Characterization of Proteins involved in Cytoplasmic and Mitochondrial Iron-Sulfur [Fe-S] Cluster Biogenesis from *Plasmodium vivax*

THESIS

Submitted in partial fulfilment
of the requirements for the degree of
DOCTOR OF PHILOSOPHY

by

Ms. BUB NIDHI KIRTIKUMAR
2017PHXF0010P

Under the Supervision of

Prof. SHILPI GARG

BITS Pilani
Pilani | Dubai | Goa | Hyderabad | Mumbai

BIRLA INSTITUTE OF TECHNOLOGY & SCIENCE
PILANI – 333031 (RAJASTHAN) INDIA

2023

BIRLA INSTITUTE OF TECHNOLOGY AND SCIENCE, PILANI

CERTIFICATE

This is to certify that the thesis titled **"Characterization of Proteins involved in Cytoplasmic and Mitochondrial Iron-Sulfur [Fe-S] Cluster Biogenesis from *Plasmodium vivax*"** submitted by **Ms. Bub Nidhi Kirtikumar**, ID No **2017PHXF0010P** for award of Ph.D. of the Institute embodies original work done by her under my supervision.

Signature (Supervisor) **:**

Name (Supervisor) : SHILPI GARG, Ph.D.

Designation **:** Professor

Affiliation **:** Department of Biological Sciences, BITS-Pilani, Pilani Campus, Rajasthan

Date :

Acknowledgments

"Life is not a problem to be solved, but a reality to be experienced." - Alan Watts

I begin by embracing the profound words of Alan Watts, which remind us that our journey through academia is not merely about finding solutions to problems but rather about embracing the experiences that shape us. With immense gratitude, I express my heartfelt appreciation to the individuals who have supported and guided me during my Ph.D. journey, enabling me to grow personally and professionally.

First and foremost, I am indebted to my exceptional Ph.D. supervisor, Prof. Shilpi Garg. Her unwavering dedication, tireless work ethic, and never-give-up attitude have been a constant source of inspiration. She fearlessly pushed me beyond my comfort zone, fostering my growth as a researcher. Her detailed guidance and unwavering belief in my potential have been instrumental in my success. I am truly fortunate to have had her as my supervisor, as she imparted invaluable research skills and provided steady support during the highs and lows of my Ph.D. journey. I am grateful for her mentorship and encouragement, which have been invaluable throughout these six years. I am truly fortunate to have had the opportunity to work under her guidance.

I extend my heartfelt gratitude to Prof. Vishal Saxena for instilling the importance of confidence and faith in my research findings. His relentless pursuit of excellence and profound insights have shaped my analytical skills. I am grateful for his critical and constructive suggestions, which have significantly enriched my research. Our scientific discussions have been invaluable, and I am thankful for the opportunities to learn from his vast knowledge. His expertise in various experimental techniques and attention to detail has also been indispensable.

I would also like to acknowledge Prof. A. K. Das, a member of my doctoral advisory committee, for his valuable advice, constructive criticism, and insightful suggestions throughout the progression of my thesis. His guidance and encouragement have played a crucial role in shaping my research work.

I want to express my gratitude to the former Vice Chancellor, Prof. Souvik Bhattacharyya, and Prof. V. Ramgopal Rao, Vice Chancellor, BITS Pilani, Pilani Campus, for allowing me to pursue Ph.D. in the excellent working atmosphere at BITS Pilani, Pilani Campus. I want to thank Col Soumyabrata Chakraborty (Retd), Registrar, BITS Pilani and former Director Prof. Ashoke K. Sarkar, and Prof. Sudhirkumar Barai, Director, BITS Pilani, Pilani campus, for providing us with a supportive atmosphere, excellent research facilities in & around the region, exposure to the scientific world and a platform to rise. I also wish to thank Prof. Sanjay Kumar Verma, Dean, Administration Division, Former Associate Dean (AGSRD), Prof. Jitendra Panwar, and Prof. Shamik Chakraborty, Associate Dean, Academic – Graduate Studies & Research

(AGSRD), and Prof. N V Muralidhar Rao, Unit Chief, Centralized Purchases Unit (CPU), for their support and helpful guidance extended throughout the research work. Moreover, I thank the contribution and dedication of the office staff of AGSRD, including Mr. Mahipal, Mr. Raghuvir, Mr. Murli, and Mr. Nitesh, for handling various evaluation documents and facilitating the submission of my thesis. Additionally, I would like to thank Mr. Nitin from the Accounts office for guiding me and helping me with various paperwork related to my doctoral fellowship.

I thank Prof. Rajdeep Chowdhury, Head of the Department, and all the Biological Sciences department faculty members for their valuable contributions and suggestions towards my Ph.D. thesis. Their expertise and guidance have been instrumental in shaping my research direction.

Special appreciation goes to Dr. Balakumaran Chandrasekar for his assistance in analyzing Mass Spectrometric data and providing guidance on career options after my Ph.D. His valuable time and expertise have been deeply appreciated. I am grateful for the valuable input and suggestions from Prof. P. R. Deepa, Prof. Sandhya Marathe, Prof. Pankaj Kumar Sharma, Prof. Sudeshna Mukherjee, and Prof. Syamantak Majumder in shaping my thesis. I sincerely appreciate their time and effort in reviewing my work and providing constructive feedback. Moreover, I would like to thank Prof. Shibasish Chowdhury for his guidance in molecular docking analyses, which have significantly enhanced my understanding of complex bioinformatics methodology.

I want to thank Prof. Prabhat Nath Jha, a valued member of the Doctoral Research Committee, for his invaluable guidance and assistance during the thesis submission process. Additionally, I am immensely grateful for the opportunity he provided me to assist him in conducting the lab course on Genetic Engineering. This experience has enriched my teaching skills and provided me with a profound understanding of instructing undergraduate and postgraduate students. Furthermore, I would like to acknowledge Mr. Ajay Kumar Yadav for his guidance, provision of essential reagents and apparatus, and assistance during the early years of my Ph.D.

My sincere regards go to the non-teaching staff of the department, namely Mrs. Kaushalya, Mr. Mukesh Saini, Mr. Subhash, Mr. Naresh Saini, Mr. Parmeshwar, Mr. Manoj, and Mr. Kamlesh Soni. Their timely assistance and support have been invaluable throughout my journey.

I am grateful to Dr. Sushil Kumar Yadav for his guidance and support during my animal studies. Additionally, I thank Mr. Vishal for teaching me the Retro-orbital bleeding technique in mice, which was crucial for completing my animal studies.

I am indebted to the collaborative efforts with Prof. Shailja Singh's Lab at Jawaharlal Nehru University, Delhi. The invaluable collaboration and the lessons learned during that period have greatly enriched my research experience. Furthermore, I am grateful to Prof. Dhanpat Kochar and Prof. Sanjay Kochar from Sardar Patel Medical College, Bikaner, for providing invaluable malaria-infected samples for my research.

I thank Dr. Vikas Kumar, my senior, for his assistance throughout my PhD journey. His guidance in troubleshooting research ideas and expertise in handling high-tech instruments have been instrumental in my growth as a researcher. I am thankful for his advice, both professionally and personally.

I am deeply grateful to Dr. Poonam Singh and Mr. Anand Tiwari for making me feel at home at BITS Pilani. Their support during challenging times, both in my Ph.D. and personal life, has been invaluable. Their attentive listening and essential advice have been a constant source of strength. I cherish our teatime discussions and the camaraderie we shared. They have taught me the value of remaining calm during chaotic situations and the importance of patience. I am grateful for the memories we have created, especially during our paneer biryani parties.

I want to thank my super seniors, Dr. Zarna Pala and Dr. Isha Pandey, for their guidance during my initial days at BITS Pilani. Their support and mentorship played a pivotal role in helping me settle into the institution. I thank Dr. Gagandeep for his assistance and guidance in various aspects of my Ph.D. work. I would also like to express my gratitude to Dr. Monika Sandhu, Dr. Panchsheela, Dr. Vikram, Dr. Shahid, Dr. Vajir, Dr. Nisha, Dr. Shradha, Dr. Tripti, Dr. Shubhra, Dr. Leena, Dr. G. Lakshmi, and Dr. Heena for their support and help throughout my Ph.D. journey.

I am grateful to my colleagues and friends who have created a stimulating environment in the lab. Special thanks to Sweta for teaching me various basic molecular biology techniques during the initial phase of my journey. I sincerely thank Subhiksha and Ankush for their unwavering support, enthusiasm, and hard work. Our collaboration yielded fruitful results that form an integral part of this thesis. Our unmatchable synergy and dedication have been a constant motivation. I also thank Srinivasan, Suryanshi, Avantika, Rohan, Suraj, and Deeptanshu for their assistance in my Ph.D. work and their inquisitive queries encouraging me to learn new things.

I thank my junior colleagues Aishwarya, Palak, Divya, Akansha, Diksha, Sayantani, Shradha, and Kanika. They have been my family at BITS Pilani, always offering their help in various experiments. Their support during the ups and downs of my Ph.D. journey has been invaluable. Our visits to the Sky Lab cafeteria and tea-time discussions have created lasting memories. Their motivation and positive approach have been precious. I am incredibly grateful to Palak and Aishwarya for always bringing a smile to my face, even during challenging times. Their active participation in significant personal and professional decisions has been deeply appreciated. Moreover, I thank Palak for nurturing my fun side and constantly motivating me with positive thoughts. Additionally, I would like to thank Aishwarya, Palak, and Sayantani for reviewing my Ph.D. thesis chapters, which have helped me immensely. Moreover, I want to thank Sampreeti, Sukrati, Gunjan, and Shreya for assisting me during my Ph.D. journey. Furthermore, I thank Priyanka and Saurabh for the exciting scientific discussions.

I sincerely thank Saumya and Aastha, my flatmates in Quarter number 7811. Our friendship has grown to new levels, and we have shared life's joys and challenges together. Thank you for providing invaluable life advice that has immensely helped me. We supported each other during the difficult times of the COVID-19 lockdown. I am grateful for your guidance in making tough decisions, as you both have known me inside out. Furthermore, I express my heartfelt gratitude to Sonia, whose constant support and guidance have been invaluable throughout my research journey. I cannot thank you enough for patiently listening to me during moments of frustration and providing comfort during the lows I experienced throughout my Ph.D.

I want to express my heartfelt appreciation to my amazing friends and colleagues, Simran, Nandita, Harshita, Shobham, Sumukh, Shreyas, Yash, Niyati, Ramakrishnan, Hansa, Ashima, Sumit, Anirudha, Proparna, Abhilasha, Vishalakshi, Tripti, and Mamta. I am grateful for the wonderful social group we have formed and cherish the moments we have spent together. I thank Ankita Daiya, Ankita Das, and Ankita Sharma for all the scientific discussions and help during my thesis work. Moreover, I would like to thank Mr. Suman Kumar for helping me during confocal microscopy and image processing, which was crucial for completing my subcellular localization studies.

I want to thank Prachi, Karan, Narendra, and Mamta for their assistance in generating the anaerobic chamber. I also thank Swati, Swetha, Kavya, Srividya, Atharva, Aishwarya, Tina, Narsimha, Moumita, Samarth, and Rajesh for their support during my Ph.D.

A special mention goes to Dr. Pooja and Aashvi, who have been significant emotional support since our time together in school. Despite the distance, you have always been there for me, providing guidance and advice when I was unsure or making wrong decisions.

I would also like to express my gratitude to Dr. Shreya and Dr. Tasnim, who have consistently cheered me up, despite the miles that separate us. Their willingness to discuss and troubleshoot research ideas has been instrumental in shaping my work. Moreover, I sincerely thank Dr. Kavya for her invaluable support and guidance throughout my research journey.

I want to acknowledge the Sky Lab cafeteria, where I spent significant time during my six-year Ph.D. journey. Countless memories have been made there, and I am grateful to Mr. Kamal Kapoor (Pappu Ji) and his staff for their hospitality. I would also like to thank Nescafe Gold for providing the best coffee, which has been a great companion throughout my Ph.D.

I sincerely thank my parents, Mr. Kirtikumar Bub and Mrs. Mina Bub. They are incredibly open-minded and supportive individuals who have always understood and respected my decisions. I thank my brother, Mr. Abhijit Bub, for engaging in discussions on history, science, and spirituality. Thank you for uplifting my mood and

always standing up for me when no one else did. Despite being younger, you have cared for me like an elder brother, and I appreciate your support throughout my Ph.D.

I take this opportunity to acknowledge the Department of Biotechnology (DBT), Government of India, New Delhi, for providing financial assistance in the form of Junior Research Fellowship and Senior Research Fellowship. This support has allowed me to conduct my work comfortably.

Last, but not least, I am deeply grateful to all the patients who generously donated their blood and the mice sacrificed during this study. Their contributions have been crucial in advancing scientific knowledge and finding potential solutions to critical issues.

In conclusion, my Ph.D. journey has been a transformative experience, filled with learning, growth, and invaluable support from mentors, colleagues, friends, and loved ones. I am grateful for everyone who has played a role in shaping my academic and personal development. Their guidance, encouragement, and assistance have been instrumental in completing this thesis. Thank you all from the bottom of my heart.

Lastly, I apologize for forgetting to acknowledge anyone who helped me.

Nidhi Kirtikumar Bub

Contents

ABSTRACT

[Fe-S] clusters are one of the most important cofactors involved in regulation of various essential biological processes such as DNA repair and metabolism, redox and non-redox catalysis, electron transport, sensing environmental stimuli etc. Four types of [Fe-S] cluster biogenesis pathways have been reported in nature namely NIF (Nitrogen fixation), SUF (Sulfur mobilization), ISC (Iron Sulfur Cluster assembly) and CIA (Cytoplasmic Iron Sulfur Cluster Assembly) pathways. Among these, majority of the components of the SUF pathway have been detailed from both the major human malaria parasites; *P. falciparum* and *P. vivax*, however, the components of the ISC pathway have been only recently elucidated from *P. falciparum*, with no reports from *P. vivax*. Recently, a few of the CIA pathway components have also been identified from *Plasmodium* database using bioinformatics tools for evolutionary studies, indicating presence of cytosolic [Fe-S] biogenesis machinery in the parasite, however, none of the components have been detailed yet from any of the *Plasmodium* species. Therefore, in the present work, we have studied the less explored Fe-S biogenesis pathways; i.e. the ISC and CIA pathways from *Plasmodium vivax*.

To investigate the [Fe-S] biogenesis pathways from *P. vivax*, we first identified various components of the CIA pathway from *P. vivax* by mining the PlasmoDB database. Based on the multifunctional role reported for Dre2 in different organisms, we selected one of the initial components of the pathway; Dre2/Anamorsin for further studies. The gene was amplified from *P. vivax* clinical isolates, cloned and expressed in a prokaryotic system. Sequence analysis revealed a highly conserved CIAPIN 1 domain at the C-terminal, with the conserved cysteine residues at Motif-I and Motif-II, reported to be involved in binding of [Fe-S] clusters. These cysteine residues were shown to interact with [Fe-S] clusters using *in silico* docking tools, which was further confirmed using *in vitro* chemical reconstitution assays, where equimolar ratio of Fe and S was found to bind to the protein. We also showed subcellular localization of *Pv*Dre2 to mitochondria. Further, to explore functions other than CIA pathway for *Pv*Dre2, interactome analysis was performed using co-immunoprecipitation and mass spectrometry analysis, where we found *Pv*Dre2 to interact with proteins involved in

Golgi trafficking, ribosome biogenesis, DNA replication and repair, suggesting the multifunctional role of protein in the parasite also.

During the heterologous expression of *Pv*Dre2 protein in *E. coli*, we observed a brown coloured pellet and surprisingly, reduced cell growth post-IPTG induction, indicating the protein's involvement in [Fe-S] dynamics. *Pv*Dre2 expression led to Fe-mediated oxidative stress and disturbances in *E. coli* membrane dynamics. However, *Pv*Dre2-mediated *E. coli* cell death recovered at late hours post induction as confirmed by the elevated expression of various stress response genes in *E. coli*. Further the *E. coli* cells were rescued from *Pv*Dre2 mediated cell toxicity when treated with exogenous Artemether indicating potential association of *Pv*Dre2 with Artemisinin and suggesting *Pv*Dre2 as one of the potential target for the drug. Artemisinin is currently the first line of drug against *P. falciparum* malaria and drug of choice to treat the severe *P. vivax* malaria, thus further investigation is required to elucidate the mechanism behind this association.

The second part of the thesis focuses on the mitochondrial ISC pathway of *P. vivax*. At the time of initiation of the thesis work, only two proteins of this pathway *IscS* and *Isd11* were reported from the parasite, where they were used for the localization studies to confirm mitochondria as the functional site of the pathway. Since a scaffold protein is an important component of any [Fe-S] cluster biogenesis pathway and the reports on the scaffold protein IscU from yeast are suggestive of it acting as a donor of intermediate moieties for the maturation of Fe-S clusters in the CIA pathway also, thus we investigated into the scaffold protein for the pathway. However, we could not retrieve any protein designated as the scaffold protein functional in ISC pathway, thus we searched the PlasmoDB database to look into mitochondrial targeted proteins having scaffold protein like features. Based on conserved domain and signature motif (LPPVK) similar to IscU proteins and the same clade with all IscU proteins in the phylogenetic tree, *Pv*NifU protein, putative was designated as *Pv*IscU protein, putative. The gene encoding this protein was amplified from *P. vivax* clinical isolates, cloned and expressed in a prokaryotic system. The purified protein was used for raising antibodies in mice, which when used for immune-localization studies confirmed mitochondria as the functional site for the protein. The purified protein was further subjected to *in vitro* chemical reconstitution, and the binding of [Fe-S] clusters onto

*Pv*IscU indicated the evolutionary conservation of its scaffold activity. To understand the physiological significance of the metamorphic property of the IscU scaffold in *P. vivax*, we investigated its binding to [Fe-S] clusters in presence of various divalent metals like Zinc, Copper and Cobalt. We observed no binding of [Fe-S] clusters in presence of these divalent metals, suggesting a shared binding site for these and [2Fe-2S] on the *Pv*IscU scaffold. In addition, the metamorphic nature of ISCU in presence of divalent metals suggests a regulatory role of these ions for formation of [Fe-S] clusters in the parasite.

In conclusion, we have characterized two [Fe-S] biogenesis proteins; Dre2 and IscU from *Plasmodium vivax* for the first time to elucidate their role in parasite life cycle. Even when the two proteins exhibited conserved nature, a few important observations like the association of Dre2 with first line drug Artemisinin, its interaction with proteins involved in pathways like Golgi trafficking, ribosome biogenesis, DNA repair etc., suggests multiple functions for the protein, which can be investigated further for designing new intervention strategies. Henceforth, the study of [Fe-S] biogenesis pathways from *Plasmodium* not only adds to the existing knowledge regarding these pathways and their interconnections but can also help find new drug targets or analyse existing antimalarial for the malaria parasites.

List of Tables

List of Figures

Abbreviations

[Fe-S] ^{int}	Intermediate Iron-Sulfur cluster
ACD	Acid Citrate Dextrose
ART	Artemisinin
ATAP	A-Type assembly proteins
ATP	Adenosine triphosphate
CDD	Conserved Domain Database
CFU	Colony Forming Units
CHC	Clathrin Heavy Chain
CIA	Cytoplasmic Iron Sulfur Cluster Assembly
CIAPIN1	Cytokine-induced anti-apoptosis inhibitor 1
CTC	CIA Targeting Complex
DAPI	4',6-diamidino-2-phenylindole
DiQ-BioID	Dimerization-induced quantitative- proximity-dependent biotin identification
DPD	N, N-Dimetthyl-p-phenylene diamine sulfate
Dre2	Derepressed for Ribosomal protein S14 Expression
DTT	Dithiothreitol
EDTA	Ethylene-diamine-tetra-acetic acid
ELISA	Enzyme linked immunosorbent assay
EPR	Electron paramagnetic resonance
$FADH_2$	Flavin Adenine Dinucleotide
Ferrozine	Disodium 3-(2-pyridyl)-5,6-bis(4-phenyl sulfonate)-1,2,4-triazine

FITC	Fluorescein Iso-Thiocyanate
FMN	Flavin mononucleotide
GSH	Glutathione
GLP3	Glutaredoxin-like protein 3
ICP-OES	Inductively coupled plasma - optical emission spectrometry
IMS	Intermembrane space
IPP	Isopentenyl pyrophosphate
ISC	Iron-Sulfur Cluster assembly
LC-MS/MS	Liquid chromatography-mass spectrometry/mass spectrometry
MSA	Multiple Sequence Alignment
MT	Methyltransferase
NADH	Nicotinamide Adenine Dinucleotide
NADPH	Nicotinamide Adenine Dinucleotide Phosphate
NIF	Nitrogen fixation
Ni-NTA	Nickel-Nitrilotriacetic acid
NOS	Nitric oxide synthases
PBMCs	Peripheral Blood Mononuclear Cells
PBS	Phosphate buffer saline
PCR	Polymerase Chain Reaction
PDB	Protein data bank
PLP	Pyridoxal phosphate
ROS	Reactive Oxygen Species
SAM	S-adenosyl-methionine

SEM	Scanning electron microscopy
S_{int}	Intermediate Sulfur moiety
SUF	Sulfur Mobilization
WHO	World Health Organization

Chapter 1

Introduction and Review of Literature

INTRODUCTION

1.1 MALARIA: The Disease

Malaria is an acute pyretic disease that spreads through the bite of female *Anopheles* mosquitoes, injecting the parasite *Plasmodium* in the host during the blood meal. In 2021 alone, approximately 241 million cases of malaria infections and 6,27,000 deaths were reported worldwide (WHO, World Malaria Report, 2022). Approximately two-thirds of the additional deaths in 2021, when compared to those in 2020 (47,000) were linked to disruptions in the provision of malaria prevention, diagnosis, and treatment during the COVID pandemic. Most of the increase was observed in the WHO African regions, which accounts for almost 90% of malaria cases and deaths globally, with six countries— Nigeria (27%), the Democratic Republic of the Congo (12%), Uganda (5%), Mozambique (4%), Angola (3.4%) and Burkina Faso (3.4%) accounting for ~55% of these cases (Oladipo et al., 2022). WHO South-East Asia Region was responsible for total 2% of the cases and out of these 79% of the cases were reported from India itself. In total 83% of the malaria deaths were reported from India only with respect to entire WHO South-East Asia region (WHO, World Malaria Report, 2022) **(Figure 1.1)**.

In humans, five species of *Plasmodium* are known to cause malaria; viz; *P. falciparum*, *P. vivax*, *P. malariae*, *P. ovale,* and *P. knowlesi* (Sato et al., 2021). Among these, *P. falciparum* and *P. vivax* account for most of the cases globally, where *P. falciparum* is the most notorious with the maximum number of cases and deaths worldwide, while *P. vivax* is the most widespread parasite. The distribution of *P. malariae* is reported as being patchy, however, it has been observed in all major malaria-endemic regions of the world especially in sub-Saharan Africa and the southwest Pacific. *P. ovale* have a much more limited distribution and its prevalence rarely exceeds 3–5%. The initial symptoms of the disease include fever, chills, headache, sweats, nausea and vomiting that are generally visible 10-15 days after the infective mosquito encounters the host. In general malaria is a treatable disease, however, if left untreated or in certain cases of delayed treatment, this mild form can develop into complicated malaria, which may also result in death. Both *P. falciparum* and *P. vivax* have been reported to cause severe manifestations like haemoglobinuria, acute respiratory distress, cerebral malaria,

hepatic dysregulation, renal failure, seizures, mental confusion, coma, and death (CDC, 2020; Kochar et al., 2009, 2005).

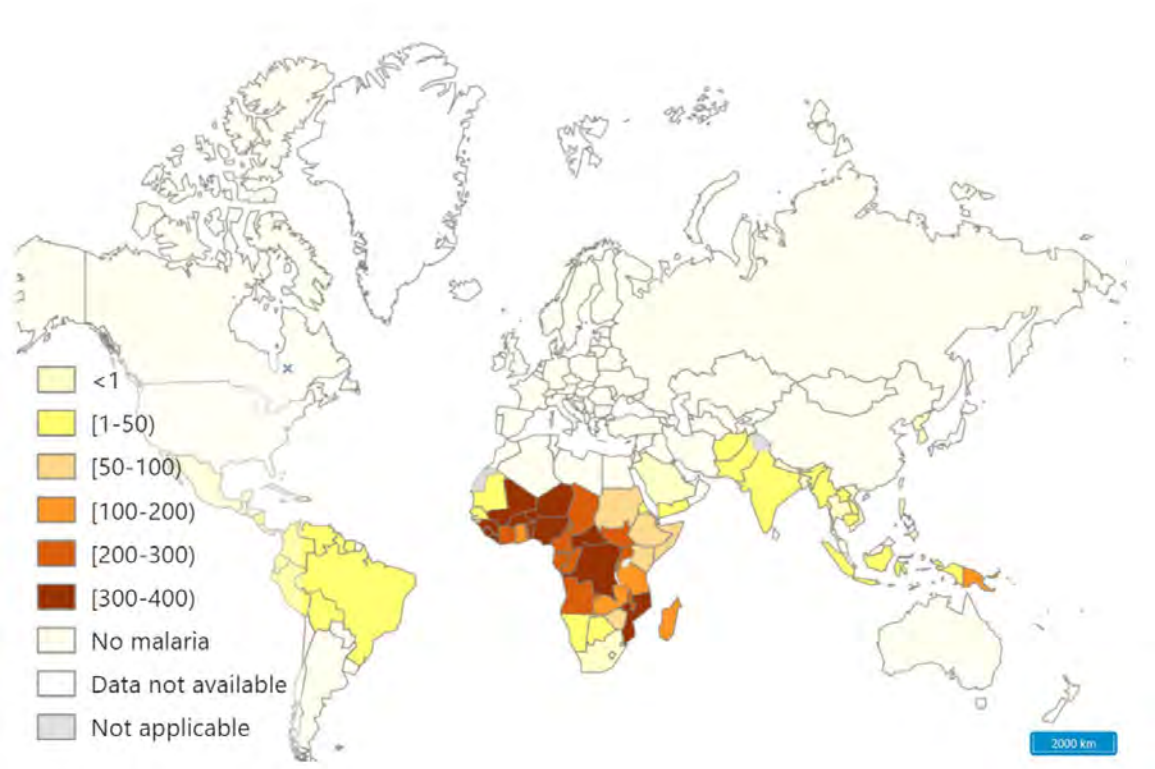

Figure 1.1: Estimated malaria incidence per 1000 population at risk in 2021
(WHO Malaria Report, 2022)

1.2 Life cycle of *Plasmodium spp.*

Plasmodium is a unicellular, eukaryotic, intracellular parasite that belongs to the Phylum Apicomplexa. It completes its lifecycle in two hosts: a vertebrate host like a human in which the parasite undergoes asexual reproduction, forms the gametocytes (sexual stage) and causes the disease malaria; and an invertebrate host such as *Anopheles* mosquito where the parasite completes its sexual cycle and which acts as a vector for transmitting the disease to the vertebrate host. The parasite's life cycle begins when an infected female *Anopheles* mosquito transfer 10-100 sporozoites present in its salivary glands into the host during blood meal (Doolan et al., 2009; Nkhoma et al., 2012). Once injected into the blood, the sporozoites head straight to the liver and within 30 minutes they invade the liver cells. Each sporozoite invades a single hepatic cell, develops, and multiplies to form 2,000- 30,000 merozoites (Jones and Good, 2006). The schizogony stage in the liver takes approximately 6 days in *P. falciparum*, 8 days

in *P. vivax*, 13 days in *P. malariae,* and 9 days in both *P. ovale* and *P. knowlesi* (www.malariasite.com/malaria-parasites; Flannery et al., 2019). However, in *P. vivax* and *P. ovale*, some of the parasites can remain in the liver for years as hypnozoites and may cause recurrent episodes of the disease.

Once the merozoite matures, they are ready to initiate the erythrocytic cycle; the symptomatic phase in the host. They break out of the hepatocytes and re-enter the bloodstream, where they invade red blood cells, grow and develops into different forms like ring, trophozoite and multinucleated schizont stage. The schizont ruptures the RBC and releases approximately 10-50 merozoites in the blood stream and the erythrocytic cycle of malaria infection continues. During the release of merozoites, the parasite also releases certain metabolites and toxins which play a key role in the development of characteristic symptoms like periodic fever and shivering (Flannery et al., 2019).

During the erythrocytic cycle, a small proportion of ring or early trophozoite gets converted into male or female gametocytes through a transcriptionally regulated mechanism. When the mosquito feeds on the vertebrate host for blood meal again, haploid gametocytes are taken along with the blood initiating the sporogony phase. After ingestion by a mosquito, male gametocytes undergo a 3-fold replication of their genome in less than 15 minutes, producing 8 motile microgametes (Janse et al., 1986). Female gametocytes (macrogametes) also mature upon entering a mosquito, but no replication or cell division occurs. The fertilization of the gamete's occurs in the mosquito's midgut, where the microgametes penetrate the macrogametes generating zygotes. The zygote becomes elongated and forms a motile ookinete. This ookinete then invades the midgut and forms oocyst, which undergoes multiple rounds of asexual division and give rise to numerous haploid sporozoites. The sporozoites in the haemocoel make their way to the salivary glands where they mix with saliva and get released into a new vertebrate host when the infected mosquito takes another blood meal. The sporogony phase lasts 8-15 days in the mosquito (Carter & Graves, 1988; Eichner et al., 2001; Flannery et al., 2019) **(Figure 1.2)**.

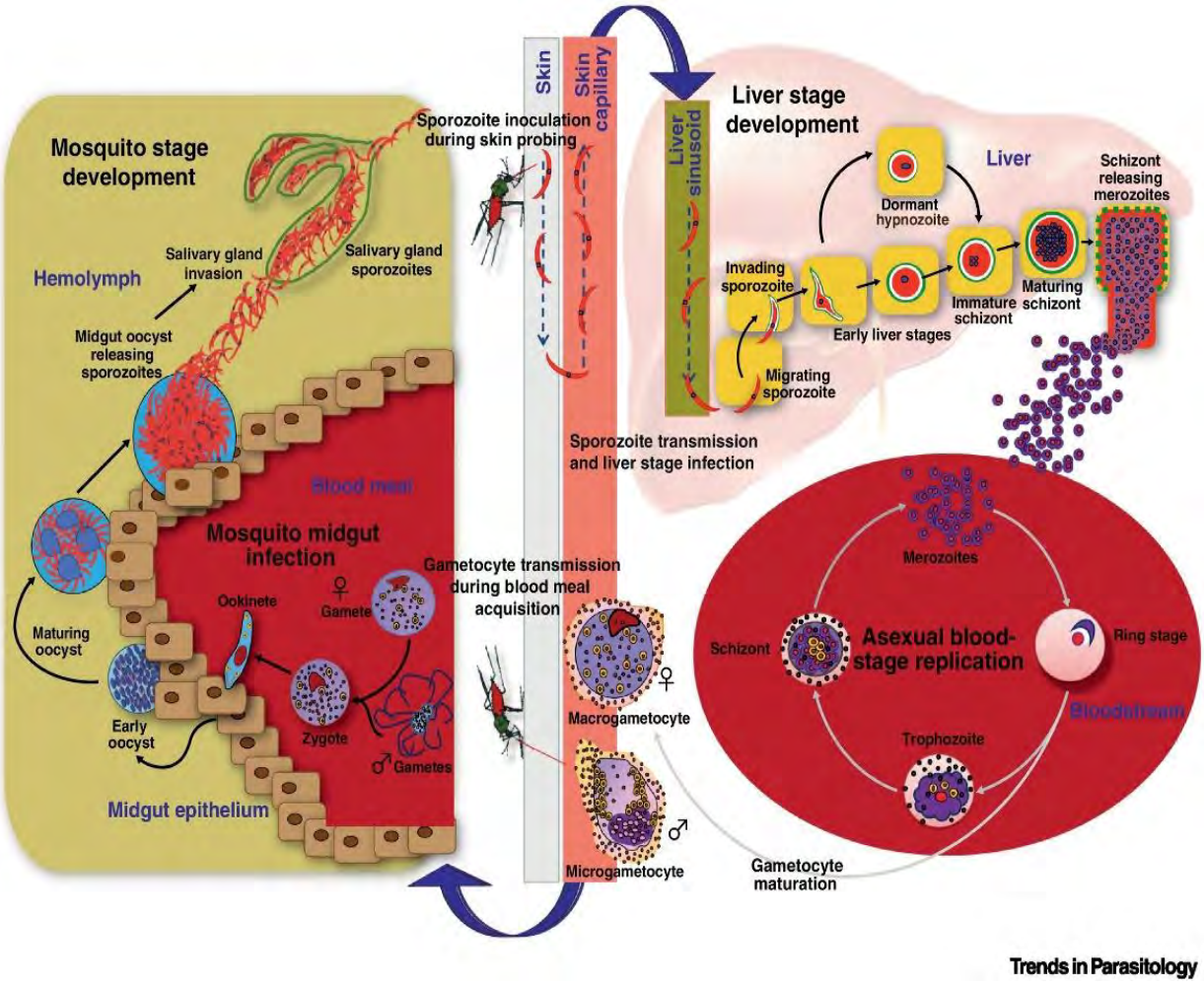

Figure 1.2: Life cycle of the malaria parasite *P. vivax* in the human host and female *Anopheles* mosquito (Flannery et al., 2019)

1.3 Burden of *Plasmodium vivax* malaria

P. vivax is geographically the most widely distributed parasite. It is most prevalent malaria parasite in the countries other than sub-Saharan regions of Africa and to be more specific in the tropical regions. More than one-third of the world's population is at risk for *P. vivax* infection, with most number of cases in South and South-East Asia, the Eastern Mediterranean region, and South America. Globally, the number of cases due to *P. vivax* increased from 4.5 million in 2020 to 4.9 million in 2021 (WHO, World Malaria Report, 2021 and 2022). While *P. vivax* infection overlaps significantly with that of *P. falciparum* in many parts of the world, there are several places in Southeast Asia such as South Korea where *P. vivax* is the exclusive cause of malaria infections (Howes et al., 2016). According to World Malaria Report 2022, approximately 71% of malaria cases in America in 2021 resulted from *P. vivax*. In 2021, Cambodia reported

a total of 1978 relapse cases. The WHO Eastern Mediterranean Region accounted for the decrease in malaria cases in 2021, however, from those reported cases, 18% of the cases in Afghanistan and Pakistan were mainly due to *P. vivax* (WHO, World Malaria Report, 2022, CDC 2022).

The WHO South-East Asia Region accounts for 53% of the global *P. vivax* malaria cases, with the majority being in India (47%) (WHO, World Malaria Report, 2022). India reported over 160 thousand cases of *P. vivax* malaria in 2021. *P. vivax* malaria is difficult to resolve when compared with the other malaria species due to many factors such as: 1) relapse due to hypnozoites, a distinct feature of *P. vivax*, 2) Poor compliance of the community for Primaquine against relapse malaria, 3) host factors such as prevalence of G6PD (glucose-6-phosphate dehydrogenase) deficiency that affect Primaquine metabolism and complicate its efficacy (Ahmad et al., 2021) **(Figure 1.3)**.

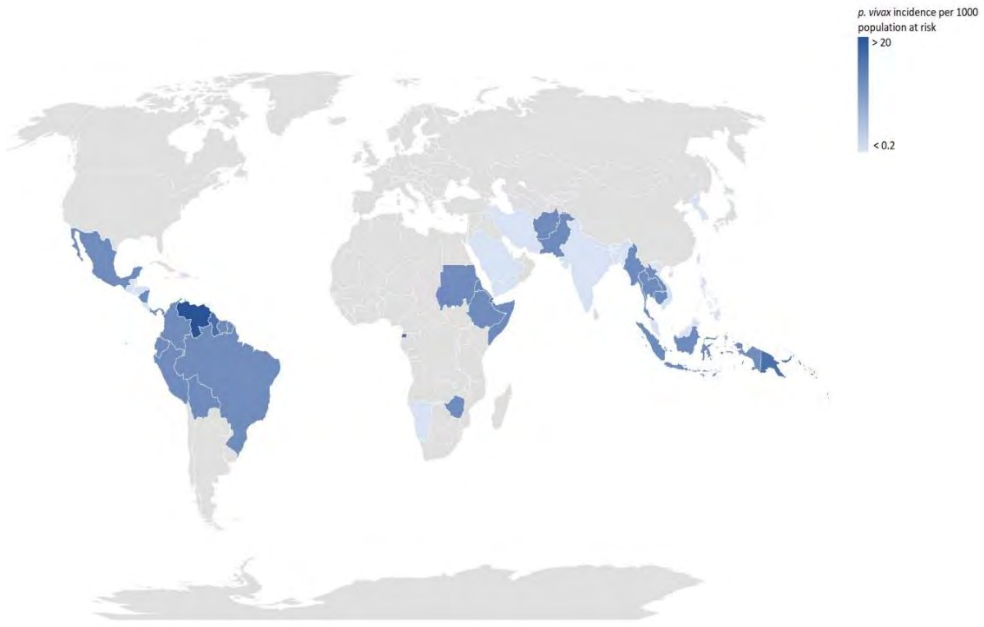

Figure 1.3: Incidence of *P. vivax* cases reported per 1000 population at risk
(WHO Malaria Report, 2022)

1.4 Treatment of Malaria

WHO-authorized various malaria prevention tools and strategies that includes effective vector control and use of preventive antimalarial drugs has significantly decreased worldwide burden of the malaria disease. Very recently in October 2021, one of the vaccines named RTS, S/AS01 has been approved by WHO against *P. falciparum*

malaria specifically for children living in high endemic areas, but its moderate efficacy remains a limitation. Hence, as of now, chemotherapeutic drugs remain the major strategy to control malaria. For long Chloroquine has been the drug of choice to treat malaria, but due to the development of resistance to the drug, it is no longer used to treat the *falciparum* malaria. However, it is still administered to patients with uncomplicated *P. vivax* malaria. In case of chloroquine resistant *Plasmodium*, four different treatment options are available that includes 1) Artemether - Lumefantrine (Coartem®) 2), Atovaquone - Proguanil (Malarone^{TM}), 3) Quinine sulfate plus doxycycline, tetracycline, or clindamycin, and 4) Mefloquine. Additionally, as *P. vivax* and *P. ovale* infections have tendency for disease relapse mainly due to the hypnozoites, they can be additionally treated with either Primaquine phosphate or Tafenoquine (Krintafel^{TM}). Patients with severe malaria manifestations such as impaired consciousness, acute kidney injury, acute respiratory distress syndrome, circulatory collapse/shock, acidosis, hepatic dysfunction, disseminated intravascular coagulation, and/or parasite density ≥5% must be given intravenous (IV) Artesunate (CDC, 2022). Recent reports on Artemisinin drug resistance has surfaced a challenge to global malaria prevention strategies in Greater Mekong sub region and more recent reports have surfaced regarding partial Artemisinin resistance in Africa. The reasons behind development of partial resistance of parasite against artemisinin is mainly poor treatment methods such as patients following drug regimen inappropriately and clinicians prescribing artemisinin-based monotherapies (CDC, 2022; WHO, World Malaria Report, 2021). Thus an immediate action must be taken to map the extent of drug resistance for designing better future intervention strategies. In addition, it is necessary to study the biology of the parasite and investigate new drug targets for the upcoming resistant strains. Thus in this work we aim to study one of the important metabolic pathway functional in the parasite i.e. the [Fe-S] biogenesis pathway which provides [Fe-S] clusters to various proteins essential for the survival of the parasite.

1.5 Iron-Sulfur Clusters

1.5.1 [Fe-S]: Primordial and important cofactor for proteins

About 3 billion years ago, the atmosphere of earth was anaerobic where oxygen concentration was less than 0.01%. In such a highly reducing environment, iron being the most versatile transition metals started forming different types of cofactors; one

such cofactor being iron sulfur [Fe-S] cluster, where iron in mostly Fe^{+2} or Fe^{+3} state reacts with reactive persulfide group (S^{-2}). Initially as the earth atmosphere was anaerobic and there was a plenty of iron and sulfur available, possibly the generation of [Fe-S] clusters would have been spontaneous. These spontaneously formed clusters would have then been incorporated into ancient proteins where they catalysed various cellular reactions and led to increased metabolic efficiency. Later, the cell came up with a highly regulated biogenesis pathways for [Fe-S] formation given the increase in the demand for the [Fe-S] as a cofactor (Rouault et al., 2008, Ratledge and Dover, 2000).

1.5.2 Different types of [Fe-S] clusters in biological system

Iron sulfur clusters are one of the most ancient cofactors that has ever existed on earth. Different number of Fe and S atoms coordinate accordingly to form variety of clusters onto respective proteins such as $Fe(Cys)_4$, [2Fe-2S], [3Fe-4S], [4Fe-4S] and [8Fe-7S]. Out of these, most common clusters used in biological processes are [2Fe-2S] and [4Fe-4S]. Many different and complex kinds of cofactors are present in prokaryotes that shows involvement of transition metals other than Fe such as Mo and Ni. These includes a) Nitrogenase, an enzyme involved in nitrogen fixation that possess iron-molybdenum cofactor i.e. [7Fe-Mo-9S] and b) hydrogenase group of enzymes having Nickel coordinated with Iron in [Ni-Fe] form. For the formation of [Fe-S] onto proteins, Iron must be present in Fe^{2+}/Fe^{3+} form and sulphur in S^{2-} form (derived from cysteine). Once the Fe and S both are present, the final coordination of [Fe-S] requires specific cysteine rich motifs in proteins along with reducing cellular environment (Maio et al., 2020) **(Figure 1.4).**

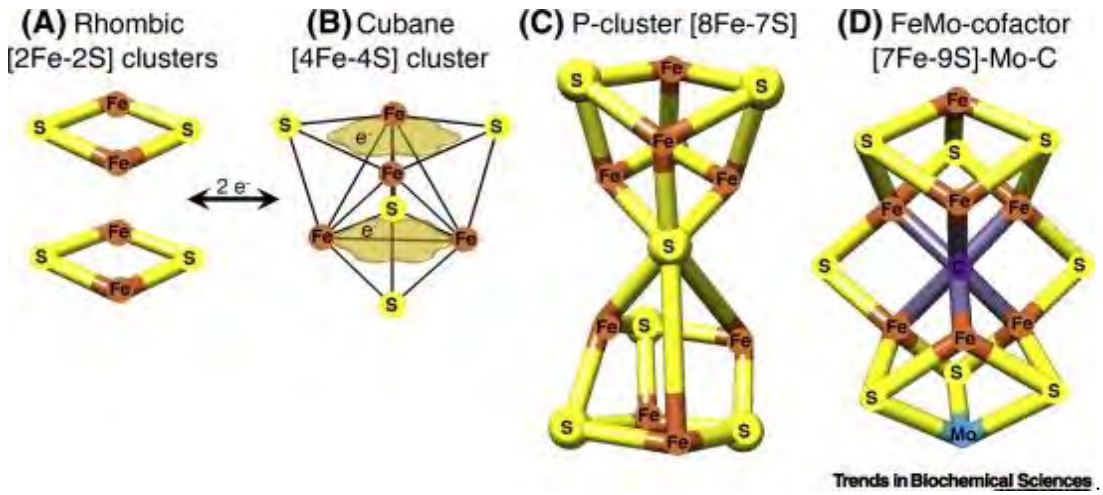

Figure 1.4: Types of Iron-Sulfur Clusters (ISCs) found in proteins (Rouault et.al 2020)

1.5.3 Functions of [Fe-S] clusters in biological system

[Fe-S] clusters play essential roles in various biological processes, and are primarily involved in maintaining physiologically relevant redox potentials, essential for the electron transfer mechanism (Kiley and Beinert, 2003). They form a series of long-range electron transfer in enzymes such as hydrogenases (microbes using or making Hydrogen for energy generation), Photosystem-I (reducing NADP upon light-mediated electron transfer), NADH-Ubiquinone oxidoreductase (Respiratory Complex-I of mitochondria), etc. **(Figure 1.5)**. They are also involved in catalytic reactions, for example [4Fe-4S] clusters of S-adenosyl-methionine enzymes reductively cleaves SAM and generates the 5′-deoxy adenosyl radical (5′-dA• radical) intermediate, which then gets involved in modification of DNA/ RNA and biosynthesis of cofactors and peptides (Ruzicka and Beinert, 1978).

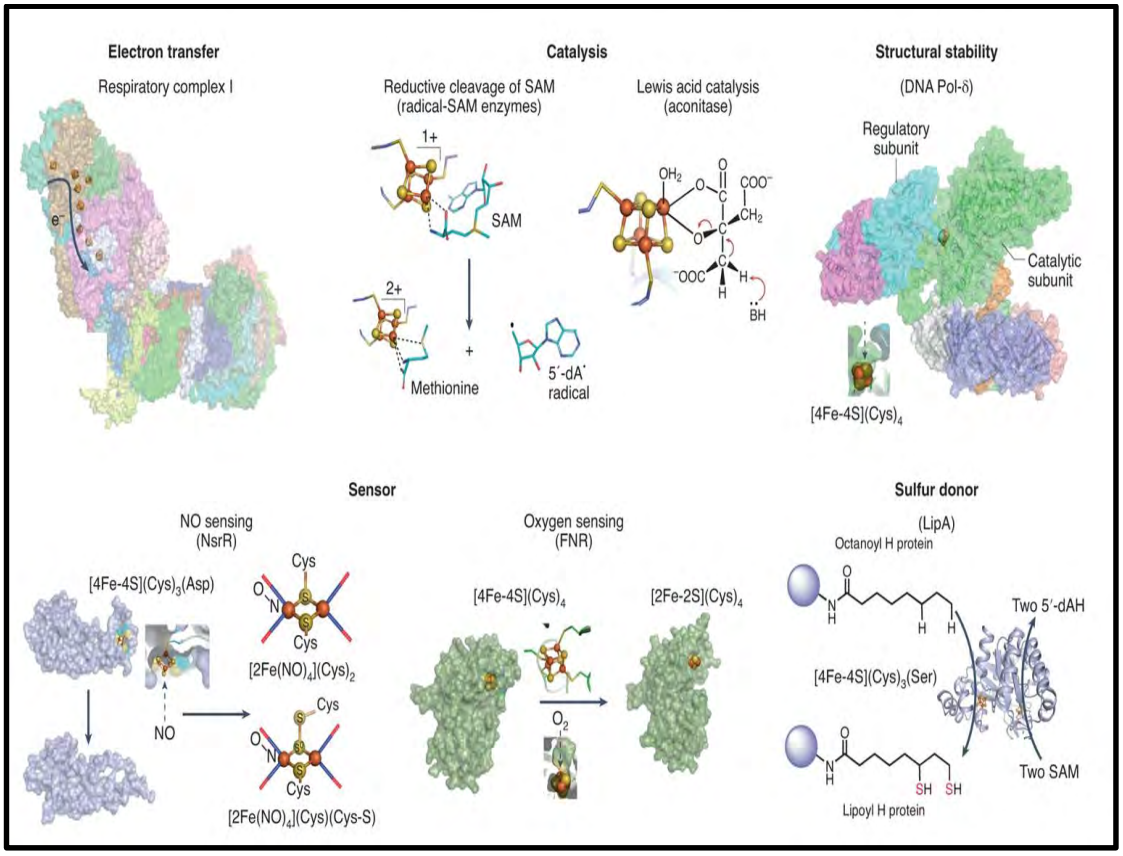

Figure 1.5: Functions of [Fe-S] clusters in various biological processes (Ebrahimi, et al., 2022)

These clusters are also essential in stabilizing protein conformation by binding to proteins or multi-protein complexes, such as stabilization of DNA polymerase δ subunit

(DNA replication and repair) upon [4Fe-4S] binding. [Fe-S] are also sensors for various environmental stimuli such as oxygen, Nitric Oxide, Hydrogen Peroxide, etc. **(Figure 1.5)**. These environmental stimuli induce changes in clusters, ultimately affecting protein conformations and controlling their functions. In some cases, [Fe-S] act as a reservoir of sulfur, such as [4Fe-4S] in lipoyl synthase (LipA), providing two sulfur atoms required to form the Lipoyl cofactor (Ebrahimi et al., 2022). Besides these functions, they are also involved in cellular apoptosis, epigenetic regulation pathways, immune defence generation, RNA modifications, anti-viral defence mechanisms, transcriptional regulation etc. (Ruzicka and Beinert, 1978).

1.6 [Fe-S] biogenesis: Cluster Biogenesis Systems and Pathways

Azotobacter vinelandii, a nitrogen fixing bacteria was the first organism in which [Fe-S] biogenesis pathway was discovered which was named as NIF (nitrogen fixation) pathway. The NIF pathway is responsible for the maturation of one of the integral enzymes; Nitrogenase which requires [Fe-S] clusters for its maturation and functionality. This was the starting point where people realized the existence of such pathways that synthesizes [Fe-S] clusters for Fe-S proteins (Jacobson et al., 1989; Frazzon and Dean, 2003). Further, as the turnover of nitrogenase enzyme was quite slow, therefore in the cells that have nitrogen fixation as their sole source of metabolic nitrogen, it was hypothesized that the reactions catalysed by NifU and NifS might have a way to increase the mobilization of iron and sulfur necessary for nitrogenase maturation and that there might also be NifU- and NifS-like "housekeeping" counterparts involved in the formation or repair of [Fe-S] clusters present in other iron-sulfur proteins (Zheng et al, 1998). Both these hypotheses were supported by evidences. The evidence of first hypothesis was indicated by the presence of a nif-specific cysE-like homolog in *A. vinelandii* to increase the cysteine pool needed for iron-sulfur cluster formation. For the second hypothesis, evidences came from genome sequencing projects that revealed the presence of NifU- and NifS-like homologs in a variety of other non-nitrogen fixing organisms, including *E. coli*, *Hemophilus influenzae*, *Saccharomyces cerevisiae* and human. This led to the identification of the ISC (Iron sulfur cluster assembly) pathway, which is the housekeeping pathway in bacteria and is reported to be distributed among most proteo-bacteria and eukaryotic mitochondria (Tokumoto et al., 2004).

The third pathway to be discovered was SUF (Sulfur mobilization) pathway, which is a conditional pathway in *E. coli* and gets activated only in oxidative stress conditions. The role of this pathway is exactly reversed in *Mycobacterium* that possess only SUF pathway for catering its needs of [Fe-S] (Blahut et al., 2020). This pathway is also functional in many eukaryotes where it is localized to the plastids, for example in case of plants it is functional inside chloroplasts whereas in case of Apicomplexans it is functional inside the plastid like organelle "Apicoplast" (Takahashi and Tokumoto, 2002). In addition to these pathways, eukaryotes also possess an exclusive machinery for [Fe-S] cluster biogenesis that is the CIA (Cytosolic Iron sulfur cluster assembly) pathway. CIA pathway is responsible for generation of extra-mitochondrial [Fe-S] clusters, which provides [Fe-S] clusters to cytosolic and nuclear Fe-S Proteins. As mentioned above, till now, three pathways have been discovered in eukaryotic cells namely ISC in mitochondria, SUF in plastids and CIA in cytosol (Leimkühler, 2020). Despite of the differences in the components, location, substrates, enzymes etc. in the [Fe-S] cluster biogenesis pathways, the mechanism of biogenesis and their transfer to apo-proteins remains highly conserved throughout living domains. However, why each compartment needs a separate [Fe-S] biogenesis pathway still needs to be elucidated **(Figure 1.6)**.

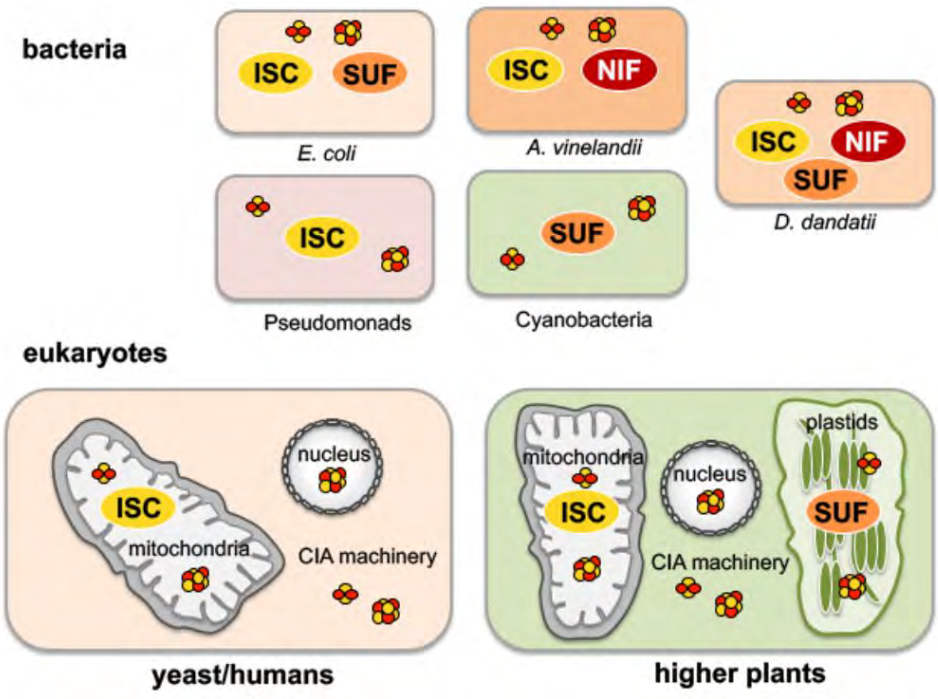

Figure 1.6: Distribution of [Fe-S] biogenesis pathways in various living domains (Leimkühler, 2020)

As the function of [Fe-S] cluster biogenesis pathways is not just assembling [Fe-S] by taking required raw materials but also to deliver these assembled clusters to the target apo-proteins, hence, to accomplish this task, there is a complex of different proteins performing dedicated roles. This complex of proteins involves an iron carrier and reductant, a cysteine desulfurase (to provide sulfide), a scaffold protein, a carrier protein (proteins mainly involved in the delivery of [Fe-S] clusters), and several accessory proteins. The basic mechanism involves sulfur retrieval from cysteine via PLP-dependent cysteine desulfurase which generates a sulphide. Further, iron from an unknown source (hypothesized to be CyaY/IscA in prokaryote; frataxin in eukaryote) alongside generated sulfide, assembles [Fe-S] clusters onto scaffold protein with the help of the electron transport chain. After generation of the mature cluster onto the scaffold, there is subsequent delivery of [Fe-S] clusters to apo-proteins which is facilitated by carrier and accessory proteins. This generalized scheme is common to all [Fe-S] cluster biogenesis pathways and is helpful for simplifying the complex steps that are involved (Barras et al., 2005; Gao et al., 2020) **(Figure 1.7)**.

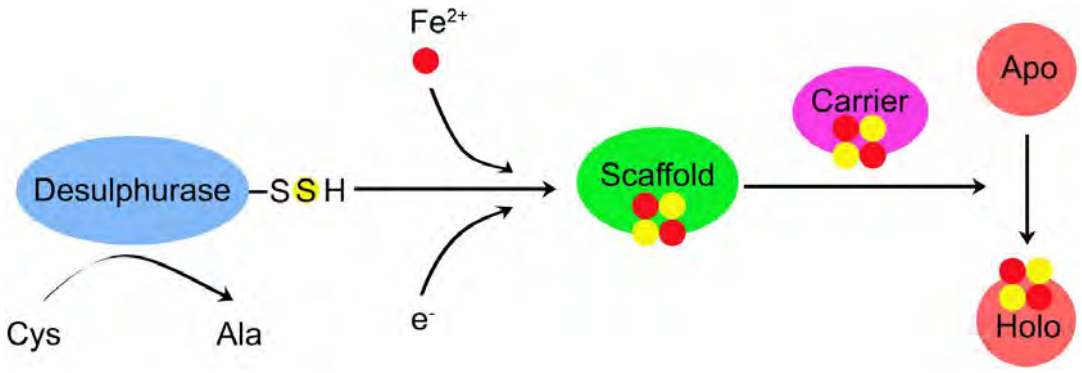

Figure 1.7: Mechanism of [Fe–S] cluster biogenesis (Gao et al., 2020)

1.6.1 ISC pathway for [Fe-S] cluster assembly

ISC pathway is the housekeeping pathway for biogenesis of [Fe-S] clusters in *E. coli* and is present in the bacterial cytoplasm. In eukaryotes, ISC pathway is functional inside the mitochondria and provides [Fe-S] clusters to mitochondrial proteins and some $[Fe\text{-}S]_{int}$ cluster or unknown sulfur moiety to cytoplasmic CIA pathway. As eukaryotic mitochondria can be evolutionary traced back to prokaryotic cellular systems, most of the mechanisms and components of the ISC system remains highly conserved from bacteria to yeast to humans (Chandramouli et al., 2007; Lill and

Freibert, 2020). Generally, the ISC pathway can be divided into three parts as mentioned below:

i) de novo [2Fe-2S] cluster synthesis on the IscU scaffold protein

The initial *de novo* assembly of [2Fe-2S] onto IscU (scaffold protein) requires a cysteine desulfurase IscS/ Nfs1, that belong to pyridoxal phosphate (PLP) dependent cysteine desulfurase group of family. The cysteine desulfurase activity is responsible for transfer of sulfur from L-cysteine to a conserved cysteine residue of IscS/NFS1 to generate a transient persulfide moiety (-SSH). This transient persulfide is then delivered directly or via sulfur relay to ISC scaffold protein where it can form the persulfide group onto the Scaffold protein. In eukaryotes, the cysteine desulfurase complex within the ISC pathway is constructed of three proteins: NFS1, ISD11, and Acyl Carrier protein 1 (ACP1), where ACP1 and ISD11 stabilize and regulate NFS1 activity **(Figure 1.8)**. The N-terminus in each NFS1 monomer contains a hydrophobic patch that is shrouded by an ISD11 monomer. This masking prevents NFS1 aggregation *in vivo* (Mühlenhoff et al., 2002). Although ISD11 does not play a direct catalytic role, NFS1 will not function in its absence due to NFS1 aggregation (Adam et al., 2006). The binding of NFS1 and Isd11 is regulated by ACP1. Insertion of a particular length of acyl chain by ACP1 protein determines its affinity to form various protein complexes such as Isd11-ACP-NFS1 or Isd11-ACP. This hydrophobic patch responsible for NFS1 aggregation is absent in the prokaryotic orthologue, explaining the absence of the ISD11 and ACP1 accessory proteins in prokaryotes, while highlighting the crucial role of these protein partners in eukaryotic ISC assembly (Hinton et al., 2022).

An iron source is needed for [Fe-S] cluster assembly which is mainly provided from the labile iron pool of the bacterial cytoplasm or mitochondrial matrix (150uM Fe^{2+}) or certain iron donor proteins. Once iron and sulfur are procured from respective donors, the electron transfer system finally assembles [Fe-S] clusters onto the scaffold protein. Ferredoxin with [2Fe-2S] clusters act as an electron donor in case of bacteria while FDX2 (homologue of Ferredoxin) plays the same role for mitochondria. In case of mitochondrial Ferredoxin (FDX2), the electrons are provided by a specific reductase, FDXR which itself gets electrons from NADPH. The significance of scaffold proteins lies in their capability to assemble transient [Fe-S] clusters and deliver it to apo-proteins having high affinity towards [Fe-S] binding rather than their assembly (Braymer et al., 2021).

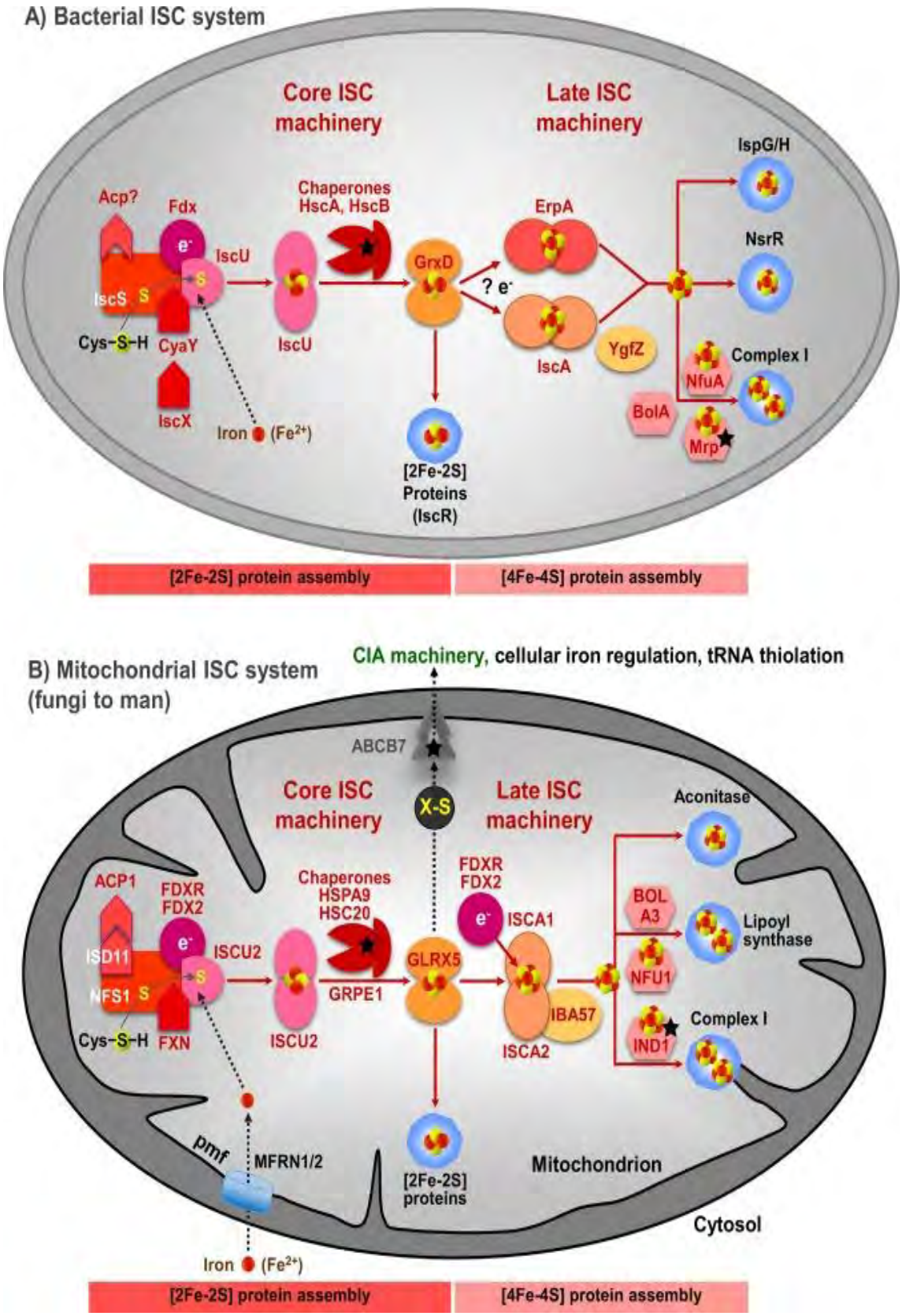

Figure 1.8: Models for the biogenesis of [2Fe-2S] and [4Fe-4S] proteins by the (A) bacterial or (B) mitochondrial ISC systems. (Braymer et al., 2021)

ii) Chaperone-Mediated Trafficking of the [2Fe-2S] Cluster and Its Insertion into Apo-proteins

Once the [2Fe-2S] clusters gets assembled onto the ISC scaffold, they are released and delivered to the downstream ISC pathway components and finally to target apo-proteins. For this purpose, a dedicated chaperone system is present in bacteria which is composed of the Hsp70 chaperone, HscA and its [Fe-S] cluster assembly-specific co-chaperone HscB. The co-chaperone HscB binds to conserved hydrophobic residues of IscU and delivers it to the ATP-bound HscA chaperone **(Figure 1.8)**. This stimulates ATP hydrolysis promoting a conformational change in ISCU, that destabilizes the bound cluster for release. The [2Fe-2S] cluster then moves from IscU to the trafficking protein GrxD, a member of the monothiol glutaredoxins, followed by rapid [2Fe-2S] cluster insertion into the polypeptide chain of target proteins. However, when the grxD was deleted, the effect on *E. coli* cell growth and Fe-S protein activities were found to be mild (Burschel et al., 2019) suggesting that either this transient [Fe-S] cluster binding component may be bypassed efficiently, or some other system, such as the SUF system may take over the maturation process. Thus, to elucidate the precise role of bacterial GrxD in ISC system, further investigation is needed.

In contrast to the bacterial ISC system, in humans, the newly made [2Fe-2S] cluster transfer is accomplished by the coordinated efforts of chaperone proteins, including: "HSCB", "HSPA9", "GRPE1", and "GLRX5". GRPE1 is a nucleotide exchange factor, that promotes the exchange of ATP with ADP on HSPA9 resulting in dissociation of ISCU2. The [Fe-S] cluster is then transferred to glutaredoxin GLRX5 and subsequently to the apo-proteins (Weiler et al., 2020). Thus the chaperone cycle for [2Fe-2S] release and transfer is similar in bacteria and Human with an exception that the ATP-ADP conversion by Hsp70 in human requires a nucleotide exchange factor GRPE1 to recover Hsp70 whereas no GrpE is required in case of bacteria. Further this Grx5-[2Fe-2S] quickly delivers cluster to [2Fe-2S] apo-proteins without any assistance from ISC pathway machinery (Braymer et al., 2021).

iii) generation of [4Fe-4S] clusters followed by insertion into target apo-proteins

The third step involves the synthesis of [4Fe-4S] clusters, their trafficking to targeting proteins, and finally their insertion into recipient apo-proteins. Various trafficking/ carrier and insertion factors plays important role in case of bacterial late ISC machinery,

which includes IscA, ErpA, YgfZ, BolA, NfuA, and Mrp. Chemical reconstitution experiments for NfuA and A-type scaffold proteins such as IscA and ErpA have shown their involvement in both [4Fe-4S] cluster assembly and transfer reactions. However, the exact mechanism of [4Fe-4S] formation and delivery by these proteins remains to be explored.

Reports in human, yeast and *Trypanosoma* have shown involvement of ISCA1-ISCA2-IBA57 proteins in [4Fe-4S] cluster biogenesis. Both ISCA proteins interact with each other, and ISCA2 preferentially binds to IBA57. Together, these three ISC proteins are responsible for the generation of virtually all mitochondrial [4Fe-4S] proteins. It is much likely that the formation of [4Fe-4S] clusters onto these A-type proteins is mediated by reductive coupling of [2Fe-2S] by GrxD/GRX5, which further requires electron transport by the core ISC machinery components NADPH- FDXR-FDX2.

In addition to these proteins, there are certain target factors such as NFU1, IND1 and BOLA3, which are responsible for [4Fe-4S] clusters delivery to target apo-proteins. There are various complex Fe-S proteins in mitochondria such as respiratory complex I & II, lipoyl synthase and aconitase that needs these targeting factors for their maturation. NFU1 and BOLA3 are shown to be involved in maturation of aconitase and Lipoyl synthase whereas IND1, a P-loop NTPase delivers clusters to Complex I of mitochondria (Braymer et al., 2021) **(Figure 1.8)**.

1.6.2 NIF Pathway for [Fe-S] cluster assembly

The NIF (nitrogen fixation) system is specifically involved in the assembly of the complex Fe-S protein Nitrogenase needed for nitrogen assimilation, and thus is predominantly found in the azototrophic (i.e. nitrogen-fixing) bacteria. It consists of two main components: cysteine desulfurase NifS, which provides sulfur for [Fe-S] cluster formation, and a scaffold protein NifU onto which [Fe-S] assembly occurs (Bandyopadhyay et al., 2008). NifS is a pyridoxal phosphate-dependent cysteine desulfurase and belongs to the class I desulfurases, like IscS or NFS1 of the ISC system (Braymer et al.,2021). On the other hand, NifU is a modular protein with multiple functionalities. It can be divided into three exclusive functional domains, N-terminal, Central, and C-terminal **(Figure 1.9)**. The N-terminal domain of NifU relates to the ISU2 protein from the ISC pathway, which acts as a scaffold protein onto which [Fe-

S] cluster assembly occurs. Initially a [2Fe-2S] cluster is assembled on it, which gets converted over time into [4Fe-4S] cluster via reductive coupling. The Central domain is a potential ferredoxin-like domain-containing protein that functions as an electron transfer system via a non-transferrable [2Fe-2S] cluster. The C-terminal domain acts as a [4Fe-4S] cluster targeting protein and binds to a labile [4Fe-4S] cluster (Braymer et al., 2021).

As mentioned, the NifU-N domain assembled [Fe-S] cluster is mainly responsible for the maturation of the nitrogenase enzyme. The nitrogenase protein complex (~300kDa) consists of dinitrogen reductase (the Fe Protein [NifH]) and dinitrogenase (the MoFe protein [NifDK]). The NifH is a [4Fe-4S] cluster containing homodimer whereas NifDK consists of two heterodimers which coordinates eight Fe ions and two FeMo cofactors. In contrast to the nitrogenase activity of N terminal, the NifU-C domain cluster has a role in [Fe-S] cluster transfer to other target Apo-proteins. Other accessory protein such as Grx5NIF and IscANIF are also encoded by nif operons and help in targeting assembled [Fe-S] clusters to apo-proteins. Recent reports have also suggested the significance of NIF pathway and its essentiality in non-nitrogen-fixing bacteria, i.e., *Helicobacter pylori,* where mutations in NIF components NifS and NifU rendered the bacteria non-viable (Olson et al., 2001; Braymer et al., 2021).

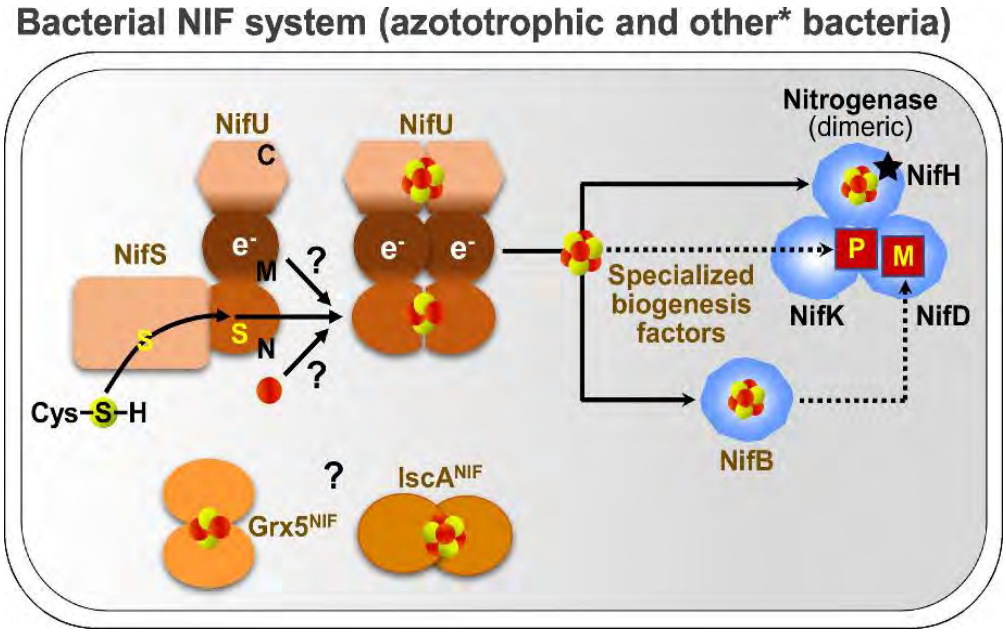

Figure 1.9: Model for [4Fe-4S] cluster synthesis by the NIF system in Azototrophic bacteria (Braymer et al., 2021)

1.6.3 SUF Pathway for [Fe-S] cluster assembly

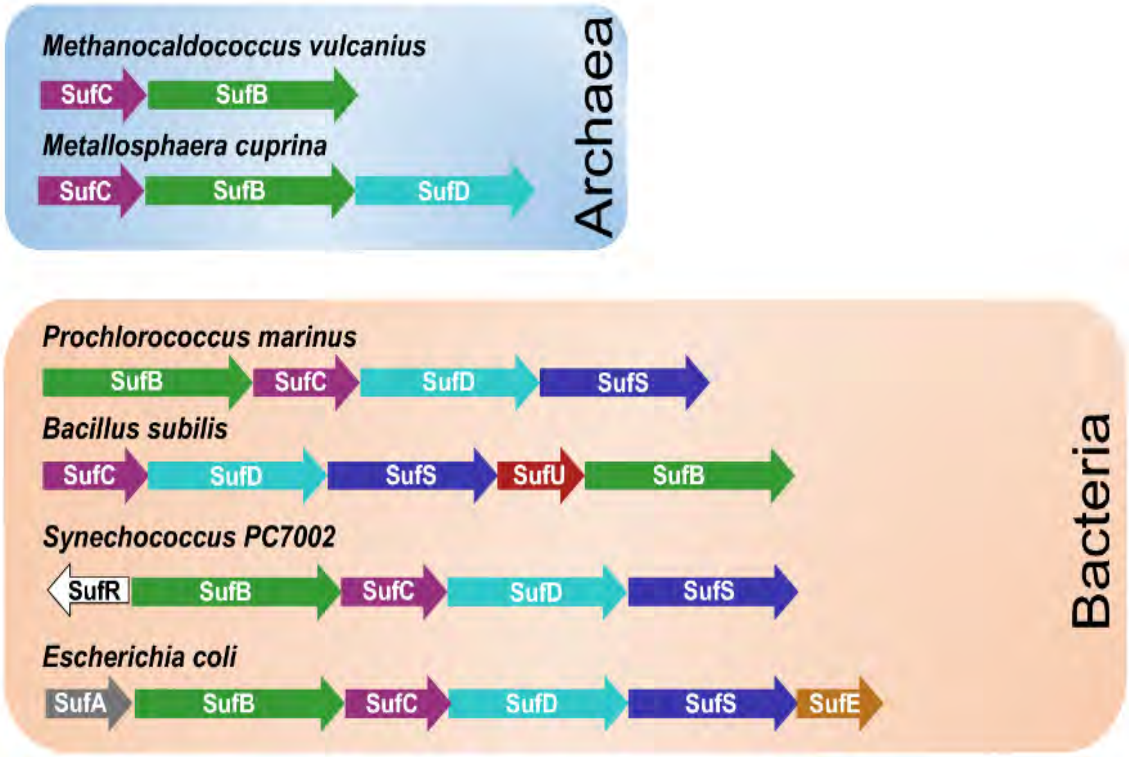

Figure 1.10: *suf* operons from Archaea and Bacteria (Pérard & deChoudens, 2018)

The SUF system is present in all the three kingdoms of life and is particularly well-adapted for [Fe-S] cluster synthesis and apo-protein maturation under aerobic and iron-limiting conditions. The *E. coli* SUF system is encoded by the sufABCDSE gene cluster (operon) in the genome **(Figure 1.10)**, which was observed to be upregulated upon inducing mutations in ISC pathway genes (Takahashi and Tokumoto, 2002). Like other [Fe-S] cluster biogenesis pathways, the SUF system also possesses a cysteine desulfurase SufS, but it belongs to class II cysteine desulfurase and has a distinct mechanism from class I desulfurases including IscS and NFS1 (Outten et al., 2004). In early studies, the poor desulfurase activity of SufS confused researchers (Mihara and Esaki, 2002), but later studies in the SUF pathway revealed another member, SufE, that binds to SufS and increases its activity to a level comparable to IscS. Thus, SufSE together can be considered as a true desulfurase rather than SufS alone. SufS is known to first shuttle the persulfide to SufE, which is then passed on to the [Fe-S] cluster scaffold protein **(Figure 1.11)**.

The scaffold complex in SUF System is distinct from the ISC system, where it exists as a tetrameric protein complex $SufB_2C_2$/ $SufBC_2D$ composed of the [Fe-S] cluster assembling protein SufB, the ABC-type ATPase SufC and/or the SufB homolog SufD. Mostly ABC transporters resides in membrane, but SufC localizes to cytoplasm, raising an important query regarding ATPase activity of this complex (Kitaoka et al., 2006). Different models have been proposed for the activity of SufC for regulating conformational changes in the [Fe-S] scaffold. One model proposes that ATP hydrolysis opens the SufB(D) dimer interface for [Fe-S] cluster synthesis, while the other proposes that ATP hydrolysis drives the release of the [Fe-S] cluster, similar to the chaperone function in the ISC system. Genetic experiments have also suggested that SufD may facilitate the delivery of iron to the [Fe-S] cluster assembly site. Reducing equivalents needed for cluster maturation onto SUF scaffold complex is unknown. However, $FADH_2$ or the NADPH-dependent thioredoxin have been postulated as potential electron sources for the SUF system. Both [2Fe-2S] or [4Fe-4S] clusters can get assembled onto SufB or SufBCD complexes *in vitro* but *in vivo* [Fe-S] nuclearities of these clusters needs to be elucidated.

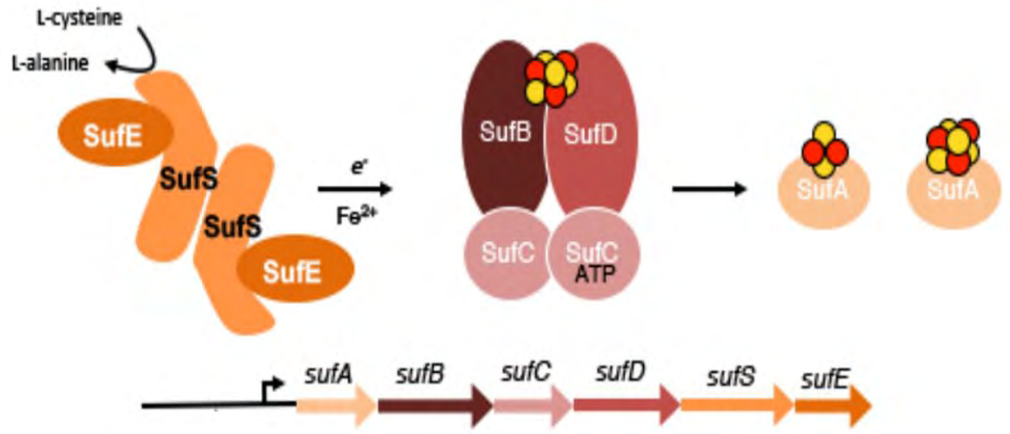

Figure 1.11: A model for [Fe-S] cluster assembly in *E. coli* by the SUF machinery (Leimkühler, 2020)

The newly assembled cluster on the scaffold protein further gets transferred to the A-type trafficking protein, SufA, which then delivers these clusters to the apo-proteins. SufA has been spectroscopically characterized as a [2Fe-2S] cluster binding protein but *E. coli* SufA can interact with the non-SUF targeting factors NfuA and the additional A-type trafficking protein ErpA, both of which bind [4Fe-4S] clusters. The [Fe-S] cluster trafficking activity of SufA has been reported not essential in *E. coli* due to the

functional overlap with the other A-type proteins IscA and ErpA, but most likely it plays a critical role under oxidative stress conditions, e.g., H_2O_2 exposure (Zheng et al., 2001). NfuA, a fusion protein with degenerate A-type module and a C-terminal NFU1 domain, has also been observed to receive [Fe-S] clusters from the $SufBC_2D$ complex.

1.6.4 CIA pathway for [Fe-S] cluster assembly

Cytosolic iron sulfur cluster assembly pathway (CIA) is responsible for providing [Fe-S] clusters to cytosolic and nuclear proteins. It is present in most eukaryotes such as *Arabidopsis thaliana*, *Saccharomyces cerevisiae*, *Blastocystis* and humans. Due to the absence of its own cysteine desulfurase, the CIA pathway is believed to be dependent on mitochondrial ISC pathway for sulfur moiety to synthesize cytoplasmic [Fe-S] clusters (Muhlenhoff et al., 2004). The pathway has been extensively studied in yeast where eight proteins were identified to be involved in the biogenesis of [Fe-S] clusters- Nbp35, Nar1, Cfd1, Tah18, Dre2, Cia1, Cia2 and MMS19 (Netz et al., 2014) as shown in **Figure 1.12**. Alongside the regular CIA pathway components, Atm1 (ABCB6 mitochondrial transporter) dependent procurement of S_{int} (intermediate Sulfur moiety) and [Fe-S] $_{int}$ via ISC pathway plays indispensable role in CIA pathway functionality (Pandey et al., 2019).

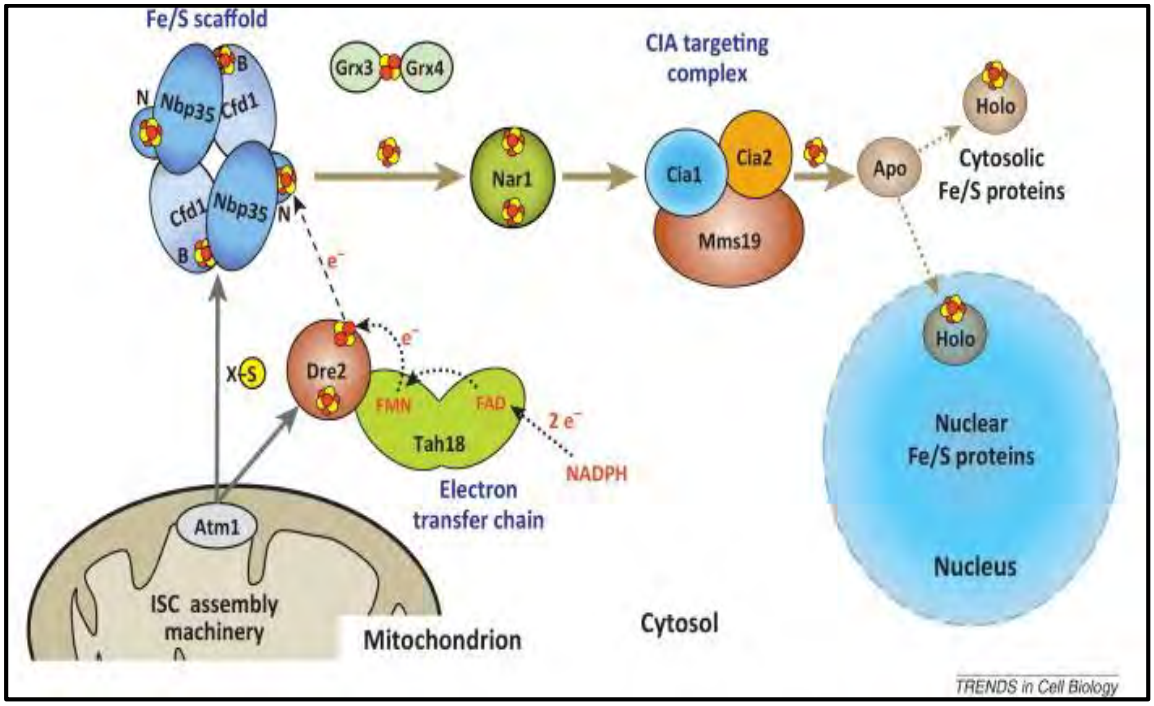

Figure 1.12: Model for maturation of cytosolic and nuclear Fe-S proteins in yeast (Netz et al, 2014)

Similar to other [Fe-S] cluster biogenesis pathways, the CIA pathway also consists of a scaffold complex consisting of Nbp35/Cfd1 and requires transfer of electrons for maturation of clusters similar to Ferredoxin. Electron transfer system of CIA system consists of NADPH, Tah18 (Diflavin Protein) and Dre2 (homolog of human CIAPIN1 protein). Later the transient [4Fe-4S] cluster is recruited onto Fe- hydrogenase like protein, Nar1 which acts as a transfer protein and delivers the assembled cluster to CIA targeting complex (CTC). CTC is the late acting component of CIA pathway consisting of Cia1, Cia2 and MMS19 proteins, responsible for final delivery of [4Fe-4S] clusters to cytosolic and nuclear Fe-S proteins. The biogenesis also requires monothiol glutaredoxins Grx3/Grx4 (GRX3 in human) for trafficking of [Fe-S] clusters (Netz et al, 2014) **(Figure 1.12)**.

1.6.4.1 CIA Scaffold: a hetero-tetrameric complex of Cfd1–Nbp35

The function of any scaffold protein in [Fe-S] biogenesis pathway is to assemble mature [Fe-S] clusters onto it. In humans and yeast, Nbp35-Cfd1 forms a hetero-tetrameric complex that facilitates [4Fe-4S] maturation through electron transfer complex (Dre2-Tah18). However, in species where Cfd1 is missing, the scaffolding function is enabled by Nbp35 homodimer complex. It is reported that Nbp35 is found ubiquitously in all lineages, but Cfd1 is mainly present in *Ophistokonta, Amoebozoa, Cryptista, Glaucophypta (Archaeplastida), Metamonada,* and *Discoba* but absent in *Chloroplastida* and *Rhodophyta (Archaeplastida)*, *SAR* (*Alveolata* group that consists of *Apicomplexa*), and *Haptista* (Ciofi-Baffoni and Andreini, 2022).

Nbp35 and Cfd1 proteins are homologous proteins involved in CIA scaffolding functions and both these proteins belongs to deviant Walker A P-loop NTPases, a branch of SIMIBI (signal recognition particle, Mind and BioD) NTPases family. This is one of the interesting features of CIA pathway scaffold because most of the U-type scaffolds in ISC and SUF pathways do not have ATPase activity. Nbp35 dimer and Nbp35-Cfd1 complexes showed ATPase activity while Cfd1 dimer doesn't have an ATPase activity of its own. A conformational shift in Cfd1 is required for the ATPase activity which is mainly induced upon Nbp35 binding to Cfd1 (Anwar et al., 2014; Grossman et al., 2019)**.**

The domain organization for Cfd1 and Nbp35 includes common signature motif "CXXC" at C-terminus located at the interface between Nbp35 and Cfd1, that is involved in binding [4Fe-4S] cluster. In addition, the N-terminal of Nbp35 protein sequence has an additional [4Fe-4S] binding domain which is absent in Cfd1 **(Figure 1.13)**. Both clusters are involved in CIA pathway functionality, however, their roles remain to be investigated (Netz et al., 2014, 2016; Tsaousis et al., 2014). The function of Nbp35-Cfd1 is to assemble [4Fe-4S] clusters onto it by using basic cluster building blocks. According to recent reports, S_{int} (intermediate Sulfur moiety) and $[Fe\text{-}S]_{int}$ are derived via mitochondrial Atm1 transporter and further gets incorporated into t-RNA for thiolation and Nbp35-Cfd1 scaffolding functions respectively. Maturation of $[Fe\text{-}S]_{int}$ onto Nbp35-Cfd1 scaffold requires reducing equivalents from Dre2-Tah18 electron transfer complex that further matures $[Fe\text{-}S]_{int}$ to [4Fe-4S] that can be further incorporated into downstream CIA pathway components (Grossman et al., 2019).

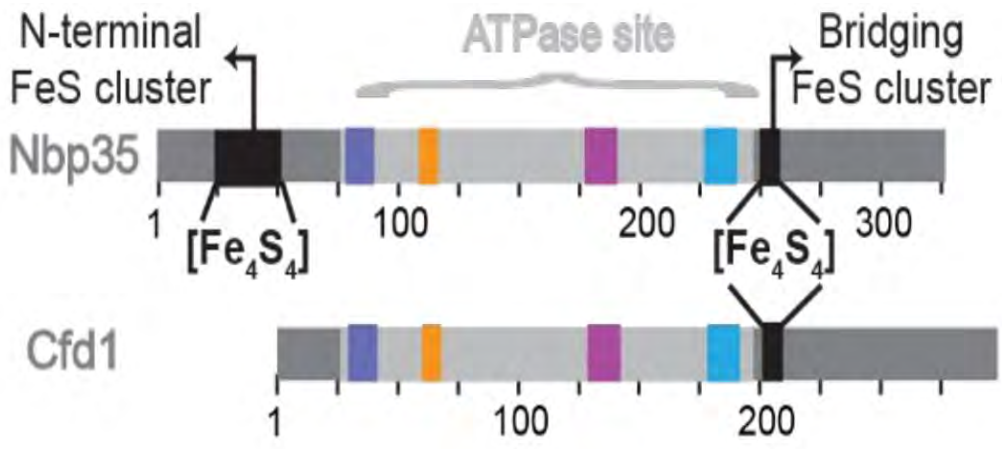

Figure 1.13: The domains and motifs of the CIA scaffold (Grossman et al., 2019) Primary structures of Nbp35 and Cfd1 highlighting the relative locations of their Fe-S binding sites (black) and the SIMIBI NTPase motifs: Walker A (purple), Switch I (orange), Switch II (magenta), and A-loop (cyan)

In addition to Cfd1 and Nbp35, there are other P-loop NTPases such as HCF101, Ind1, and AbpC. Out of these, HCF101 is distributed in plastids of photosynthetic eukaryotes mainly involved in maintenance of [Fe-S] assembly in photosystem I. One of its paralogs is also present in mitochondria of some phyla such as *Cryptista, Haptista,* and *SAR*. However, in Apicomplexans (*T. gondii*) HCF101 is reported to be localized at cytoplasm and Nbp35 in mitochondria (Pyrih et al., 2021).

1.6.4.2 CIA electron transfer complex: a complex of Dre2–Tah18

Dre2, a homolog of human Anamorsin (Banci et al., 2011) is an Fe-S protein and one of the early components of CIA pathway, acting upstream to Nbp35. It is also termed as CIAPIN1 (Cytokine Induced Apoptosis Inhibitor 1) protein due to its role in cytokine-based anti-apoptosis mechanism (Shibayama H et. al. 2004). In yeast, the C-terminal CIAPIN 1 domain of Dre2 consists of two signature cysteine motifs: Motif I and Motif II (residues 252–325), that are involved in [Fe-S] coordination of [2Fe-2S] and [4Fe-4S] clusters respectively. However, the stoichiometry of types of clusters present on Motif II remains a bit controversial given their studies in yeast Dre2 and human Anamorsin which suggested presence of [4Fe-4S] clusters in yeast and [2Fe-2S] clusters in humans (Netz et al., 2016; Matteucci et al., 2021).

The C-terminal CIAPIN1 also shows interaction with Diflavin reductase, TAH18/NdorI possessing two prosthetic groups FMN and FAD at their respective binding domains, which then transfers electrons to [2Fe-2S] of CIAPIN1 domain via cytosolic NADPH (Netz et al., 2010). *In vitro* and *in vivo* analysis have proved stable complex formation of Dre2-TAH18, which is reported to be involved in cell death regulation mechanism apart from its canonical role in CIA pathway. In yeast, Dre2-TAH18 complex has been shown to be essential for its viability. Its successful replacement in yeast with its Human ortholog; Anamorsin-NdorI, suggests evolutionary conservation of this electron transfer complex (Netz et al., 2010).

For the diflavin reductase group of enzymes like Tah18, the transfer of electrons from $FMNH_2$ to substrate requires a conformational shift from close to open. NdorI in closed conformation receives electron from NADPH and generates hydroquinone state of FMN. This binding of NADPH increases the population of open NdorI species, which exposes to the solvent the FMN moiety and allows the formation of a transient interaction with the [2Fe-2S] cluster region of anamorsin located in the CIAPIN1 domain. The latter interaction allows an efficient transfer of one electron from the hydroquinone state of FMN to the [2Fe-2S] cluster. This type of Dissociative electron transfer of Anamorsin-NdorI justifies their role in regulation of cellular death/survival, emphasizing the requirement of constant interaction between these two proteins to maintain continuous flow of electrons. Any disturbance in this electron flow might lead to disruption of essential biological processes (Banci et al., 2013) **(Figure 1.14).**

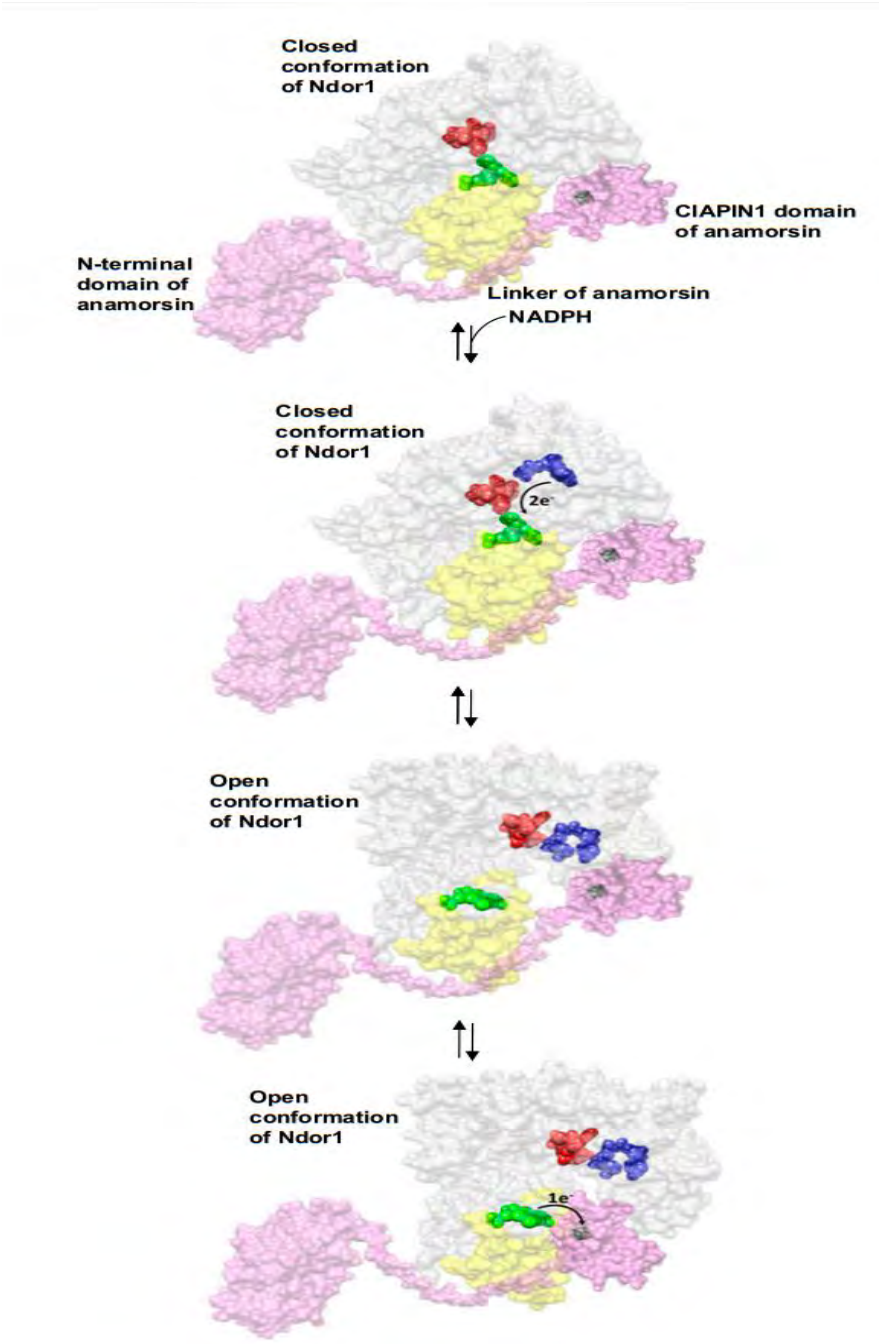

Figure 1.14: Model of the electron transfer process between Ndor1 and Anamorsin (Banci et al., 2013)

1.6.4.3 Nar1: an [FeFe]-hydrogenase-like protein

Another component of CIA pathway is Nar1 which is a transfer protein delivering the assembled [4Fe-4S] clusters to late acting CIA pathway components i.e., CIA targeting complex (CTC) consisting of Cia1, Cia2 and MMS19. Domain analysis of Nar1 revealed an [FeFe]- hydrogenase-like protein containing domain; however, it does not possess any hydrogenase like activity (Tsaousis et al., 2014). Nar1 protein consists of

four cysteine residues for [4Fe-4S] cluster binding towards the N-terminal domain, whereas another four cysteine are distributed across central and C-terminal part of the protein. Depletion of Nar1 protein resulted in decreased activity of CIA dependent Fe-S protein; Isopropylmalate isomerase (Leu1) in yeast, suggesting essentiality of functional Nar1 in CIA pathway (Braymer et al., 2021).

Earlier studies suggest that [Fe-S] clusters are important for Nar1 to perform its downstream CIA functions. For these [Fe-S] clusters, Nar1 depends on early acting CIA components such as Dre2 and TAH18. In humans, it is reported that Cfd1 shows interaction with Nar1 and is involved in [4Fe-4S] maturation on Nar1. Thus, it could be possible that Nar1 might also be acting as an intermediate protein in between CIA scaffold protein and Cia targeting complex (Netz et al., 2014; 2016).

1.6.4.4 CIA Targeting Complex (CTC): Cia1, Cia2 and MMS19

CIA scaffold protein assembles [4Fe-4S] clusters, that are delivered to CTC complex (Cia1, Cia2 and Met18 in yeast and CIAO1, CIAO2B and MMS19 in human) through Nar1 (CIAO3 in human), an intermediate protein. CTC further delivers these clusters to client cytosolic and nuclear Fe-S proteins through direct physical interactions. CIAO1 has seven bladed WD40 repeats with beta-propeller domain and may serve as a docking site for Nar1 and other CIA pathway proteins like CIAO2B and MMS19. CIAO2B is one of the smallest proteins of CTC that possess a reactive cysteine residue (Cys 93 in human and Cys 161 in yeast) with possible role in [4Fe-4S] cluster transfer. MMS19 is an adapter protein that is involved with the client apo-protein recognition such as DNA repair and replication proteins. Depletion of MMS19 showed reduction in [4Fe-4S] cluster incorporation in DNA metabolism proteins leading to DNA damage.

The low-resolution cryo-EM analysis of CTC complexed with Fe-S proteins (DNA2 and primase) revealed that CTC consists of two high affinity binding sites for client apo-protein recognition. The first high affinity binding site resides in CIAO1 which generally recognizes most of the client apo-proteins whereas the second binding site is present in MMS19 that identifies various DNA metabolism proteins. Various CTC combinations exists in humans such as i) CIAO1and CIAO2B for GPAT and Viperin maturation, ii) CIAO1 and CIAO2A for IRP1 maturation iii) CIAO1, CIAO2B, MMS19 and adapter complex [ORAOV1 and YAE1] for Rli1 (ABCE1) maturation etc.

These different combinations of CTCs exhibit different binding preferences and affinity for client apo-proteins (Braymer et al., 2021). Conformational flexibility of MMS19 also plays an essential role in accommodating client apo-proteins since CIAO1-CIAO2B complex shows some rigidity. Other than CTCs, CIAO3 (Nar1) might be required for bridging CIAO2B to client apo-proteins while transferring these [Fe-S] clusters (Kassube and Thomä, 2020; Braymer et al., 2021) **(Figure 1.15)**.

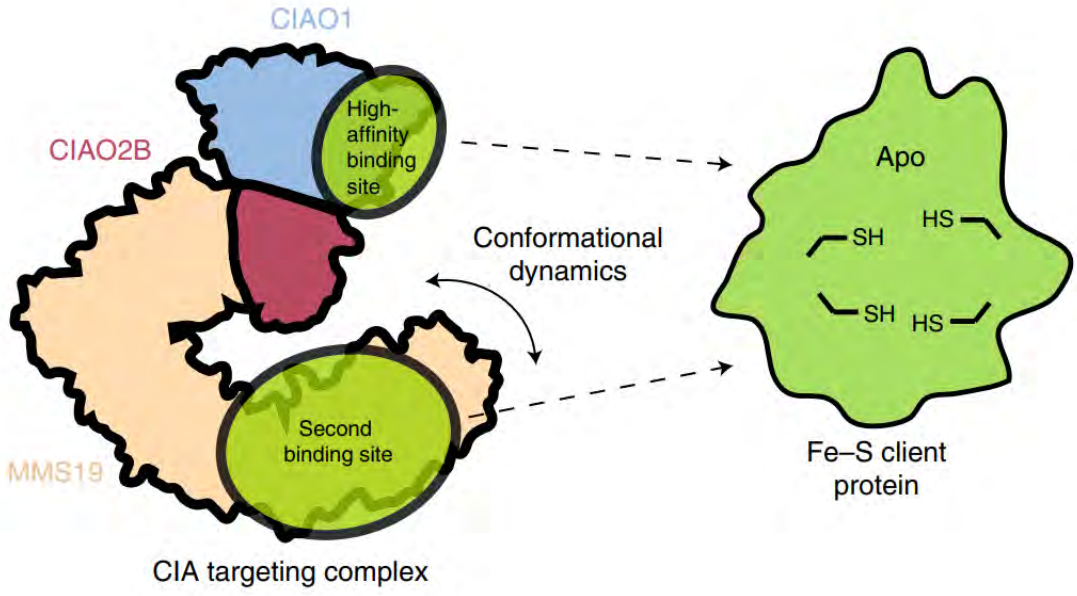

Figure 1.15: Proposed mechanism of Fe–S client protein recruitment by the CTC complex (Kassube and Thomä, 2020)

1.6.4.5 Grx3/Grx4

Recent reports suggest involvement of monothiol glutaredoxins such as Grx3 and Grx4 in maintaining iron homeostasis in CIA pathway. Cytoplasmic monothiol glutaredoxins GRX3 (grx3 in yeast) has been reported to be involved in [2Fe-2S] cluster transfer to the C-terminal CIAPIN1 domain of human Anamorsin, where N-terminal GRX3 plays essential role in molecular recognition and cluster transfer. Deletion of GRX3 results in non-functional Anamorsin, one of the early acting CIA pathway components (Frey et al., 2016). Other than Anamorsin/Dre2, cytosolic glutaredoxins also interacts with CTCs, Cia1 (CIAO1 in human), Mms19, and Cia2, but the biochemical mechanism behind the same remains unknown (Berndt et al., 2021). Depletion of monothiol glutaredoxins leads to deregulated cellular iron uptake, resulting in impairment of cytosolic Fe-S proteins. Along with Fe-S biogenesis pathway disturbances, glutaredoxin depletion leads to iron overload and huge cellular GSH increase

suggesting importance of Glutaredoxin mediated iron trafficking (Lill and Freibert, 2020)

1.7 [Fe-S] biogenesis pathways in *Plasmodium*

Of all the above mentioned [Fe-S] biogenesis pathways, majority of the components of the ISC and SUF pathway have been studied in detail from at least one of the *Plasmodium* species, suggesting their functionality in *Plasmodium*. NFU, one of the components of NIF pathway has also been characterized for its dispensability in *P. berghei*. Very recently, CIA pathway components have also been identified from *Plasmodium* using bioinformatics tools for evolutionary studies, indicating presence of cytosolic [Fe-S] biogenesis machinery in the parasite (Tsaousis et al., 2014; Ke and Mather, 2017). However, many of these [Fe-S] cluster biogenesis components especially related to CIA pathway and few components from other three pathways still need to be detailed from the parasite.

1.7.1 SUF Pathway in Plasmodium

In *Plasmodium*, the SUF pathway is functional inside the plastid like organelle, Apicoplast and provides [Fe-S] clusters to the proteins present in the organelle. Unlike the *E. coli* operon, SUF pathway genes in *Plasmodium* are present on different chromosomes. Majority of the genes of SUF pathway are nuclear encoded with the exception of SufB which has an Apicoplast origin. In *Plasmodium*, The SUF pathway starts with SufS, a PLP-dependent cysteine desulfurase that converts cysteine to alanine to generate persulfide moiety. However, SufS activity requires SufE for its heightened cysteine desulfurase activity, where SufE has been reported to increase desulfurase activity by many folds (Charan et al., 2014; Pala et al., 2019). Mutation studies in *Pf*SufS suggested that Cys497Ala mutant lacks cysteine desulfurase activity indicating Cys497 as an essential residue for the same (Charan et al., 2014). After sulfur generation, SufE quickly transfers sulfur to the scaffold protein. In *Plasmodium*, two hypotheses have been given for the scaffold protein. According to the first hypothesis, in *P. falciparum*, the SufBCD complex is shown to function as a scaffold protein in *in vivo* cross-linking assays. *Pf*SufC, a member of the ABC transporters exhibited a characteristic ABC ATPase motif, but without a transmembrane domain (Koenderink et al., 2010; Kumar et al., 2011). Hydrodynamic characterization studies reported the

ABC ATPase motifs of *Pf*SufC in close proximity to the *Pf*SufC–*Pf*SufD interaction pocket, suggesting an increase in ATPase activity of *Pf*SufC due to interaction with *Pf*SufD (Petrovic et al., 2008). Following the experimental validation of SufBCD interaction, Charan et al. further reported a stoichiometry of 1:2:1 for the *Pf*SufB: *Pf*SufC: *Pf*SufD complex, to maintain the correct orientation of the proposed [4Fe–4S] binding site for [Fe–S] cluster assembly (Charan et al., 2017).

Another hypothesis, based on a *P. vivax* study, indicated [Fe–S] cluster coordination on an A-type carrier protein, SufA, acting as a scaffold protein (Pala et al., 2016). In *E. coli*, along with SufBCD, another protein, SufA, forms [Fe–S] clusters *in vitro* (Gupta et al., 2009). Based on this, Pala et al. through *in vitro* reconstitution assays, confirmed the assembly of [4Fe–4S] clusters on SufA protein, suggesting its role as a scaffold and a carrier protein for the assembly and transfer of [Fe–S] clusters in *P. vivax* (Pala et al., 2016). The *in-silico* interaction between *Pv*SufA and *Pv*SufB suggested conjunction of both these for the assembly and transfer of the [Fe–S] clusters in *Plasmodium*.

The essentiality of SUF pathway for Apicoplast maintenance was demonstrated by Gisselberg et al. where by generating dominant negative mutant of *P. falciparum* SufC, they showed that the mutant was toxic to the cell, but viable in the presence of IPP, suggesting the requirement of [Fe-S] clusters for proper functioning of isoprenoids biosynthesis pathway (Gisselberg et al., 2013). Similarly, the pivotal role of SufS for the development of oocysts in mosquito stages was also reported by Charan et al., 2017, by knocking out SufS gene and demonstrating that the parasite lacking SufS was unable to infect and grow in a mammalian host (Charan et al., 2017). The indispensability of SufC and SufD has also been reported for *P. berghei* blood stage infection (Haussig et al., 2014).

1.7.2 ISC machinery in Plasmodium

Majority of the components of the *P. falciparum* ISC pathway has been identified only recently. The ISC pathway proteins, *Pf*IscS, *Pf*Isd11, *Pf*IscU, *Pf*IscA1, and *Pf*IscA2, have been shown to localize to the mitochondria, suggesting mitochondria as the functional site for the ISC pathway in *Plasmodium* as well (Gisselberg et al., 2013; Sadik et al., 2021). As reported from many organisms, including bacteria and humans, the ISC pathway remains conserved in *Plasmodium*, except the two unusual findings,

as reported by Sadik et al, 2021: 1) In *P. falciparum*, *Pf*IscU scaffold can directly assemble and transfer [4Fe-4S] clusters to apo-proteins (AcnB) in a more efficient manner when compared with various other secondary carrier proteins such as *Pf*IscA2 and 2) The organization of the entire ISC scaffold complex in *Plasmodium* is maintained as *Pf*IscS tetramer instead of IscS/NFS homodimers, as mentioned in *E. coli* and humans (Sadik et al., 2021).

Other nuclear-encoded ISC pathway components such as A-type assembly proteins (*Pf*IscA1 and *Pf*IscA2) have also been explored by Sadik et al., 2021. Spectral studies demonstrated that only *Pf*IscU and *Pf*IscA2 were able to transfer [4Fe–4S] cluster to the target apo-protein while *Pf*IscA1 and *Pf*NifU-like protein had very low or insignificant [Fe–S]-carrier activity. It was observed that the *Pf*IscU scaffold assemble and transfer [4Fe-4S] clusters to apoproteins (AcnB) more efficiently than any other secondary carrier proteins such as *Pf*IscA2. *Pf*IscA1 was found to primarily bind iron, suggesting its potential role as a Fe^{2+} carrier/donor. Other than these critical findings, the homologs of ISC pathways accessory proteins such as ferredoxin, ferredoxin reductase, glutaredoxin-like protein, Bol, Hsp70, and Hsp20 were also identified from *P. falciparum* (Sadik et al., 2021).

1.7.3 Other [Fe-S] cluster biogenesis proteins from Plasmodium

In addition to the proteins involved in SUF and ISC pathways, few more proteins have been identified and characterized from *Plasmodium*. One such [Fe-S] protein is *Pb*NFUapi which showed a NIFU-like domain, suggesting its potential as a scaffold protein. The NFUapi protein has been confirmed to be localized to Apicoplast in both *Toxoplasma gondii* (TGME49_021920) and *Plasmodium*. It was discovered that loss-of-function mutants for *Pb*NFUapi were easily generated *in vivo,* suggesting its dispensability for the parasite. According to a thorough examination of life cycle progression, *Pb*NFUapi is reported not necessary for any stage of host switching, stage conversion, or colonization of new host cells. It was suggested that NFUapi might enhance the release of merozoites via merosomes from the hepatocyte cell line. Furthermore, this data suggested the increased expression and possible utilization *of Plasmodium yoelii* NFUapi in late liver stages (Haussig et al., 2013).

Furthermore, an HCF101-like protein (P-loop NTPases) implicated in the assembly of [4Fe–4S] proteins in plant plastids have been reported to be universally present in the plastids, even in non-photosynthetic organisms – like apicomplexans, including *Plasmodium*, *T. gondii*, and *Cryptosporidium parvum*; however, their role in [Fe–S] cluster assembly in these organisms is yet to be elucidated (Schwenkert et al., 2010).

1.8 Gap in existing Research

As the majority of the proteome of *Plasmodium* consists of hypothetical/putative proteins, it is imperative to understand the role of these proteins, especially the ones involved in the major metabolic pathways of the parasite, and to elaborate their function experimentally in order to identify their importance in *Plasmodium* biology to design novel intervention strategies. One such less studied process is the [Fe-S] cluster biogenesis mechanism in *Plasmodium*, which is important for its survival and may be utilized for the development of new antimalarial.

In *Plasmodium*, while there are ample reports on the two major [Fe-S] cluster biogenesis pathways; the SUF and ISC pathways, the components of the CIA pathway have not been investigated till date. Recently, a few homologs of CIA pathway proteins have been identified from Apicomplexans including *Plasmodium* (Tsaousis et al.,2014; Ke and Mather, 2017), but these proteins still remain functionally uncharacterized from these parasites. Hence, further investigations are required to identify all CIA pathway genes to get a complete picture of this pathway as well as the major components of the pathway for their functional role in the life cycle of the parasite.

Reports have suggested interdependence of the CIA pathway on the mitochondrial ISC pathway, which can also be explored and further proven experimentally. While recently, the core components of the ISC pathway have been delineated from *P. falciparum* (Sadik et al., 2021), there are no reports on this pathway from another major parasite species, *Plasmodium vivax*, and thus it needs to be investigated. Given the metamorphic nature of the ISC scaffold protein, which marks a starting point for this pathway, it is also important to reveal the conformational effect of various ligands on the scaffold as well.

1.9 Research Objectives

Keeping the above gaps in mind, to explore more into [Fe-S] cluster biogenesis pathways, the following objectives were proposed –

- *In silico* analysis of the protein(s) involved in cytoplasmic and mitochondrial [Fe-S] cluster biogenesis pathways from *Plasmodium vivax*.
- Functional characterization of the candidate [Fe-S] cluster biogenesis protein(s) from *Plasmodium vivax* using molecular and biochemical approaches.
- Identification of interacting partners/ ligands of the characterized [Fe-S] cluster biogenesis proteins

Chapter 2

Materials and Methods

Materials and Methods

2.1 Identification of genes involved in Cytosolic and mitochondrial [Fe-S] cluster assembly pathway from *Plasmodium*

[Fe-S] cluster biogenesis pathways are crucial for providing [Fe-S] clusters to proteins involved in various housekeeping and metabolic pathways in all domains of life. While these pathways have been studied extensively from higher eukaryotes such as yeast, human and *Arabidopsis*, studies on these pathways for most of the apicomplexans including *Plasmodium* have been initiated only in the last decade. For long it was believed that *Plasmodium* harbours only two [Fe-S] cluster biogenesis pathways: the SUF pathway functional in the apicoplast and the ISC pathway residing in the mitochondria. Among these, the components of the SUF pathway have been detailed and characterized from both *P. falciparum* and *P. vivax* (Pala et al., 2016; Charan et al., 2017), but the proteins associated with ISC pathway were only recently identified and characterized (Sadik et al., 2021). The first report on CIA pathway homologs in *Plasmodium* was by Tsaousis et al., 2014, who identified few of the proteins involved in the pathway for their evolutionary significance suggesting a functional CIA pathway in the parasite (Tsaousis et al., 2014). Thus to further understand the [Fe-S] cluster assembly in the malaria parasite, in the present study, the proteins hypothesized to be functional in the CIA and ISC pathway were identified from the PlasmoDB database (Aurrecoechea et al., 2009) based on the presence of conserved domains and signature motifs as predicted by Conserved Domain Search tool from NCBI (Marchler-Bauer et al., 2015) and PROSITE from ExPASy (Sigrist et al., 2002), respectively.

The identified proteins were further subjected to various *in silico* targeting software's, to identify their functional site as mitochondria, apicoplast or cytosol. PlasmoAP; an algorithm that uses amino-acid frequency and distribution to identify putative Apicoplast-targeting peptides, was used to determine the Apicoplast transit peptide (Foth et al., 2003). We also checked for mitochondrial targeting using servers like MitoProtII (Claros and Vincens, 1996), which calculates the N-terminal protein region that can support a mitochondrial targeting sequence and the cleavage site. To identify if any of these proteins are localized to nucleus, we used NLS mapper that identifies nuclear localization signals in the sequences (Kosugi et al., 2009). Shortlisted proteins

were also subjected to STRING database to identify their networking partner proteins (Szklarczyk et al., 2016).

2.2 Study site and Malaria infected blood sample collection

P. vivax infected patient's blood samples (3-6 ml) were collected by trained clinicians at P. B. M. and associated group of Hospitals, Bikaner, Rajasthan, India. They were preserved either in acid citrate dextrose (ACD) anticoagulant for DNA isolation or in Tri-Reagent for RNA isolation after separating RBCs from Peripheral Blood Mononuclear Cells (PBMCs). For RBC separation, the parasite infected blood was subjected immediately to density gradient centrifugation using Histopaque 1077 (Sigma Aldrich, USA). The RBC pellet was washed with phosphate buffered saline (1X PBS), lysed using Tri-Reagent (Sigma Aldrich, USA) and preserved in −80°C. All the samples were then transported in dry ice to BITS, Pilani for further processing. The infections in these samples were clinically detected by standard Microscopy and Rapid Diagnostic Tests (OptiMAL® and Falcivax). All patient material was collected on informed consent according to the Hospital guidelines and the study was formally approved by the Institute's Human Ethics Committees (IHEC Approval no. IHEC/BITS/A/05/20).

2.3 Parasite DNA isolation

Parasite DNA was extracted from the blood samples preserved in ACD using standard/ Lab standardized protocols (Russell and Sambrook, 2001; Saxena et al., 2007).

Reagents

1. Lysis buffer
   Buffer A: 10mM NaCl; 50mM Tris (pH=8.0); 10mM EDTA (pH=8.0)
   Buffer B: 10mM NaCl; 50mM Tris (pH=8.0); 10mM EDTA (pH=8.0); 1% SDS
2. Proteinase K (20mg/mL) (Merck Bioscience)
3. 3M Sodium Acetate (pH 5.2)
4. Tris-saturated Phenol (pH 8.0)
5. Chloroform: Isoamyl alcohol (24:1)
6. Absolute and 70% Ethanol (Merck Bioscience)

The malaria parasite infected frozen blood samples were thawed at room temperature and transferred to a micro-centrifuge tube. The cells were lysed by adding equal volume of Buffer A and Buffer B and incubating the mixture at 37 °C for 45 min. To digest the proteins, Proteinase K (Merck, Germany) was added to a final concentration of 100µg/ml and mixture was incubated at 50°C for 2-3 hrs with intermittent mixing. A conventional phenol: chloroform: iso-amyl alcohol (25:24:1) extraction was performed to remove digested proteins and DNA was precipitated from the aqueous phase using chilled absolute ethanol in the presence of 0.3M sodium acetate at -20°C overnight. The precipitated DNA was pelleted by centrifuging the tubes at 8,000 rpm for 30 min at 4°C. The pellet was then washed with 70% ethanol (Merck, Germany) to remove excess of salts, air dried and re-dissolved in appropriate amount of 1X TE buffer (pH 8.0). Integrity of DNA was checked using agarose gel electrophoresis and DNA fragments were viewed in UV gel documentation system (BioRad, USA) **(Figure 2.1)**.

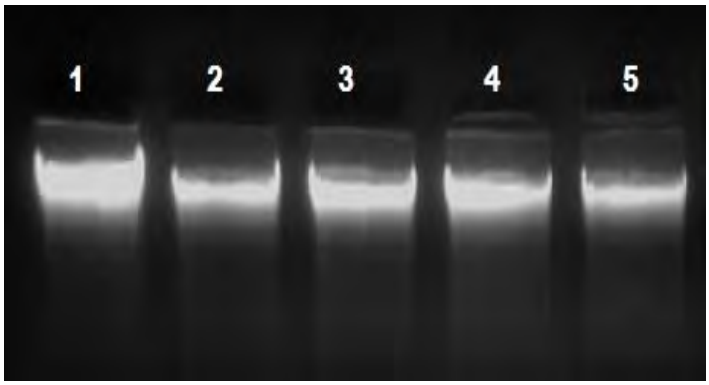

Figure 2.1: Parasite DNA isolation from *Plasmodium* infected patients' blood sample (1-5: clinical isolates)

2.4 RNA/DNA Extraction from samples preserved in Tri-Reagent

Total RNA and DNA was extracted from the RBC fraction of the parasite infected blood sample preserved in Tri Reagent using manufacturers protocol (Sigma, USA).

Reagents:

1. Diethyl Pyro carbonate (DEPC) (SIGMA): 0.1%
2. Back Extraction Buffer: 4M Guanidine thiocyanate, 50mM Sodium citrate, 1M Tris (pH= 8.0).
3. Bromo-chloro propane (BCP) (SIGMA)
4. Isopropanol

5. 70% ethanol
6. 5% Bleach Agarose gel
7. 3% Hydrogen Peroxide solution

Before proceeding for RNA isolation, all the plastic-wares and glass-wares were treated with DEPC and autoclaved. Reagents were prepared in DEPC treated and autoclaved MilliQ water. To isolate RNA, briefly, the Tri-reagent preserved blood samples were thawed on ice and BCP (1/10th volume of Tri reagent) was added to these sample followed by vigorous shaking for 15 seconds. Further the samples were incubated at room temperature (RT) for 15 min. To separate the phases, the sample was centrifuged at 12,000 rpm for 15 min at 4°C. Two phases were obtained: a pink phase containing DNA and protein and a transparent phase containing RNA. The transparent phase was separated, precipitated with isopropanol, and incubated for 20 minutes at RT. RNA pellet was obtained by centrifugation at 12,000 rpm for 10 min at 4°C. Supernatant was discarded and the pellet was washed with 70% ethanol twice. After air drying the pellet, it was resuspended in 80-90µl DEPC treated water and stored at -80°C. RNA integrity was assessed using bleach agarose gel **(Figure 2.2)** and RNA purity and concentration was checked by the Nano UV-Vis Spectrophotometer (Simpli Nano GE, UK).

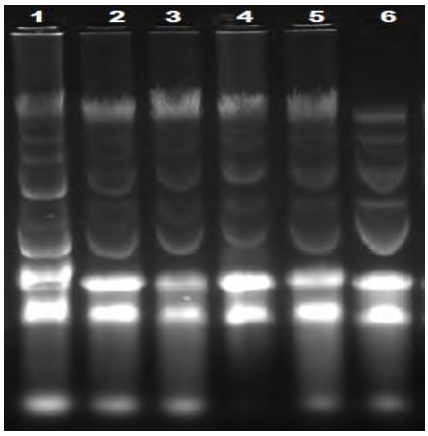

Figure 2.2: Bleach gel for RNA isolation (1- 6 clinical samples)

For DNA isolation, the pink phase obtained initially was mixed with back extraction buffer and shaken vigorously for 15 sec followed by incubation at RT for 15 min. After centrifugation at 10,000 rpm for 10 min at 4°C, DNA was obtained in aqueous phase that was precipitated with isopropanol. DNA pellet was washed twice with 70% ethanol and resuspended in 100µl of 1X TE buffer. The isolated DNA was used to confirm the

infection using either the 18S rRNA based multiplex PCR (Das et al., 1995; Kochar et al., 2005; Pakalapati et al., 2013b) or 28S rRNA based nested PCR (Pakalapati et al., 2013a).

2.5 Confirmation of type of parasite infection

At the time of collection at hospitals, the samples were thoroughly checked by trained technicians for the type of infection using Microscopy or Rapid-Diagnostic Kits (RDTs) such as Optimal (for *P. falciparum* and non- *P. falciparum* antigens) or FalciVax (for both *P. falciparum* and *P. vivax* antigens). However, in areas like Bikaner where both *P. falciparum* and *P. vivax* infection coexists, there are chances of misdiagnosis. Thus a confirmatory diagnostic PCR based on 18S rRNA gene (Das et al., 1995; Kochar et al., 2005) and 28S rRNA gene (Pakalapati et al., 2013) amplification was performed to ensure the type of infection as *P. falciparum* or *P. vivax* or a combination of both.

2.5.1 Diagnostic PCR based on 18S rRNA gene

The multiplex PCR based on 18S rRNA gene involves a single forward universal primer for the genus *Plasmodium* 5' ATC AGC TTT TGA TGT TAG G GT ATT G 3'and two reverse species-specific primers for *P. vivax* 5' TAA CAA GGA CTT CCA AGC C 3' and *P. falciparum* 5' GCT CAA AGA TAC AAA TAT AAG C 3'. The reaction conditions used were 93°C for 3min followed by 30 cycles of denaturation at 93°C for 1.5 min, annealing at 52°C for 2 min and extension at 72°C for 3 min (Kochar et al., 2005; Pakalapati et al., 2013b). The presence of *P. falciparum* was indicated by a ~1400bp amplicon whereas, *P. vivax* shows an amplification at ~500bp (**Figure 2.3)**.

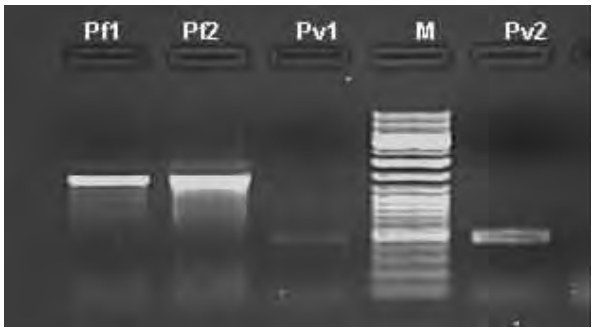

Figure 2.3: Multiplex PCR based on 18S rRNA gene. Pf1 and Pf2: *P. falciparum* samples (amplification at ~ 1400bp) and Pv1 and Pv2: *P. vivax* samples (band at ~500bp), M- DNA ladder SM0331

2.5.2 Nested PCR based on 28S rRNA gene

This PCR involves two reactions; the primary reaction based on amplification of a region common to 28S rRNA gene of human, *P. falciparum* and *P. vivax* followed by a nested PCR that is specific for *P. falciparum* or *P. vivax* for final diagnoses of the type of infection (Pakalapati et al., 2013a; Das et al., 2017). For the primary reaction, the primers NUF: 5' GAT TTC TGC CCA GTG CTT TGA ATG T 3' and NUR: 5'AAT GAT AGG AAG AGC CGA CAT CGA A 3' were used that gave an amplification of ~790bp. The amplicon from this reaction was used for nested PCR 1 using primers NPV2: 5' TCG GTT CGC CGG GTA TTC ATA TT 3' and NPVR: 5' CAC AGT AGG AAG ATA AAT TCC T 3' that amplifies a region of ~294bp specific for *P. vivax*, and the nested PCR 2 using the primers NPF1: 5' TAT CCT TCG GGA AGG CAT TCT G 3' and NPF2: 5' CTA TAT GCA CAG TAG TAA GTA ATT TA 3'to amplify ~286bp region specific for *P. falciparum*. The reaction conditions utilized are shown in **Figure 2.4**. The samples showing the band positive for *P. vivax* mono-infection were utilized for further studies **(Figure 2.5)**.

Primary Reaction conditions (common to Human, *P. falciparum* and *P. vivax*): -

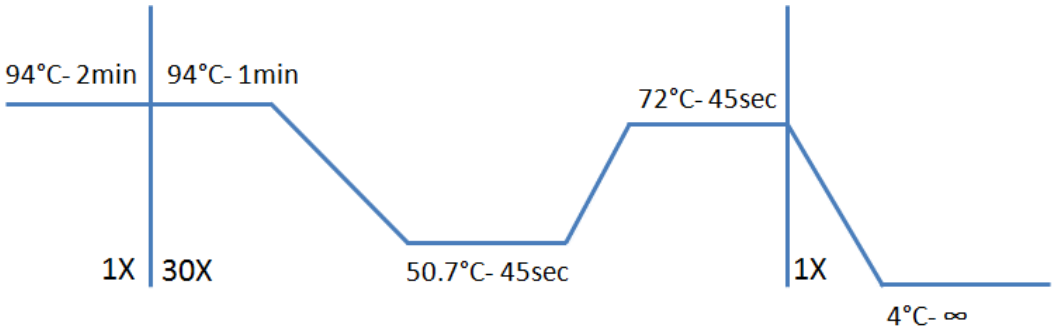

Nested PCR 1 (*P. vivax* specific) Reaction conditions: -

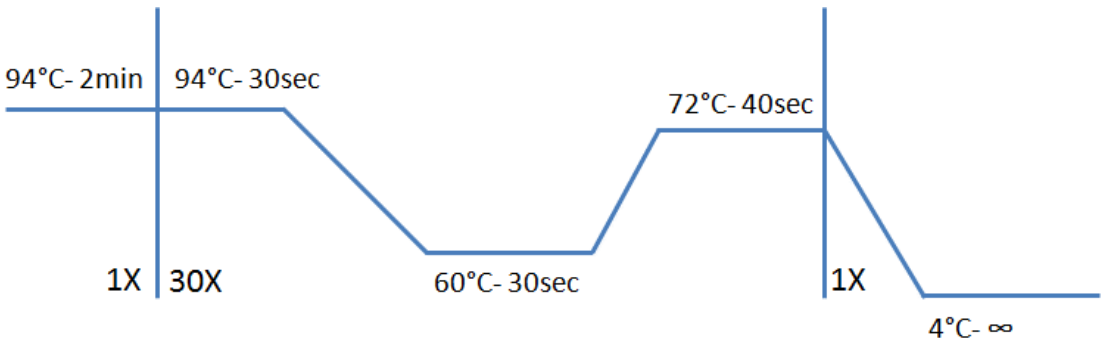

Nested PCR 2 (*P. falciparum*) Reaction conditions:

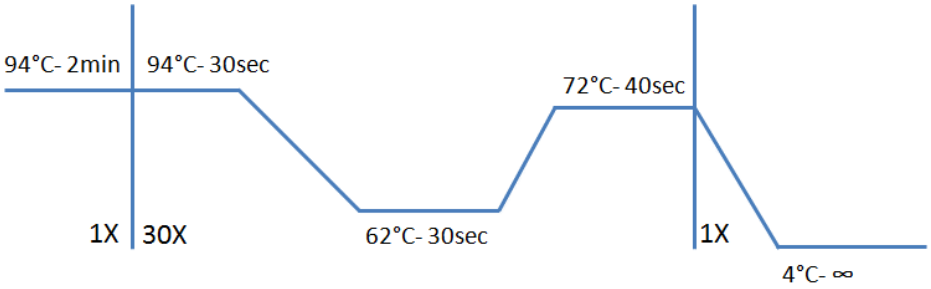

Figure 2.4: Reaction conditions used for primary and nested PCR

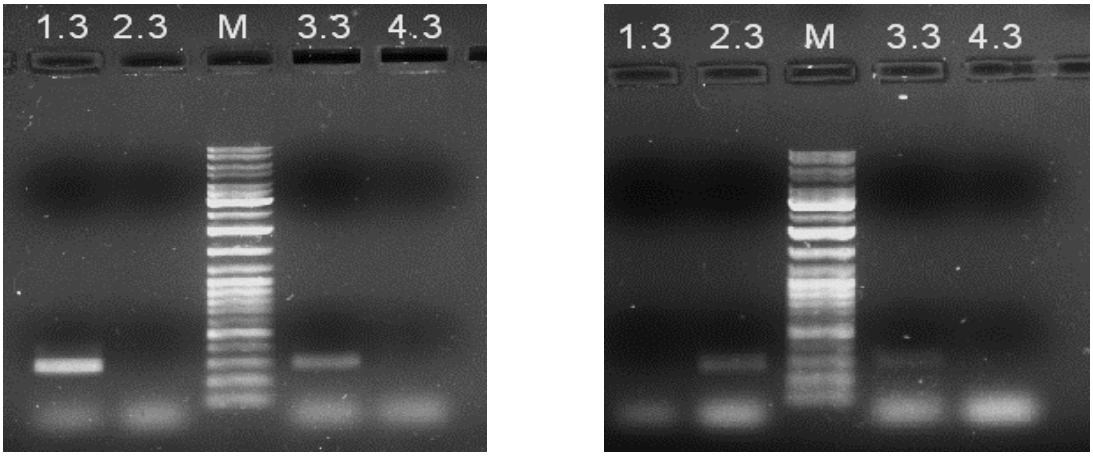

Nested PCR 1 **Nested PCR 2**

Figure 2.5: Parasite infection confirmed by Nested PCR based on 28S rRNA gene amplification. 1.3-4.3: Samples; M= Gene ruler DNA Ladder mix (SM0331)

2.5.3 cDNA synthesis

The RNA samples isolated from the confirmed *P. vivax* mono-infections were used to synthesize the first Strand cDNA using a Quantitect Reverse Transcription kit (QIAGEN, Germany) as per the manufacturers protocol. For the same, first the genomic DNA contamination, if any was removed using the Genomic DNA wipe-out buffer followed by treatment with reverse transcriptase to synthesize the cDNA strand.

Genomic DNA elimination reaction

Template RNA	1µg (RNA quantitated and sample added accordingly)
gDNA Wipeout buffer (7X)	2µl
RNA free water q. s.	14µl

Incubate at 42˚C for 2 minutes and transfer it to ice immediately.

Reverse Transcription master mix:

Above mix	14µl
Reverse Transcription Primer mix	1µl
Reverse Transcription Buffer (5X)	4µl
Reverse transcriptase	1µl
Total	20µl

Incubate the reaction mixture at 42°C for 30 mins followed by enzyme inactivation at 95°C for 3 mins. After the completion of reaction, cDNA sample was diluted (to 50µl or as per the quantity) by adding TE buffer and stored at -80°C till further use.

2.6 Amplification of genes involved in CIA and ISC pathways

2.6.1 Primer Designing

Primers were designed for genes participating in Cytoplasmic (CIA) and mitochondrial (ISC) Fe-S biosynthesis pathway of *P. vivax* using sequences available at PlasmoDB database (Aurrecoechea et al., 2009) or NCBI. For designing the primers, freely available online software's like Gene Runner (Hasting Software's Inc., USA), Primer3 (Untergasser et al., 2012) and Primer-BLAST (Ye et al., 2012) were used. Various parameters like complementarity of the two primers, Tm of hairpin loop if any, GC percentage, restriction site to be incorporated etc. were taken into consideration while designing the primers. The sequences of the primers designed are given in respective chapters.

2.6.2 Amplification and sequence analysis

The desired genes were amplified from cDNA/ DNA isolated from *P. vivax* infected patients using standardized PCR conditions, as given in the respective chapters. The PCR amplicons obtained were commercially sequenced for both strands following Sanger's dideoxy method using ABI automated DNA Sequencer (Applied Biosystems, USA). To check whether the correct gene is amplified and if there are any changes in the sequence of clinical isolates with respect to those available in different databases, nucleotide BLAST tool available at NCBI was used (Altschul et al., 1997). Further, the percentage similarity between homologous and orthologous protein sequences of *Plasmodium spp*., Apicomplexans, and other Higher Eukaryotes was determined using the multiple sequence alignment generated from Clustal omega (Larkin et al., 2007).

2.7 Cloning of *Pv*Dre2 and *Pv*NIFU/IscU genes

To functionally characterize the desired proteins involved in *P. vivax* CIA and ISC pathways and decipher their role in *Plasmodium* life cycle, the amplicons obtained from *P. vivax* clinical isolates were cloned in different cloning and expression vectors like TA cloning vector and pRSETA plasmid using the restriction sites incorporated in primers at the time of primer designing. The complete cloning process is a multi-step process that includes preparation of the required competent cells like *E. coli* DH5α or BL21(DE3) pLys cells, plasmid isolation, restriction digestion of vector (plasmid) and insert (amplified gene) using appropriate restriction enzymes, preparation of recombinant molecule by ligating the digested vector and insert, transforming the recombinant molecule in cloning or expression host, and screening of desired recombinant clone. The protocols for each of these procedures are discussed in detail in the following sections.

2.7.1 Competent cell preparation

A single colony of *E. coli* strains such as DH5-alpha and BL21 (DE3) pLysS (protein expression strain) were picked, inoculated in 10ml LB broth with required antibiotics and incubated overnight at 37°C for 12-14hr. The following day, inoculum in the ratio of 1:40 was added from this primary culture to a flask containing 50ml fresh LB broth. This was incubated at 37°C with shaking till the culture OD_{600} reached 0.3-0.4 (~2-3 hrs). Once the required OD was achieved, the culture was cooled on ice for 10 minutes followed by centrifugation at 6000 rpm for 8 minutes at 4°C. The supernatant was discarded, and the pellet was re-suspended slowly in one-third of the initial bacterial culture volume of ice-cold 0.1M Calcium Chloride ($CaCl_2$) and incubated on ice for 20 min, after which it was again centrifuged at 6000 rpm, 4°C for 8 min. The supernatant was discarded, the pellet was re-suspended in 2ml of ice-cold 0.1M $CaCl_2$ and Glycerol (to a final concentration of 15%) with gentle stirring. 300µl of this cell suspension was further aliquot in micro-centrifuge tube. Immediately the tubes were closed and kept at -20°C for 2hr and then stored at -80°C for further use (Russell and Sambrook, 2001).

2.7.2 Plasmid DNA Isolation

Reagents:

1. Solution I: 50mM Glucose; 25mM Tris-Cl (pH=8.0); 10mM EDTA (pH=8.0)

2. Solution II: 0.2N NaOH; 1% SDS (should be prepared fresh each time).
3. Solution III: 3M Sodium acetate (pH=5.2)
4. Lysozyme (50mg/ml stock solution) (Sigma-Aldrich)
5. RNAse A (20mg/ml) (Genei)
6. Phenol solution (Tris saturated pH-8) (Sigma-Aldrich)
7. Chloroform: Isoamyl alcohol (24:1) solution (Sigma-Aldrich)

A single colony of the desired plasmid like pRSETA was inoculated in 10ml LB broth containing appropriate antibiotics and allowed to grow for 12-14 hrs at 37°C, with shaking at 150-200 rpm. Alkaline Lysis method by Bimboim and Doly, was followed to isolate the plasmid from this bacterial culture (Bimboim and Doly, 1979). Briefly, the overnight grown culture was centrifuged at 6000 rpm for 5 min to pellet the cells. The supernatant was discarded and the bacterial pellet was re-suspended in ice-cold Solution I by vortexing followed by lysozyme (100µg/ml) treatment. After incubating the mixture for 3 min at RT, freshly prepared Solution II was added. The tubes were immediately shifted to the ice bucket and incubated for 4-5 minutes. Chilled Solution III was added to the above mix, mixed gently, and incubated on ice for 4 min. The lysed material was centrifuged at 10,000 rpm for 10 min at 4°C, and the supernatant was transferred to a fresh tube. RNase A treatment (20µg/ml) was given to the supernatant for 30 min at 37°C. A phenol: chloroform: isoamyl alcohol treatment was given to remove the proteins. The DNA was precipitated overnight by adding twice the volume of absolute ethanol in the presence of Na–acetate (one-tenth of the initial volume). The precipitated DNA was pelleted by centrifuging the tubes at 10,000 rpm for 30 min at 4°C. The supernatant was discarded, and the pellet was washed with 70% ethanol. The pellet was air-dried and suspended in an adequate amount of 1X TE buffer (Sambrook & Russell, 2001). The integrity of the plasmid DNA was checked by running on 1% agarose gel **(Figure 2.6)**

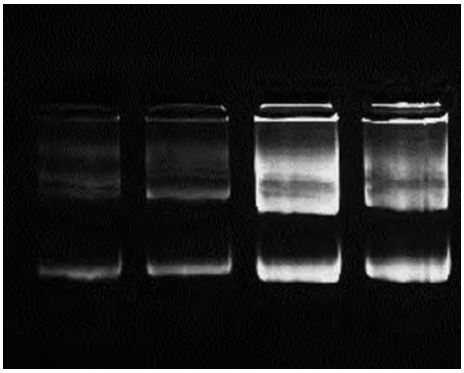

Figure 2.6: Plasmid Isolation using Alkaline Lysis method

2.7.3 Gel elution of insert

The insert being a PCR product was purified using QIAquick Gel extraction kit (QIAGEN, Germany) following the manufacturer's protocol to remove any non-specific amplifications or primer dimers. Briefly, the desired DNA band was excised from gel using a clean scalpel and the gel slices were melted in three volumes of QG buffer (w/v) by incubating at 50°C in a water bath. Later one volume of isopropanol was added to the tubes and incubated at RT for 3 min. The above mixture (max ~730µl at a time) was applied to QIAquick spin column to bind the DNA, and the column was centrifuged at 13,000 rpm for 1 min. This was repeated if the volume was more. After decanting the flow through, the spin column was washed with 500µl QG buffer to remove any agarose remnants and then with 720µl PE buffer to remove the salts by centrifuging it at 13,000 rpm for 1 min. After an empty spin, the column was transferred to fresh 1.5ml micro-centrifuge tube and DNA was eluted by using 1X TE/ elution buffer by centrifuging at 13,200 rpm for 1.5 min. The integrity of DNA was analysed by running 1µl of above eluted product on agarose gel.

2.7.4 TA Cloning

As the PCR product was gel eluted using the Qiaquick Gel extraction kit, to ensure the poly-A tail at the 3' end, a treatment of insert with dATP was performed as follows:

Poly-A Tailing:

Gel eluted amplicon (Gene of interest)	9.5µl
Taq DNA Polymerase (1U/µl)	0.5µl
Taq DNA Polymerase Buffer (10X)	1.2µl
dATP	0.8µl

Incubate the reaction mix for 1 hr at 72°C.

After the adenylation, the insert was ligated to the TA vector using the TA cloning kit procured from Genetix Asia Pvt Ltd. as follows:

Ligation with TA Vector:

Poly-A Tailed Gene of Interest	6µl
TA Vector	2µl
Ligation Buffer A (10X)	1.1µl
Ligation Buffer B (10X)	1.1µl
T4 DNA Ligase	1µl

Reaction mix was incubated for 12 hrs at 4°C.

The ligation mixture was then transformed in *E. coli* DH5α competent cells using the heat shock method. Briefly, competent cells (stored at -80°C) were thawed on ice and 10µl of ligated mix was added to 100µl of competent cells and mixed properly. Cells were incubated on ice for 25 min. The samples were thereafter given a heat shock in a water bath at 42°C for 90 seconds, after which 800µl of fresh LB broth medium was added to this mixture in a laminar hood. After incubating these cells for 45 mins at 37°C, the cells were pelleted by centrifugation at 3000 rpm for 5 min. 800µL of supernatant was removed and cells were resuspended in remaining 100µl of supernatant and plated on LB Agar plates containing the desired concentration of antibiotics. These plates were incubated at 37°C overnight and the colonies obtained were further screened for presence of recombinant clones by performing assays described in Section 2.7.6.

2.7.5 Cloning in pRSETA

For the sticky end directional cloning or sub-cloning, the isolated pRSETA plasmid vector and the gene insert were double digested with appropriate restriction enzymes as follows:

Restriction digestion of Vector and Gene Insert

Template DNA/ Plasmid DNA	500ng – 1µg
Restriction Enzyme	3 – 5U
Buffer (10X)	5µl
Sterile MilliQ Water q.s.	50µl

The reaction mix was incubated at the temperature specific to the restriction enzyme (mostly 37°C) for 1 – 2 hours, after which the complete digestion was checked by running 1µl of digested plasmid/ insert on 1% agarose gel. The digested vector and insert were then purified to remove any salts as well as enzyme using QIAquick Gel Extraction kit (QIAGEN, Germany) as discussed above.

Ligation of insert with vector

For setting up the ligation, first the concentration of vector and insert was checked by loading equal quantity of each on an agarose gel **(Figure 2.7)**. They were also quantified using Nanodrop (G.E. Healthcare) prior to the ligation. Finally, for ligation, the Insert and vector were mixed in the ratio of 3:1 and ligated using T4 DNA ligase enzyme as follows:

Vector (plasmid DNA)	100ng
Gene of interest	300ng
T4 DNA ligase buffer (10X)	2µl
T4 DNA ligase (5U/µL) (Thermo Scientific)	1µl
Sterile Deionized water q.s.	20µl

The reaction mix was incubated for 16 hrs at 22°C in a circulating water bath after which it was transformed into *E. coli* DH5α competent cells as described above.

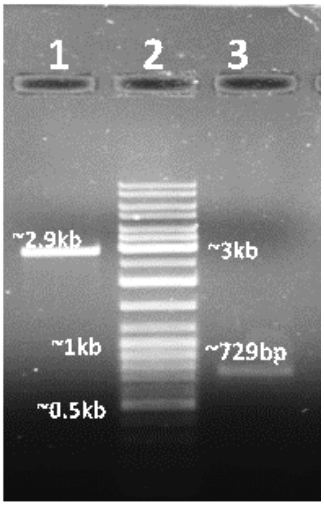

Figure 2.7: Double digested Vector and insert concentration check prior to ligation
1= Vector, 2= Gene ruler DNA Ladder mix (SM0331 Fermentas) and 3= Insert

2.7.6 Identification of recombinant clones

The obtained colonies were further screened for recombinant clones by following assays mentioned below:

2.7.6.1 Gel shift assay

The gel shift assay was initially used to examine the obtained colonies for the presence of recombinant molecule after the transformation of the ligated product (Sekar, 1987). For the same, a single colony was picked and treated with 50µl of lysis buffer (0.5mM EDTA; 10% Sucrose; 0.25% SDS; 100mM NaOH; 60mM KCl). After mixing the bacterial cells properly, the tubes were given a series of additional incubations, including 5 minutes at 65°C (water bath), 5 minutes on ice, 5 minutes at room temperature followed by centrifugation at 8000 rpm for 5 minutes. The obtained supernatant (10-15µl) was loaded on the gel to analyse band profiles. Due to the difference in size of the recombinant plasmid

with respect to plasmid without any insert, a shift in the DNA bands is observed which indicates the presence of a clone **(Figure 2.8)**.

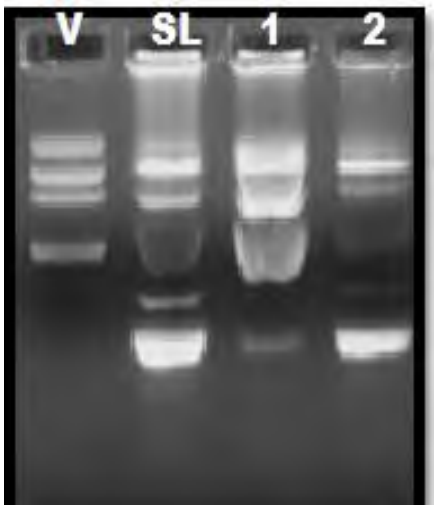

Figure 2.8: Gel shift pattern obtained after lysis for clone identification [SL: self-ligated; V= vector; 1-2 = colonies obtained after ligation. Lane 1 indicates a positive shift.

2.7.6.2 Colony PCR

After the gel shift assay, shortlisted colonies (exhibiting the shift with respect to controls) were subjected to colony PCR using gene-specific primers to screen positive clones. For this, colonies were picked from the plate under sterile conditions, suspended in 50µl of nuclease-free water, and vortexed to ensure proper suspension. The tubes were further incubated for 5 minutes at 100°C (water bath) followed by 5 minutes on ice. After keeping the tubes for five minutes at RT, the bacterial cells were pelleted by centrifuging at 10,000 rpm. After centrifugation, 10µl of the supernatant was used as a template to prepare the PCR reaction mixture. The self-ligated colonies or Vector alone served as controls.

2.7.6.3 Restriction Digestion Analysis

The recombinant colonies with positive colony PCR results were further used for plasmid isolation using the previously detailed alkaline lysis procedure. The resulting plasmid was digested using one or more restriction enzymes to confirm the clone's appropriate size and the insert's presence as well as the correct orientation. The validation of the clone and potential for frameshift were next determined by sequencing the recombinant plasmid using T7 promoter/terminator and gene-specific primers. The verified recombinant molecules were further used for protein expression analysis.

2.8 Protein Expression

Reagents

1. 1.5M Tris (SIGMA) (pH=8.8)
2. 0.5M Tris (pH=6.8)
3. 30% Acrylamide solution (29.2g Acrylamide and 0.8g N, N'-Methylene Bis-Acrylamide) (SIGMA)
4. 10% Ammonium Persulfate (SRL)
5. Sodium Dodecyl Sulfate (1% SDS)
6. Tetra methyl ethylene diamine (TEMED; SIGMA)
7. 2X Sample lysis buffer (Merck Bioscience, Germany)
8. Electrophoresis Running Buffer: 25mM Tris; 192mM Glycine; 0.1% SDS
9. Protein Molecular Weight Marker
10. Staining solution: 0.2% Coomassie Brilliant Blue (CBB) R-250 (HiMedia); 5% Methanol; 10% Acetic acid
11. Destaining solution: 40% Methanol; 7% Acetic acid in deionized water

To initiate protein expression, the recombinant plasmid (for the gene of interest) and the plasmid alone (as control) were freshly transformed in *E. coli* BL21(DE3) pLysS host cells. A single colony from this transformed plate was inoculated in fresh LB broth with appropriate antibiotic(s) after which it was incubated overnight at 37°C. 5% inoculum of this primary culture was used to inoculate fresh culture after 10-12 hours. When this secondary culture attained an OD_{600} of 0.4-0.6 (~2hrs), it was induced with 0.5mM IPTG. 1ml aliquot was withdrawn from these test (recombinant plasmid) and control (plasmid vector alone) culture flasks at regular intervals (0hrs, 2hrs, 4hrs, 6hrs and 8hrs). The collected samples were lysed by adding 2X sample lysis buffer and heating at 100°C for 10min after which the samples were checked for protein induction by running the preheated samples on a denaturing polyacrylamide gel and staining it with Coomassie Brilliant Blue. After destaining the gel, the bands obtained for recombinant clone (uninduced and induced) samples were compared with vector (uninduced and induced) samples to check the protein induction at proper size and position.

2.9 Western Blotting

To confirm the expression of desired proteins, the recombinant protein was analysed for its binding with antibodies raised against fusion tags present in the vector/ recombinant proteins. As the expression vector used in the study was pRSETA, which has a His tag as fusion protein, thus anti-His antibodies (Qiagen, Germany) were used for the protein detection.

Reagents:

1. Tris buffered saline (TBS) (50mM Tris; 150mM NaCl; 100mM KCl; pH=7.5)
2. Transfer buffer: 48mM Tris; 39mM Glycine; 20% Methanol
3. Wash buffer (1X TBST): (1X TBS with 0.05% Tween20)
4. Blocking buffer: (5% Skim milk powder (HiMedia) in 1X TBST)
5. Anti-His antibodies (QIAGEN)
6. Goat anti-mouse IgG HRP labelled antibodies (Merck Bioscience, Germany)
7. Substrate solution: TMB/H_2O_2 (SIGMA)
8. Nitrocellulose membrane (Schleicher & Schuell, Germany)

For Western blot, the recombinant protein (induced with IPTG and uninduced) along with pRSETA vector was run on an SDS-PAGE. This gel (unstained) was used to transfer the protein on the nitrocellulose membrane (soaked in the pre-cooled transfer buffer) utilizing the wet transfer method. Assembly was set with the gel at the negative electrode and the membrane at the positive end and proteins were transferred to the membrane by electro transfer (50V, 2hrs). The entire transfer was performed in cold room to avoid heating of the apparatus. After the transfer process, the membrane was stained with Ponceau-S (Merck Bioscience, Germany) for 15 min at 37℃ to check the transfer efficiency. After confirming the successful transfer of the desired band; the Ponceau-S stain was removed by excessive washing with deionized water, followed by blocking the membrane with blocking buffer (5% Skim milk powder in 1X TBST) for one and half hrs at 37℃ to prevent any non-specific binding. Later the membrane was soaked in primary antibody (dilution of antibodies varies according to the protein targeted) for 2 hours at 37°C. The membrane was washed thrice with wash buffer (1X TBST) followed by incubation with secondary HRP conjugated antibody for 1½ hours at 37°C. After washing the membrane again with wash buffer thrice (as mentioned

above), it was incubated for 15-20 min with TMB/H_2O_2 substrate solution in dark. The reaction was stopped by adding distilled water to avoid band saturation.

2.10 Protein Purification

Once the protein expression was confirmed with Western Blotting, the recombinant protein was purified using Ni-NTA columns.

Reagents

1. Lysis Buffer/ Equilibration buffer: (25mM Tris-Cl; 0.3M NaCl; 8M Urea; 20mM β-mercaptoethanol (pH 8.0)
2. Phenyl methyl sulphonyl fluoride: (PMSF; 100mM stock in Isopropanol) (SIGMA)
3. Lysozyme (50mg/ml stock) (Ameresco)
4. Wash buffer: [Equilibration buffer (pH 6.3)]
5. Elution buffer: [Equilibration buffer (pH 4.5)]

To purify protein in bulk amount, the bacterial culture containing the recombinant protein was harvested at the time point of maximum protein induction and pelleted. PMSF (final concentration of 1mM) was added to these pellets to inhibit any protease activity and the pellets were stored at -20°C if not in immediate use. To release recombinant protein from *E. coli* cells, the induced cell pellet was treated with Lysis buffer and lysozyme (final concentration of 1mg/ml) at 30°C for 20 min. This was further subjected to sonication (10 watts, 10 sec pulse; 10-15 times) on ice followed by centrifugation at 3000 rpm for 15 min at 4°C to pellet down the broken cellular debris of *E. coli* cells. The supernatant (soluble protein fraction) and pellet (insoluble protein fraction) were separated, and SDS-PAGE was performed to look for desired band. The soluble fraction was purified using Ni-NTA chromatography (QIAGEN, Germany). For this firstly, the soluble fraction of the protein is mixed with the Ni-NTA agarose resin which was then incubated for 30-45 min on rocking shaker in cold conditions. The slurry of protein and agarose resin was then loaded onto previously equilibrated (with equilibration buffer pH-8) polypropylene column (QIAGEN, Germany). After the settlement of the Ni-NTA agarose resin, the sample was allowed to flow through the column. Once the lysate completely passes out of the column, it was washed with wash buffer (pH -6.3) to remove any non-specifically bound proteins. Further the column

was treated with elution buffer (pH-4.5) to elute the bound recombinant protein. These eluted fractions were then subjected to SDS-PAGE for the determination of the purification efficiency. Once eluted, the protein was precipitated using ethanol and quantified using the popular Bradford method (Bradford, 1976). The Bradford method relies on the electrostatic and hydrophobic interaction of sulfonic acid groups in Coomassie Brilliant Blue G250 dye to positively charged, aromatic, basic amino acids present in the protein at low pH. After the binding of protein, the absorbance maxima of CBB dye shifts from 465 to 495nm, which can be then assessed using UV-visible spectrophotometer (Shimadzu, Japan). BSA at different concentrations ranging from 5µg to 100µg was used to plot the standard curve for protein estimation. By extrapolating the absorbance obtained for the unknown protein sample on this standard curve, the concentration of the protein was determined.

2.11 Biochemical Activity Assay

To characterize [Fe-S] cluster biogenesis proteins at molecular and functional level, various *in vivo* and *in vitro* biochemical assays were performed such as **1)** ICP-OES to analyse metal content in *E. coli* cells expressing protein of interest **2)** Reconstitution of [Fe-S] clusters on the protein(s) and UV-vis spectrometry and **3)** Determination of oxidative stress generated in *E. coli* cells due to recombinant protein expression using fluorescence spectroscopy.

2.11.1 Inductively coupled plasma optical emission spectrometry (ICP-OES)

After IPTG induction of the bacterial cells with recombinant plasmid, to analyse any iron accumulation in the cell, ICP-OES was performed. For the same, 10ml of IPTG induced bacterial culture expressing protein of interest were taken and cells were harvested through centrifugation (4000 rpm, 15 min). Clone un-induced bacterial culture, and induced bacterial culture with pRSETA alone were taken as controls. After removing any residual media, the bacterial pellet was dried at room temperature for 24 hr. The dried bacterial pellet was treated with 1ml of 30% HNO_3 solution and further incubated at room temperature for 48 hr. The mixture was then sonicated 5 times at 10kHz/10sec after which it was centrifuged at 13000 rpm for 20 minutes. The obtained supernatant was passed through 0.2µ syringe filter to remove the cellular debris. The filtrate was then diluted 1:5 with autoclaved Milli-Q water and subjected to ICP-OES

(Optima 8000 PerkinElmer) analysis. Three Fe standards (Merck) of 1ppm, 10ppm and 50ppm were used for the standard curve preparation and Fe quantification. Three different biological replicates for each sample were analysed for Fe accumulation by ICP-OES at the wavelength of 238.204 nm (Tu et al., 2012).

2.11.2 Chemical Reconstitution assay

Reagents

1. Reconstitution buffer (50 mM Tris-HCl, 200 mM NaCl, pH-8)
2. Iron releasing agent (0.6M HCl and 0.142M $KMnO_4$)
3. Iron chelating reagent (6.5mM ferrozine, 13.1mM neocuprine, 2M ascorbic acid and 5M ammonium acetate)

As the [Fe-S] clusters are sensitive to oxygen and the purification of proteins were done in aerobic conditions, it resulted in the oxidation of protein which ultimately led to the removal or no formation of [Fe-S] clusters on the protein. Thus to determine the [Fe-S] cluster binding ability of the proteins under study, the [Fe-S] clusters were chemically reconstituted on the protein(s) under anaerobic conditions. For the same, specific concentrations of purified proteins were anaerobically incubated in Reconstitution buffer for 30 min to 1hr at 25°C in a reaction chamber. Further the protein was incubated with 10mM Dithiothreitol (DTT) prepared in Tris-Cl (pH-8) for 1.5 hr to generate reducing environment. Once the desired reducing environment and buffered conditions were established, five-fold molar excess of Na_2S and Fe $(NH_4)_2$ $(SO_4)_2$ were added sequentially dropwise and whole reaction mixture was incubated for 2hrs at 25°C. After this, to remove excess iron, sulfur, and other unbound metals, the reaction mix was subjected to desalting with Amicon Ultra-4 filters 10K (Merck Millipore, UK). The removal of residual metals was done strictly under anaerobic conditions. To further validate the [Fe-S] formation, the UV-vis spectra (200nm-800nm) of purified protein with and without chemical reconstitution was taken by UV-vis spectrometer (Shimadzu, Japan). The obtained UV-vis spectra of purified protein with and without reconstitution was correlated with the signature peaks of spectra reported for [Fe-S] cluster biogenesis proteins from other organisms (Bernard et al., 2013; Netz et al., 2016; Zhang et al., 2016).

After the chemical reconstitution of [Fe-S] clusters on the protein, the molar ratio of bound iron and sulfur with the protein(s) was determined using the Ferrozine (for iron) and methylene blue (for sulfur) assay respectively (Fish, 1988; Siegel, 1965). To determine the iron content by Ferrozine assay, iron standards ranging from 1µg – 6µg/ml were prepared by dissolving required concentration of ferrous ethylene di-ammonium sulfate tetra hydrate salt (SIGMA, USA) in 0.01M HCl. Further, all the standards and test samples were subjected to acid digestion for 2hr at 60°C by adding iron releasing agent, followed by addition of reducing, iron chelating reagent (chromophore). The solution was incubated at room temperature for 30 min after which the absorbance of standards and protein samples were recorded at 562nm (Fish, 1988). The graph obtained by plotting the absorbance of iron standards were used to deduce the regression equation for determining the unknown values of test samples.

To determine sulfur content by methylene blue assay, sulfur standards ranging from 0.01mM to 0.1mM were prepared by dissolving sodium sulfide in sodium carbonate buffer (pH 9.0). The sodium sulfide standards and test samples were then treated with 0.02M N, N-Dimethyl-p-phenylene diamine sulfate (DPD) and 0.03 M Ferric Chloride ($FeCl_3$). After incubation at room temperature for 10 min, absorbance was recorded at 650nm (Siegel, 1965) and the sulfur released was determined in similar manner as iron by plotting the concentration against the absorbance and deducing the value of test from standard graph.

2.11.3 Reactive Oxygen Species (ROS) detection

The cell-permeable free radical sensor 2′,7′-dichlorodihydrofluorescein diacetate (H_2DCFDA, Invitrogen, San Diego, CA) was used to measure intracellular ROS levels. After inducing the bacterial cells containing recombinant plasmid with IPTG, 1ml of bacterial culture was collected at 0, 2, 4, 6 and 8h respectively. Uninduced bacterial cells with recombinant plasmid were used as negative control whereas for positive control these cells were treated with H_2O_2 (1 mM). Vector alone without induction and with induction were also used to confirm that the change in ROS generation is not due to the addition of IPTG. The collected samples were washed with phosphate-buffered saline (1X PBS) and further dissolved in 1X PBS for downstream treatment. H_2DCFDA (10 µM) was added to all the tubes and incubated for 30 min in the dark at RT. The ROS generation in the sample was detected by measuring fluorescence with

excitation/emission at 485nm / 530nm using Fluorescence Multiplate Reader (VICTOR Nivo^{TM}, PerkinElmer).

2.12 Scanning Electron Microscopy

Reagents

1. Chromic acid solution
2. 1X PBS buffer (pH 7.2)
3. 2.5% Glutaraldehyde solution prepared in 1X PBS.
4. Ethanol solution: 30%, 50%, 75%, 90% and 100%

To analyse bacterial morphology upon heterologous protein expression, surface analysis was done using FEI-Apreo S LoVac (Thermo Fisher Scientific, USA) scanning electron microscope. For SEM analysis, 1 ml of bacterial cells harbouring recombinant molecule were collected before (uninduced) and post-IPTG induction at various time points as mentioned above. We also collected 1 ml of bacterial culture for pRSETA (induced) as control. All the bacterial cells were pelleted at 4000 rpm for 5 min and the pellet was washed twice with 1X PBS by centrifugation at 300 x g for 5 min. After the second spin, the supernatant was gently poured off leaving 50-60µl of supernatant for smear preparation. The bacterial pellet was resuspended in remaining supernatant and a simple smear was prepared onto the pre-cleaned autoclaved slide (small squares cut into 1 X 1 cm). These smears were treated with 2.5% glutaraldehyde solution and incubated overnight at 4°C. After incubation, excess glutaraldehyde solution was removed with a gentle wash of 1X PBS. The slides were then dried and dehydrated with series of different ethanol concentrations: 30%, 50%, 75%, 90% and 2X 100%. Gold coating was done by exposing the smears for 30-60 seconds in sputter coater instrument and finally SEM analysis was performed to analyse bacterial morphology.

2.13 Cell viability assays

2.13.1 Colony Forming Unit (CFU) analysis

To analyse cellular toxicity due to heterologous protein expression in *E. coli* BL21 (DE3) pLysS cells, CFU/ml was assessed at different time points after induction (Srivastava et al., 2019). The collected bacterial samples were diluted with fresh LB media to prepare 10^{-1}, 10^{-3} and 10^{-5} dilutions. 5 µl of these respective dilutions were

spread on LB agar plates and incubated at 37°C. Colony forming units were quantified and CFU/ml graph was plotted accordingly. Proper controls were set such as *E. coli* cells with empty plasmid (plasmid without gene of interest) and *E. coli* cells with recombinant plasmid (with gene of interest) but no protein induction.

2.13.2 Hoechst H33342/Propidium Iodide staining

To further validate *E. coli* cellular death due to heterologous protein expression, Hoechst 33258 (Sigma-Aldrich, USA) and Propidium Iodide (PI) (Sigma-Aldrich, USA) based live/dead staining was performed. Hoechst is a nuclear-specific dye used to stain live or fixed cells during experimentation, while on the contrary PI is impermeable to live cells making it significant to differentiate dead cells. Bacterial suspension was collected from test and control at regular intervals post-IPTG induction. A sample volume of 1ml was pelleted at 3000 rpm for 5 min, washed once with 1X PBS and stained with Hoechst (10µg/ml) and PI (5 µg/ml) sequentially, according to manufacturer's protocol. The Hoechst responsive cells (blue coloured) were detected with excitation/emission at 350nm/ 461nm wavelength whereas, PI responsive cells (red coloured) were detected with excitation/ emission at 545nm/ 590nm, using Fluorescence Microscope (Zeiss ApoTome 2.0).

2.14 Expression profile of *E. coli* stress genes upon heterologous expression

Reagents:

1. Diethyl Pyro carbonate (DEPC) (SIGMA)
2. RNA stabilization solution (0.2% SDS, 19% ethanol, 1% water saturated Phenol)
3. TRI-reagent® (Sigma Aldrich, USA)
4. Lysozyme (4mg/ml) (SIGMA, USA)
5. Chloroform (SIGMA, USA)
6. Isopropanol (SIGMA, USA)
7. 70% ethanol (Merck, Germany)
8. 5% Bleach Agarose
9. 3% Hydrogen Peroxide solution

E. coli response to ROS generation and cellular toxicity due to heterologous protein expression was analysed by checking the expression of genes involved in stress response pathway. 1 ml of bacterial culture was collected at regular time points from different samples including Clone induced, Vector Induced and Clone Uninduced. The bacterial cells were pelleted by centrifuging the samples at 6000 rpm for 10 minutes at 4°C. The obtained pellet was resuspended in 500µl of RNA stabilization solution (Srikumar et al., 2015). Total RNA was isolated from these samples using TRI-reagent® (Sigma Aldrich, USA) following manufacturers protocol with a minor modification of pre-treating collected bacterial samples with Lysozyme (4mg/ml) at 37°C for 20 min. RNA integrity was assessed using denaturing agarose gel and its purity and concentration was checked by the Nano UV-Vis Spectrophotometer (Simpli Nano GE, UK)). cDNA was prepared from these samples using QuantiTect Reverse transcriptase kit (QIAGEN, Germany) as per manufacturers protocol. Quantitative RT-PCR for stress genes was carried out with technical and biological duplicates using a 10µl reaction volume on CFX Connect Real-Time PCR Detection System (Bio-Rad Laboratories, USA) and conditions as described before (McQuillan and Shaw, 2014; Pareek et al., 2022). The 10µl reaction mixture was prepared by mixing 5µl of iTaq TM Universal SYBR® Green Supermix (BIORAD, USA), 1µl of forward and reverse gene specific primer (10 pmol/ µl), 2 µl of nuclease-free water, and 1µl of cDNA template. The relative fold change in the mRNA expression level was determined using the $2^{-\Delta\Delta Ct}$ method keeping 16S rRNA gene as internal control (Livak and Schmittgen, 2001).

2.15 Protein sub-cellular localization and Antibody binding studies

To determine subcellular localization of protein in parasite, immunofluorescence microscopy was performed on methanol fixed *P. vivax* thin smears prepared using blood collected from malaria patients. To detect the protein, antibodies specific to the recombinant molecule were raised in Swiss albino mice and used along with secondary antibody and other organelle specific reagents.

2.15.1 Antibody raising and ELISA

Reagents

1. Freund's Complete/Incomplete Adjuvant (Merck Bioscience, Germany).
2. Coating Buffer (Carbonate bicarbonate buffer, pH 9.4).

3. Blocking Buffer (5% skim milk powder prepared in 1X PBS)
4. Wash Buffer (1X PBS containing 0.2% Tween 20)
5. Goat anti-mouse IgG HRP conjugate (Merck Bioscience, Germany).
6. TMB/H_2O_2 for ELISA (Merck Bioscience, Germany).
7. Stop Solution: 2N H_2SO_4

To raise antibodies against shortlisted protein, 25-30µg of purified recombinant protein was injected intra-peritoneal/ subcutaneously per mice along with Freund's adjuvant. Freund's complete adjuvant was used at the time of primary immunization while the subsequent booster doses were given with Freund's incomplete adjuvant. Mice in which no protein was added was taken as control group. Each group (Test and control) consisted of 5 female Swiss albino mice of 4 to 5 weeks. These mice were bred under contamination free conditions and maintained throughout in Animal House facility, BITS Pilani, Rajasthan. Before injecting protein inside mice, they were pre-bled to check for the presence of any pre-existing antibodies against the protein of interest. After pre-bleed, the mice were kept under recovery period of 5-7 days. All the protocols mentioned hereby were approved by the Institute's Animal Ethics committee (Approval no. IAEC/RES/28/6). Three booster doses were given after primary immunization, where a 21-day incubation was followed for Protein-Adjuvant injection. After every injection, on 9th day, mice blood was collected for sera separation using Retro-orbital bleeding. For the sera separation, the collected blood was kept at 37°C for 1 hr, followed by overnight incubation at 4°C and final centrifugation at 10,000 rpm for 10 min at 4°C. The supernatant (serum) was collected in a fresh micro-centrifuge tube and stored at -20°C till further use.

Antibody titre specific to recombinant protein was measured by performing ELISA. 96 well micro-titre plate with flat bottom (Nunc) was used where 100 µl of 1ng/ul of recombinant protein prepared in coating buffer was coated in each well while keeping few wells uncoated that served as controls. The plates were kept for an overnight incubation at 4°C. Next day, after giving three washes of 5 minutes each with wash buffer, the plates were kept in blocking buffer for 2 hr at 37°C to prevent non-specific binding. Again, washing was done as mentioned above after blocking step. Serum samples (primary antibody) with varying dilutions starting from 1:50 to 1:5000 were added to the plates for binding to the coated recombinant protein. After incubating the

plate with primary antibody for 2hrs at 37°C, and washing thrice with wash buffer, antibodies specific to recombinant protein were detected using HRP conjugate goat anti-mouse IgG (diluted to 1:1000 in blocking buffer). TMB/H_2O_2 substrate was used for the generation of chromogenic reaction and the reaction was stopped by adding dilute H_2SO_4 solution. The absorbance was recorded at 450nm/650nm on ELISA plate reader (Multiskan, Thermofisher). All the tests were performed in duplicates and antibody levels were expressed as an average concentration unit. The specificity of these antibodies was further confirmed by western blot analysis using parasite lysate.

2.15.2 Immuno-localization studies

Reagents:

1. 0.05% Saponin in 1X PBS
2. 0.1% Triton X-100
3. Blocking Buffer (3% Bovine Serum Albumin (BSA) in 1X PBS)
4. DAPI (Life Technologies, USA)
5. Goat anti-mouse IgG FITC Conjugate (Merck, Germany)
6. Prohibitin Polyclonal Rabbit Antibody [PA5-27329] (Invitrogen, USA)
7. Goat anti rabbit IgG Alexa 647 conjugate (Invitrogen, USA)
8. Qdot® 565 Streptavidin conjugate (Life Technologies, USA)
9. VECTASHIELD (Vector Laboratories, USA)

For localization studies, first the thin smeared pre-fixed slides were washed with 1X PBS for 5 min on rocking shaker at low speed. Afterwards they were treated with 0.05% Saponin at RT for 30 min, followed by 0.1% Triton-X treatment for 3 min 30 sec at RT for permeabilization. Once the permeabilization step was over, slides were washed thrice with 1X PBS (5 min each wash) and kept for overnight blocking (3% BSA) in static condition at 4°C. After blocking, the slides were incubated with primary antibody prepared in blocking buffer for 3 hr at 37°C. To remove any unbound antibodies, the slides were again washed with 1X PBS Tween-20 (0.05%), repeating it for 4 more times. All the subsequent steps after this were performed in dark conditions as the fluorescence molecules were now added to the slides. Firstly, the slides were subjected to FITC 488 conjugate Goat anti-mouse IgG secondary antibody (1:200 dilution) and incubated for 1hr 30 min at 37°C. Washing was repeated as mentioned above. Further to stain mitochondria, slides were treated with mitochondria specific Prohibitin

Polyclonal Antibody (Invitrogen, USA) diluted to 1:500 followed by 1:200 dilution of goat anti rabbit IgG Alexa 647 conjugate (Invitrogen, USA). To stain Apicoplast, slides were treated with 20nM Qdot 565 streptavidin conjugate for one and a half hour at 25°C. For staining the nucleus, 75ng/ul solution of DAPI (Sigma) was added to the slides and incubation was done for 10 min at 25°C. After counterstaining of the parasite, slides were washed twice with 1X PBS (5 min each) and air dried. The slides were finally mounted with VECTASHIELD anti-fade mounting medium and observed in confocal microscope (ZEISS LSM 880) under a 63X oil immersion lens. The excitation and emission wavelengths for the fluorescent dyes is given in **Table 2.1**

Table 2.1: Fluorescent dyes and their excitation and emission wavelength peaks

Filter Set Description	Excitation	Emission	Remarks
DAPI	359 nm	461 nm	Violet EX / Blue EM
FITC antibody conjugate	495 nm	519 nm	Blue EX / Green EM
Qdot® 565 Streptavidin conjugate	300 nm	564 nm	Yellowish orange
Goat anti rabbit IgG Alexa 647 conjugate (Invitrogen, USA)	651 nm	671 nm	Red

2.16 Parasite Lysate Preparation

Reagents:

1. Saponin Lysis Buffer: 0.03% Saponin in 1X PBS (pH – 7.5)
2. Parasite Lysis Buffer: 10% SDS, 10% TritonX-100 in 1X PBS
3. Protease Inhibitor Cocktail-P8465 (Sigma, USA)

After thawing at room temperature, 1.5ml of the parasite-infected blood sample was transferred to a 15 ml falcon tube. The cells were washed with an equal volume of 1X PBS by centrifugation at 5000 rpm for 5 min at 4˚C. The washes were repeated (five-six washes) until the red colour disappeared from the cellular pellet. Further, the pellet was resuspended in 500µl of 1X PBS and transferred to a 2ml micro-centrifuge tube. To the above mixture, 200µl of Saponin lysis buffer was added along with 2µl of Protease Inhibitor Cocktail and the tubes were incubated on ice for 15 min followed by centrifugation at 13,200 rpm for 5 min at 4˚C. The resulting pellet was washed again with 500µl of 1X PBS at 13,200 rpm for 5 min at 4˚C. After washing, the pellet was

treated with 350µl of parasite lysis buffer and centrifuged at 13,200 rpm for 5 min at 4˚C, and the supernatant and pellet were collected in separate tubes. The pellet was resuspended in 500µl of 1X PBS. An equal volume of 2X sample lysis buffer was added to the supernatant and pellet and a small volume of these were subjected to SDS-PAGE.

2.17 *In vitro* co-immunoprecipitation (Co-IP)

Dynabeads Protein G (Life technologies) cross-linked with antibodies raised against the shortlisted proteins were used for the immuno-precipitation reactions. For crosslinking, 50µl (1.5 mg) of Dynabeads were taken in a vial, and 100µl of *Pv*Dre2 antibody (1:50 dilution of *Pv*Dre2 anti-sera prepared in 1X PBST-Tween-20) was added. Pre-immune sera were also cross-linked to Dynabeads Protein G in a similar manner, to be used as control. These mixtures were incubated at 4˚C for 2-3 hrs. Afterwards, the antibody conjugated Dynabeads were washed thrice with 1X PBST (00.1% Tween 20 in 1X PBS). After washing, 500µg of parasite lysate was added to Dynabead-antibody conjugate (test and control) and incubated overnight with slow rocking at 4˚C. After immunoprecipitation of the target antigen, the sample was washed with 1X PBST thrice to remove any unbound proteins. Target proteins were eluted by incubating samples at 70˚C for 10 min in 1X Laemmli buffer and stored at 4˚C till further processing.

2.18 Protein Identification with Liquid chromatography tandem mass spectrometry (LC-MS/MS)

The immune-precipitated sample was subjected to SDS-PAGE and stacked just above the resolving gel. The stacked sample was then excised and stored in 50% methanol and 10% acetic acid solution and sent to Centre for Cellular and Molecular Platforms (C-CAMP), Bangalore, for mass spectrometry analysis following the standard protocols. Orbitrap Fusion Tribrid Mass Spectrometer coupled to a Thermo EASY nanoLC 1200 chromatographic system (Thermo Scientific™, USA) was used to conduct mass spectroscopy. The protein was digested with Trypsin (Promega) and 3µl of the sample was injected into a C8 LC column (EASY SPRAY PEPMAP RSLC C18 2µm; 15cm x 50µm; 100Å). Chromatographic separation was performed at a flow rate of 300 nl/min using a gradient elution program. Exact gradient parameters are given in **Figure 2.9**. The generated data were searched for the identity of the peptides on the

Proteome Discoverer 2.2 (Thermofisher Scientific Inc, USA) using the UniProt database [uniprot-organism_plasmodium_2022]. The Parent Mass Error Tolerance was set at 10.0 ppm with the Fragment Mass error Tolerance of 0.6 Da, with max missed cleavage of 2. The data obtained for *Pv*Dre2 specific antibodies was compared with the control (pre-immune sera). The significant hits with the Peptide Spectrum Match (PSM) of 5 or more, and two or more unique peptides were taken into consideration.

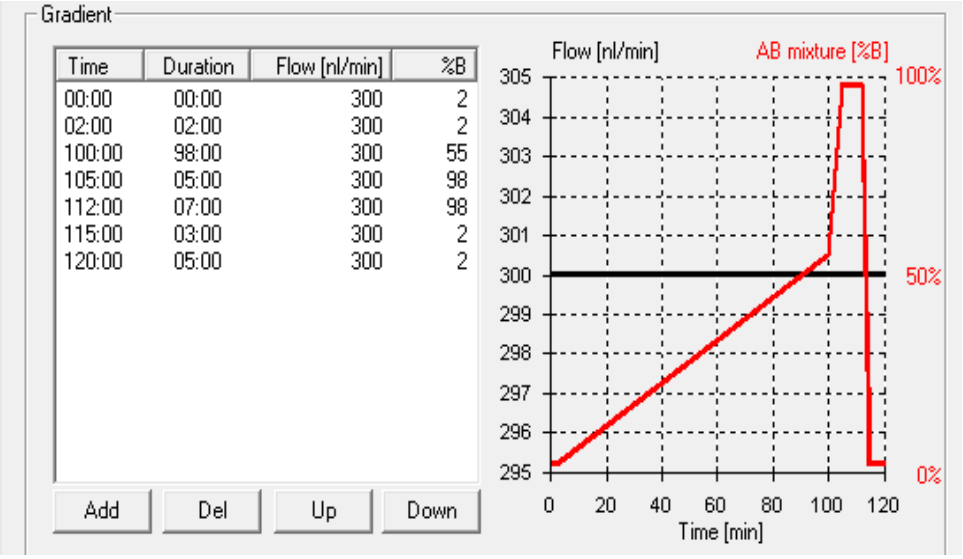

Figure 2.9: LC gradient program used for Mass spectroscopic analysis. Buffer A:0.1% Formic acid; Buffer B:80% Acetonitrile + 0.1 % formic acid (in LCMS water)

2.19 Phylogenetic Analysis

To estimate the evolutionary distance between various *Plasmodium* species, as well as other apicomplexans, higher eukaryotes, and prokaryotes for the proteins implicated in the CIA and ISC pathways, the phylogenetic tree was generated and examined. Evolutionary analysis was performed using MEGA X software, using the Neighbour-joining method (Kumar et al., 2018; Saitou and Nei, 1987). A matrix of pairwise distances was calculated using a JTT model that was subjected to neighbour-join and BioNJ algorithms to produce the phylogenetic tree. The topology with the highest log likelihood value was chosen (Kumar et al., 2018). The evolutionary history of the taxa under study was represented by the bootstrap consensus tree, inferred from 1000 iterations. All places with gaps and missing data were removed (Felsenstein, 1985). The obtained tree was then analysed to predict the evolutionary position of *Plasmodium* with respect to other species.

2.20 Protein Structure Prediction

2.20.1 Secondary structure prediction

Prediction of secondary structure is a useful intermediate step, that can facilitate the process of 3D structure prediction and help to identify conserved domains. Secondary structures of proteins in our study were generated using PSI-PRED server (McGuffin et al., 2000) to find out the total number of α-helices and β-sheets present and to depict the conformation of amino acid residues that were repeatedly seen in the proteins.

2.20.2 Prediction of three-dimensional structure of proteins

To generate three dimensional models for the shortlisted proteins, first the homology modelling approach was adapted using MODELLER 9v18 (Eramian et al., 2006; Šali and Blundell, 1993). For this, the translated amino acid sequence of the desired protein was uploaded on the HHpred web server (Söding et al., 2005). Based on the sequence similarity of the target sequence with the template and resolution of the template structure, the best structure was selected, for predicting the protein structure by MODELLER. Among the various models generated, the structure with the lowest discrete optimized protein energy (DOPE) was chosen. In case we could not find a good match or resolution for the structure in HHpred, *ab initio* modelling was used to generate the protein structure. The RoseTTAFold method available at Robetta server developed by Baker's lab's (https://robetta.bakerlab.org/) was used for *ab initio* modelling (Baek et al., 2021).

The steps that generate a protein structure are followed with Energy Minimization (EM) strategies to achieve ideal folding for a protein. The internet server YASARA (Krieger et al., 2009) and the AMBER tool from Chimera were used for energy minimizations (Pettersen et al., 2004). The energy minimized three-dimensional protein structures were analysed for their quality and for the environment profile surrounding protein residues using a variety of online servers, including PROCHECK (Laskowski et al., 1993), VERIFY3D (Eisenberg et al., 1997) and ERRAT (Colovos and Yeates, 1993). The WHAT IF program that assesses atomic contacts and side chain packing in the final improved models (Vriend, 1990) and Ramachandran plot that displays the statistical distribution of all the possible backbone dihedral angle combinations were also used to evaluate the derived models (Lovell et al., 2003; Hollingsworth and Karplus, 2010).

2.20.3 Substrate docking

Any protein/ enzyme participating in biological processes, such as [Fe-S] cluster biogenesis pathways, will likely have binding sites/ pockets for substrates or cofactors. Based on literature available from other organisms, a binding pocket constituted by conserved amino acid residues was identified. Docking studies were performed using AutoDock Vina (Trott and Olson, 2010). The structures of [4Fe-4S] and [2Fe-2S] ligands were obtained from PubChem (https://pubchem.ncbi.nlm.nih.gov/) (Kim et al., 2023) in .sdf format, which was then converted into .pdb format using Chimera software (Pettersen et al., 2004). These [Fe-S] structures were then docked to the respective protein models by following below steps:

(i) preparation of ligand ([Fe-S]) and receptor (Protein) coordinate file (. pdbqt) using AutoDock Vina tool,
(ii) pre-calculation of atomic affinities using AutoGrid,
(iii) generation of the configuration file, and
(iv) docking of receptor and ligand.

Preparing receptor/ ligand.pdbqt files involved deleting water molecules, adding polar hydrogen atoms in their respective .pdb files, and saving them as [Fe-S]. pdbqt and Protein. pdbqt. To prepare the grid map, first, [Fe-S]. pdbqt and Protein. pdbqt files were opened in AutoDock tools and then defined into macromolecule (receptor) and ligand. Binding cavities were located on these proteins and selected as constraints, which were further used as a site for docking. The cubic grid box was prepared manually with a grid edge length of appropriate size covering conserved residue sites of protein (receptor). The output of the grid dimension file was saved as grid.txt. In the configuration file, receptor (Protein. pdbqt) and ligand ([Fe-S]. pdbqt) files, x, y, and z centers, length of the grid box for x, y, and z dimensions, energy range (default value = 2), and exhaustiveness parameter (default value = 8) were defined. The output file was saved as config.txt. The following docking command was given from the command prompt to execute AutoDock vina – (C:\program files(x86) \The Scripps Research Institute\Vina\vina.exe). The log.txt and Output. pdbqt files were the output of the docking process. The Log.txt contained information on amino acids participating in interactions and their proximity to the ligand in Protein-[Fe-S] docked models. Output. pbdqt is the model generated from docking. Once the simulation was over, docking results were imported from the output directory together with the pose organizer. In the

pose organizer, all the poses were analysed manually to check the interaction between protein and ligand molecules using Pymol (The PyMOL Molecular Graphics System, Version 2.0) and Discovery Studio software (Dassault Systèmes, 2016). By measuring the distances (A° values), the affinity of conserved amino acid residues toward ligand molecules was estimated.

Materials used for various reactions

Vector and Bacterial strains used

pRSET A	Invitrogen, USA
TA cloning vector	Genetix Biotech, Asia
E. coli strain DH5α	Thermo Scientific, USA
E. coli strain BL21 (DE3) pLysS	Novagen, Germany

Various kits used in this study

Anti-His Antibody kit	QIAGEN®, Germany
Qiaquick Gel extraction kit	QIAGEN®, Germany
Ni-NTA agarose Resin	QIAGEN®, Germany
PCR purification kit	QIAGEN®, Germany
Plasmid miniprep kit	QIAGEN®, Germany
Quantitect Reverse Transcriptase kit	QIAGEN®, Germany

Antibodies and Fluorescence dyes

Prohibitin Polyclonal Rabbit Antibody [PA5-27329]	Invitrogen, USA
Goat anti-Mouse IgG HRP conjugate	Merck, Germany
Goat anti-Mouse IgG FITC conjugate	Merck, Germany
Qdot® 565 Streptavidin conjugate	Life Technologies, USA
DAPI	Life Technologies, USA
Goat anti rabbit IgG Alexa 647 conjugate	Invitrogen, USA
2′,7′-dichlorodihydrofluorescein diacetate	Invitrogen, San Diego, CA)
VECTASHIELD	Vector Laboratories, USA

Other reagents used in the study

Certipur® Iron standard solution (1000mg/l)	Merck, Germany
Artemether [>98.0% pure] [Cat: A2190]	Tokyo Chemical Industry Ltd, Japan
Hydrogen Peroxide 30%	Merck, Germany
Isopropyl β-D-1-thiogalactopyranoside	Sigma Aldrich, USA

Composition of common buffer and solution used in the study

Acid Citrate Dextrose (1000ml)	Sodium citrate 13.2gm Citric acid: 4.8gm Dextrose: 14.7gm Filter sterilize using 0.2µm syringe filter
DNA loading buffer (6X) 10ml	9mg Bromophenol blue 9mg Xylene cyanol FF Dissolve in 8.8ml of 60% Glycerol and add 1.2ml of 0.5M EDTA
Phosphate Buffered Saline pH 7.4 (10X) for 50ml	1.37mM NaCl (4g) 27mM KCl (0.1g) 100mM Na_2HPO_4 (0.709g) 18mM KH_2PO_4 (0.12g)
TE buffer (1X; pH 8.0)	10mM Tris-Cl (pH 8.0) 1mM EDTA (pH=8.0)
TAE buffer (50X; 1000ml)	40mM Tris-acetate 1mM EDTA (pH 8.0) 57.1 ml Glacial acetic acid

Accession Numbers for Sequences used to perform MSA and generate phylogenetic tree of Dre2:

S. No.	Organism	Accession No.
1.	*Plasmodium vivax Sal-I*	PVX_089130
2.	*Plasmodium_falciparum_3D7*	PF3D7_0824600
3.	*Plasmodium malariae UG01*	PmUG01_05021400
4.	*Plasmodium reichenowi CDC*	PRCDC_0823900
5.	*Plasmodium ovale curtisi GH01*	PocGH01_05016300
6.	*Plasmodium cynomolgi strain B*	PCYB_051660
7.	*Plasmodium inui San Antonio 1*	C922_02656
8.	*Plasmodium knowlesi strain H*	PKNH_1318600
9.	*Plasmodium yoelii yoelii YM*	PYYM_0706200
10.	*Plasmodium chabaudi chabaudi*	PCHAS_0715300
11.	*Plasmodium vinckei petteri*	YYG_04228
12.	*Plasmodium berghei ANKA*	PBANKA_0706000
13.	*Toxoplasma gondii*	TGVEG_216900
14.	*Arabidopsis thaliana*	At5g18400
15.	*Saccharomyces cerevisiae*	P36152
16.	*Trypanosoma brucei brucei*	Tb927.8.1750
17.	*Mus musculus*	Q8WTY4
18.	*Caenorhabditis elegans*	T20B12.7
19.	*Xenopus laevis*	Q4V7N8
20.	*Babesia bovis*	BBOV_I003760
21.	*Oryza sativa subsp. Japonica*	Q5W6R4
22.	*Homo sapiens*	Q6FI81
23.	*Eimeria brunetti*	EBH_0015930
24.	*Theileria parva*	TA20710
25.	*Neospora caninum*	BN1204_059410

Accession Numbers for Sequences used to perform MSA and generate phylogenetic tree of IscU/ NifU:

S. No.	Organism	Accession No.
1.	*Plasmodium vivax Sal-I*	PVX_117755
2.	*Plasmodium berghei ANKA*	PBANKA_0706000
3.	*Plasmodium malariae UG01*	PmUG01_05021400
4.	*Plasmodium falciparum 3D7*	PF3D7_0824600
5.	*Plasmodium chabaudi chabaudi*	PCHAS_0715300
6.	*Plasmodium vinckei petteri*	YYG_04228
7.	*Plasmodium reichenowi CDC*	PRCDC_0823900
8.	*Plasmodium ovale curtisi GH01*	PocGH01_05016300
9.	*Plasmodium cynomolgi strain B*	PCYB_051660
10.	*Plasmodium inui San Antonio 1*	C922_02656
11.	*Plasmodium knowlesi strain H*	PKNH_1318600
12.	*Plasmodium yoelli yoelli*	PYYM_1319000
13.	*Saccharomyces cerevisiae*	Q03020
14.	*Arabidopsis thaliana*	At3g01020
15.	*Mus musculus*	Q9D7P6
16.	*Oryza sativa*	Os01g0662600
17.	*Homo sapiens*	Q9H1K1
18.	*Escherichia coli*	P0ACD4

Chapter 3

Characterization of cytoplasmic [Fe-S] cluster biogenesis (CIA) pathway protein Dre2 from *P. vivax*

Characterization of cytoplasmic [Fe-S] cluster biogenesis (CIA) pathway protein Dre2 from *P. vivax*

3.1 Introduction

[Fe-S] clusters are one of the most critical cofactors regulating various essential biological processes such as DNA repair and metabolism, electron transfer reactions, transcription, sensing environmental stimuli, maintaining protein conformations etc. In prokaryotes, three [Fe-S] biogenesis pathways have been reported viz: ISC, SUF, and NIF, that provides [Fe-S] clusters to the bacterial cytoplasm. But in eukaryotic organisms, due to compartmentalization, the ISC and SUF pathways have been transferred to mitochondria and plastids respectively. In addition, a third pathway, the CIA pathway has also been reported to fulfil their cytosolic and nuclear need for [Fe-S] clusters. While the CIA pathway and its components have been extensively studied from various organisms such as *Arabidopsis thaliana*, *Saccharomyces cerevisiae*, and humans (Imlay et al., 2006; Ayalo-Castro et al., 2008), they have not been detailed as yet from any of the Apicomplexans, including *Plasmodium*, except a recent report where few of the homologs of CIA pathway have been identified from *Plasmodium falciparum* and *Toxoplasma gondii,* suggesting a functional CIA machinery in these parasites (Tsaousis et al., 2014; Ke and Mather, 2017). Thus to study this pathway in detail from *Plasmodium*, we identified all the major players of the CIA pathway from one of the major human parasite *Plasmodium vivax*, based on conserved domain analysis and BLAST results. Further we characterized one of these proteins; Dre2 to elucidate its function during the life cycle of the parasite.

In *Arabidopsis*, hypomorphic Dre2 mutant and mutants of other CIA pathway components [(AE7 (Cia2), MET18 (MMS19), ATM3 (Atm1), and GRXS17 (GLRX3)] led to the accumulation of DNA damage and activated DNA damage response (Wang et al., 2019), suggesting the essentiality of CIA components in the living system. Reports have shown that deficiency in the Dre2-Tah18 complex elicits DNA damage checkpoint and iron regulon, which is associated with maintaining genome integrity. In yeast, Dre2-depleted cells resulted in deficiency of cytoplasmic [Fe-S] clusters where the scaffold protein Nbp35 was unable to form [4Fe-4S] clusters onto it, suggesting the importance of this initial component of CIA machinery (Pena-Diaz et

al., 2018; Netz et al., 2016). Visualising the importance of this protein in functionality of an organism and the fact that this protein has not been studied from any of the Apicomplexans including *Plasmodium*, we characterized the Dre2 protein from *Plasmodium vivax*. For the same, we amplified the gene encoding the Dre2 protein from *P. vivax* infected patients blood, cloned it and expressed the recombinant protein in a prokaryotic based heterologous system. Further to decipher the functional role of Dre2 in the parasite, we performed immune-localization studies to identify the functional site of the protein, analysed its ability to bind [Fe-S] clusters (both *in silico* and *in vitro*) for its own activity as well as for their transfer to scaffold/ apo protein and finally identified the interacting partners to assess its role in different essential life processes of the parasite.

3.2 Results

3.2.1 Identification of components of CIA pathway from Plasmodium vivax

In yeast, eight major proteins have been identified for the cytosolic biogenesis of [Fe-S] clusters - Nbp35, Nar1, Cfd1, Tah18, Dre2, Cia1, Cia2, and MMS19 (Netz et al., 2014; Tsaousis et al., 2014). Thus, to initiate our studies, we mined the PlasmoDB database to search homologues of components of CIA pathway from *P. vivax* based on conserved domain, multiple sequence alignments and signature motifs **(Table 3.1)**. We could identify all the major components of the CIA pathway from *Plasmodium vivax* as shown in **Figure 3.1** (Gene ID shown overlapping their counterparts from *S. cerevisiae*).

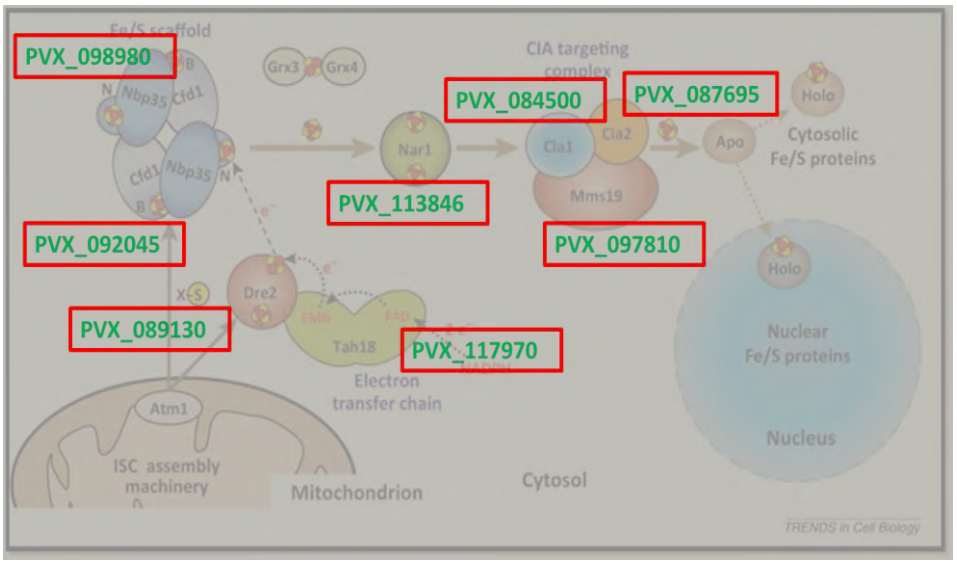

Figure 3.1: *P. vivax* homologs of the CIA pathway as identified from PlasmoDB

Table 3.1: Identification of Cytoplasmic [Fe-S] cluster assembly proteins from *P. vivax*

PlasmoDB Id	PlasmoDB Nomenclature	Conserved Domain Analysis	Function
PVX_098980	Cytosolic [Fe-S] cluster assembly factor NBP35, putative	ParA: NUBPL iron-transfer P-loop NTPase	Scaffold complex, assembly, transient binding of [4Fe–4S] cluster
PVX_092045	Hypothetical protein, conserved	Mrp_NBP35: Mrp/NBP35 ATP-binding protein family	Scaffold complex, assembly, and transient binding of [4Fe–4S] cluster
PVX_089130	[Fe-S] cluster assembly protein DRE2, putative	Cytokine-induced anti-apoptosis inhibitor 1(CIAPIN1) Superfamily	Electron acceptor from NADPH–Tah18
PVX_117970	Flavodoxin domain-containing protein	CyPoR like: NADPH cytochrome p450 reductase (CYPOR)	Electron transfer from NADPH to Dre2
PVX_113846	Cytosolic [Fe-S] cluster assembly factor NAR1, putative	Nar1: Iron only hydrogenase large subunit	CIA adaptor protein, mediates contact between early and late parts of CIA machinery
PVX_084500	Cytosolic iron-sulfur protein assembly protein 1, putative	WD40: WD40 domain	Docking site of the CIA targeting complex
PVX_087695	Hypothetical protein, conserved/ Cia2 putative*	Uncharacterized conserved protein	Component of CIA targeting complex
PVX_097810	Hypothetical protein, conserved	MMS19_N: Dos2-interacting transcription regulator of RNA-Pol-II	Insertion of [Fe-S] clusters into target apo-proteins

After identification of components of the CIA pathway, we proceeded with the amplification, cloning and characterization of Dre2 protein from the parasite.

3.2.2 Amplification of Dre2 gene from P. vivax infected patient's blood sample:

The genomic and mRNA sequence of Dre2, putative from *P. vivax* Salvador I (PVX_089130) was retrieved from PlasmoDB and used for designing the primers. The gene is 1789bp in length and is present on chromosome no. 5, spanning the region between 335,358 - 337,146 (- strand). It consists of an upstream 5'UTR and four introns and codes for an mRNA of length 1177bp, including the UTR region. Three primers were designed to amplify the complete *Pv*Dre2 coding gene from the cDNA isolated from *P. vivax* clinical isolates **(Figure 3.2)**. The sequence of the primers used is given in **Table 3.2**. The 1177bp region spanning the 5' UTR was amplified using the forward primer PVDREFU and the reverse primer PVDRER, while the forward primer PVDREF along with PVDRER was used to amplify 729bp region without the UTR region **(Figure 3.3)**. For both the amplifications, 200 ng of cDNA was subjected to a PCR cycle at 94 °C for 3 min followed by 35 cycles at 94 °C for 1 min, 58 °C for 1 min and 72 °C for 2 min, followed by post-extension of 72 °C for 4 min. The obtained amplicons were purified using a QIAquick Gel Extraction kit (Qiagen, Germany) and sequenced commercially.

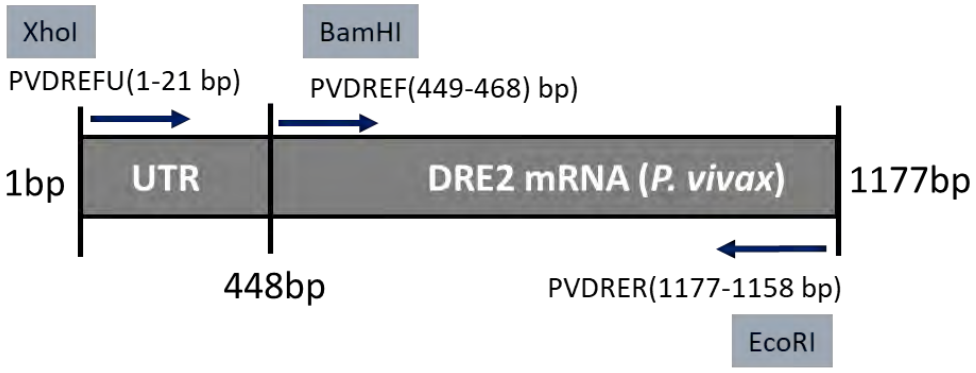

Figure 3.2: Primers designed for amplification of *Dre2* gene from *P. vivax*

Table 3.2: Primer sequences for amplification of the *Pv*Dre2 gene

Lab Id	Primer sequence	Rest. Site
PVDREFU	5′ GCACTCGAGAAAAAGGCATACTAAAAAGGC 3'	XhoI
PVDREF	5′ CAAGGATCCATGATGAACTTCGCAGATAC 3'	BamHI
PVDRER	5′ CCGGAATTCTCAGTTAGGTTCATTGTCCA 3′	EcoRI

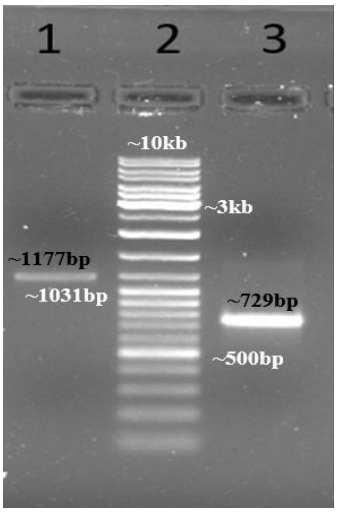

Figure 3.3: *P. vivax Dre2* full gene amplification from cDNA. 1: *PvDre2* gene with 5' UTR, 2: Gene Ruler Ladder mix SM0331, 3: *PvDre2* gene without 5' UTR

3.2.3 Sequence Analysis and Multiple Sequence Alignment

The Dre2 sequences obtained from *P. vivax* Indian isolates (5 isolates) were analysed both at the nucleotide and amino acid level, by performing multiple sequence alignment with its homologues and orthologues from *P. vivax* Salvador I, different *Plasmodium spp.,* apicomplexans and various eukaryotes. The Indian *Pv*Dre2 isolates showed a complete match to *P. vivax* Sal-1 (PVX_089130), except in one isolate where a change from Asparagine to Tyrosine was observed towards the N- terminal of the protein at codon 116 **(Figure 3.4)**.

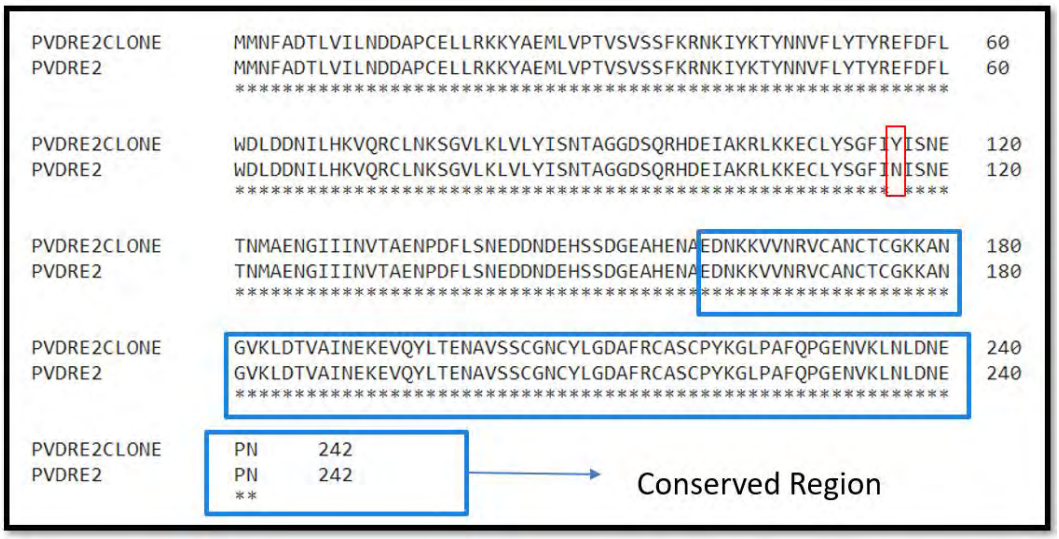

Figure 3.4: Sequence alignment of *Pv*Dre2 Indian isolate (*Pv*Dre2 clone*)* with *P. vivax Sal-1* (*Pv*Dre2). A change of amino acid from N→Y detected at 116 codon

Within the *Plasmodium* genus, *Pv*Dre2 showed a percent identity of ~60% to ~94%, suggesting high sequence conservation for Dre2 **(Figure 3.5A)**. Multiple sequence alignment of *Plasmodium* Dre2 with that from other Apicomplexans, showed percent identity in the range of ~23% to ~34% **(Figure 3.5B)**, while when compared with orthologues from higher eukaryotes, *Pv*Dre2 showed percent identity in the range of ~23% to ~29% **(Figure 3.5C)**.

A)

1:	Plasmodium_vivax_Indian	100.00	63.90	68.05	63.07	67.23	93.39	90.08	89.67	61.98	61.16	60.74	62.24
2:	Plasmodium_falciparum	63.90	100.00	67.18	98.12	67.77	65.15	63.07	64.32	63.89	61.75	62.15	64.54
3:	Plasmodium_malariae	68.05	67.18	100.00	66.41	73.55	69.29	67.22	67.22	65.08	65.74	65.74	65.34
4:	Plasmodium_reichenowi	63.07	98.12	66.41	100.00	67.77	64.32	62.24	63.49	64.29	62.15	62.55	64.94
5:	Plasmodium_ovale	67.23	67.77	73.55	67.77	100.00	68.91	66.39	67.65	67.90	65.70	65.70	66.94
6:	Plasmodium_cynomolgi	93.39	65.15	69.29	64.32	68.91	100.00	92.15	92.98	61.98	61.57	61.16	62.24
7:	Plasmodium_inui	90.08	63.07	67.22	62.24	66.39	92.15	100.00	89.26	61.16	60.33	59.92	61.41
8:	Plasmodium_knowlesi	89.67	64.32	67.22	63.49	67.65	92.98	89.26	100.00	61.98	60.74	60.33	62.24
9:	Plasmodium_yoelii	61.98	63.89	65.08	64.29	67.90	61.98	61.16	61.98	100.00	91.27	91.67	96.03
10:	Plasmodium_chabaudi	61.16	61.75	65.74	62.15	65.70	61.57	60.33	60.74	91.27	100.00	98.41	93.23
11:	Plasmodium_vinckei	60.74	62.15	65.74	62.55	65.70	61.16	59.92	60.33	91.67	98.41	100.00	94.02
12:	Plasmodium_berghei	62.24	64.54	65.34	64.94	66.94	62.24	61.41	62.24	96.03	93.23	94.02	100.00

B)

1:	Plasmodium_vivax_Indian	100.00	63.90	61.98	62.40	26.88	22.77	30.21	28.40	29.37	33.12	27.54	22.75	24.77
2:	Plasmodium_falciparum	63.90	100.00	61.75	64.54	28.04	23.04	27.92	24.42	27.61	31.88	28.30	21.96	24.20
3:	Plasmodium_chabaudi	61.98	61.75	100.00	93.25	30.16	25.00	28.21	27.91	28.40	31.25	29.05	23.36	22.58
4:	Plasmodium_berghei	62.40	64.54	93.25	100.00	29.63	24.51	28.72	27.91	28.40	31.25	29.52	22.90	22.58
5:	Dictyostelium_discoideum	26.88	28.04	30.16	29.63	100.00	23.66	29.31	30.50	31.15	30.16	29.32	26.43	28.21
6:	Cryptococcus_neoformans	22.77	23.04	25.00	24.51	23.66	100.00	25.68	23.20	33.18	28.27	24.23	25.21	23.24
7:	Babesia_bovis	30.21	27.92	28.21	28.72	29.31	25.68	100.00	27.11	29.61	37.18	38.06	30.88	28.28
8:	Paramecium_tetraurelia	28.40	24.42	27.91	27.91	30.50	23.20	27.11	100.00	31.74	35.38	29.17	31.36	28.63
9:	Cryptomonas_curvata	29.37	27.61	28.40	28.40	31.15	33.18	29.61	31.74	100.00	35.88	35.44	31.55	33.33
0:	Eimeria_brunetti	33.12	31.88	31.25	31.25	30.16	28.27	37.18	35.38	35.88	100.00	36.08	47.09	43.83
1:	Theileria_parva	27.54	28.30	29.05	29.52	29.32	24.23	38.06	29.17	35.44	36.08	100.00	31.53	28.42
2:	Besnoitia_besnoiti	22.75	21.96	23.36	22.90	26.43	25.21	30.88	31.36	31.55	47.09	31.53	100.00	64.86
3:	Toxoplasma_gondii	24.77	24.20	22.58	22.58	28.21	23.24	28.28	28.63	33.33	43.83	28.42	64.86	100.00

C)

1:	Plasmodium_vivax_Indian	100.00	61.98	61.41	61.00	62.24	25.00	27.46	28.72	26.29	27.18	28.42	27.07
2:	Plasmodium_yoelii	61.98	100.00	91.27	91.67	96.03	27.00	30.57	28.06	28.72	29.08	28.42	29.83
3:	Plasmodium_chabaudi	61.41	91.27	100.00	98.41	93.23	27.50	30.05	27.18	28.87	28.72	28.96	30.39
4:	Plasmodium_vinckei	61.00	91.67	98.41	100.00	94.02	27.50	30.05	27.18	28.87	28.72	28.96	30.39
5:	Plasmodium_berghei	62.24	96.03	93.23	94.02	100.00	27.00	30.57	27.55	28.35	28.72	28.96	29.83
6:	Saccharomyces_cerevisiae	25.00	27.00	27.50	27.50	27.00	100.00	29.89	24.73	27.64	27.34	27.16	26.27
7:	Schizosaccharomyces_pombe	27.46	30.57	30.05	30.05	30.57	29.89	100.00	29.53	34.52	31.76	28.26	29.07
8:	Xenopus_laevis	28.72	28.06	27.18	27.18	27.55	24.73	29.53	100.00	60.20	61.56	34.88	35.34
9:	Mus_musculus	26.29	28.72	28.87	28.87	28.35	27.64	34.52	60.20	100.00	82.20	33.85	33.87
10:	Homo_sapiens	27.18	29.08	28.72	28.72	28.72	27.34	31.76	61.56	82.20	100.00	35.77	35.06
11:	Arabidopsis_thaliana	28.42	28.42	28.96	28.96	28.96	27.16	28.26	34.88	33.85	35.77	100.00	51.34
12:	Oryza_sativa	27.07	29.83	30.39	30.39	29.83	26.27	29.07	35.34	33.87	35.06	51.34	100.00

Figure 3.5: Percent identity matrix for *P. vivax* Dre2 from Indian isolates with A) other *Plasmodium* species B) Other apicomplexans C) higher eukaryotes

3.2.4 Conserved Domain Analysis of PvDre2

The general domain architecture for Dre2 includes highly divergent N- terminal domain, a disordered linker region and an evolutionary conserved C- terminal CIAPIN1 (Cytokine Induced Apoptosis Inhibitor 1) domain. The N-terminal domain of Dre2 has structural similarity with S-adenosyl-L-methionine-dependent methyl transferases, but has not been reported to bind S-adenosyl-L-methionine (Song et al., 2013). It is said to be required for correct assembly of the [2Fe-2S] clusters. The linker part of Dre2, which is highly disordered or less foldable, plays a significant role in acting as a platform for interaction with various other proteins, such as Tah18/NDOR1 and glutaredoxins (Wang et al., 2019). The C-terminal of Dre2 has two types of conserved cysteine Motifs: Motif I arranged in a slightly variable CX_nCX_2CXC pattern (with n = 5–15 residues), followed at a ~42 residue distance by Motif II with the invariable $CX_2CX_7CX_2C$ pattern (C is Cysteine and X is any amino acid). These motifs are responsible for binding of two types of [Fe-S] clusters: [4Fe-4S] at Motif II and [2Fe-2S] at Motif I. The Motif-II bound [4Fe-4S] is highly sensitive towards oxygen and readily converts to [2Fe-2S], while Motif-I bound [2Fe-2S] is labile in presence of oxygen (Netz et al., 2016; Zhang et al., 2016).

The obtained *Plasmodium vivax* Dre2 sequences when subjected to a Conserved domain analysis using NCBI Conserved Domain Search showed the presence of Cytokine-induced anti-apoptosis inhibitor 1 (CIAPIN1) domain towards the C-terminal end from amino acid position 168-235. But no SAM-methyl transferase-like domain at N-terminal was observed for *P. vivax* **(Figure 3.6)**.

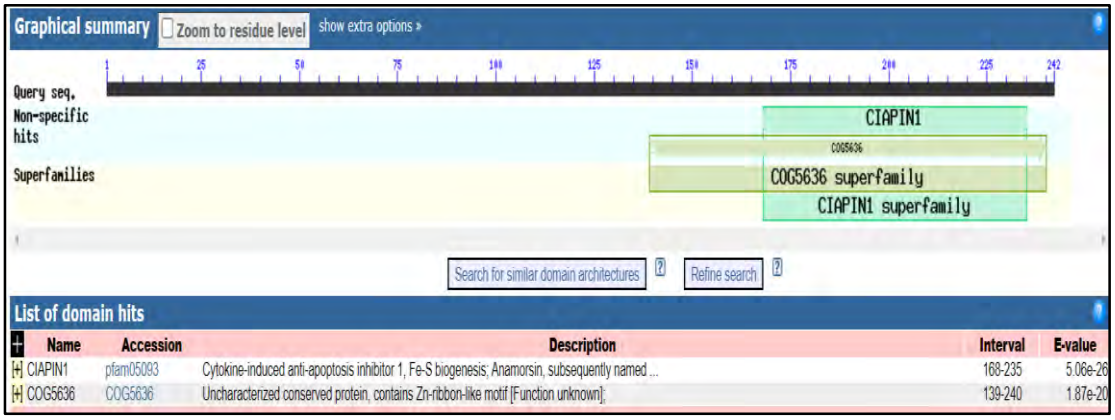

Figure 3.6: Conserved domain analysis of *Pv*Dre2 protein

As mentioned above, the C-terminal CIAPIN1 domain consists of two conserved cysteine motifs: Motif I (CX_nCX_2CXC) and Motif II ($CX_2CX_7CX_2C$). When we aligned the C-terminal CIAPIN1 domain of the obtained *Pv*Dre2 sequences with other *Plasmodium sp*, Apicomplexans, and higher eukaryotes using Clustal Omega, we found the first cysteine residue of Motif 1 to be missing in both *P. falciparum* and *P. vivax* Dre2 sequences **(Figure 3.7 a1)**, as reported previously for *Plasmodium* and *Encephalitozoon* species (Netz et al., 2016). However, when the Dre2 sequences of the rodent malaria parasites (*P. berghei*, *P. chabaudi*, *P. yoelii,* and *P. vinckei*) were aligned with other higher eukaryotes and apicomplexans, it showed perfect alignment for Motif-I sequence **(Figure 3.7 b1)** with all the four cysteine residues conserved. Motif-II was found to be highly conserved in *Plasmodium* **(Figure 3.8 a2 & b2)** and all eukaryotes with the structured twin CX2C motif.

a1

```
Plasmodium_vivax_Indian     EAHENAEDNKKVVNRVCANCTCGKKANGVKLD-TVAINEKEVQYLTENAVSSCGNCYLGD   212
Plasmodium_vivax            EAHENAEDNKKVVNRVCANCTCGKKANGVKLD-TVAINEKEVQYLTENAVSSCGNCYLGD   212
Plasmodium_knowlesi         EAYQNAEDNKKVVNRVCANCTCGKKTNGVKLD-KVTINEKEVQYLTENAVSSCGNCYLGD   212
Plasmodium_cynomolgi        EAYENAEDNKKVVNRVCANCTCGKKANGVKLD-KVAINEKEVQYLTENAVSSCGNCYLGD   212
Plasmodium_malariae         EAYEDEDDKKKVVNRVCDNCTCGKKKNAINQE-KII-IGENVEYITENVVSSCGNCYLGD   236
Plasmodium_reichenowi       DIYNNEDDKKKVVNRVCDNCTCGKKEKLLNSENKVLINEKDGEYITENVVSSCGNCYLGD   236
Plasmodium_ovale            ETYENKEDNKKVVNRVCDNCTCGRKKNDVNLE-KISISGNEVEYVTENVVSSCGNCYLGD   213
Plasmodium_inui             EAYENAEDNKKVVNRVCANCTCGKKTTGIKLD-KVAINEKEVQYLTENAVSSCGNCYLGD   212
Plasmodium_falciparum       DLYNNEDDKKKVVNRVCDNCTCGKKEKLLNSENKVLINEKDGEYITENVVSSCGNCYLGD   236
Plasmodium_yoelii           EIYEKCEDKKKVVNRVCDNCTCGKKEKAMNLE-KIKINDNEVEYSTENVVSSCGNCYLGD   223
Plasmodium_chabaudi         EINEKCEDKKKAVNRVCDNCTCGKKEKAMNLE-KIQINSNEVEYNTENVVSSCGNCYLGD   222
Plasmodium_vinckei          EINEKCEDKKKAVNRVCDNCTCGKKEKAMNLE-KIKINSNEVEYNTENVVSSCGNCYLGD   222
Plasmodium_berghei          EIYEKCEDKKKVVNRVCDNCTCGKKEKAMNLE-KIKINDNEVEYNTENVVSSCGNCYLGD   222
                            :  :. :*:**.***** *****:* . :: : .:    :: :* ***.***********
```

b1

```
Plasmodium_berghei          SSDEE--------------IYEKCED-KKKVVNRVCDNCTCGKKEKAMNLEKIKI-----   199
Plasmodium_chabaudi         SSDDE--------------INEKCED-KKKAVNRVCDNCTCGKKEKAMNLEKIQI-----   199
Plasmodium_vinckei          SSDDE--------------INEKCED-KKKAVNRVCDNCTCGKKEKAMNLEKIKI-----   199
Plasmodium_yoelii           SSDEE--------------IYEKCED-KKKVVNRVCDNCTCGKKEKAMNLEKIKI-----   200
Homo_sapiens                DSDELLDPEDLKKPDPASLRAASCGEG---KKRKACKNCTCGLAEELEKEKSR-------   263
Mus_musculus                DSDELLDPEDLKRPDPASLKAPSCGEG---KKRKACKNCTCGLAEELEREQSK-------   261
Saccharomyces_cerevisiae    EEEELIDEDGSGKSMI---TMITCGK-SKTKKKKACKDCTCGMKEQEENEINDIRSQQDK   287
Arabidopsis_thaliana        DEDSLLTEEDLMKPQLP--VASGCE-----TTKKACKNCVCGRAEIEEKAVKLGL-----   221
Caenorhabditis_elegans      DEDGLLQEEDFEKPTGDQLKAGGCGPDDPNKKKRACKNCSCGLAEQEELEKM--------   191
Xenopus_laevis              DSDELLDQEDLKKPAPSSLLASGCGEGS-EKKRKACKNCTCGLAEELEAEKTP-------   262
Babesia_bovis               -------SLDDYIPSAP--AAESCD-----TKPRPCANCNCGRAERVNTDAKE-------   207
Toxoplasma_gondii           DESTLIDPTESYQPLGK--DRSSCA-----SRPKACPNCTCGRKEAEEAAEKEER-----   367
Eimeria_brunetti            DEDSLIDPKETYTPLGK--GRSDCA-----SRPRACANCTCGRKEMEEKAEKEKF-----   167
Theileria_parva             -------PIDGYISKAP--DYESCS-----TKPRACANCTCGRAERENLNSTDSNANSTD   250
Neospora_caninum            DEATLIDPAEAYQPLGK--DRSSCA-----SRPKACPNCTCGRKEAEEAAEK--T-----   223
                                                          *        : * :* **  *
```

Figure 3.7: Conserved cysteine residue analysis of Motif I of CIAPIN1 domain of Dre2. a1: MSA of Motif-I of *P. vivax Indian* sequence with another *Plasmodium spp*. **b1:** MSA of Motif-I of Rodent *Plasmodium spp*. with higher eukaryotes and Apicomplexans. The highlighted residues indicate conserved cysteine residues.

a2

```
Plasmodium_vivax_Indian   GVKLD-TVAINEKEVQYLTENAVSSCGNCYLGDAFRCASCPYKGLPAFQPGENVKLNLDNEPN--   242
Plasmodium_vivax          GVKLD-TVAINEKEVQYLTENAVSSCGNCYLGDAFRCASCPYKGLPAFQPGENVKLNLDNEPN--   242
Plasmodium_knowlesi       GVKLD-KVTINEKEVQYLTENAVSSCGNCYLGDAFRCASCPYKGLPAFQPGENVKLNLDNEPN--   242
Plasmodium_cynomolgi      GVKLD-KVAINEKEVQYLTENAVSSCGNCYLGDAFRCASCPYKGLPAFQPGENVKLNLDNEPN--   242
Plasmodium_malariae       AINQE-KII-IGENVEYITENVVSSCGNCYLGDAFRCASCPYKGLPAFQPGENVKLNLNNESN--   266
Plasmodium_reichenowi     LLNSENKVLINEKDGEYITENVVSSCGNCYLGDAFRCASCPYKGLPAFQPGENVKLNLNNESN--   266
Plasmodium_ovale          DVNLE-KISISGNEVEYVTENVVSSCGNCYLGDAFRCASCPYKGLPAFQPGENVKLNLNNESN--   243
Plasmodium_inui           GIKLD-KVAINEKEVQYLTENAVSSCGNCYLGDAFRCASCPYKGLPAFQPGENVKLNLDVRQNEG  244
Plasmodium_falciparum     LLNSENKVLINEKDGEYITENVVSSCGNCYLGDAFRCASCPYKGLPAFQPGENVKLNLNNESN--   266
Plasmodium_yoelii         AMNLE-KIKINDNEVEYSTENVVSSCGNCYLGDAFRCGSCPYKGLPAFQPGENVKLNLNNEQN--   253
Plasmodium_chabaudi       AMNLE-KIQINSNEVEYNTENVVSSCGNCYLGDAFRCGSCPYKGLPAFQPGENVKLNLNNDQN--   252
Plasmodium_vinckei        AMNLE-KIKINSNEVEYNTENVVSSCGNCYLGDAFRCGSCPYKGLPAFQPGENVKLNLNNDQN--   252
Plasmodium_berghei        AMNLE-KIKINDNEVEYNTENVVSSCGNCYLGDAFRCGSCPYKGLPAFQPGENVKLNLNNEQN--   252
                           :: : .:    :: :* ***.***************.******************:   *
```

b2

```
                                                  *          : * :* **  *
Plasmodium_berghei        -N------------------DNEVEYNTENVVSSCGNCYLGDAFRCGSCPYKGLPAFQP      239
Plasmodium_chabaudi       -N------------------SNEVEYNTENVVSSCGNCYLGDAFRCGSCPYKGLPAFQP      239
Plasmodium_vinckei        -N------------------SNEVEYNTENVVSSCGNCYLGDAFRCGSCPYKGLPAFQP      239
Plasmodium_yoelii         -N------------------DNEVEYSTENVVSSCGNCYLGDAFRCGSCPYKGLPAFQP      240
Homo_sapiens              ------------------------EQ-MSSQPKSACGNCYLGDAFRCASCPYLGMPAFKP      298
Mus_musculus              ------------------------AQ--SSQPKSACGNCYLGDAFRCANCPYLGMPAFKP      295
Saccharomyces_cerevisiae  ----VVKFTEDEL-------TEIDF-TIDGKKVGGCGSCSLGDAFRCSGCPYLGLPAFKP      335
Arabidopsis_thaliana      ------------------------TED-QIENPQSSCGSCGLGDAFRCGTCPYKGLPPFKL      257
Caenorhabditis_elegans    ------------------------GQ-IAAEPKSSCGNCSLGDAFRCSTCPYLGQPPFKP      226
Xenopus_laevis            ------------------------ST-VPKAAPSACGNCYLGDAFRCASCPYLGMPAFKP      297
Babesia_bovis             ------------------------STVNADGPTSSCGKCYLGDAFRCANCPYRGMPAFAP      243
Toxoplasma_gondii         ------------------------RRKLETGEIRSSCGNCYLGDAFRCAGCPYRGMPAFKP      404
Eimeria_brunetti          ------------------------KKQLETGAIRSSCGNCYLGDAFRCAGCPYRGLPAFRP      204
Theileria_parva           FNANSTDFNGVDLTTNSKDVSGVDLVVDVDAPTSSCGNCYLGDAFRCDSCPYKGLPAFKP      310
Neospora_caninum          ------------------------RRKLESGEIRSSCGNCYLGDAFRCAGCPYRGMPAFKP      260
                                                  ..**.* *******  *** * * *
```

Figure 3.8: Conserved cysteine residues present in Motif II of CIAPIN1 domain of Dre2. a2: MSA of Motif-II of *P. vivax Indian* sequence with other *Plasmodium spp* **b2:** MSA of Motif-II of Rodent *Plasmodium spp*. with higher eukaryotes and Apicomplexans. The highlighted residues indicate conserved cysteine residues.

3.2.5 Phylogenetic analysis

The obtained Dre2 sequence along with homologues and orthologues from various other organisms was also subjected to MEGA X software to ascertain the evolutionary position of *Pv*Dre2 (Kumar et al., 2018; Saitou et al., 1987). The MSA was generated using 24 amino acid sequences including *Plasmodium spp*. (primate, rodent and avian), other Apicomplexan parasites (such as *T. gondii, B. bovis, N. caninum*), single-cell eukaryotes (*S. cerevisiae* and *D. discoideum*) and higher eukaryotes (Humans, Mice, *A. thaliana*, *X. laevis*) following the Neighbor-Joining approach. The evolutionary history of the organisms under study was represented by the bootstrap consensus tree

estimated from 1000 iterations. Branches corresponding to partitions reproduced in fewer than 50% of bootstrap replicates were collapsed. The evolutionary distances, measured in terms of the number of amino acid changes per site, were calculated using the JTT matrix-based approach. Less than 5% alignment gaps, missing data, and ambiguous bases were permitted at any location. All positions with less than 95% site coverage were eliminated. The final dataset contained 601 locations altogether **(Figure 3.9**).

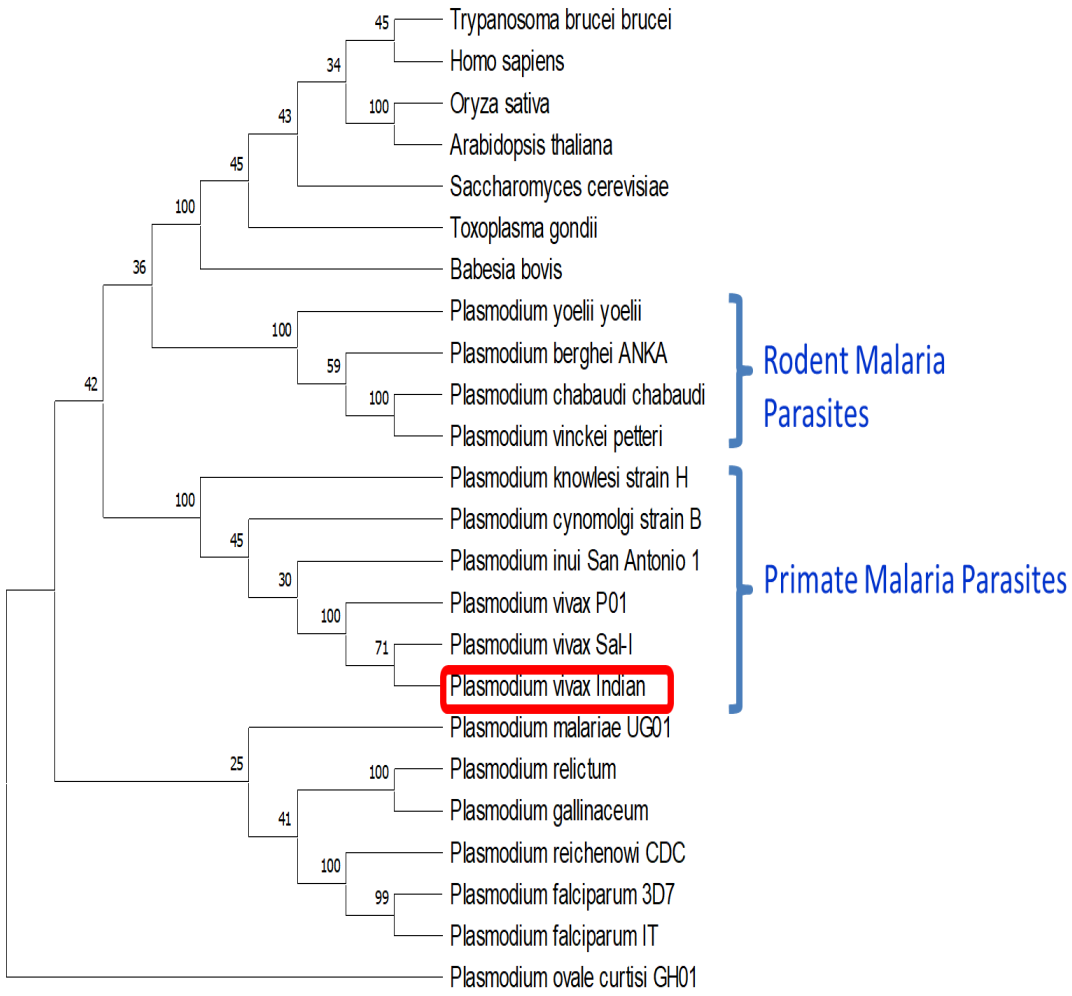

Figure 3.9: Phylogenetic analysis of Dre2 protein sequences. [Dre2 protein sequence of Indian *P. vivax* with orthologues]. Bootstrapping was done for 1000 iterations, and the percentage of trees in which the associated taxa clustered is shown next to branches.

Evolutionary analysis of *Pv*Dre2 sequence with different orthologs resulted in a tree where *Pv*Dre2 closely associated with other primate parasites *P. cynomolgi, P. knowlesi*, and *P. inui*. All the rodent malaria parasites formed a separate clade

indicating evolutionary divergence. All apicomplexans and higher eukaryotes formed a separate clade diverging from both rodent and primate malaria parasites **(Figure 3.9).**

3.2.6 Cloning of PvDre2 gene in pRSETA vector

Once the *Pv*Dre2 amplicon sequences were confirmed by Sanger sequencing and CDD analysis, they were subjected to cloning in pRSETA expression vector. For the same, the vector (pRSETA) and insert (*Pv*Dre2 amplicon) were double digested by BamHI and EcoRI restriction endonucleases and ligated using T4 DNA ligase **(Figure 3.10)**.

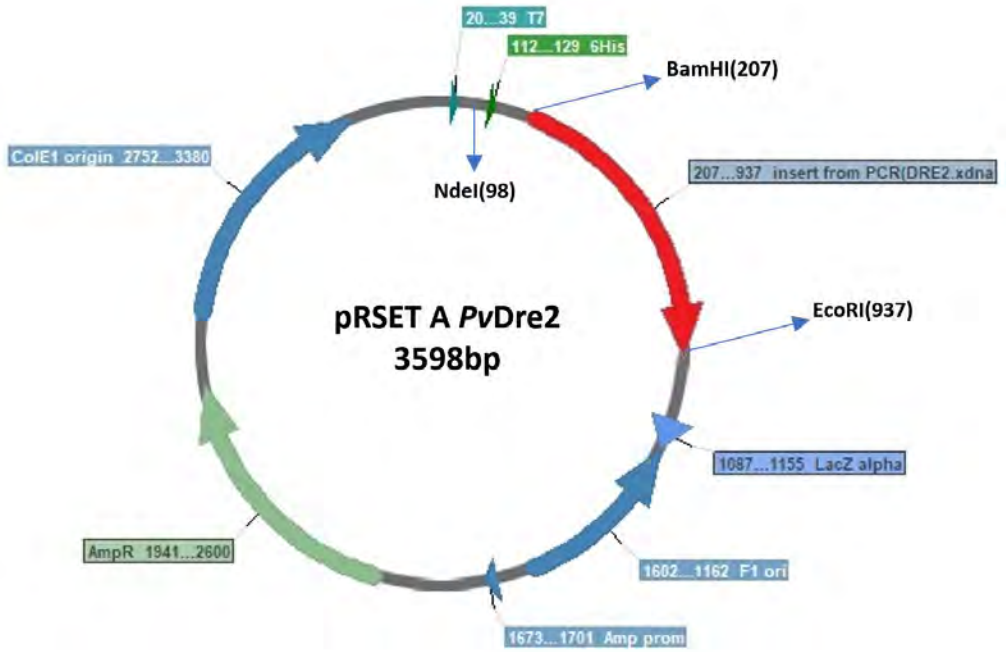

Figure 3.10: The pRSET A-*Pv*Dre2 clone map: The red region depicts the *Pv*Dre2 gene in the pRSETA backbone

To confirm the presence of Dre2 gene in the obtained recombinant colonies, various confirmation methods as described in Materials and Methods chapter were used:

1) G**el shift assay**: The band profiles for putative clones (colony no. 1 to 5) on agarose gel were different from a self-ligated plasmid and vector alone **(Figure 3.11a)**
2) **Colony PCR**: Using *Pv*Dre2 specific gene primers, we obtained amplification of *Pv*Dre2 gene which indicates the presence of *Pv*Dre2 recombinant plasmids in colony no. 1 to 5 **(Figure 3.11b)**
3) **Restriction endonucleases digestion**: The obtained *Pv*Dre2 recombinant molecule when digested with BamHI (RE site present in insert), linearized the putative clone plasmid. The linearized putative clone (~3.6 kb) when compared with linearized

pRSETA (~2.9 kb) exhibited the desired size difference **(Figure 3.11c)**. Once the *Pv*Dre2 clone was confirmed, to check the gene orientation *Pv*Dre2-pRSETA (recombinant molecule) clone was digested with EcoRI (RE site in insert) and NdeI (which was present in the pRSETA at the 98th position). The obtained bands at ~2.7kb and ~850bp confirmed the presence of *Pv*Dre2 in the correct orientation **(Figure 3.11d)**.

4) **Sequencing:** Final validation of the *Pv*Dre2 clone was performed by **Sanger sequencing** using T7 (T7 promoter and terminator) and gene-specific (*Pv*Dre2) primers, confirming the start codon presence in-frame.

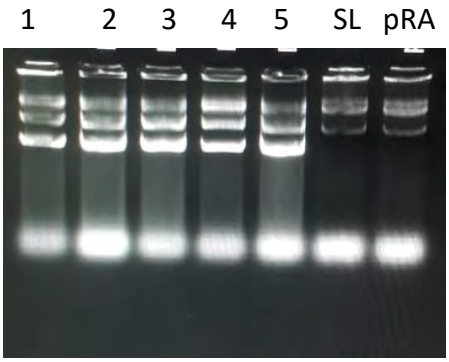

a)

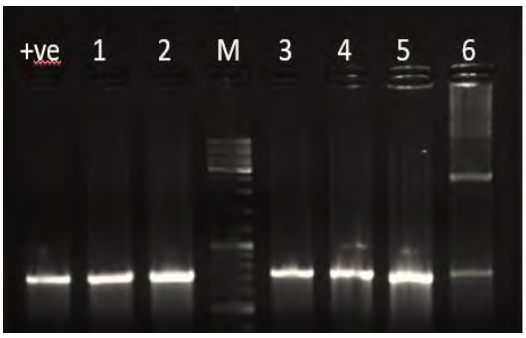

b)

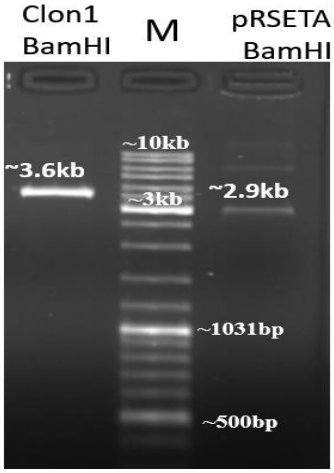

c)

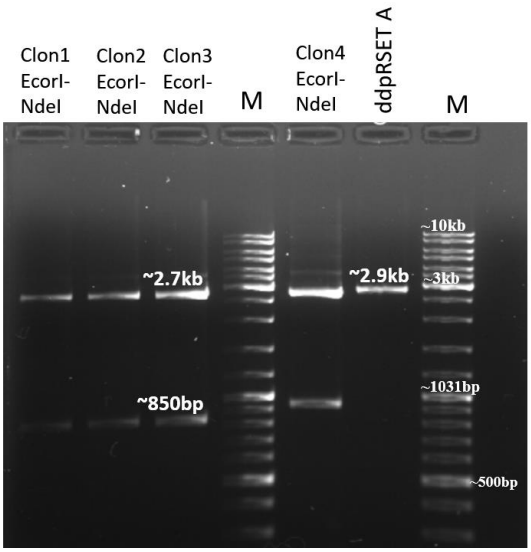

d)

Figure 3.11: Confirmation of Clone by a) Gel shift assay b) Colony PCR c) Restriction digestion using BamHI and d) Orientation check using restriction enzymes EcoRI and NdeI (M: Gene Ruler DNA Ladder Mix Fermentas SM0331; 1- 6: colony number after vector insert ligation and transformation; SL: self-ligated colony plasmid +ve: PCR Positive control; pRA: pRSETA vector)

3.2.7 PvDre2 Protein Expression in a prokaryotic heterologous system

To express the *Pv*Dre2 protein, the recombinant clone was transformed in *E. coli* BL21(DE3) pLysS cells. A single colony from these transformed cells was grown overnight at 37 °C from which the secondary culture was prepared by inoculating fresh media with 5% inoculum at 10^{th} hr. Once the OD_{600} reached 0.45-0.5, bacterial culture was induced with 0.5mM IPTG, after which 1 ml sample was collected at regular intervals from *Pv*Dre2 clone-induced, clone-uninduced, vector-induced, and vector-uninduced samples. These were subjected to SDS-PAGE to check for the presence of *Pv*Dre2 protein between 30-35kD **(Figure 3.12)**.

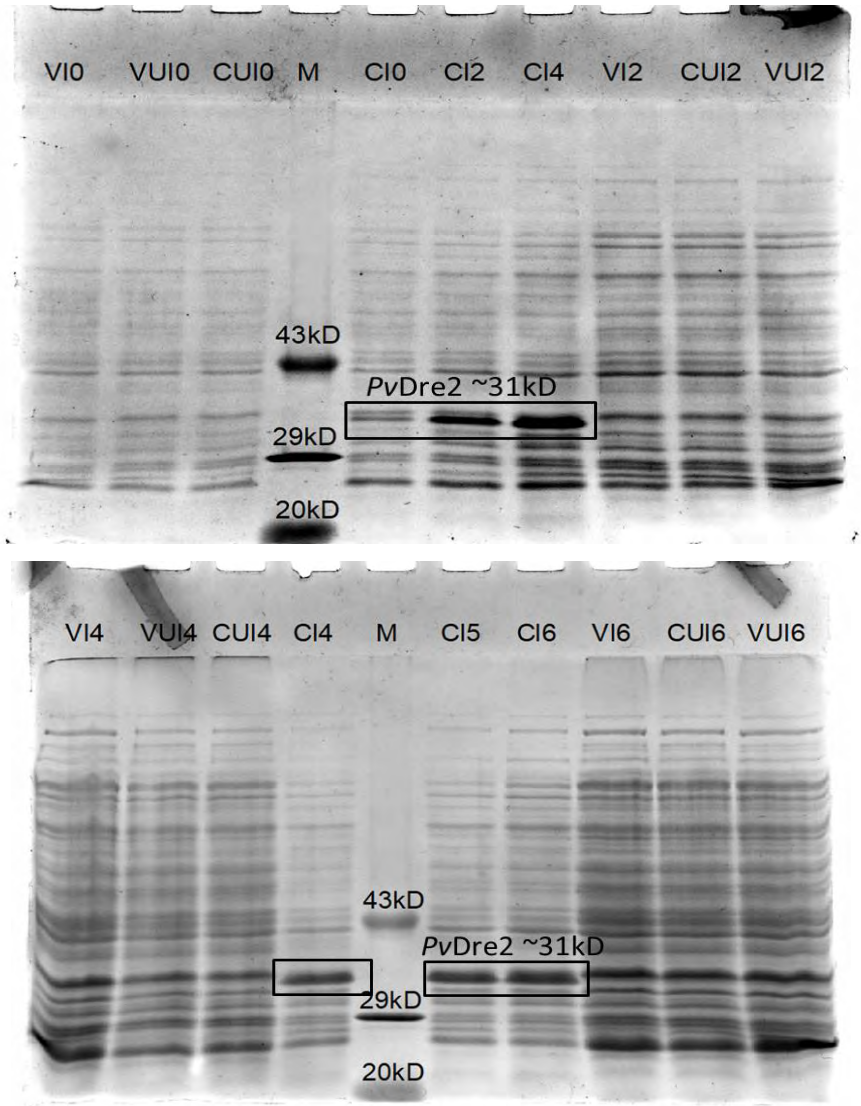

Figure 3.12: Overexpression of full-length *Pv*Dre2 Protein in *E. coli* BL21(DE3) pLysS cells. M: Protein Low Molecular Weight Marker (Genei); VUI: pRSETA vector uninduced sample; VI: pRSETA vector induced sample; CUI: pRSETA *Pv*Dre2 clone uninduced sample; CI: pRSETA *Pv*Dre2 clone induced sample

The protein expression was further validated by western blot analysis of the bacterial lysate **(Figure 3.13)** using the His fusion tag and anti-His antibodies (Qiagen, Germany). A band at ~31kD in the recombinant clone-induced sample shows the presence of desired protein.

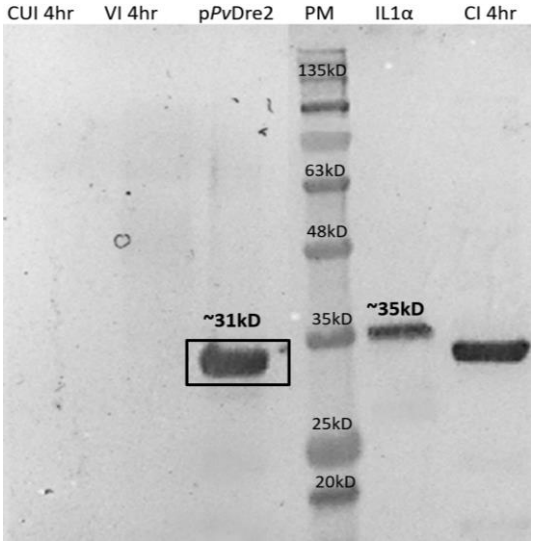

Figure 3.13: Confirmation of *PvDre2* protein expression using anti-His antibodies in a western blot. Control: IL1α, Human; PM: Prestained protein molecular weight marker (BLUeye, BR Biochem life sciences); VI: pRSETA vector induced sample; CUI: pRSETA *Pv*Dre2 clone uninduced sample; CI: pRSETA *Pv*Dre2 clone induced sample; p*Pv*Dre2: Ni-NTA Purified Dre2

3.2.8 Protein purification

After successfully confirming the over-expression of *Pv*Dre2 protein in bacterial cells, the protein was purified for further downstream experiments such as biochemical reconstitution, sub-cellular localization and co-immune precipitation assays using Ni-NTA chromatography **(Figure 3.14)**. The eluent fraction with maximum intensity for the required band and minimum/absence of non-specific bands were included for further experiments.

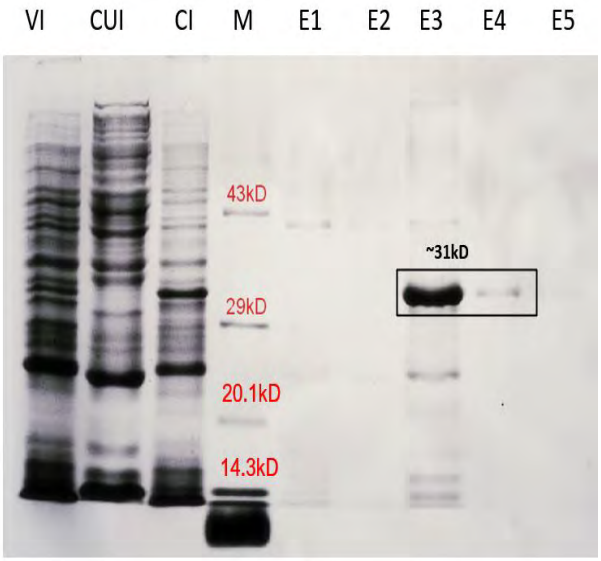

Figure 3.14: Purification of His-Tagged *Pv*Dre2 Protein. M: Protein Molecular Weight Marker -Lower range (Merck); CI: pRSETA-*Pv*Dre2 clone induced sample; CUI: pRSETA- *Pv*Dre2 clone uninduced sample; VI: pRSETA induced sample, E1-E5-eluent fractions

3.2.9 Subcellular localization of PvDre2 protein

3.2.9.1 In silico targeting predictions for PvDre2

In higher eukaryotes such as humans, *Arabidopsis*, and yeast, Dre2 is shown to be localized at multiple subcellular locations such as cytosol, mitochondria, and nucleus, due to its multifunctional roles (Buzas et al., 2014; Yoshikawa et al., 2016; Wang et al., 2019; Yamaguchi et al., 2019). Thus to predict the functional site of *Pv*Dre2 we subjected the *Pv*Dre2 (PVX_089130) protein sequence to various online available tools such as cNLS Mapper (nuclear targeting), PlasmoAP (Apicoplast targeting), and Mitoprot II (mitochondrial targeting). cNLS Mapper suggested both Monopartite (consisting of a single stretch of basic amino acids) and Bipartite (consisting of two stretches of basic amino acids separated by a linker region) type of nuclear localization signals. The scores between 3 to 5, suggested dual targeting for the protein to the cytosol and nucleus **(Figure 3.15)**. When the *Pv*Dre2 sequence was submitted to PlasmoAP, it showed "0" score for both signal peptide and apicoplast targeting peptide suggesting that the protein is not localized to the Apicoplast. The Mitoprot analysis showed a very low score of 0.04 and no cleavage site could be identified, indicating no targeting to mitochondria for the protein. However, the *Pv*Dre2 protein consists of twin cysteine motifs (CXXC) at Motif-II of CIAPIN1 domain. These cysteine twin motifs are responsible for the translocation and retainment of these proteins into the mitochondrial intermembrane space (IMS) (Banci et al., 2011) **(Figures 3.16)**, suggesting the *Pv*Dre2 protein to be associated with mitochondrial membrane.

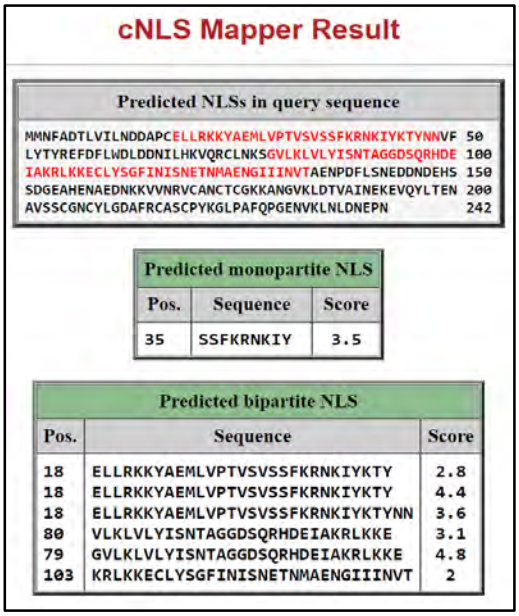

cNLS Mapper Result

Predicted NLSs in query sequence

```
MMNFADTLVILNDDAPCELLRKKYAEMLVPTVSVSSFKRNKIYKTYNNVF 50
LYTYREFDFLWDLDDNILHKVQRCLNKSGVLKLVLYISNTAGGDSQRHDE 100
IAKRLKKECLYSGFINISNETNMAENGIIINVTAENPDFLSNEDDNDEHS 150
SDGEAHENAEDNKKVVNRVCANCTCGKKANGVKLDTVAINEKEVQYLTEN 200
AVSSCGNCYLGDAFRCASCPYKGLPAFQPGENVKLNLDNEPN         242
```

Predicted monopartite NLS

Pos.	Sequence	Score
35	SSFKRNKIY	3.5

Predicted bipartite NLS

Pos.	Sequence	Score
18	ELLRKKYAEMLVPTVSVSSFKRNKIYKTY	2.8
18	ELLRKKYAEMLVPTVSVSSFKRNKIYKTY	4.4
18	ELLRKKYAEMLVPTVSVSSFKRNKIYKTYNN	3.6
80	VLKLVLYISNTAGGDSQRHDEIAKRLKKE	3.1
79	GVLKLVLYISNTAGGDSQRHDEIAKRLKKE	4.8
103	KRLKKECLYSGFINISNETNMAENGIIINVT	2

Figure 3.15 Prediction of targeting for *Pv*Dre2 using cNLS Mapper

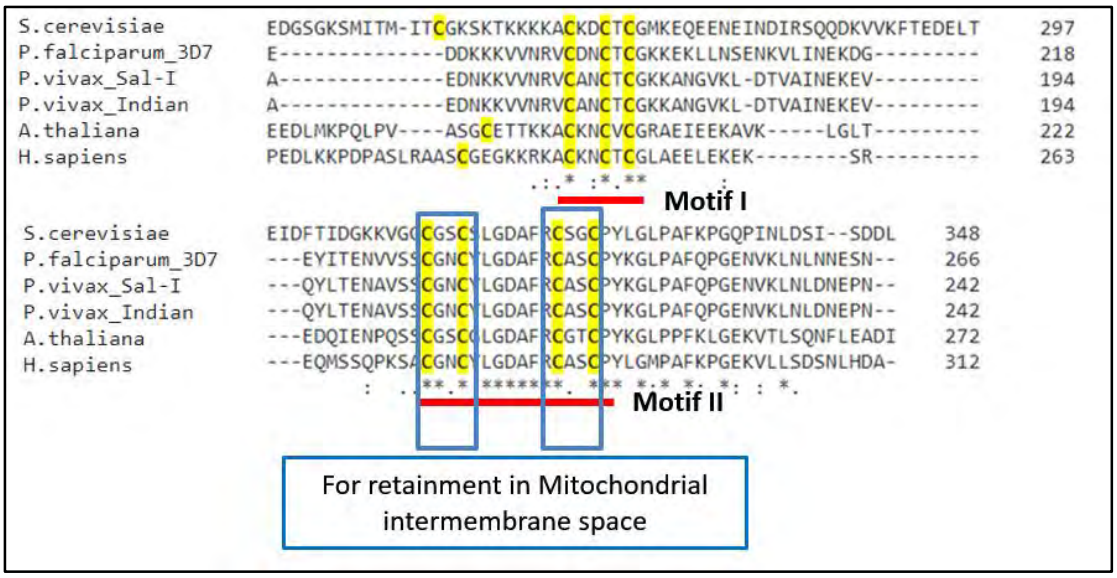

Figure 3.16 Cysteine twin motifs in *Pv*Dre2 responsible for IMS targeting

3.2.9.2 Antibody Raising and Immuno-localization

Our preliminary *in silico* targeting predictions suggested multiple subcellular localizations for the protein. Thus, to confirm the subcellular localization of *Pv*Dre2, antibodies were raised against recombinant *Pv*Dre2 protein in mice. For this, 25-30µg of purified protein along with Freund's adjuvant was injected in mice followed by three booster doses at regular interval of 21 days (details in Chapter 2). Sera was collected after each booster dose and subjected to ELISA to determine the antibody titer. Sera collected from mice injected with 1X PBS and Freund's Adjuvant was used as a control. Pre-immune sera (PB) were also collected to check for any cross-reactive antibodies. An increased antibody titer was observed after the booster doses **(Figure 3.17)** and the sera with best antibody titer was used for downstream experiments.

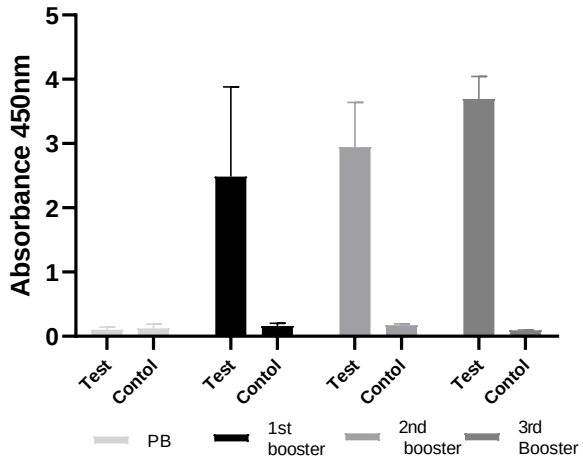

Figure 3.17: Estimation of antibody titre for *Pv*Dre2 protein using ELISA [Antibody dilution 1:1000; PB: Pre-bleed sera

The specificity of antibodies towards *Pv*Dre2 protein was also confirmed by western blot analysis with pure protein and *P. vivax* parasite-infected blood lysate, where a specific band at the desired position was obtained **(Figure 3.18)**.

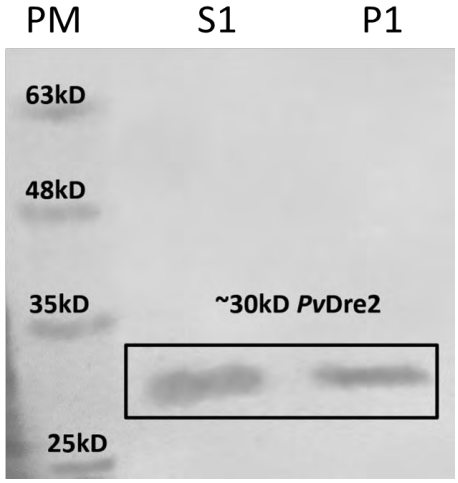

Figure 3.18: Western Blot of Parasite Lysate using *Pv*Dre2 antibodies. S1 and P1: Supernatant and Pellet fraction of Lysate, PM: Pre-stained Protein marker)

The raised antibodies were then used to localize *Pv*Dre2 protein on methanol fixed *P. vivax*-infected blood smears. Initially the cells were permeabilized with treatment of 0.05% Saponin and 0.1% Triton-X 100. After permeabilization, mouse polyclonal anti-*Pv*Dre2 sera (1:500) followed by FITC 488 conjugate (1:200) were added sequentially. Further cells were treated with 1:500 dilution of mitochondria-specific antibody [Prohibitin Polyclonal Rabbit Antibody] followed by goat anti-rabbit IgG Alexa 647 conjugate (1:200 dilution). The cells were later counterstained with DAPI and Qdot 565 Streptavidin Conjugate to visualize parasite's nucleus and Apicoplast respectively before mounting it with Vectashield. Slides were observed using the appropriate lens and filters, where a bright field was used to identify the RBCs infected with the parasite, green fluorescence to localize *Pv*Dre2 protein, blue, red, and pink fluorescence for the nucleus, mitochondria, and apicoplast respectively **(Figure 3.19)**.

The *Pv*Dre2 protein was localized as a green fluorescing spot with an overlapping red spot of mitochondria giving a yellow colour. However, the *Pv*Dre2 green fluorescing spot did not coincide with the pink and blue fluorescence, indicating it not to be localized to either Apicoplast or Nucleus. This study confirms the mitochondrial localization of the *Pv*Dre2 protein (**Figure 3.19)**.

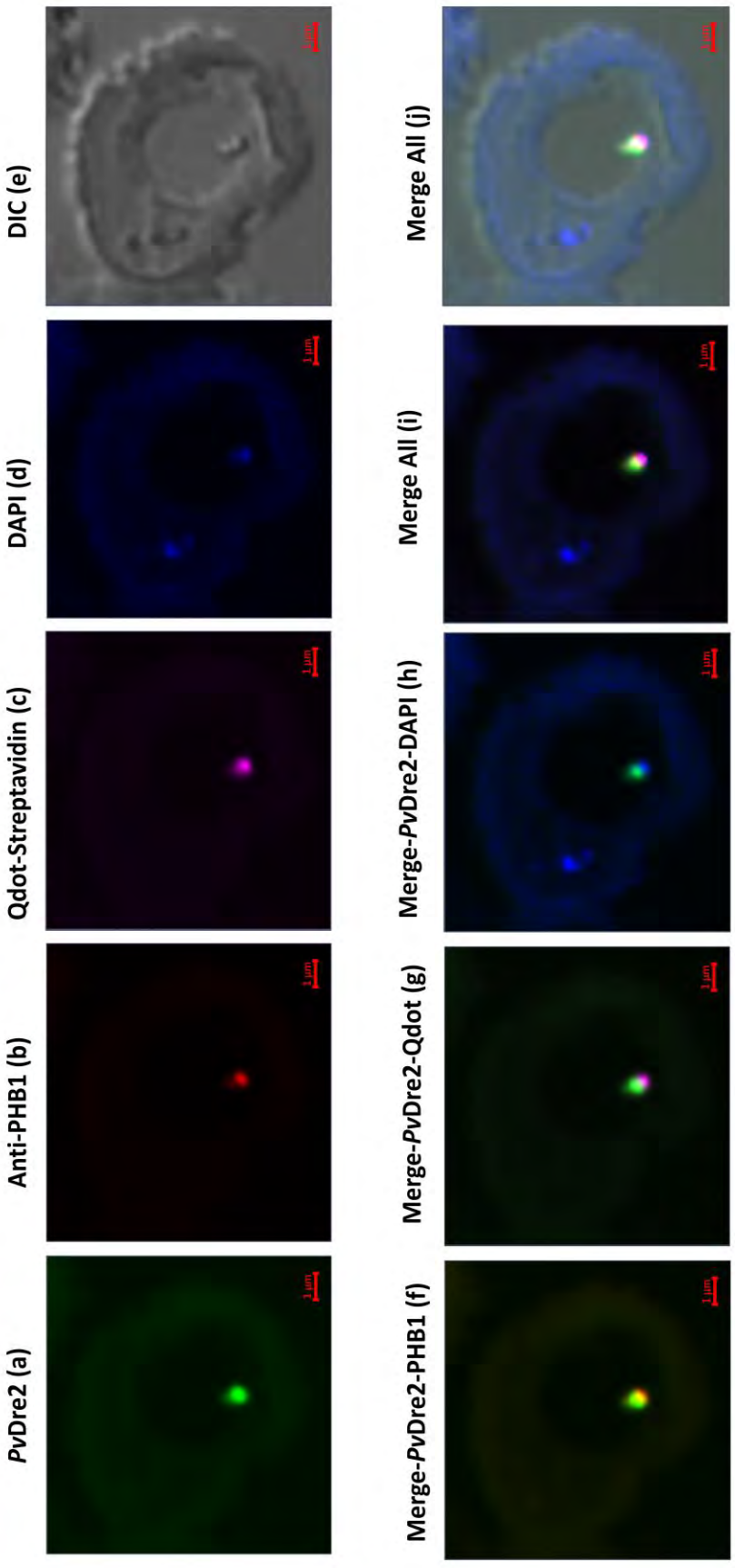

Figure 3.19: Sub-cellular localization of *Pv*Dre2 protein in smears prepared from *P. vivax* Indian field isolates. 63X Magnification a) The full-length *Pv*Dre2 protein was tagged with FITC 488 and visualized as green fluorescence. **b)** The parasite's mitochondria was stained with Mitochondria specific antibodies [Prohibitin Polyclonal Rabbit Antibody] and Alexa 647 (red), **c)** The parasite's Apicoplast was stained with Q-dot 565 (pink), and **d)** DAPI (blue) to identify the nucleus. **e)** The DIC bright field image shows the presence of a Parasite inside an infected RBC. Image z-stacks were deconvolved and then presented as a single combined image. The merged image of *Pv*Dre2 with different antibodies/ dyes is given as **[f to j]**.

3.2.10 Identification of interacting partners of Dre2 protein using anti-PvDre2 antibodies and LC-MS/MS analysis

To identify the role of Dre2 protein in the parasite life cycle, we performed co-immunoprecipitation (co-IP) using *Pv*Dre2 antibody to pull down *Pv*Dre2-associated protein partners from the parasite lysate. For the same, 1.5 mg of Dynabeads Protein G were cross-linked with *Pv*Dre2 antibody and were incubated at 4˚C for 2-3 hrs. Pre-immune sera were also cross-linked to Dynabeads in a similar manner, to be used as control to eliminate similar protein hits from *Pv*Dre2 antibody eluted proteins. After removing any unbound antibodies with 1X PBST (00.1% Tween 20 in 1X PBS), 500µg of parasite lysate was added to this Dynabead-antibody conjugate (test and control) and incubated overnight at 4˚C. After removing any unbound proteins, target proteins were eluted by incubating samples at 70˚C for 10 min with 1X Laemmli buffer. The eluted samples were sent for Mass spectrometry to identify potential associated partners (Methodology detailed in Chapter 2).

A list of interacting proteins identified through LC-MS/MS of the *Pv*Dre2 co-immune precipitated sample is given in **Table 3.3**. The major interacting partners for Dre2 protein include: 1) **Clathrin heavy chain**, which is reportedly involved in vesicular endocytosis and cellular homeostasis (Prichard et al., 2022), 2) **Letm1**; An inner mitochondrial membrane protein reported to be involved in mitochondrial ion regulation (K^+/H^+ Exchanger) (Li et al., 2019; Chang et al., 2019) and regulation of autophagy and apoptosis in case of hepatocellular carcinoma (Zhou et al.,2021), 3) **ribosomal biogenesis proteins** such as 50S ribosomal protein L33, Small ribosomal subunit assembling AARP2 protein, and various splicing factors 4) Nuclear targeted proteins such as **ES2, DNA replication licensing factor MCM2**, etc.; 5) a few Merozoite Organizing proteins; 6) proteins related to post-translational modifications and proteasome degradation; 7) and various conserved/hypothetical groups of proteins.

Table 3.3: Identification of proteins immuno-precipitated in parasite lysate using anti-*Pv*Dre2 antibody by LCMS–MS analysis

SN	PlasmoDB Id	# PSMs	MW [kD]	Sequences of peptides identified
1	PVX_123620 (PF3D7_1219100) Clathrin heavy chain, putative	56	225.8	NLQNLLILTAIK [6], VLSLVDSSLYNNENAEFARQFGNY SNNYQEK [1],

				LLLPWLESR [3], DPENFLKNNNFYDK [1], LQEATSILLDFLK [1], ALENYTNLSDIKRVINK [1]
2	PVX_089955 (PF3D7_0417300) LETM1-like protein, putative	12	86.3	TGILLFLTNMKISK [2], QNVNNNNNNNNNANSSDNNNNHANSSNIDDKQK [1], NSLAKVRDAQIK[1]
3	PVX_100730 (PF3D7_1235600) serine hydroxyl-methyl transferase	12	121.9	VLLNKWGYRR [1], IAAVACQLKEVNTPFFK [2], NHINLSICK [1]
4	PVX_083255 (PF3D7_1347100) DNA topoisomerase 3, putative	10	101.6	NPNININGNIINEINENKDINNIVNNQYHNEK [1]
5	PVX_099270 (PF3D7_0917000) Merozoite organizing protein	10	218	QITMLSLLR [3], EDETMKYHDINKNEDIQNVVHFDNK [2], SILLIIIEKGIAITNRSNIIELVYK [1], KNINESVDETNEQQTKHINK [1]
6	PVX_085565 (PF3D7_1417800) DNA replication licensing factor MCM2	9	111.4	RIENLKNVIVSSSAYEPIPQDLLQK [1], TVQQMIQRQNLK [1], DILNNFKGGHTIRGDINVLLLGDPGLGK [1]
7	PVX_100660 Protein of unknown function (DUF2439)/AAA domain	9	205.9	ISVSYTNIRNFNK [1], EKNQQISLR [1]
8	PVX_113635 (PF3D7_0609700) hypothetical protein, conserved	8	19.5	LSSHGRTQFCKNPLGLVAYYR [1]
9	PVX_091290 (PF3D7_1112800) hypothetical protein, conserved	7	52.1	NNSYYIQLQCHDMTRQK [1], NININININKNINININK [1]
10	PVX_091195 (PF3D7_1110900) ES2 protein, putative	6	61.5	GVFNLLHEKNGYKYVNTPIIEAGK [1]
11	PVX_123805 (PF3D7_1223500) hypothetical protein, conserved	6	556.2	ISLSKISYYFDIQKDYINHIINMSSFYPK [1], NEWVNFMKQYVNK [1], KENSNISFNIIHKR [1], KNNSYQNDTLIHSGDQGENTHK [1]
12	PVX_003970 (PF3D7_0210400) 50S ribosomal protein L33, putative	5	19.3	VHVNLISSCASNYIYSTYISPSK [1]
13	PVX_083410 (PF3D7_1350300)	5	37.5	NLSLGIGNNKKIQENHK[2], KMTLPYLDK [1]

	hypothetical protein, conserved			
14	PVX_094385 (PF3D7_1003700) MKT1 domain-containing protein, putative	5	132.9	SIDNNILIIFELLKFGFLTTHPLLPPNGKK [1], KVRDSSEGNNNESEEGK [1], IIRNYNNYYKNILNTDNQNFNSILCIVYYMFLENLGIFTK [1]
15	PVX_083075 (PF3D7_1343600) UDP-N-acetylglucosamine pyrophosphorylase, putative	5	67.6	IFKQCNNFITNFNFDVLMKNHNTVLTAPGGNGTIFK [1]
16	PVX_087800 (PF3D7_0705100) conserved protein, unknown function	5	110.4	NNKYIFGYFILILANQIK [1], NQMINNFIINYNMKKENDINQINEINEINGTNQSVNR [1]
17	PVX_087800 (PF3D7_0705100) conserved protein, unknown function	3	109	NNKYIFGYFILILANQIK [1], NEHNEEYTLEEYINKSKYNNNVK [1]
18	PVX_084335 and PVX_117005 (PF3D7_1206000 and PF3D7_1469200) shewanella-like protein phosphatase 2 and shewanella-like protein phosphatase 1	5	35.6	KILLTENIIDEENNAIR [1]
19	PVX_095315 (PF3D7_0318300) conserved protein, unknown function	5	115.6	IQDILAQLR [1], ISPMSHINAYIISNNGR [1], EAGGENPTGEKPTGEKPTGEK [1]
20	PVX_088210 (PF3D7_0634231) protein tyrosine phosphatase, putative	5	139	TFPYFYISEKNNIK [1], DEMNEKENLIFKLNFLNR [1], DYNSMNNMNNIDK [1]
21	PVX_094615 (PF3D7_1008400) 26S protease regulatory subunit 4, putative	5	52.2	TMLELLNQLDGFDSR [1]
22	PVX_081435 (PF3D7_0106700) small ribosomal subunit assembling AARP2 protein/ribosome biogenesis protein BMS1, putative	5	148.9	DIINFHALENPKLAAR [1], KYYNYDIENKLR [1]
23	PVX_117805 (PF3D7_1453500) NAD(P) trans hydrogenase, putative/ pyridine nucleotide transhydrogenase, putative	5	332.5	KKSILNHTTIMNINEGNNK [1], ILEEDNMIKGISSK [1]

1) Clathrin is the most prominent endocytic protein in yeast and mammalian cells (Prichard et al., 2022) required to recycle plasma membrane components, such as integrins and cadherins, essential for cell adhesion and also reported to be critical for maintaining cell shape and polarity (Le et al., 1999; Ezratty et al., 2009; Morse et al., 2014). However, Pieperhoff et al., 2013 and Wolfgang et al 2018, in their work on homologue of the Clathrin Heavy Chain (CHC) from *Toxoplasma gondii* and *P. falciparum* respectively suggested it to function at the Golgi compartment for post translational trafficking and reported it not to be involved in endocytosis (Pieperhoff et al., 2013 and Jonscher et al 2018). In *Toxoplasma*, CHC1 is reported essential for vesicle formation at the trans-Golgi network and functional ablation of CHC1 has been shown to result in Golgi aberrations, a block in the biogenesis of the unique secretory microneme and rhoptry organelles, and of the pellicle. Vesicles resembling clathrin coated vesicles, have also been observed budding off from the Golgi in *Plasmodium* (Bannister et al., 2000) which is in agreement with data obtained from *Toxoplasma* where clathrin mediates secretory trafficking from the trans-Golgi to the apical organelles (Pieperhoff et al., 2013). Wolfgang et al 2018 also found CHC to be refractory to gene disruption in *P. falciparum* blood stages and showed that inducible inactivation of CHC using knock sideways leads to reduced parasite growth.

Further to elucidate more on the type of post Golgi trafficking pathway associated with CHC in Apicomplexans, a functional retromer trafficking from the Golgi to the early endosome has been described in *T. gondii* (Sangare et al., 2016). The identification of elements of the retromer like sortilin (Pan et al., 2017) in the DiQ-BioID experiments with the *P. falciparum* CHC, is an indication of Clathrin performing Golgi derived trafficking in *P. falciparum* in a possibly retromer type from Golgi to endosomal or lysosomal compartments. This is also in agreement with the finding that CHC localization is completely altered after treatment of the parasite with the retromer-inhibitor Retro-2. The interaction of Dre2 and CHC in the co-immunoprecipitation experiment suggests some association of the *Pv*Dre2 protein in/ with the Trans Golgi post translational trafficking possibly via the retromer pathway through endosomal or lysosomal compartments. A recent report by Frey et al 2016, has suggested the degradation of apo- Dre2 protein via possibly an auto-phagosomal /lysosomal route indicating a possibility of Ciapin1 as a component of a large cytosolic complex that turns over via autophagy rather than the proteasome (Frey et al.,2016). However, the

exact function that Dre2 might be performing by interacting with CHC needs to be further investigated.

2) The second interacting partner for Dre2; Letm1 is a conserved protein found in eukaryotic organisms predominantly localized to the inner membrane of mitochondria. Its primary role is to maintain the electrochemical gradient across the inner mitochondrial membrane by facilitating potassium-hydrogen ion exchange. In yeast, depletion of Letm1 has been shown to result in various pathological conditions such as mitochondrial dysfunction, increased potassium contents, and massively swollen mitochondria. Recent studies have also implicated Letm1 in regulating mitochondrial calcium homeostasis, with knockdown or deletion of the protein resulting in elevated mitochondrial calcium levels and subsequent cell death. In a study by Chang et al., it was found that the depletion of *Tg*Letm1 in the protozoan parasite *Toxoplasma gondii* led to a significant decrease in the parasite's growth rate and alterations in mitochondrial morphology and function. Furthermore, it was demonstrated that *T. gondii* Letm1 could rescue the growth defects of yeast cells lacking their own Letm1, suggesting the protein to be functionally conserved across species (Chang et al., 2019). As Dre2-Tah18 complex has been reported to be associated with mitochondrial integrity in yeast (Vernis et al., 2009) and Dre2 has also been shown to localize to mitochondrial membrane, its interaction with Letm1 in co-immunoprecipitation reaction indicates some role of Dre2 in maintaining mitochondrial integrity in the parasite.

Additionally, it has been shown that the Letm1 knockdown can also significantly drop ATP levels, which can modify the ADP or AMP/ATP ratio and activate AMP-activated protein kinase (AMPK). This bioenergy sensor (AMP/ATP ratio) promotes the creation of auto phagosomes (Cárdenas et al., 2010). According to reports, both *in vitro* and *in vivo* Letm1 silencing reduced the growth of HCC (hepatocellular carcinoma) and increased autophagy and death. Thus as per Frey et al. 2016 it might also be possible that the interaction of Dre2 and Letm1 may be required for auto-phagosomal /lysosomal degradation for turns over of Ciapin1 via autophagy (Frey et al.,2016). However, as mentioned above, further investigations are required to decipher the exact function of Dre2 along with Letm1.

3) Other than CHC and Letm1, one of the interacting partners for *Pv*Dre2 protein in Co-IP data was MCM2, which is a component of the MCM2-7 hexamer complex (helicase). MCM2-7 hexamer complex is involved in DNA unwinding during the replication process (Saito et al., 2022). Association of *Pv*Dre2 with MCM2 strengthens Dre2 (CIA component) involvement in [Fe-S] assembly onto certain DNA maintenance proteins, which is in accordance with the reports from *Arabidopsis thaliana*, where the hypomorphic Dre2 mutants (viable mutants) generated upon adding Methyl methane sulfonate (a DNA damage compound) showed accumulation of DNA damage and upregulation of DNA Damage Response (DDR) genes. Overexpression of wild type Dre2 reversed the Dre2 mutant-related DNA damage (Wang et al., 2019).

4) In addition, Dre2 showed interactions with certain ribosome biogenesis proteins such as 50S ribosomal protein L33 and AARP-2/ BMS-1 involved in the biosynthesis of the 40S ribosomal subunit. Previously it has been reported in yeast that Dre2 is also responsible for providing the [Fe-S] clusters to ABCE1, which is a cytoplasmic/ nuclear Fe-S protein necessary for ribosomal maturation and translation (Zhang et al., 2008; Ciofi-Baffoni and Andreini, 2022). Depletion of ABCE1 have resulted in nuclear export defect of the small and large ribosomal subunits and subsequently a translational arrest. Similar results were observed in Dre2 depleted cells where GFP-tagged proteins of the large and small ribosomal subunits, Rpl25 and Rps2, were retained in the nucleus and nucleolus, indicating defective ribosome assembly functions. Thus the interaction of *Pv*Dre2 with the proteins related to the ribosomal biogenesis, suggests its potential role in these mechanisms.

3.2.11 Binding of [Fe-S] clusters on PvDre2 Protein

As discussed above, the Dre2 C-terminal CIAPIN1 domain has been shown to coordinate [Fe-S] clusters at Motif-I and Motif-II, respectively. Our CDD and signature motif analysis also showed that *Pv*Dre2 possesses the CIAPIN1 domain and the reported cysteine residues. In addition, Dre2, being Fe-S protein, itself requires [Fe-S] clusters for its functionality and other downstream processes. Thus to analyze the binding of Fe-S clusters on the *Pv*Dre2 protein, first we generated three dimensional structure of *Pv*Dre2 protein followed by *in silico* docking of [Fe-S] clusters on the protein to check the binding affinity of the cluster and to identify the residues that

interact with [Fe-S] clusters. Later we biochemically reconstituted the [Fe-S] clusters on *Pv*Dre2 protein to analyze the *in vitro* binding of clusters on *Pv*Dre2 protein.

3.2.11.1 Three Dimensional Model generation for C-terminal CIAPIN1 domain of PvDre2 protein

To generate the three dimensional model, we submitted the C-terminal domain sequence of *Pv*Dre2 protein to the HHPred software, however, no proper template could be identified for the protein. The reason for the same might be that CIAPIN1 domain is reported to be highly unstable and undergoes degradation. Thus, *Pv*Dre2 CIAPIN1 domain (C- terminal) was modelled *ab initio* using a freely available online software "Robetta" **(Figure 3.20)**.

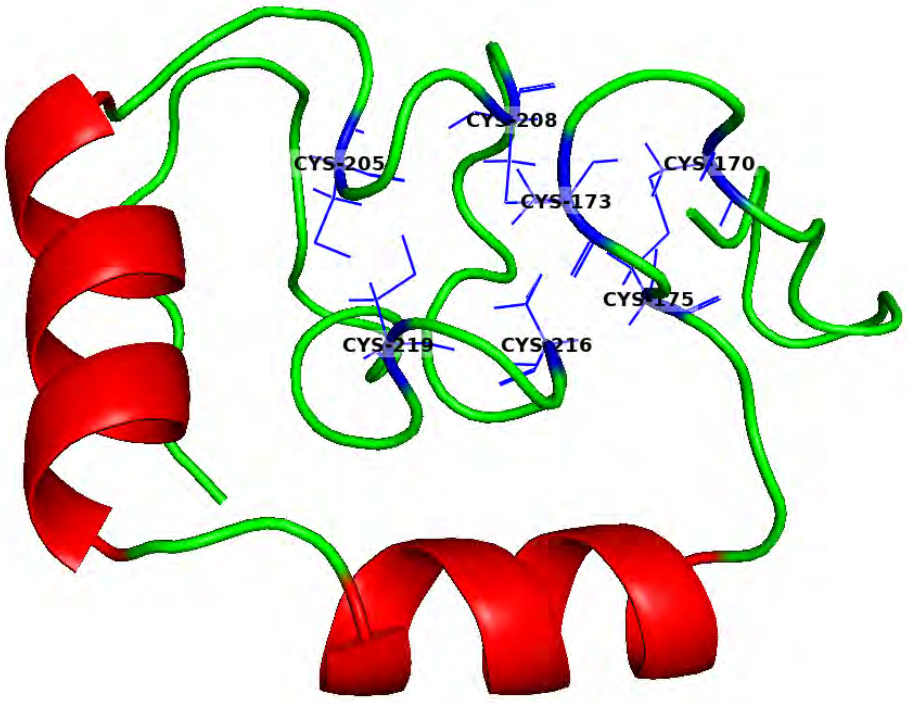

Figure 3.20: Three dimensional model of *P. vivax* Dre2 C-terminal CIAPIN1 domain. The conserved cysteine in Motif-I and Motif-II are represented in blue.

The generated structure was further evaluated for model integrity and stability using different online servers available on UCLA-DOE LAB SAVES v6.0. The structure when subjected to PROCHECK, showed a G- factor 'BETTER.' All the amino acid residues in Ramachandran Plot were placed in favorable regions, with 90.9 % residues in the most favored region and 9.1% in additionally allowed regions **(Figure 3.21a)**. The VERIFY3D for *Pv*Dre2 N-terminal model showed that 90.91% of the residues had

averaged 3D-1D score >= 0.2 while the ERRAT score of 83.82 represented that molecular geometry of the model is of good quality **(Figure 3.21 b).**

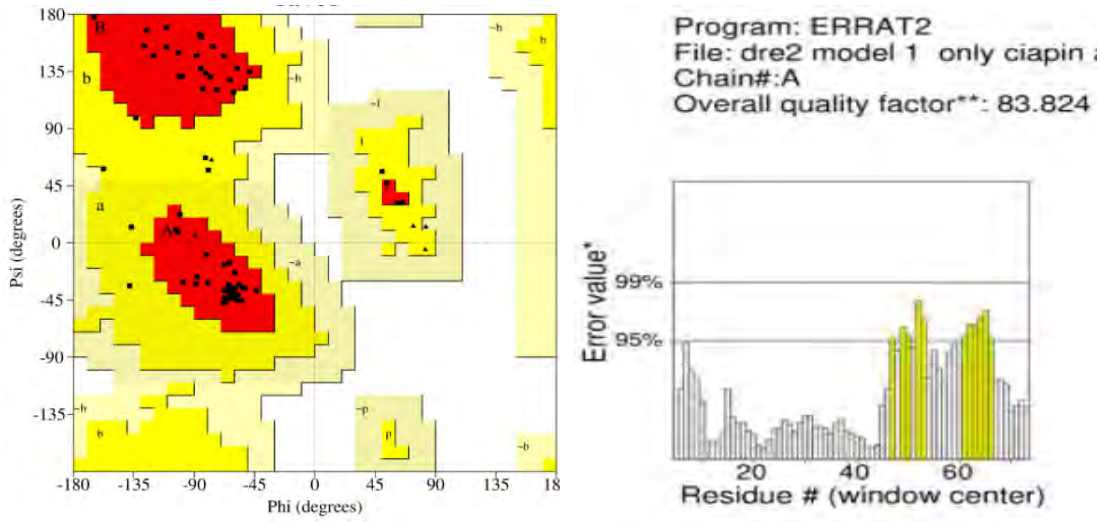

Figure 3.21: Validation of 3D structure of *Pv*Dre2 C-terminal CIAPIN1 domain using a) Ramachandran Plot and b) ERRAT score.

The 3D structure of the *Pv*Dre2 CIAPIN1 domain consisted of two alpha helices connected with loop regions and showed a high level of conservation of cysteine residues in Motif-I (Cys170, Cys173, and Cys175) and Motif-II (Cys205, Cys208, Cys216, and Cys219) required for binding of [Fe-S] clusters. **(Figure 3.20)**.

3.2.11.2 In silico docking of [Fe-S] clusters on the PvDre2 Protein

To analyse the [Fe-S] cluster binding of *Pv*Dre2, the protein model was docked against [2Fe-2S] and [4Fe-4S] clusters at Motif-I and Motif-II, respectively. A conformational shift was observed in protein upon [Fe-S] cluster docking, including disulphide bond formation between Cys208-Cys173 and Cys170-Cys175. At Motif-I, the two cysteine residues Cys170 and Cys173 were observed to interact with the [2Fe-2S] cluster, along with Asn172 and Asn207. However, at Motif-II, all the 4 cysteine residues i.e. Cys205, Cys216, Cys219, and Cys208 interacted with the [4Fe-4S] cluster, along with Gly206, Asp212, and Ala213. **(Figure 3.22)**. All these interactions were within a distance of 4 A°. The amino acid residues involved in the interaction with the [2Fe-2S] and [4Fe-4S] clusters are given in **Table 3.4**.

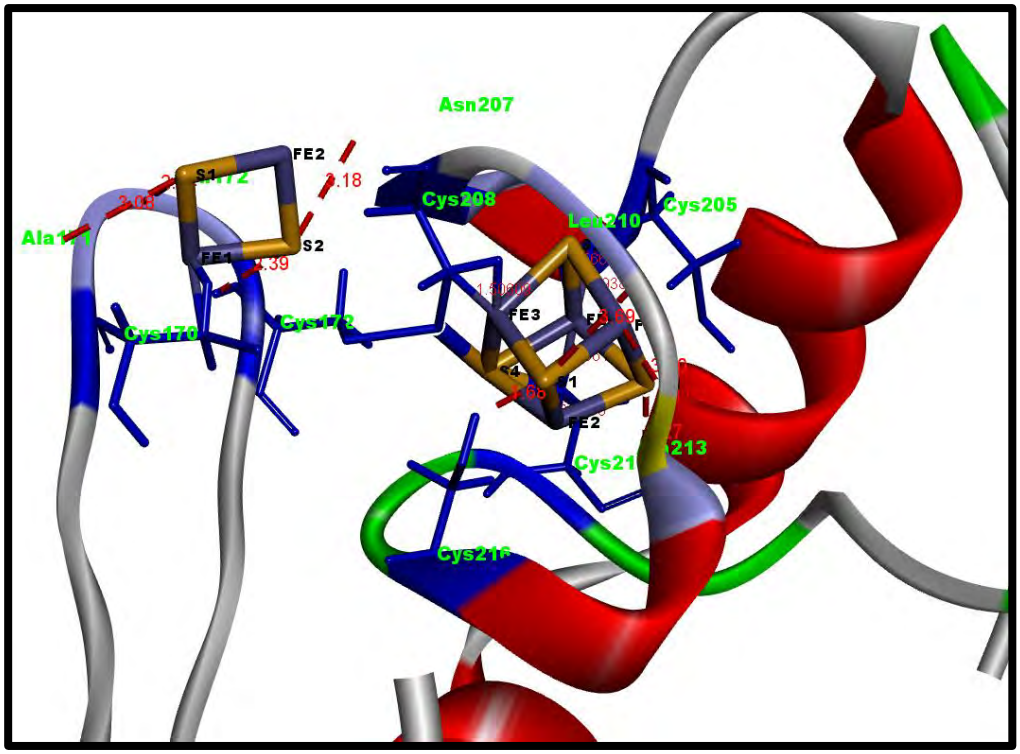

Figure 3.22: *P. vivax* Dre2 CIAPIN1 domain model docked with [2Fe-2S] and [4Fe-4S] at Motif-I and Motif-II respectively. The side chains of interacting Cysteine residues are shown in blue.

Table 3.4: Residues interacting with [2Fe-2S] and [4Fe-4S] clusters at Motif-I and Motif-II respectively

[2Fe-2S] Motif-I	Interacting Residues
FE1	Cys170 [2 Å]
S1	Ala171 [3.08 Å], and Asn172 [2.34 Å]
S2	Cys170 [3.54 Å], Cys173 [2.39 Å], and Asn207 [3.18 Å]

[4Fe-4S] Motif-II	Interacting Residues
FE1	Cys205 [1.38 Å], and Cys219[1.86 Å]
FE2	Ala213 [2.14 Å], and Cys219 [2.3 Å]
FE3	Cys208 [1.51 Å]
FE4	Ala213[2.25 Å], and Gly206 [2.74 Å]
S1	Cys208 [3.28 Å], Leu210 [3.69 Å], and Cys216 [1.68 Å]
S2	Cys205 [1.57 Å]
S3	Ala213 [1.5 Å], and Cys219 [2.23 Å]
S4	Cys208 [1.94 Å],Cys219 [1.96 Å], and, Asp212[3.06 Å]

As mentioned above, Motif-I binds to [2Fe-2S], and Motif-II binds to [4Fe-4S] in the case of Yeast Dre2. However, Matteucci et al. recently reported that human Anamorsin binds to two [2Fe-2S], one each at Motif-I and Motif-II (Matteucci et al., 2021). Hence, we also performed the docking of [2Fe-2S] at both Motif-I and Motif-II of the *Pv*Dre2 CIAPIN1 domain simultaneously to analyse the residues interacting with [2Fe-2S] clusters **(Figure 3.23).** Upon docking [2Fe-2S] at Motif-II, all the 4 cysteine residues; Cys205, Cys216, Cys219, and Cys208 were still found interacting with the [2Fe-2S] cluster, and the interactions were also within a distance of 4 A°. However, the distance between the interacting residues were found to be more for the [2Fe-2S] clusters at Motif-II. Along with the above conserved Cysteine residues, Ser204, Tyr209, Leu210, Gly211, Asp212, Ala213, and Phe227 were also found associated with the [2Fe-2S] cluster **(Figure 3.23)**. Additionally, in the presence of [2Fe-2S] at Motif-II, the [2Fe-2S] at Motif-I showed new interactions with residues Tyr209 and Leu210. All the residues involved in the interaction with the [2Fe-2S] clusters at Motif-I and Motif-II are given in **Table 3.5**.

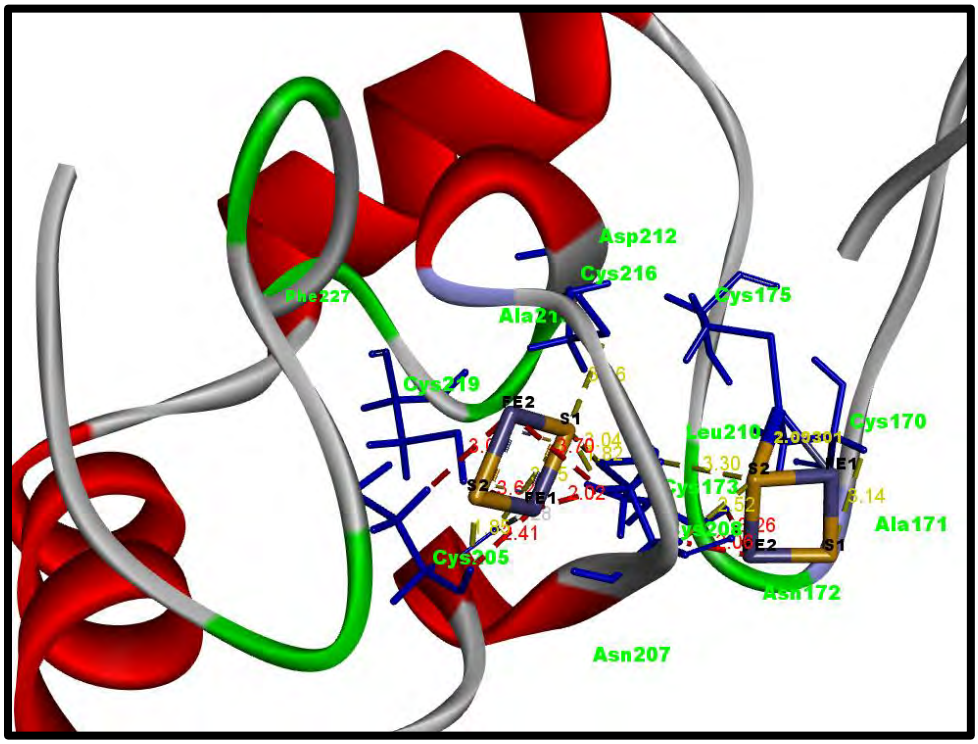

Figure 3.23: *Pv*Dre2 C-terminal CIAPIN1 domain docked with [2Fe-2S] at both the Motif-I and Motif-II. The side chain of interacting Cysteine residues 205, 208, 216, and 219 at Motif II are shown in blue.

Table 3.5: Residues at Motif-I and Motif-II interacting with the [2Fe-2S] clusters (Docked together).

[2Fe-2S] at Motif-I	Interacting Residues
FE1	Ala171 [3.43 Å], Asn172 [3.78 Å], and Cys170 [2.18 Å]
FE2	Asn172 [1.77 Å], Cys173 [3.25 A], Asn207 [3.80 Å], Cys208 [2.05 Å], and Tyr209 [3.29 A]
S1	Cys170 [3.14 Å], Ala171 [3.13 Å], Asn172 [2.34 Å], Cys208 [3.04 Å]
S2	Leu210 [3.17 Å], Cys173 [3.30 Å], Cys208 [2.51 Å], Cys170 [2.09 Å]

[2Fe-2S] at Motif-II	Interacting Residues
FE1	Ser204 [3.33 Å], Cys205 [2.40 Å], Cys208 [2.01 Å], Tyr209 [3.13 Å], Leu210 [2.80 Å], Ala213 [3.13 Å], and Cys219 [3.61 Å]
FE2	Cys205 [3.07 Å], Cys208 [3.70 Å], Leu210 [3.11 Å], Gly211 [3.52 Å], Asp212 [3.46 Å], Ala213 [1.46 Å], and Phe227 [2.80 Å]
S1	Cys205 [3.52 Å], Cys208 [1.82 Å],Cys216 [3.46 Å], Leu210 [2.38 Å], and Ala213 [2.48 Å]
S2	Ser204 [3.34 Å], Cys205 [1.85 Å], Leu210 [2.78 Å], Ala213 [2.60 Å], and Phe227 [2.60 Å]

Once we confirmed the *in silico* docking of [Fe-S] clusters at both Motif-I and Motif-II, we further confirmed the formation of [Fe-S] clusters on the protein *in vitro* by chemically reconstituting these clusters on the *Pv*Dre2 protein by externally providing the Fe and S source.

3.2.11.3 Chemical Reconstitution of [Fe-S] clusters on Purified PvDre2 protein

As the protein was purified in aerobic conditions resulting in removal of [Fe-S] clusters, thus we chemically reconstituted [Fe-S] clusters onto *Pv*Dre2. For the same, we anaerobically incubated purified protein with a five-fold molar excess of Na_2S and Fe $(NH_4)_2(SO_4)_2$ in the presence of Dithiothreitol (DTT). After incubation for 2-3 hrs, the formation of [Fe-S] clusters were validated using UV-vis spectroscopy. The UV-visible spectral analysis showed a shoulder in between 450- 550 nm with a peak at ~500nm for *Pv*Dre2 suggesting the formation of [Fe-S] clusters for both the protein concentrations (10µM and 20µM *Pv*Dre2) **(Figure 3.24).** However, no such peak was visible in the case of apo-*Pv*Dre2 (purified protein without reconstitution) spectral analysis.

We also further validated chemically reconstituted *Pv*Dre2 spectral data for the type of clusters present using the Fit-Fes tool, which is used to analyse [Fe-S] quantitatively and qualitatively (Betinol et al., 2021). For this, we subjected chemically reconstituted *Pv*Dre2 spectral data to the Fit-Fes software and found that both [2Fe-2S] (~28%) and

[4Fe-4S] (~9%) are present. This data supports the presence of both [2Fe-2S] and [4Fe-4S] clusters in the *Pv*Dre2 protein at Motif-I and Motif II respectively. The presence of greater amount of [2Fe-2S] clusters may be attributed to the available reports from different organisms that suggest that the [4Fe-4S] bound to Motif-II slowly gets converted into [2Fe-2S] (Netz et al., 2016; Zhang et al., 2016). However, Fit-FeS displays only semi-quantitative data, which further needs validation by EPR studies to establish types of [Fe-S] clusters.

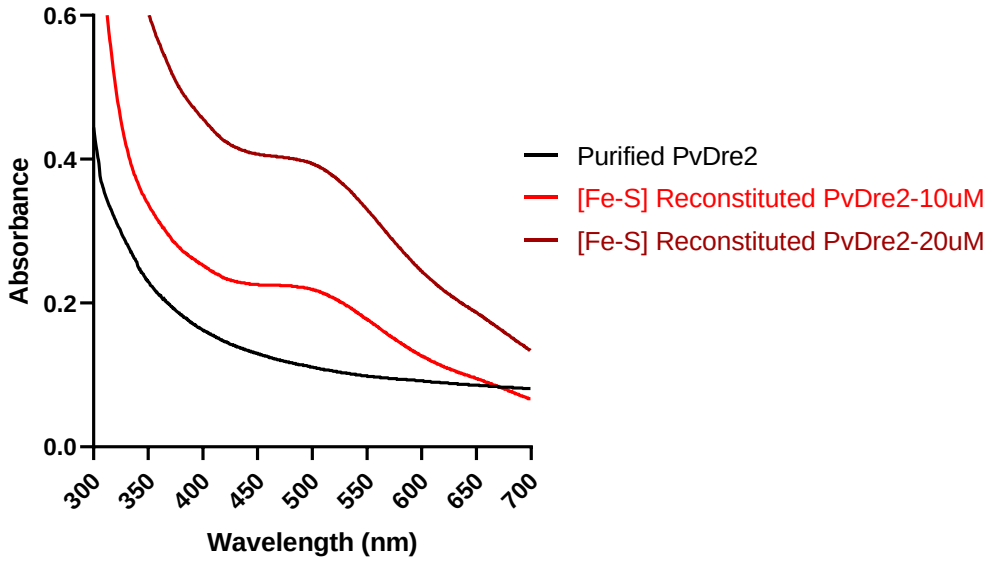

Figure 3.24: UV-vis spectral analysis of chemically reconstituted *Pv*Dre2. *Pv*Dre2 at 10µM and 20µM protein concentrations showed significant [Fe-S] cluster peak after Chemical reconstitution (Red and Crimson Red, respectively) when compared to apo-*Pv*Dre2 before Reconstitution (Black).

3.2.11.4 Rapid Colorimetric Assay: Iron and Sulphur Determination

After chemical reconstitution and [Fe-S] peak validation through UV-vis spectrometry, the molar ratio of bound iron and sulfur to *Pv*Dre2 was determined by using Ferrozine and methylene blue assays respectively as mentioned in Materials and Methods. First the standard graphs for iron (1µg – 6µg/ml ferrous ethylene di-ammonium sulfate tetra hydrate salt (SIGMA, USA) in 0.01M HCl.) and sulfur (0.01mM to 0.1mM sodium sulfide in sodium carbonate buffer (pH 9.0)) were generated based on the obtained absorbance for different known concentrations **(Figure 3.25 and 3.26)**. Further, the molar concentration of iron and sulfur for the chemically reconstituted *Pv*Dre2 was extrapolated from these standard graphs. The total iron and sulfur content of

reconstituted *Pv*Dre2 was calculated as 4.15µM (µmole protein)$^{-1}$ and 4.46µM (µmole protein)$^{-1}$ respectively, indicating binding of [Fe-S] clusters to the *Pv*Dre2 protein.

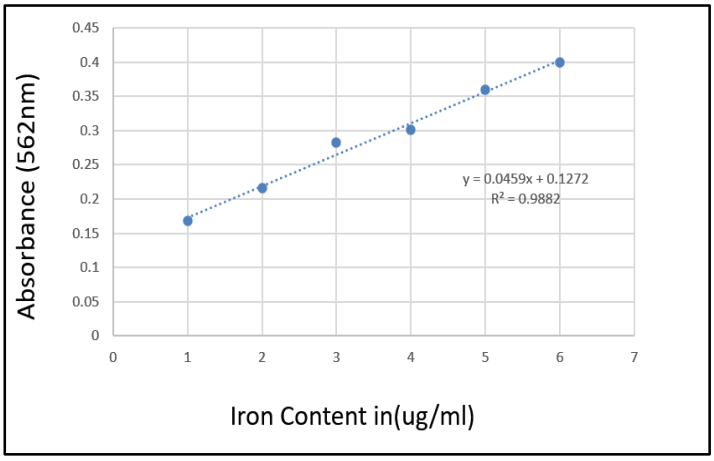

Figure 3.25: Estimation of iron content in reconstituted *Pv*Dre2 protein using Ferrozine assay

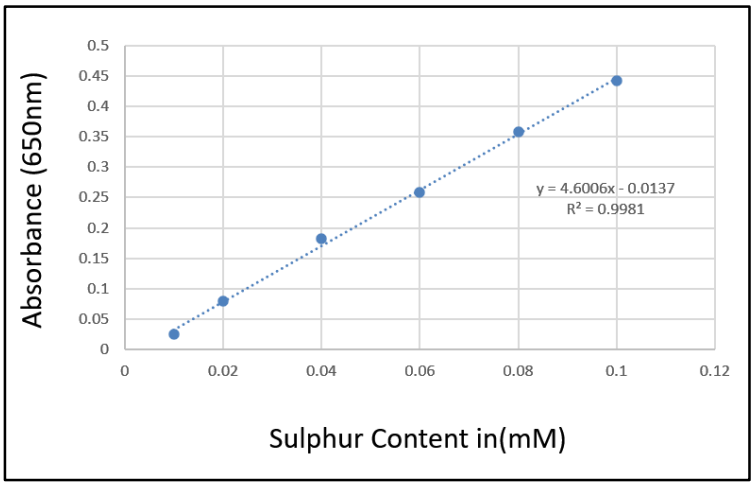

Figure 3.26: Estimation of Sulfur content in the reconstituted *Pv*Dre2 protein using Methylene Blue assay

3.2.12 Protein Model generation for N-terminal of PvDre2

To further investigate into the complete structure of *Pv*Dre2 protein, we proceeded with secondary structure prediction for *Pv*Dre2 N-terminal (1-115 a.a.) region using PSIPRED software. Further we also generated a three-dimensional (3D) model of *Pv*Dre2 using Robetta software, as no proper template was available for this region for homology modeling **(Figure 3.27 and 3.28).** To determine model integrity, the predicted structure was evaluated using different online servers available on UCLA-

DOE LAB SAVES v6.0. The structure when subjected to PROCHECK, showed a G-factor 'BETTER.' 91.1% of the amino acid residues in Ramachandran Plot were placed in favorable regions where 83.2% were in the most favored region, 12.1% in additionally allowed, and 3.7% in generously allowed **(Figure 3.29 a)**. The VERIFY3D for *Pv*Dre2 N-terminal model showed 98.26% of the residues had averaged 3D-1D score >= 0.2 while obtained ERRAT score 89.72 represented that molecular geometry of the models is of good quality **(Figure 3.29 b)**.

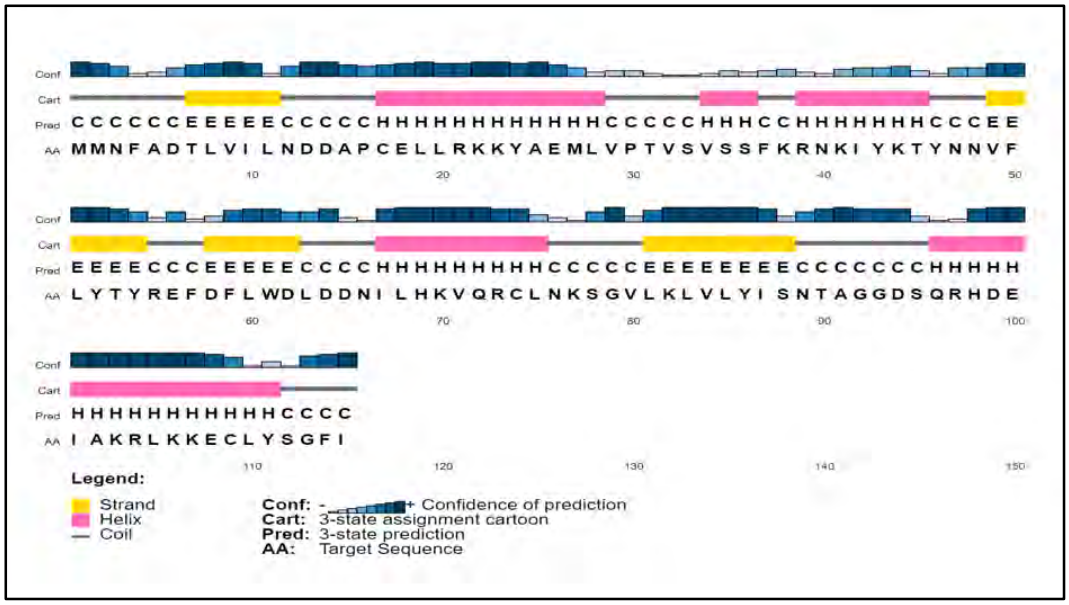

Figure 3.27: Secondary structure prediction of N-terminal of *Pv*Dre2 protein

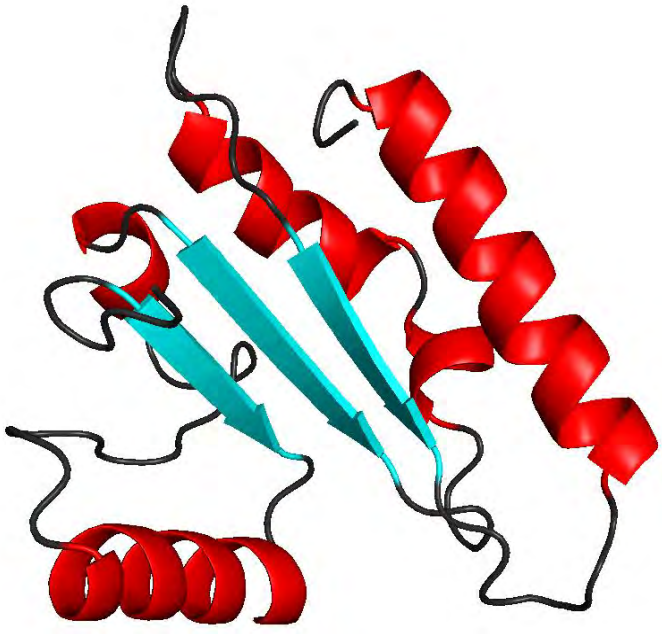

Figure 3.28: Three Dimensional structure of N-terminal of *Pv*Dre2 protein

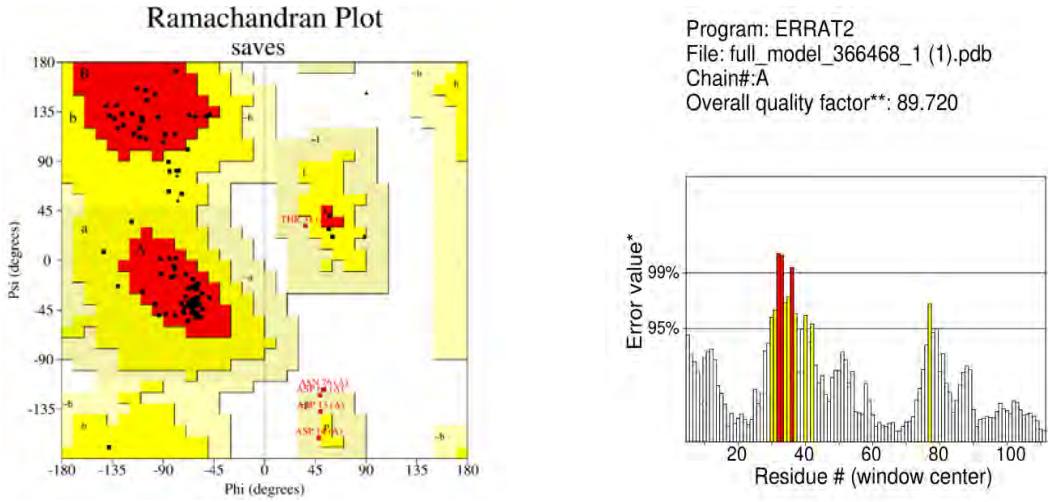

Figure 3.29: Validation of 3D structure of *Pv*Dre2 N-terminal region using a) Ramachandran Plot b) ERRAT score

The obtained *Pv*Dre2 N-terminal structure consisted of four alpha helices, three parallel beta helices, and in-between loop regions with beta-alpha-alpha-beta-alpha-beta-alpha topology as shown in **Figure 3.27 and 3.28**. The *PvDre2* N-terminal 3D model when compared to the Yeast N-terminal Dre2 PDB structure (2KM1) also showed the presence of a hydrophobic patch onto the last alpha helix (**Figures 3.30 a and b)** similar to yeast (Soler et al., 2012). This patch is required to recognize certain substrates and involves residues such as Ile101, Ala102, Leu105, Leu110, Tyr111, Gly113, Phe114, Ile115, and a spatially nearby Ile87.

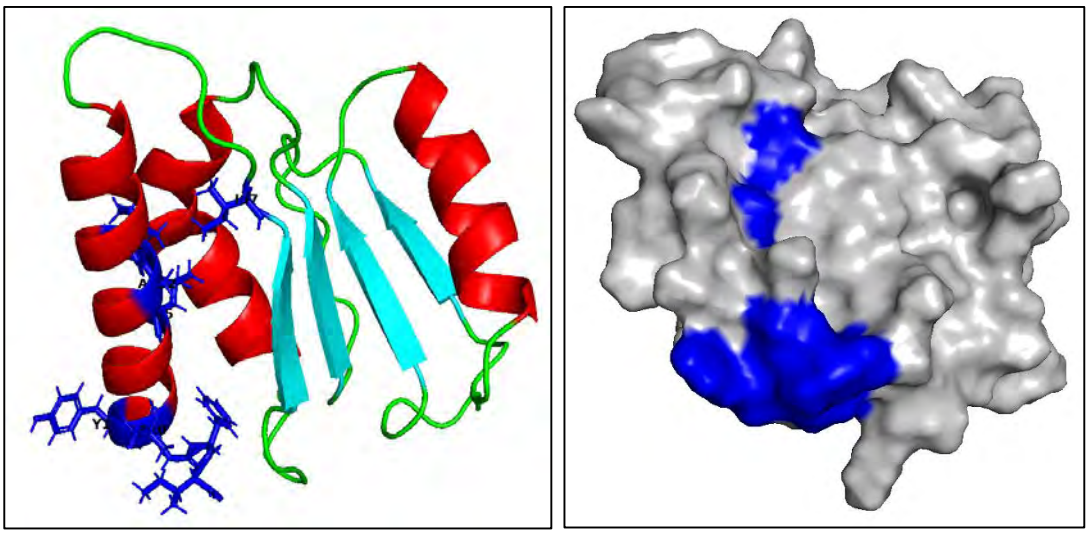

Figure 3.30: Hydrophobic patch on N- terminal of *Pv*Dre2: a) 3D structure and b) Surface model. Hydrophobic Residues are labelled in blue colour

3.2.13 Folding prediction of linker region of PvDre2 protein

As mentioned above, a linker region is present downstream to the N-terminal of the Dre2 protein, which is reported to be a highly disordered region to enable interaction of Dre2 with various other proteins. Thus to analyse and predict if there is any disordered region present in the linker region of *Pv*Dre2, we used FoldIndex software (Prilusky et al., 2005). Similar to other eukaryotes, the disordered/unfolded region was also present in *P. vivax* Dre2 and it also covered the initial portion of the CIAPIN1 domain containing the Motif-I (Banci et al., 2011) **(Figure 3.31 a and b)**. However, when we analysed the *Pf*Dre2 protein, we observed more disordered with multiple stretches of unfolded regions in comparison to *P. vivax* Sal-I Dre2 and Indian *Pv*Dre2 **(Figure 3.31 c)**.

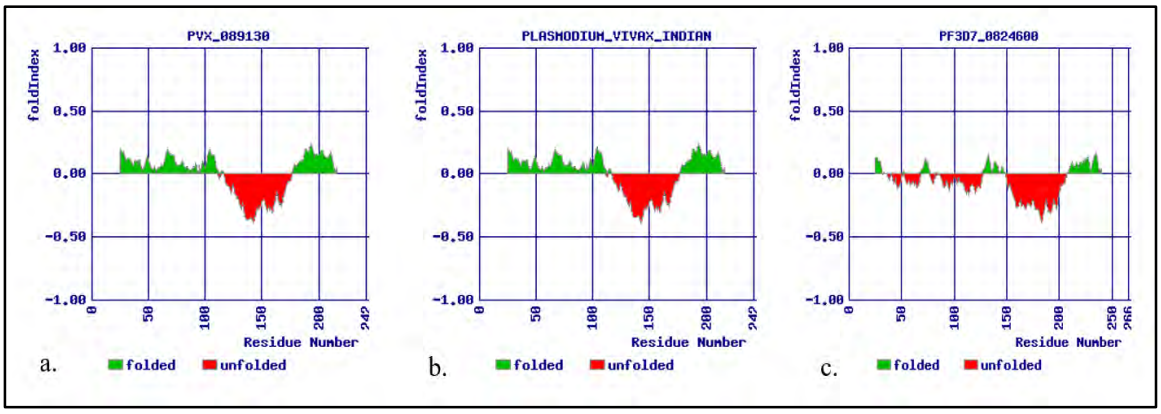

Figure 3.31: Folding prediction of Dre2 derived from the FoldIndex program. Regions shaded in green are predicted to be folded, whereas red-shaded regions are expected to be unfolded. **a)** PVX_089130 Disordered region: 116-176 a.a. **b)** *Pv*Dre2 *Indian* Disordered region: 117-176 a.a. **c)** PF3D7_0824600 Disordered region: 150-207 a.a. [most extended disordered regions are only mentioned]

3.3 Discussion

[Fe-S] clusters are one of the essential cofactors involved in various metabolic and regulatory functions in the cell. While the SUF pathway has been extensively explored from both the major human parasites, *P. falciparum,* and *P. vivax*, only recently core ISC machinery functional in mitochondria have been reported from *P. falciparum* (Kumar et al., 2011; Charan et al., 2014, 2017; Pala et al., 2016, 2018, 2019; Sadik et al., 2021). The third [Fe-S] cluster biogenesis pathway, the CIA pathway has not been elucidated till date from any of the Apicomplexans, including *Plasmodium*. Thus, in

this study, we have identified the various components of the CIA pathway from one of the major human malaria parasite; *Plasmodium vivax* and have characterized the initial components of the pathway i.e. Dre2 protein from the parasite, to establish its importance in the parasite life cycle.

Dre2 protein along with TAH18 has been reported to provide electrons to Nbp35-Cfd1 scaffold complex for maturation of the [4Fe-4S] cluster. Conserved domain analysis of *Pv*Dre2 showed the presence of CIAPIN1 at the C-terminal but no S-adenosine methyl transferase-like domain could be detected at the N-terminal of *Plasmodium* Dre2. The Rossmann-like α/β topology or partial S-adenosyl methionine methyl transferase (SAM) fold specific for the methyl-transferase family of proteins was absent in Dre2 from both *P. falciparum* and *P. vivax*, suggesting no methyl-transferase activity for Dre2 (Soler et al., 2012; Song et al., 2014). Foldindex analysis revealed the presence of a highly disordered stretch of amino acids between the N- and C- terminal of the *Pv*Dre2 sequence, indicating the presence of a linker region (Prilusky et al., 2005). This disordered stretch of amino acids in protein indicates its role in multi-organelle targeting and as a platform for protein-protein interactions, as reported from different organisms like humans, yeast, and *Arabidopsis* where it is shown targeted to the cytoplasm, mitochondria, and nucleus (Bondos et al., 2022).

The Dre2 protein, when sequenced from *P. vivax,* exhibited ~23-94% identity with other eukaryotic orthologues. Multiple sequence alignment of *Pv*Dre2 with other *Plasmodium* spp, Apicomplexans, and higher eukaryotes suggested high conservation for Motif-II (CX2CX7CX2C) involved in binding of [4Fe-4S] clusters. However, only three cysteine residues were present for Motif-I instead of four cysteine residues (CXnCX2CXC). This is in agreement with previous reports suggesting that *Plasmodium* and Encephalitozoon species lack first cysteine residue from Motif-I compared to other species (Netz et al., 2016). Interestingly, we observed that while the primate *Plasmodium* species, including *Pv*Dre2, lack this first cysteine, the rodent malaria parasites such as *P. berghei, P. chabaudi, P. yoelii*, and *P. vinckei* possess this fourth cysteine residue in Motif-I. This cysteine residue has been reported to be required but not essential in yeast for [Fe-S] cluster coordination and function of Dre2 protein, as when this cysteine was mutated to alanine, it did not have lethal effect on yeast viability but showed a marked decrease in the *in vivo* binding of [Fe-S] clusters

to Dre2 (Netz et al., 2016). To analyse the effect of this cysteine on the [Fe-S] cluster biogenesis in *Plasmodium*, further mutation studies needs to be performed.

Dre2, is an iron-sulfur cluster protein, known to coordinate [Fe-S] clusters at Motif-I and Motif-II of CIAPIN1, essential for its own functionality and its function as an electron transfer complex in CIA machinery (Netz et al., 2010; Peña-Diaz et al., 2018). Detailed spectroscopic analysis of types of [Fe-S] clusters and their binding onto yeast Dre2 have suggested binding of [2Fe-2S] clusters at Motif-I and [4Fe-4S] clusters at Motif-II of CIAPIN1 domain (Zhang et al., 2016; Netz et al., 2016; Zhang et al., 2008). However, studies on human Dre2 has revealed the presence of both [2Fe-2S] and [4Fe-4S] clusters at Motif II. In a study by Zhang et al, 2016, similar g values were observed for bound [Fe-S] clusters from both Human Anamorsin and yeast Dre2 through EPR studies. It was hypothesized that in the presence of Oxygen, the Motif-I bound [2Fe-2S] shows degradation, whereas Motif-II bound [4Fe-4S] gets converted to [2Fe-2S] (Zhang et al., 2016; Netz et al., 2016). Another report on Human Anamorsin suggested that both Motif I and Motif II can bind [2Fe-2S] clusters independently, however, the binding of one cluster mutually exclude the binding of other. Also, only the [2Fe-2S] clusters present at Motif-I are involved in the electron transfer with Ndor-1 for its function in the CIA pathway (Banci et al., 2013). Recently, Matteucci et al. through *in cellulo* EPR and Mossbauer spectroscopy also indicated that human Anamorsin, when expressed in *E. coli* cells can coordinate two [2Fe-2S] clusters at each motif (M1 and M2) (Matteucci et al., 2021). Thus, to evaluate [Fe-S] coordination dynamics of *Pv*Dre2, we generated an *ab initio* model for the *Pv*Dre2 C-terminal CIAPIN1 domain and docked it with [Fe-S] clusters. In correlation with existing literature, docking of [Fe-S] at *Pv*Dre2 CIAPIN1 (M1 and M2) was performed in two different combinations i) as reported in yeast: binding of [2Fe-2S] and [4Fe-4S] at M1 and M2 respectively and ii) as reported in Human: binding of [2Fe-2S] at both M1 and M2 respectively. In the case of combination i), we could observe the binding of [2Fe-2S] at M1 and [4Fe-4S] at M2 respectively similar to yeast, and all the interactions were within 4A°. However, in combination ii), even when we could observe the binding of [2Fe-2S] at M1 and [2Fe-2S] at M2, and most of the interactions were under 4A°, the distance between the interacting residues increased when compared to combination (i). These results indicate more possibility of [4Fe-4S] clusters at Motif II than [2Fe-2S] in *Plasmodium*, similar to yeast.

Further, to validate the [Fe-S] cluster interaction with Dre2, we chemically reconstituted the [Fe-S] clusters on *Pv*Dre2 under anaerobic conditions. We observed a reddish-brown colour indicating the formation of [Fe-S] clusters, which gradually faded to white colour upon air exposure indicating the sensitivity of [Fe-S] clusters towards oxygen. UV-vis spectral analysis showed a shoulder at ~500nm for holo-*Pv*Dre2 (after reconstitution), which is in accordance with the reports from yeast and *Arabidopsis* (Bernard et al., 2013; Netz et al., 2016). We further analysed chemically reconstituted *Pv*Dre2 spectral data using the Fit-FeS tool, to analyse the type of clusters in the reconstituted mixture (Betinol et al., 2021). We recorded both [2Fe-2S] (~28%) and [4Fe-4S] (~9%) type of clusters. Less [4Fe-4S] species were recorded when compared to [2Fe-2S], which might be due to the conversion of Motif-II bound [4Fe-4S] to [2Fe-2S] as reported in yeast Dre2 (Ciofi-Baffoni and Andreini, 2022). However, UV-vis spectral data-based techniques only displays semi-quantitative data, which further needs validation by EPR spectroscopy (Betinol et al., 2021).

It is reported that Anamorsin/Dre2 is a multi-targeted protein localized to various cellular compartments, including cytoplasm, mitochondrial inter-membrane space, and nucleus (Hao et al., 2006; Park et al., 2011). Thus we used various online targeting software's such as Signal P, Mitoprot II, and NLS Mapper to predict *Pv*Dre2 localization inside the parasite cell, which suggested Dre2 to be targeted to both cytoplasm and nucleus, but no targeting to mitochondria was observed. But studies performed in other organisms have suggested Dre2 to be localized to inner mitochondrial membrane space (Banci et al., 2011; Peleh et al., 2014; Fraga and Ventura, 2012), thus we performed the immuno-localization studies using antibodies raised in mice against the recombinant protein to confirm its functional site. The protein was found to be localized to mitochondria in *P. vivax* infected blood smears which is in alignment with humans, yeast, and *Arabidopsis*, suggesting evolutionary conservation of the functional site.

To add to its role as a multifunctional protein, the hydrophobic patch on helix E towards the end region of the N-terminal, having a significant role in protein-protein binding, was also present in *Pv*Dre2 suggesting multiple binding partners for the protein (Soler et al., 2012). Even the interactome analysis of *Pv*Dre2 using co-immunoprecipitation studies revealed potential associations of *Pv*Dre2 with multiple partners, including

Clathrin heavy chain, Letm1, MCM2 and ribosomal biogenesis proteins, suggesting its involvement in various cellular processes, like Golgi-derived trafficking, mitochondrial integrity, ribosome biogenesis and DNA replication and damage response etc. However, further investigations are required to unravel the precise functions of *Pv*Dre2 and its interactome.

Overall, *Pv*Dre2 is an evolutionary conserved protein with conserved cysteine motifs for [Fe-S] cluster binding required for its functionality and transfer to other apo-proteins. Its interaction with various proteins involved in Golgi endosomal trafficking, ribosome biogenesis and DNA replication and repair suggests its multifunctional role in the parasite, that need to be further investigated in detail to get a holistic picture of its role in the parasite.

Chapter 4

P. vivax Dre2 protein as a plausible target of Artemisinin:

Mechanistic insights from a prokaryotic heterologous system

P. vivax Dre2 protein as a plausible target of Artemisinin: Mechanistic insights from a prokaryotic heterologous system

4.1 Introduction

As detailed in Chapter 3, Dre2 (Derepressed for Ribosomal protein S14 Expression) also known as Anamorsin or CIAPIN1 (cytokine-induced apoptosis inhibitor 1) is an essential iron sulfur (Fe-S) protein which plays as essential role in electron transfer mechanism alongside with Tah18 (Netz et al., 2016) for cytosolic [Fe-S] cluster biogenesis. However, in addition to its role in CIA pathway, various non-canonical roles have also been assigned to Dre2. Many studies in eukaryotic organisms such as human, yeast and *Arabidopsis*, have reported involvement of Dre2 in different life processes such as Apoptosis, Epigenetic modifications, Immunity against pathogens, and Multi drug resistance mechanisms **(Figure 4.1)**.

In normal conditions, Dre2 and Tah18 forms a cytoplasmic complex for their function as an electron transfer system in CIA pathway. However, under oxidative stress conditions, this complex disassembles and free Tah18 is targeted to mitochondria where it performs mitochondria-dependent apoptosis. Tah18 has recently been reported to possess Nitric oxide synthase (NOS) activity where it generates NO, which then leads to cellular death or Apoptosis. Dre2 over-expression can suppress Tah18 growth defects suggesting its anti-apoptotic role. Thus, Dre2-Tah18 complex regulates cell death and act as a molecular switch by responding to various external environmental cues (Vernis et al., 2009; Yoshikawa et al., 2016) **(Figure 4.1).**

In *Arabidopsis*, Dre2 has been reported to have an epigenetic role in maternal activation in the endosperm lineage (EDL) via DNA demethylation. It was reported that mutated Dre2 led to decrease in Flowering Wageningen (FWA) gene expression; a target of DME (DEMETER) a base-excision glycosylase enzyme, suggesting that Dre2 and DME act together for activation of the FWA gene. Using RT-qPCR, it was identified that the expression of all the DME target genes was reduced in the *At*Dre2 mutant compared with WT *At*Dre2, indicating that *At*Dre2 is essential for maternal activation in the endosperm lineage (Buzas et al., 2014) **(Figure 4.1).**

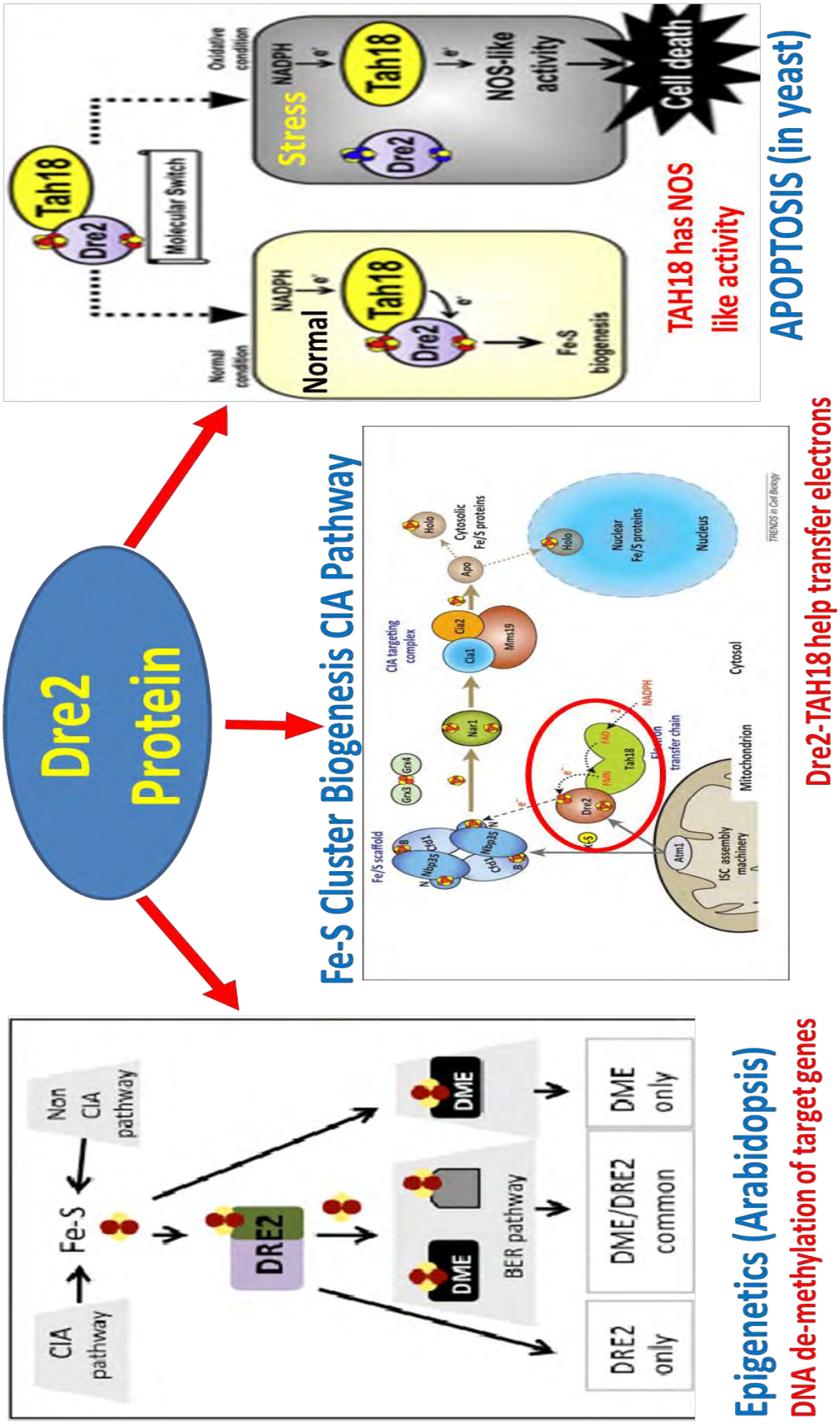

Figure 4.1: Dre2/Anamorsin: An Fe-S protein with Pleiotropic functions

Dre2 has also been reported to have a role in regulation/development of multidrug resistance (MDR), as observed in gastric cancer cell lines. It was observed that over-expression of Dre2 led to increased expression of P-glycoprotein (P-gp or MDR-1) and multidrug resistance associated protein 1 (MRP-1) while silencing of Dre2 resulted in their down regulation. This suggests that there is less accumulation of drugs in case of Dre2 over expression while more accumulation of drug when Dre2 was knocked down. Dre2 not only increased resistance of cells against anticancer drugs which are substrates of MDR-1 and MRP-1 but also against anticancer drugs which are not substrates of MDR-1 and MRP-1 (Hao et al., 2006).

In Rice there are two homologs of Dre2 namely *Os*DRE2a and *Os*DRE2b which shows 98% identity. Among these, *Os*DRE2a is a possible interactor of *Os*RLCK185 (rice receptor-like cytoplasmic kinase 185), a key regulator in chitin mediated signaling in rice. It was observed that there was an upregulation of the Dre2 homologs (*Os*DRE2a and *Os*DRE2b) in presence of chitin. Silencing of Dre2 homologs resulted in decreased chitin induced ROS species (MAPK dependent ROS generation), indicating a role for *Os*DRE2a in *Os*RLCK185 mediated rice immunity (Yamaguchi et al., 2019)

Thus, Dre2, being a multifunctional protein shows potential for its role in inter and intra connected pathways, yet this protein has not been characterized from *Plasmodium*. Recently, Siddiqui et. al. through chemical proteomics revealed interaction of peroxide antimalarial such as Artemisinin with various proteins involved in redox homeostasis and *Pf*Dre2 was one of them. Artemisinin is the first-line treatment for malaria, especially *P. falciparum* malaria as the parasite has gained resistance for most of the other common antimalarial drugs in use. Many artemisinin derivatives of the first generation, such as Dihydroartemisinin, Artemether and Artesunate, have been used to treat malaria. This class of medications (artemisinin) contains an intra-molecular peroxide bridge important for parasite destruction. If the endo-peroxide bridge remains intact after synthesizing artemisinin, the medicine retains its anti-parasitic activity. Even artemisinin enantiomers such as trioxane and other comparable modules had no stereo selective behavior, indicating that its mode of action in parasites is not target specific (Wang et al., 2010). The artemisinin endo-peroxide bridge is cleaved by Fe^{2+} or heme groups found in *Plasmodium*. Endoperoxide bridge cleavage produces oxygen radicals, which eventually rearrange to form primary or secondary carbon-centered radicals.

These carbon-centered radicals are one of the causes of parasite protein alkylation, which leads to parasite cell death. Artemisinin may also disrupt redox balance by interacting with $FADH_2$ in the parasite's glutathione reductase or flavoenzymes, resulting in the formation of reactive oxygen species (Haynes et al., 2010; Ismail et al., 2016).

In the previous chapter, we have detailed the overexpression of *Pv*Dre2 in *E. coli* BL21 (DE3) pLysS cells to characterize the protein at molecular and functional level. However, in ours trials to express this protein in the bacterial system, we observed *Pv*Dre2 mediated cellular toxicity upon IPTG induction, that led to decreased cellular growth. Thus in this chapter, we have tried to understand the possible reasons behind this cell death phenomenon. In addition, we have exploited this cellular death window post-IPTG induction of *Pv*Dre2 to analyze the interactions between *Pv*Dre2 and Artemether.

4.2 Results

4.2.1 PvDre2 Overexpression led to E. coli cellular toxicity

As discussed in Chapter 3, *Pv*Dre2 gene was cloned in pRSETA vector and samples were collected post-IPTG induction at regular intervals for protein expression analysis. However, while collecting samples post-IPTG induction we came across two interesting observations for *Pv*Dre2 induced culture in comparison with vector induced or clone uninduced: 1) the bacterial pellet appeared brown in colour Post IPTG induction **(Figure 4.2)** and 2) decrease in the cell density post IPTG induction **(Figure 4.3)**.

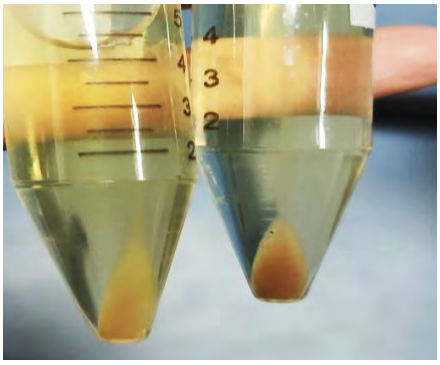

Figure 4.2: Brown colour bacterial pellet visible after *Pv*Dre2 overexpression 4hr post-IPTG induction

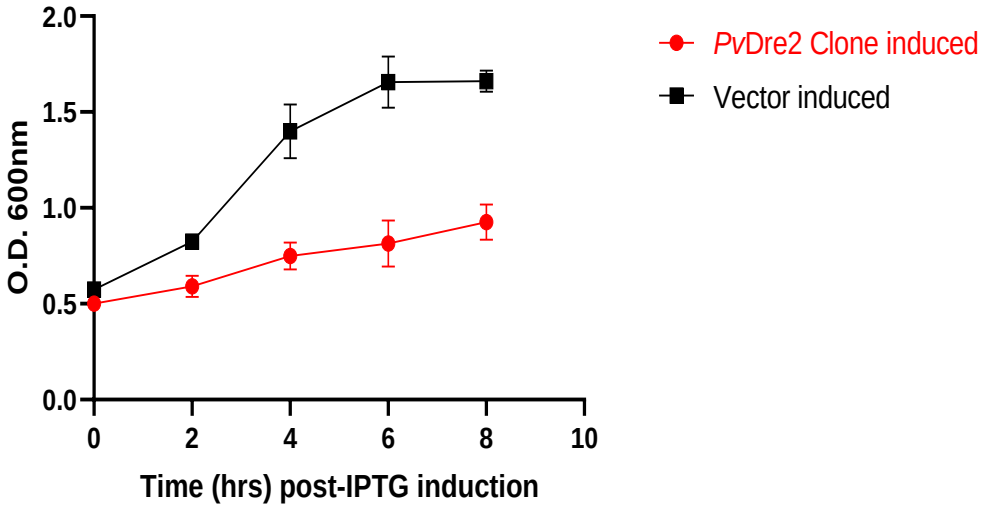

Figure 4.3: *E. coli* growth kinetics post-IPTG induction for *Pv*Dre2 at different time points. *Pv*Dre2 Clone induced (red) and pRSETA vector induced (black).

4.2.2 ICP-OES analysis of Recombinant PvDre2

We were intrigued by these observations, so we went into the available literature where we came across following reports: 1) Zhang et. al. showed that when yeast Dre2 was overexpressed and purified from *E. coli*, the protein was brown in colour and that colour was mainly due to the [Fe-S] binding to the Dre2 (Zhang et al., 2008). 2) Another report by Corless et. al. suggested a positive correlation between iron occupancy and Fe-S proteins [Note: Fe-S proteins are protein which required [Fe-S] clusters for its own functionality] (Corless et al., 2020). Hence, we collected samples every 2 hours (0hr-8hr) post IPTG induction from *Pv*Dre2 clone induced, clone uninduced and vector induced (empty vector) bacterial cultures and performed ICP-OES to quantify the iron present in these samples. In addition, to analyse if heterologous expression based Fe accumulation is unique to *Pv*Dre2 or whether all [Fe-S] cluster biogenesis proteins accumulate iron, we took another [Fe-S] cluster biogenesis protein *Pv*IscU, a component of ISC pathway as a control (refer chapter 5 for details about overexpression of *Pv*IscU in *E. coli* system). For ICP-OES, the collected bacterial samples (*Pv*Dre2, *Pv*IscU and Control) were pelleted and dried at RT for 24 hr. The dried bacterial pellet was treated with 30% HNO_3 solution and further incubated at RT for 48 hr. The mixture was then sonicated and centrifuged and the obtained supernatant was filtered, diluted and subjected to ICP-OES (Optima 8000 PerkinElmer) analysis. Three Fe standards of 1ppm, 10ppm and 50ppm were used for the standard curve preparation.

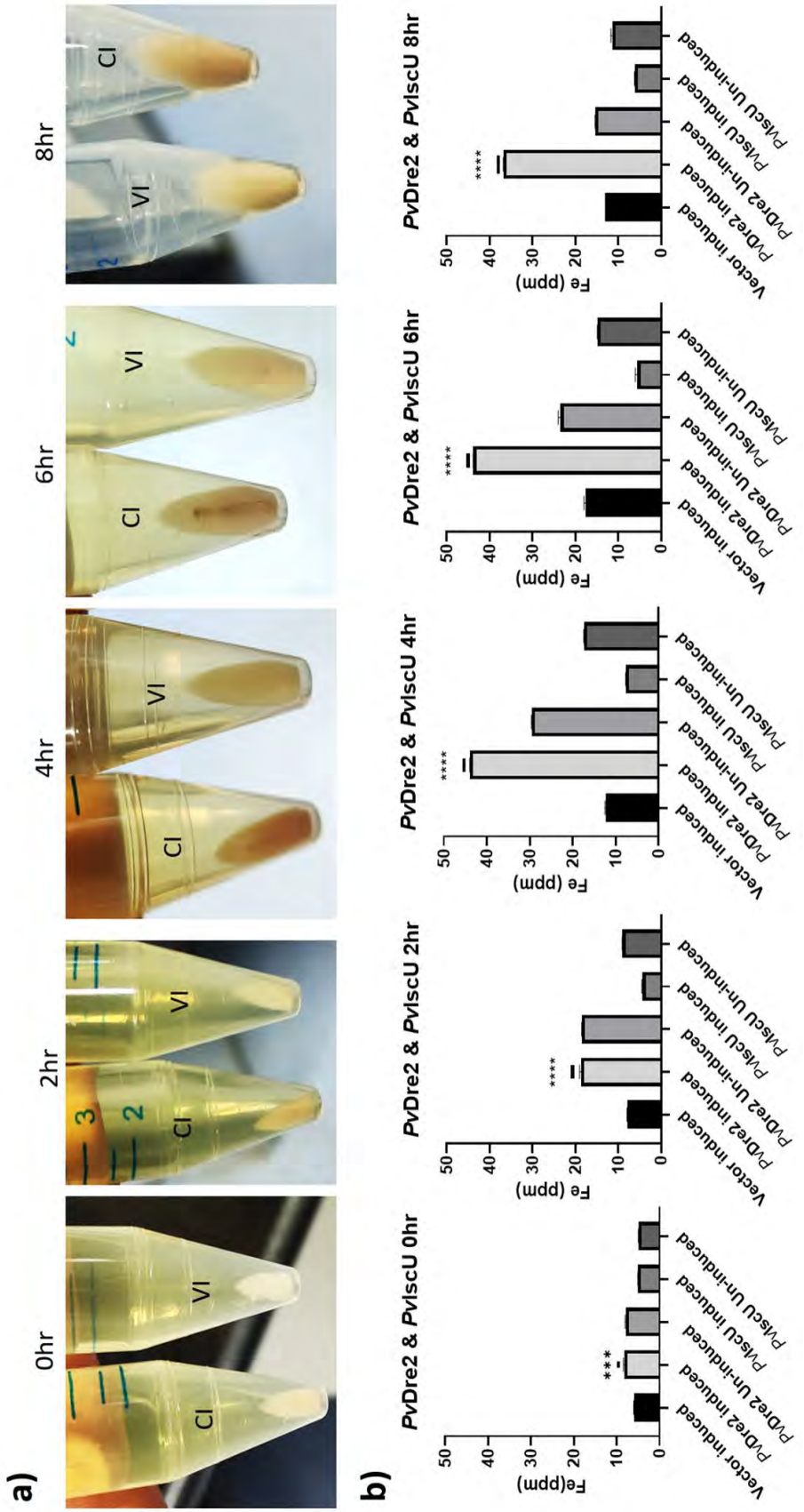

Figure 4.4: Accumulation of iron in *Pv*Dre2 and *Pv*IscU overexpressed *E. coli* cells. a) Brown colour bacterial pellet visible after *Pv*Dre2 overexpression at regular intervals post IPTG induction at 0, 2, 4, 6, and 8hr b) Inductively Coupled Plasma Optical Emission Spectroscopy (ICP-OES) measurement of Iron in Vector induced, *Pv*Dre2 Induced, *Pv*Dre2 Un-induced, *Pv*IscU Induced, *Pv*IscU Un-induced samples (ordinary one-way ANOVA, SD, n=2, *p<0.05)

Three different biological replicates for each sample were analysed for Fe accumulation by ICP-OES at the wavelength of 238.204 nm (Tu et al., 2012). We observed ~3-4 times more iron accumulation in the *Pv*Dre2 induced bacterial culture compared to *Pv*Dre2 uninduced and Vector (pRSETA) induced bacterial culture. Also the iron content was found to be more in the *Pv*Dre2 induced bacterial culture when compared with *Pv*IscU induced and uninduced cultures. The brown colour was observed only for the *Pv*Dre2 induced bacterial culture **(Figure 4.4)**. These results suggest that the tendency to accumulate iron is specific to *Pv*Dre2 as no iron accumulation was observed for *Pv*IscU induced cultures. This intracellular increase in the iron also might be one of the reasons for bacterial death**.**

4.2.3 Colony forming unit assay and Hoechst PI assay for assessing E. coli growth upon PvDre2 overexpression

As mentioned above, we observed a decrease in OD_{600} of bacterial culture post IPTG induction in *Pv*Dre2 induced bacterial culture when compared to vector induced or clone uninduced bacterial cultures **(Figure 4.3)**, suggesting *Pv*Dre2 mediated cellular toxicity in *E. coli*. Thus, to validate the decrease in OD_{600} for *E. coli* cells and to associate it with cellular death, we performed bacterial colony forming unit assay to determine the bacterial cell growth and cell viability assay using Hoechst/Propidium Iodide (PI) dyes to differentiate between live and dead cells. For performing CFU, the induced and uninduced bacterial samples were diluted with fresh LB media to prepare 10^{-1}, 10^{-3} and 10^{-5} dilutions and 5 µl of these respective dilutions were spread on LB agar plates and incubated at 37°C. Colony forming units were quantified and CFU/ml graph was plotted accordingly. We observed decrease in CFU/ml for the 2^{nd} and 4^{th} hour post IPTG induction, confirming cellular toxicity due to overexpression of *Pv*Dre2 protein **(Figure 4.5)**.

In this assay, Hoechst dye can stain both live and dead cells while PI will only be able to stain dead cells by penetrating their damaged membranes. Also the Hoechst-PI staining indicated an increase in cellular death in *Pv*Dre2 induced cells with increasing time points post IPTG induction, as more PI staining was observed for *Pv*Dre2 expressing bacterial cells when compared to vector induced or clone uninduced bacterial cells. This validates our results regarding *Pv*Dre2 mediated *E. coli* cellular toxicity **(Figure 4.6 a and b)**.

Time	0hr		2hr		4hr		6hr		8hr	
Dilution factor	10 -1	10 -3	10-1	10 -3	10 -1	10 -3	10 -1	10 -3	10 -1	10 -3
E. coli strain	BL21 pLysS	BL21 pLysS	BL21 pLysS	BL21 pLysS	BL21 pLysS	BL21 pLysS	BL21 pLysS	BL21 pLysS	BL21 pLysS	BL21 pLysS
VI	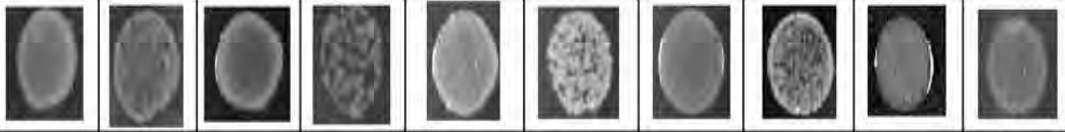									
CI	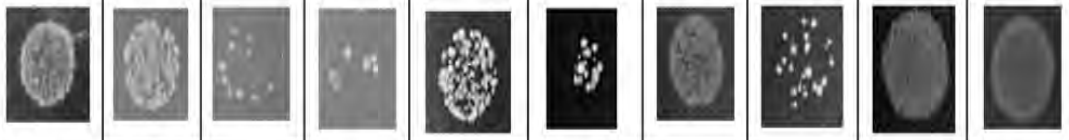									
CUI	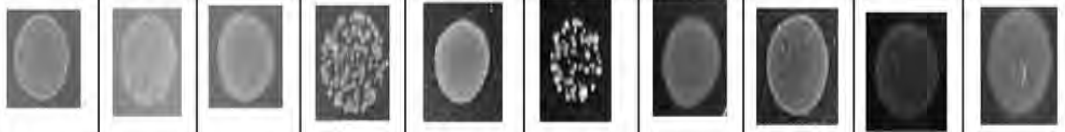									

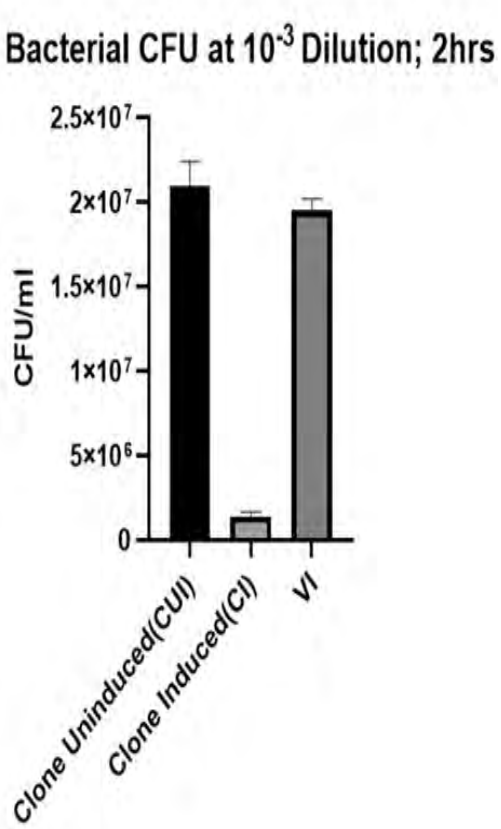

Figure 4.5: Colony Forming Units assay for Bacterial cell growth determination. Bacterial samples [VI, CI and CUI] plated for CFU/ml study at 0hr, 2, 4, 6 and 8 hr. the experiment was performed twice. Bacterial CFU graph was prepared for 2hr Post IPTG-induction at 10^{-3} dilution. Note: For CFU/ml assay 5µl was plated from respective dilutions prepared at different time points (CI: Clone induced, VI: Vector Induced, CUI: Clone uninduced), (ordinary one-way ANOVA, SD, n=2, *$p<0.05$)

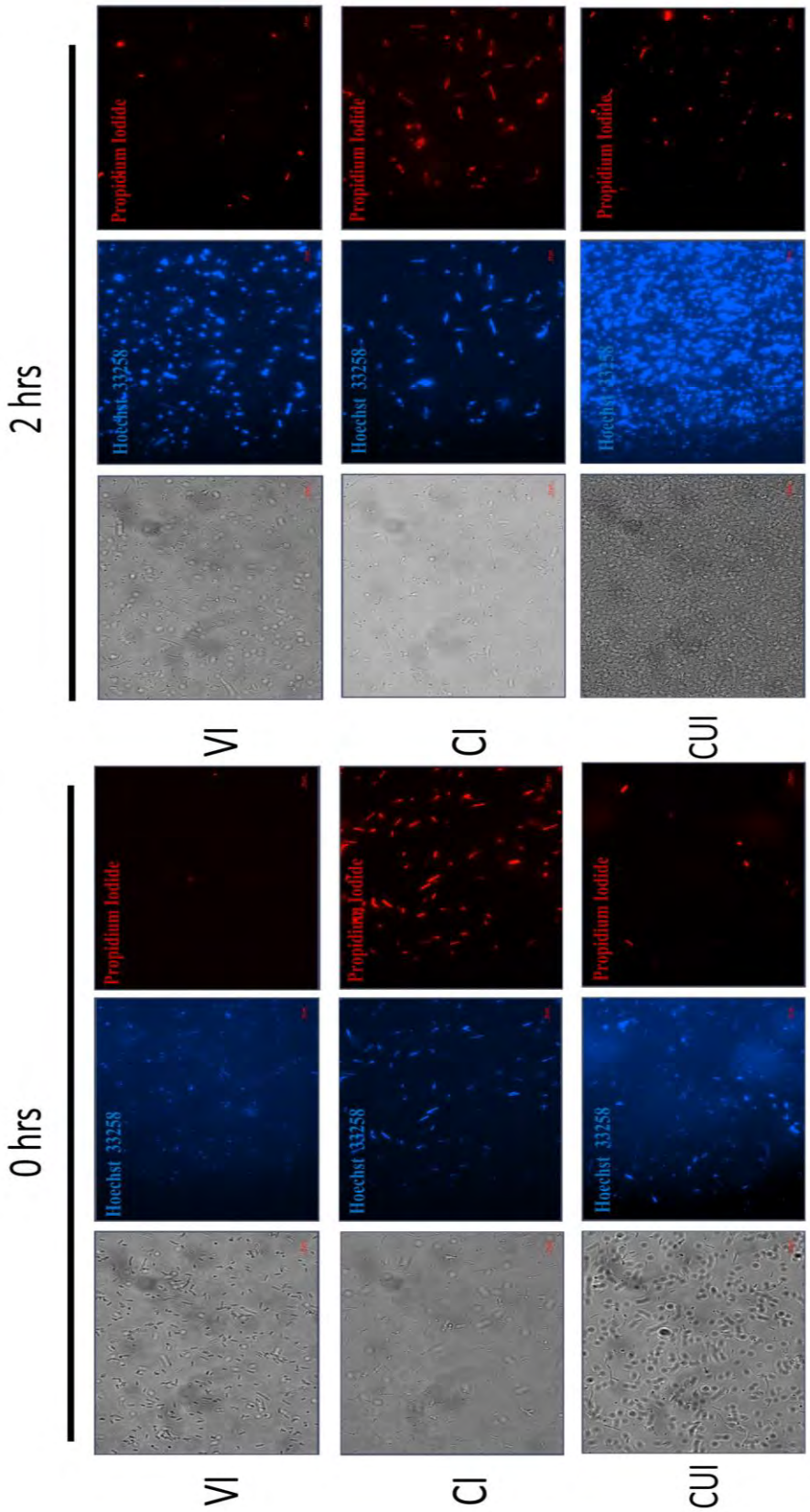

Figure 4.6a: Viability assay for *E. coli* cells expressing *Pv*Dre2 protein using Hoechst/PI (63X magnification): live-dead staining for CI, VI and CUI at 0 and 2hr post IPTG-induction (CI: Clone induced, VI: Vector Induced, CUI: Clone Uninduced)

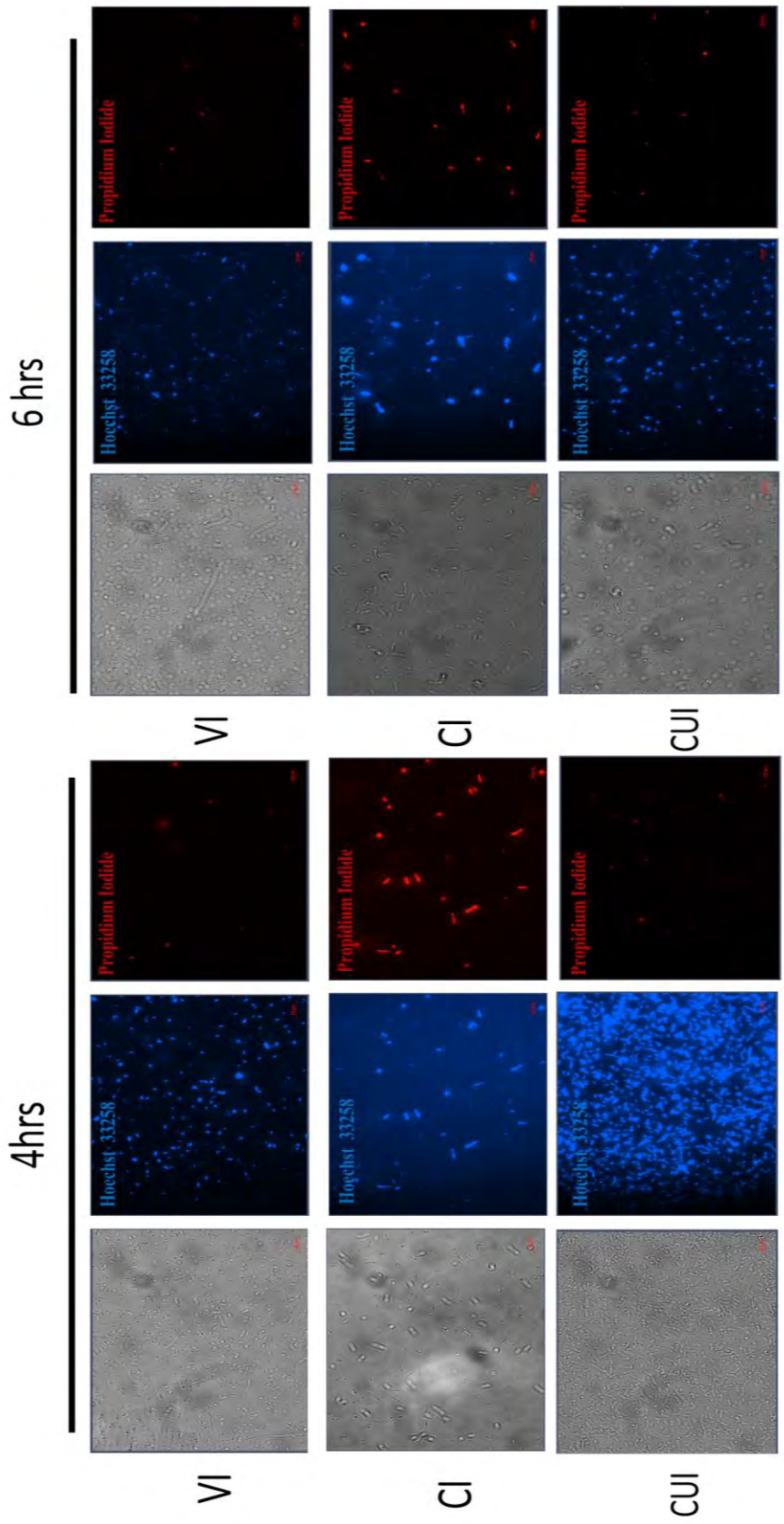

Figure 4.6 b: Viability assay of *E. coli* cells expressing *Pv*Dre2 protein using Hoechst/PI (63X magnification) live-dead staining for CI, VI and CUI at 4 and 6hr post IPTG-induction (CI: Clone induced, VI: Vector Induced, CUI: Clone Uninduced)

4.2.4 Reactive Oxygen Species (ROS) detection by H2DCFDA

As confirmed through cell growth and viability assays that the overexpression of *Pv*Dre2 protein results in cellular toxicity, further we examined whether the intracellular increase in the iron observed might be one of the reasons for bacterial death**.** Studies by Imlay, have reported that ROS and [Fe-S] clusters are intimately linked and [Fe-S] clusters seem to be both the source and the target of ROS. He also suggested that the iron atoms that are released upon cluster destruction can react with hydrogen peroxide to generate hydroxyl radicals, which can cause substantial DNA damage (Imlay 2003; 2006)**.** Thus to check whether there is any oxidative stress induced in the *E. coli* cells expressing *Pv*Dre2 protein due to iron accumulation that might be responsible for their death, we quantified the ROS levels in these cultures at regular intervals post IPTG induction using H2DCFDA. We also used another [Fe-S] cluster biogenesis protein; *Pv*IscU to check if other [Fe-S] binding proteins also generate oxidative stress. There was a significant increase in ROS production post IPTG induction (**Figure 4.7)** that correlates with the decrease in the cellular absorbance OD_{600}. However, no ROS generation was observed in *Pv*IscU induced samples when compared with vector induced and clone uninduced (*Pv*IscU) (**Figure 4.7)**. These experiments suggest that *Pv*Dre2 upon heterologous expression generates oxidative stress possibly through the accumulation of iron.

4.2.5 PvDre2 mediated cell toxicity results in upregulation of Stress genes in E. coli

During our ICP-OES, Hoechst PI and ROS generation assays, we came across an interesting observation. While there was decrease in *E. coli* growth possibly due to iron accumulation and ROS generation at 2^{nd} and 4^{th} hour post IPTG induction, complete cellular recovery was observed at later time points i.e. 6^{th} and 8^{th} hour post IPTG induction. This suggests that with time, the *E. coli* cells somehow undergoes recovery**.** This initiated us to analyse the gene expression levels of *E. coli* stress genes such as *mazF, soxS* and *recA* to examine whether the *Pv*Dre2 overexpression led toxicity has any effect on the stress pathway of *E. coli*. For the same, *Pv*Dre2 expressing *E. coli* samples were collected at 0, 2, 4, 6 and 8 hr post-IPTG induction, and total RNA was isolated from these samples. cDNA was prepared from these samples using QuantiTect Reverse transcriptase kit and this cDNA was used for Quantitative RT-PCR. The 10µL reaction mixture contained 5µL of iTaq^{TM} Universal SYBR® Green Supermix, 1µL of each forward and reverse gene specific primers (10 pmol μL^{-1}) synthesized for *E. coli*

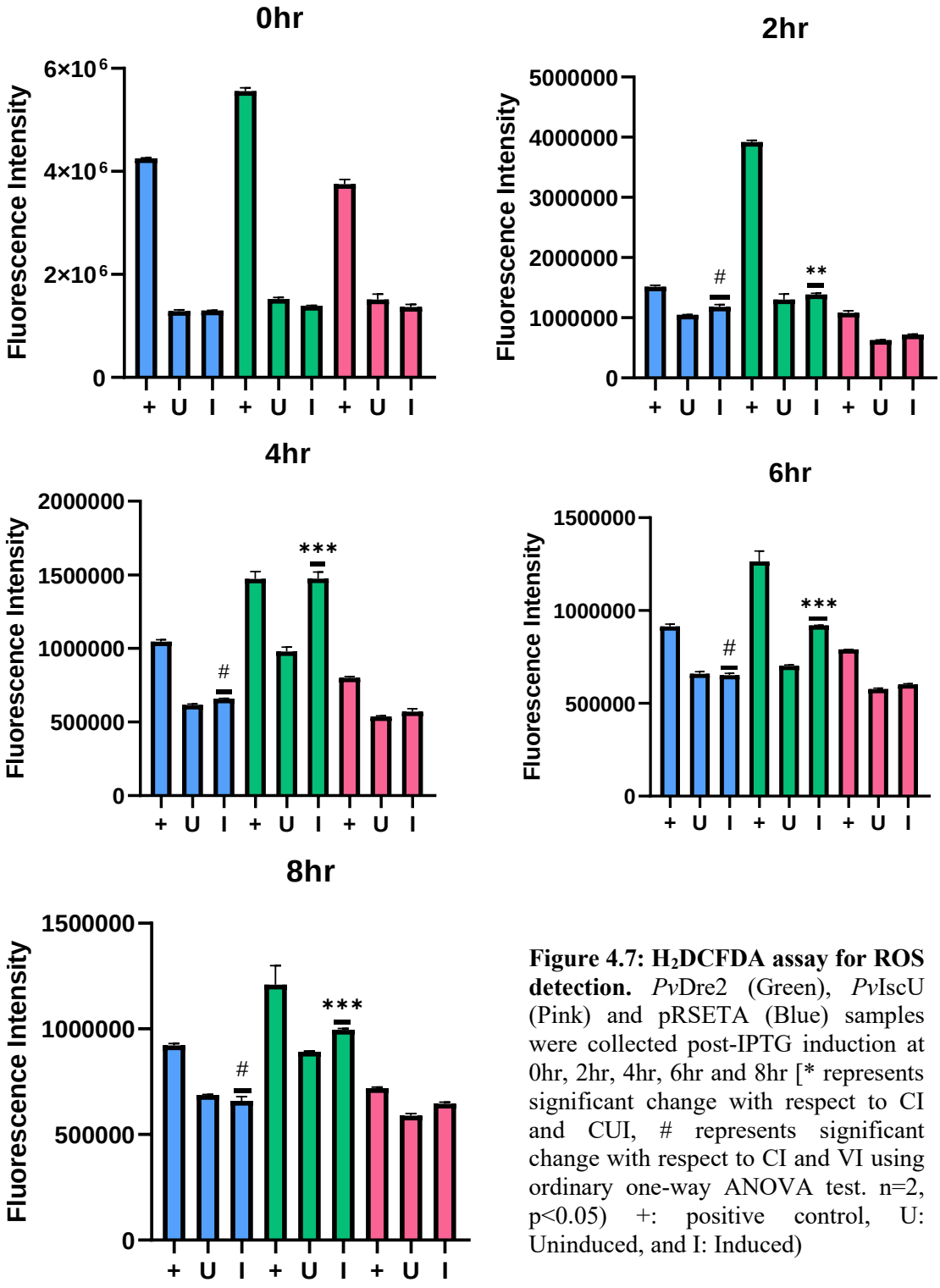

Figure 4.7: H_2DCFDA assay for ROS detection. *Pv*Dre2 (Green), *Pv*IscU (Pink) and pRSETA (Blue) samples were collected post-IPTG induction at 0hr, 2hr, 4hr, 6hr and 8hr [* represents significant change with respect to CI and CUI, # represents significant change with respect to CI and VI using ordinary one-way ANOVA test. n=2, $p<0.05$) +: positive control, U: Uninduced, and I: Induced)

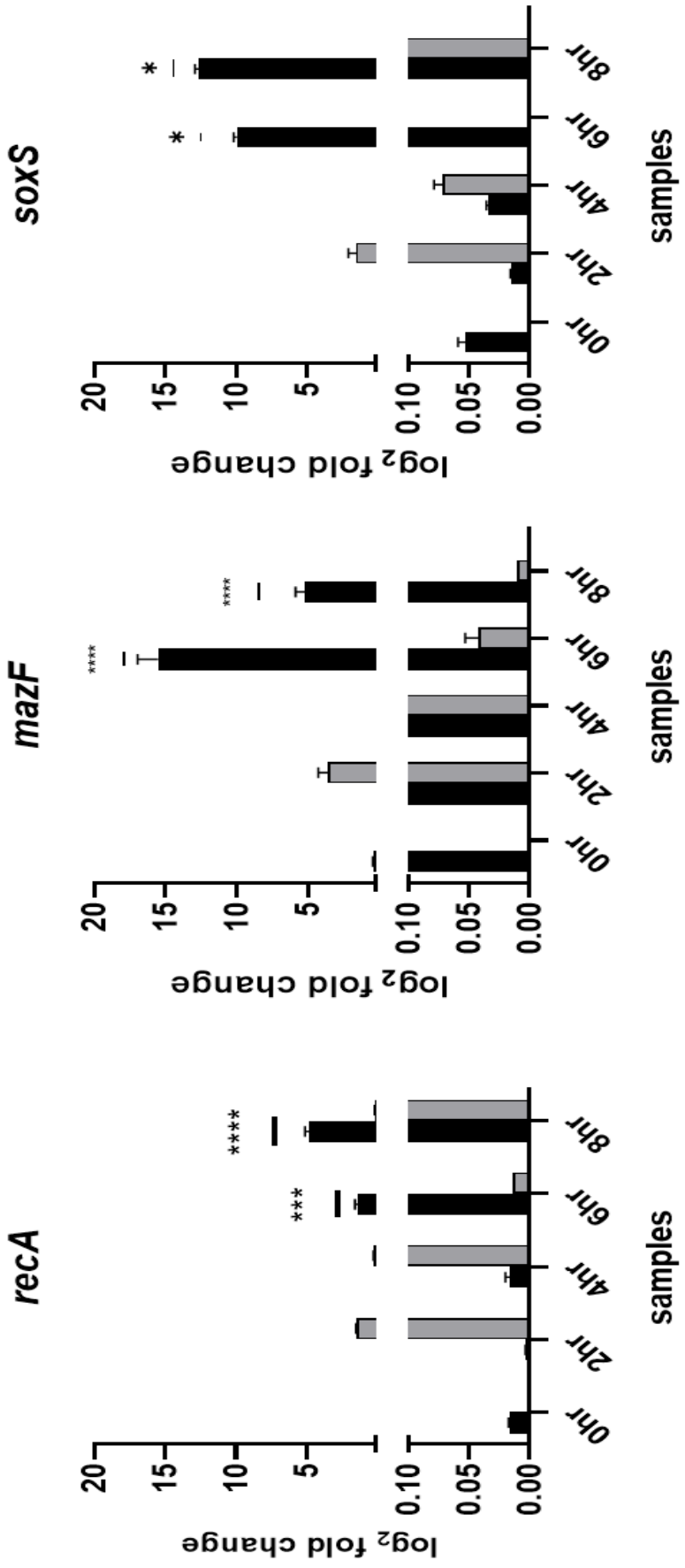

Figure 4.8: Quantitative Real time PCR for *E. coli recA*, *mazF* and *soxS* gene. X axis: *Pv*Dre2 Induced and *Pv*Dre2 Uninduced samples at different time points post-IPTG addition; Y axis: log fold change for *E. coli* stress genes in *Pv*Dre2 induced (Black) and *Pv*Dre2 Uninduced (Grey) samples when compared with pRSETA Induced bacterial samples (VI). (Two-way ANOVA, mean ±SD, n=2, *p<0.05) [*, **, and **** represents statistical significance]

stress genes viz. *recA, mazF and soxS*, 2µL of nuclease-free water and 1µL of diluted cDNA template. Thermal cycling was performed as follows: 94°C for 2 min followed by 30 cycles of 94°C for 1 min, 54°C for 1min, and 72°C for 40 sec followed by a cycle of 72°C for 5 minutes. The relative fold change in the mRNA expression level was determined according to the $2^{-\Delta\Delta Ct}$ method described (Livak and Schmittgen, 2001) by keeping 16S rRNA gene as an internal control. We observed an increase of these transcripts in *Pv*Dre2 clone induced samples at later time points i.e., $6^{th,}$ and 8^{th} hr, which suggests activation of *E. coli* stress machinery in these cells ultimately leading to *E. coli* cellular growth recovery **(Figure 4.8)**.

4.2.6 Heterologous expression of PvDre2 results in Membrane Pathologies

In chapter 3, we have shown the mitochondrial localization of Dre2 in *P. vivax* infected blood smears. Also the Dre2 protein in yeast, humans and *Arabidopsis* is reported to be localized in inter-membranous space of mitochondria. Thus to analyse bacterial membrane dynamics due to *Pv*Dre2 heterologous overexpression, *Pv*Dre2 overexpressing bacterial cells were compared against normal bacterial cells using Scanning Electron Microscopy (SEM) for any defects, that may be responsible for cell death. SEM analysis for *Pv*Dre2 induced bacterial cells showed variety of membrane pathologies upon *Pv*Dre2 overexpression, while the vector induced cells exhibited normal morphology. As shown in **Figure 4.9**, normal *E. coli* cells (untreated) present smooth surface and perfect rod shaped cells with approximate size of 0.5 to 1.5µm whereas *Pv*Dre2 expressing cells were elongated, deformed, flattened and filamentous in shape representing cell morphology defects. The membrane defects were visible even at the early time points after *Pv*Dre2 induction in the cells and kept on increasing at later time points. Additional membrane deformities in case of *Pv*Dre2 overexpressing cells include membrane blebbing, outer membrane vesicular structures (OMVs), membrane cavity formation, membrane rupturing leading to intracellular exudation etc **(Figure 4.9)**. Hence, *Pv*Dre2 overexpression in *E. coli* led to variety of membrane pathologies suggesting its possible role in membrane dynamics/interaction.

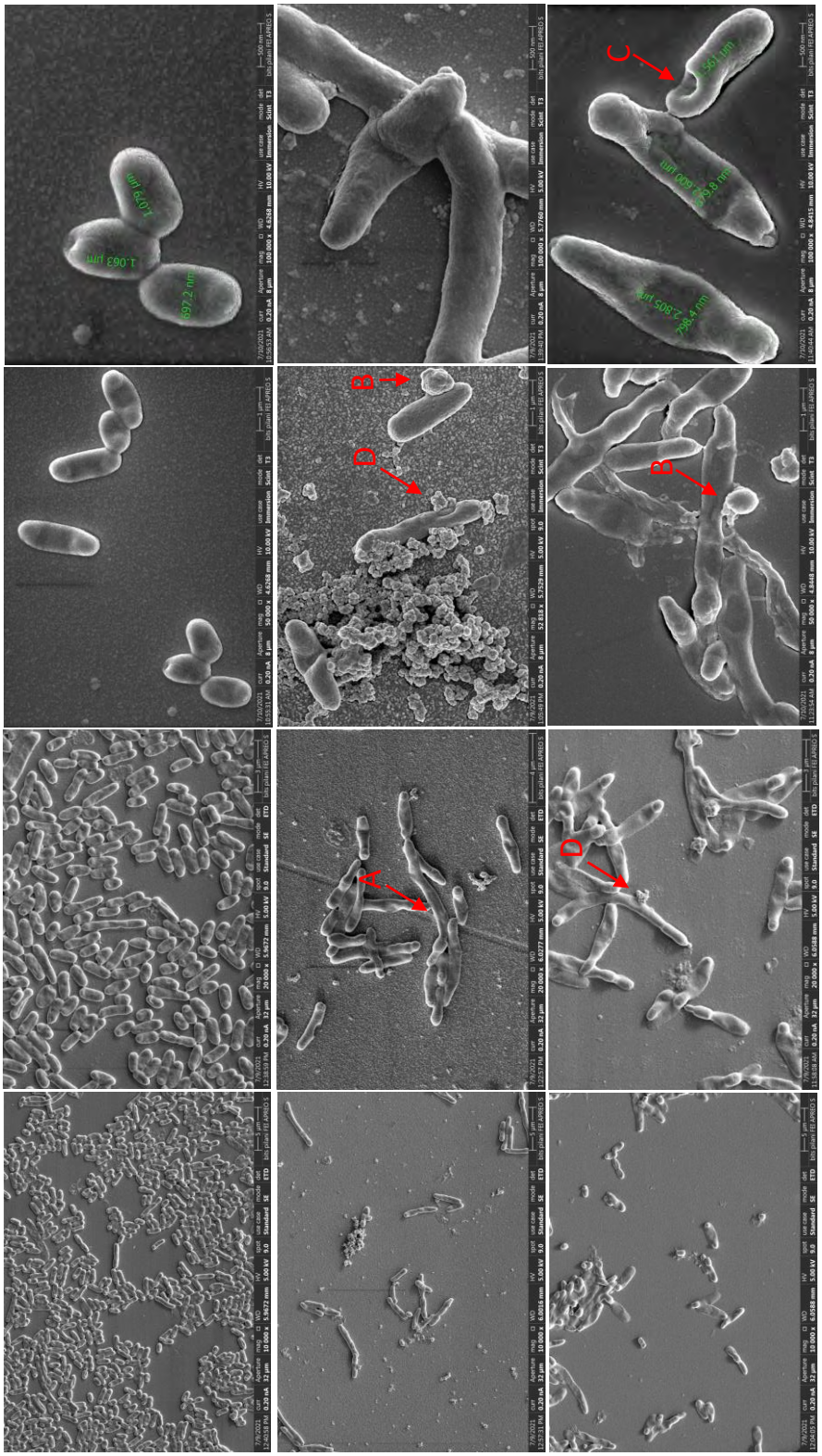

Figure 4.9: Scanning Electron Microscopy for Morphological changes in *E. coli* cells with *Pv*Dre2 overexpression [VI: Vector Induced and CI: Clone (*Pv*Dre2) Induced] Arrow mark: A=filamentous shape, B= membrane blebbing, C= membrane cavity formation, D= rupturing of membrane leading to intracellular exudation

4.2.7 Artemether binds to PvDre2 and rescues the E. coli cells expressing PvDre2

As mentioned above, *Pv*Dre2 heterologous expression led to *E. coli* cellular toxicity majorly due to Fe accumulation mediated oxidative stress and membrane pathologies. Proteomic studies have identified *Pf*Dre2 as one of the proteins that shows interaction with Dihydroartemisinin (DHA) (Siddiqui et al., 2022). Thus to further evaluate if Artemisinin has any effect on *Plasmodium* Dre2 overexpression induced toxicity in heterologous system, we performed the Colony Forming Unit (CFU) assay and analysed the growth for induced r*Pv*Dre2 cultures at different time points with and without exogenous Artemether. We observed that in the presence of Artemether, bacterial growth was restored to normal even at early time points suggesting that Artemether reverses the *Pv*Dre2 mediated growth retardation in bacteria **(Figure 4.10)**. These results indicate that *Pv*Dre2 is possibly a plausible target of Artemether.

Furthermore, to analyse, whether Artemether has any effect on the induction of *Pv*Dre2 in *E. coli*, we collected bacterial cultures expressing *Pv*Dre2 at different time points (0, 2, 4, and 6hr) post-IPTG induction with and without Artemether. These samples were then subjected to SDS-PAGE analysis with various controls **(Figure 4.11)**. We could see no change in *Pv*Dre2 protein expression in the presence of Artemether. This observation suggests Artemether could interact directly with *Pv*Dre2 protein rather than modulating *Pv*Dre2's expression inside *E. coli* cells.

Time	0hr			2hr			4hr			6hr		
Dilution factor	10 -1	10 -3	10 -1	10-1	10 -3	10 -1	10 -1	10 -3	10 -1	10 -1	10 -3	10 -1
E. coli strains	BL21 pLysS	BL21 pLysS	DH5α	BL21 pLysS	BL21 pLysS	DH5α	BL21 pLysS	BL21 pLysS	DH5 α	BL21 pLysS	BL21 pLysS	DH5α
Uninduced	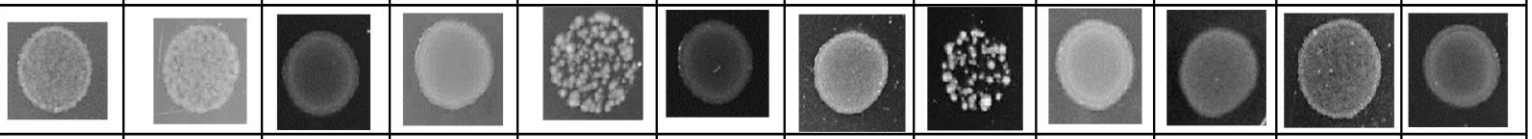											
Induced	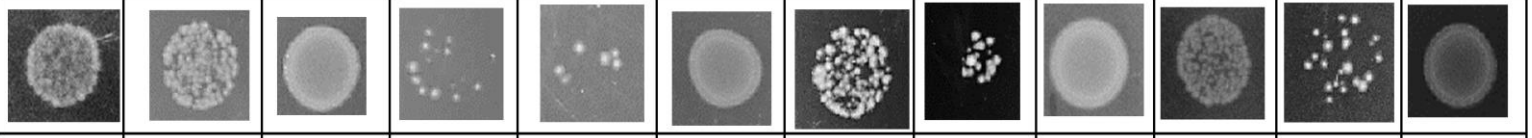											
Induced+ 20nM Artemether	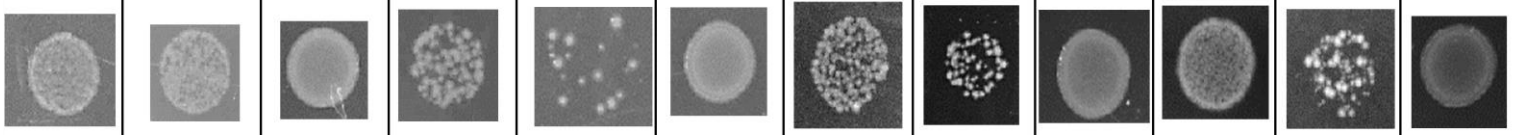											

Figure 4.10: **Effect of r*Pv*Dre2 expression on growth of *E. coli* cells in presence and absence of exogenously supplied 20nM Artemether.** Colony forming units (CFU) were measured at 2hr, 4hr and 6hr time points. For CFU assay, 10^{-1} and 10^{-3} dilutions were prepared at desired time points and then 5µL was plated from each dilution.

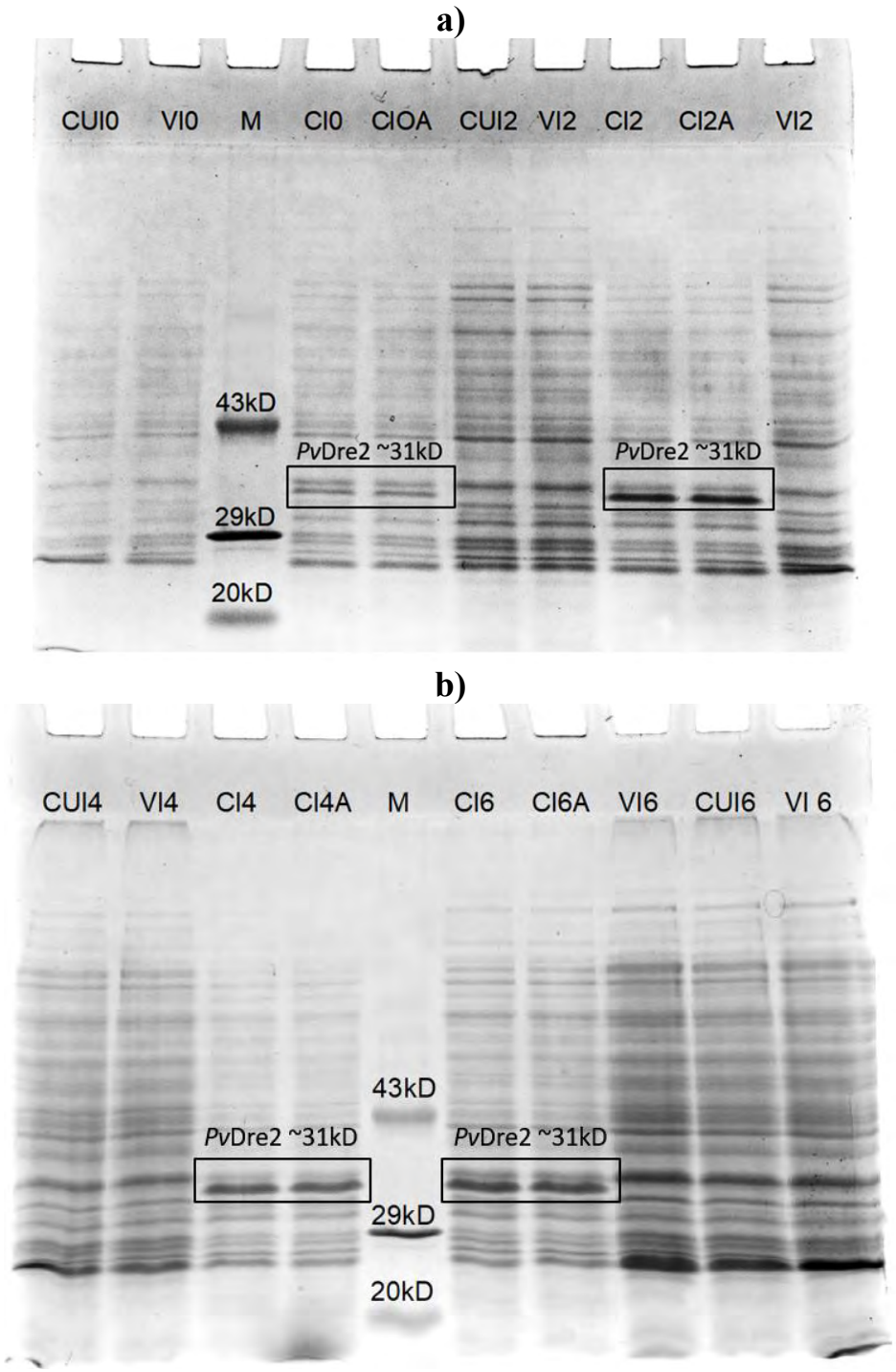

Figure 4.11: Overexpression of full-length *Pv*Dre2 Protein in *E. coli* with and without Artemether (M: Protein Molecular Low Weight Marker (PMWL Genei); VUI: pRSETA uninduced; VI: pRSETA induced; CUI: pRSETA *Pv*Dre2 clone uninduced; CI: pRSETA *Pv*Dre2 clone induced; and CIA: pRSETA *Pv*Dre2 clone induced sample with Artemether; the number in the lane represents time interval post-IPTG induction i.e., CI0A is clone induced with Artemether at 0hr post-IPTG Induction)

4.3 Discussion

Dre2 is shown to be involved in multiple housekeeping pathways, such as apoptosis, epigenetic regulation and immune responses, alongside conventional [Fe-S] cluster biogenesis CIA pathway (Buzas et al., 2014; Hao et al., 2006; Wang et al., 2019; Yamaguchi et al., 2019; Yoshikawa et al., 2016). Even the co-immunoprecipitation analysis performed by us suggested its interaction with multiple partners from various pathways such as ribosome biogenesis, Golgi trafficking etc. as discussed in Chapter 3. In this chapter we have discussed the possible reasons for the toxicity effects of overexpression of *Pv*Dre2 in a prokaryotic heterologous *E. coli* system. Later we have shown the interaction of *Pv*Dre2 with Artemether to rescue the bacteria from *Pv*Dre2 induced toxicity, which adds on to another non-canonical role for Dre2.

During heterologous *Pv*Dre2 protein expression in *E. coli*, detrimental effects of overexpression of *Pv*Dre2 protein was observed for *E. coli* growth at 2nd and 4th hr post IPTG-induction, as analysed by reduced pellet size and bacterial density analysis at OD_{600}. The growth defects in *E. coli* due to *Pv*Dre2 overexpression were also confirmed using Colony Forming Unit assay and Live-dead staining (Hoechst/PI). In addition to reduced *E. coli* growth post IPTG induction, we also observed that the bacterial pellet after *Pv*Dre2 expression in *E. coli* was reddish brown in colour. According to reports, the Dre2 protein in its wild-type form exhibits a brown coloration following its purification under native conditions, which can be attributed primarily to the existence of [4Fe-4S] and [2Fe-2S] clusters on the protein (Netz et al., 2016; Zhang et al., 2008). Thus we quantified iron through ICP-OES which revealed a noticeable increase of approximately ~2 to 3.5 times in iron concentration (ppm) in *Pv*Dre2-induced *E. coli* cells compared to Vector-induced bacterial culture. These findings suggest a potential involvement of *Pv*Dre2 in the accumulation of iron in the *E. coli* system. To ensure that this iron accumulation is specific to *Pv*Dre2 and not to other [Fe-S] cluster biogenesis proteins in general, we also performed an ICP-OES analysis for *Pv*IscU, the scaffold protein involved in ISC machinery. However, *E. coli* cells overexpressing *Pv*IscU at similar time points as that of *Pv*Dre2 did not show any increase in iron when compared with vector induced samples. This observation signifies the peculiar role of *Pv*Dre2 in iron accumulation.

As elevated intracellular iron concentrations have been reported to lead to Fenton reaction, i.e., ROS generation, we correlated *Pv*Dre2 mediated bacterial iron accumulation with ROS generation. ROS analysis in *Pv*Dre2 expressing *E. coli* cells also revealed significant ROS production at the 2nd and 4th hr post IPTG induction. We also noted decreased CFU/ml counts and more PI staining at later time points post-IPTG induction in *Pv*Dre2 expressing cells which perfectly aligned with our ROS analysis. Hence, the *E. coli* cellular toxicity seems to be mainly due to iron mediated oxidative stress inflicted by *Pv*Dre2 overexpression.

To analyse *Pv*Dre2-induced *E. coli* cell death at the morphological level, we also performed Scanning Electron Microscopy. SEM analysis showed several membrane deformities in *Pv*Dre2 expressing *E. coli* cells, such as elongated *E. coli* cells, membrane blebbing and cavity formation as well as rupturing of cells releasing cellular exudates. The membrane deformities increased from 0 hr post-IPTG Induction of *Pv*Dre2 protein to 4th hr with the time showing a direct correlation with *Pv*Dre2 overexpression. Thus *Pv*Dre2 may play a role in membrane dynamics or interaction possibly by translocating to the periplasmic space. Even evolutionary IMS of mitochondria can be traced back to the periplasmic space of prokaryotes. Because of their shared history, most proteins directed to these compartments become structurally stabilized by disulfide bond formation, which helps keep them in the IMS/Periplasm (Backes et al., 2019). Banci et al. has also reported that Mia-40, an IMS resident oxidoreductase, interacts with Dre2 in humans and catalyses the formation of disulfide bonds at the CXXC twin motif (Motif II) that eventually traps Dre2 in IMS (Banci et al., 2011).

In addition to *Pv*Dre2-mediated membrane pathologies, we also noticed outer membrane vesicular structures during SEM. Outer membrane vesicles (OMV) formation through blebbing happens due to accumulation of peptidoglycan fragments or misfolded protein into the periplasmic space of bacteria. This membrane deformity generally happens due to turgor pressure generated onto outer membrane that leads to outer membrane vesicles (OMV) release (Toyofuku et al., 2019). Also as per a recent study, iron-limiting conditions impact phospholipid transporter genes in *V. cholera*, *E. coli*, and *H. influenzae*, causing OMV development. But little is known about how environmental stress alters other genes in OMV development (McBroom & Kuehn, 2007; Roier et al., 2016).

As mentioned above, the CFU/ml data in *Pv*Dre2 expressing *E. coli* showed cellular death at 2 and 4 hr post IPTG-induction, but later at 6 and 8 hr, an increase in CFU/ml counts was observed indicating cellular recovery for *E. coli* despite the ongoing stress. Till date, three distinct programmed cell death pathways have been identified in *E. coli*, viz i) mazEF pathway (toxin-antitoxin module): A quorum-sensing based pathway that requires a penta-peptide named Extracellular death factor (EDF) for the initiation of the pathway, ii) Apoptosis like death (ALD) pathway: this pathway is initiated by recA and lexA, and iii) Thymine Less Death pathway (TLD): this pathway is initiated by ssDNA breaks, generated by Thymine scarcity and ultimately leads to DNA breakage and blockage of replication forks. TLD can be activated at the molecular level through recA-dependent and recA-independent mechanisms. (Lee & Lee, 2019). ALD pathway is functional at the individual cell level and shows *recA*-dependent activation, which means it will get activated only at the time of DNA damage. In contrast, the EDF-mazEF pathway gets activated through various stresses like DNA damage, high temperature, and oxidative stress (Hazan et al., 2004). According to some reports, the EDF-mazEF pathway in *E. coli* represses the *recA*-mediated ALD pathway by lowering *recA* mRNA levels; however, the opposite is not true. (Erental et al., 2012).

In the present study, an increase in the expression of bacterial stress genes (*recA, mazF*, and *soxS*) was observed post IPTG induction at 6^{th} and 8^{th} hr in cells expressing *Pv*Dre2. However, while comparing the *recA* and *mazF* gene expression data for *Pv*Dre2-induced *E. coli* cells, we observed that the 6^{th} hr *recA* transcript is less expressed than the *mazF* transcript. The *recA* and *mazF* gene expression observations from *Pv*Dre2-induced *E. coli* cells are consistent with prior reports, which suggests inhibition of the *recA*-mediated ALD pathway by the EDF-mazEF pathway. EDF-mazEF cell death pathway gets activated in both ROS-dependent and ROS-independent manner. MazF induction during oxidative stress synthesizes different protein groups (i) ygcR and yfbU, ii) elaC, iii) clpP, slyD, and yfiD) essential for moving bacteria towards different cell death pathways, eventually leading to massive population death. However, MazF also produces proteins (yajQ, rsuA, deoC, SoxS, and SoxR) essential for the survival of small subpopulations. Significant ROS generation was seen in *Pv*Dre2-induced *E. coli* at the 2^{nd} and 4^{th} hr. The *soxS* transcript was subsequently elevated in *Pv*Dre2-induced *E. coli* cells to preserve a small subpopulation due to the activation of the ROS-dependent EDF-mazEF pathway. Therefore, when *Pv*Dre2 was expressed as a heterologous protein in

E. coli, iron mediated oxidative stress (ROS) was generated, which activated the ALD and EDF-mazEF cell death pathways in *E. coli* (Amitai et al., 2009).

Recently *Pf*Dre2 has been recognized by proteomic studies as one of the candidates for Dihydroartemisinin (DHA) binding (Siddiqui et al., 2022). Since artemisinin is the first line of drug used to treat malaria, we also examined how Artemether affected bacterial cultures harbouring *Pv*Dre2 after IPTG induction to assess the binding of Artemisinin derivatives with Dre2 and their impact on bacterial growth. We discovered that bacterial growth returned to normal in the presence of Artemether, indicating that Artemether reverses the *Pv*Dre2-mediated inhibition of bacterial growth. Additionally, the presence of Artemether did not result in any apparent alteration in the expression of the *Pv*Dre2 protein. The above observation implies that Artemether may directly interact with the *Pv*Dre2 protein instead of exerting an effect on *Pv*Dre2 gene expression within *E. coli* cells. These findings clearly suggest that Dre2 may be an Artemisinin target. However, it is yet unclear how Artemisinin and Dre2 interact to produce further activity, which requires further experimentation.

Chapter 5

Characterization of mitochondrial [Fe-S] cluster biogenesis scaffold protein IscU from *P. vivax*

Characterization of mitochondrial [Fe-S] cluster biogenesis scaffold protein IscU from *P. vivax*

5.1 Introduction

As detailed in earlier chapters, till now, three [Fe-S] cluster biogenesis pathways have been recorded in *Plasmodium spp*. that includes SUF pathway functional in the Apicoplast, ISC pathway localized to the mitochondria and the cytoplasm based CIA pathway that provides the [Fe-S] clusters to the cytoplasmic and nuclear proteins. As mentioned earlier, most of the components of the ISC pathway have only been recently explored from the malaria parasite *P. falciparum* (Sadik et al., 2021), however there are no reports on this pathway from *P. vivax*. Thus, after exploring into the initial component of the CIA pathway, to delve more into the [Fe-S] cluster biogenesis in the parasite, we focussed on the ISC pathway from *P. vivax.*

The mitochondrial ISC pathway has been extensively studied from bacteria, yeast and humans, which has given significant insights about the various integral steps and the vital proteins involved in the pathway. The similarity of components involved in the ISC pathway in prokaryotes and eukaryotes highlights the evolutionary conservation of this pathway (Lill and Freibert, 2020). In general, for the [Fe-S] cluster biogenesis via this pathway, initially the [Fe-S] clusters need to be assembled onto the ISC scaffold protein ISCU. To achieve this, the sulfur is acquired from the cysteine residue by a cysteine desulfurase enzyme; NFS1 in yeast and humans and IscS in bacteria, which mobilizes the sulfur in association with Isd11. However, the source of iron is still under investigation. Frataxin was once hypothesized to function as an iron chaperone for the pathway, but this hypothesis is no longer supported (Pastore and Puccio, 2013; Gervason et al., 2019; Patra et al., 2019). In fact, recently frataxin has been reported as an allosteric regulator of NFS1 where its binding to NFS1 increases the sulfur transfer rate (Tsai and Barondeau, 2010; Colin et al., 2013). Further, for the assembly of iron-sulfur cluster on the scaffold, Ferredoxin reductase serves as electron transfer protein that donates reducing equivalents to Ferredoxin which further provides these equivalents for initial [Fe-S] cluster assembly and maturation. After maturation, these assembled [Fe-S] clusters get released via a specific chaperone-co-chaperone system. They can be directly transferred to target apo-proteins or can be received by

transfer/carrier proteins such as NFU1, ISCA1, ISCA2, GLRX5, and BOLA3 (Braymer and Lill, 2017; Maio and Rouault, 2020). Other than providing [Fe-S] clusters to apo-proteins of mitochondrial matrix, ISC pathway also provides intermediate [4Fe-4S] clusters or unknown sulfur moiety to cytosolic CIA pathway via mitochondrial ATM1 transporter for the maturation of cytosolic and nuclear Fe-S proteins (Pandey et al., 2019).

In *Plasmodium*, the proteins involved in the ISC pathway were first identified from the *Plasmodium* database using bio-informatics tools. Seeber (2002) reported homologues of the core components of the mitochondrial iron-sulphur cluster biogenesis machinery, including the NFS (PF3D7_0727200) and two homologues of ISCA (PF3D7_0207200 and PF3D7_0322500) (Seeber, 2002). Later the accessory proteins involved in [Fe–S] cluster biogenesis, such as ferredoxin (PFL0705c), ferredoxin NADP+ reductase (PF11_0407), Isd11 protein (MAL13P1.53), FAD linked sulfhydryl oxidase ERV-1 (PFA0500w), Glutaredoxins-like protein (GLP3), Bol, Hsp70, and Hsp20 also were shown to have the mitochondrial homologs in *P. falciparum* (Dooren et al., 2006; Ke and Mather, 2017). However, no homologue of Frataxin could be retrieved from *P. falciparum*.

After identifying the components of the ISC pathway from the parasite, the functional site of the pathway was investigated. In 2003, Sato et al., showed that the N-terminal leader sequence of IscS protein targeted the green fluorescent protein (GFP) to the mitochondrion (Sato et al., 2003), providing evidence that this process occurs in the *Plasmodium* mitochondrion. ACP (acyl carrier protein), which is associated with accessory protein Isd11 in human mitochondrial ISC scaffold (Cory et al., 2017), also have 2 homologues in the parasite, one associated with the apicoplast and other with mitochondria (Waller, 2000). Later in 2013, Gisselberg et al., reported the localization of the ISC desulfurase complex components *Pf*IscS and *Pf*Isd11 to the *P. falciparum* mitochondrion (Gisselberg et al., 2013), confirming mitochondria as the site for ISC pathway in the parasite. Recently Sadik et al. 2021, have characterized most of the core ISC pathway components from *P. falciparum* and shown mitochondria as their functional site.

In addition to localization studies, Sadik et al., 2021 also showed that the scaffold protein *Pf*IscU along with the cysteine desulfurase complex *Pf*IscS–*Pf*Isd11 has the capability to directly assemble [4Fe–4S] clusters without the prior formation of [2Fe–2S] clusters. As a deviation from reported complexes from other organisms, the *P. falciparum* desulfurase-scaffold complex assembles around a *Pf*IscS tetramer instead of a dimer, resulting in a symmetric hetero-hexamer [2 x (2*Pf*IscS – 2*Pf*Isd11 – 2*Pf*IscU)]. Other than deviations at the assembly level, *Pf*IscU was also reported to exhibit changes at the transfer level, where in addition to transfer of clusters via carrier proteins such as chaperones - GLP3, A-Type Assembly Proteins, and *Pf*NifU-like protein, it also has the capability to directly transfer [4Fe–4S] clusters to the apo-protein without any requirement of intermediary proteins. It was also reported that *Pf*IscA1 can primarily bind iron, suggesting its potential role as a Fe^{2+} carrier/donor (Sadik et al., 2021). However, the ISC pathway components from *P. vivax* still remains to be elucidated.

Thus in this study, we have characterized the IscU protein from *P. vivax* clinical isolates. For the same, we have amplified the gene encoding the IscU protein from *P. vivax* infected patients blood samples, cloned it and expressed the recombinant protein in a prokaryotic based heterologous system. Further to decipher the functional role of IscU in the parasite, we performed immune-localization studies on *P. vivax* infected blood smears to identify its functional site and analysed its ability to bind [Fe-S] cluster both *in silico* and *in vitro*. Additionally, we also explored [Fe-S] cluster binding ability of *Pv*IscU in the presence of divalent metal ions to get insights into ISC scaffold's metamorphic property.

5.2 Results

As mentioned above, when we started our work, at that time, only few reports were available for the ISC pathway and they also majorly reported about the mitochondrial localization of proteins involved in ISC pathway. Considering the significance of the mitochondrial ISC pathway scaffold protein in cluster assembly and its role in releasing these assembled [Fe-S] clusters to the apo-proteins of the mitochondrial matrix and cytoplasmic CIA pathway through various mediator proteins and ATM1 transporter (Pandey et al., 2019) respectively, we decided to focus on the scaffold

protein of the ISC pathway for our study. Data mining of PlasmoDB for the scaffold protein involved in the ISC pathway did not retrieved any results at that time. Therefore, we searched and analyzed the Fe-S proteins related to scaffolding activity using *in -silico* tools, which resulted in three proteins with NIFU-like domains in the malarial parasite including two proteins that were targeted to mitochondria, namely NIFU, putative, and NFU1 protein, and one protein targeted to the Apicoplast, called NFUapi (Haussig et al., 2013). Since the ISC pathway is functional inside mitochondria, we focused on the proteins with mitochondrial localization, namely NIFU, putative, and NFU1 protein from *P. vivax*.

5.2.1 Conserved Domain Analysis

To identify the conserved domains of the NIFU, putative (PVX_117755), and NFU1 protein (PVX_087160) from *P. vivax*, we conducted CDD analysis where we identified the IscU-like superfamily domain (47-160 aa) for *P. vivax* NIFU, putative **(Figure 5.1)** and the NifU superfamily domain (85-143 aa) for the protein designated as *P. vivax* NFU1 **(Figure 5.2)**. The identification of the IscU-like superfamily domain in *P. vivax* NIFU, putative, indicates its potential association with the mitochondrial ISC pathway.

Figure 5.1: Conserved domain analysis of *P. vivax* NIFU, putative protein. The region of interval 47-160 shows the presence of the IscU-like superfamily domain.

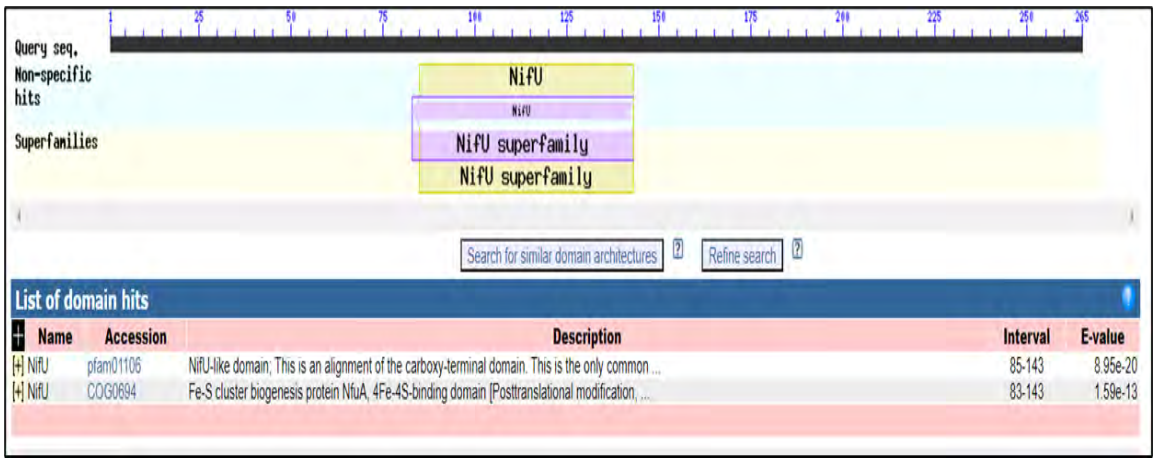

Figure 5.2: Conserved domain analysis of *P. vivax* NFU1 protein. The region of interval 85-143 shows the presence of the NifU superfamily domain.

5.2.2 Phylogenetic Analysis

To further analyze the above two mitochondrial targeted NifU-like domain containing proteins, we determined the evolutionary position of *P. vivax* NIFU, putative and *P. vivax* NFU1 by subjecting the corresponding protein sequences to MEGA11 software for phylogenetic tree generation (Saitou N. et al., 1987; Kumar S et al., 2018). The analysis involved 29 amino acid sequences, including *Plasmodium spp.*, *E. coli* (prokaryote), and higher eukaryotes. All ambiguous positions were eliminated for each sequence pair using the pairwise deletion option. The final dataset comprised 301 positions. The Neighbor-Joining method was employed to infer the evolutionary history of the taxa examined. A bootstrap consensus tree was generated from 1000 replicates to represent the analyzed taxa's evolutionary history **(Figure 5.3)**.

The obtained phylogenetic tree of *P. vivax* NIFU, putative, and *P. vivax* NFU1 with various *Plasmodium spp.*, eukaryotic species, and *E. coli* showed two separate clades: one consisting of NIFU, putative and other with NFU1 **(Figure 5.3)**. The clade with NIFU, putative had all the members belonging to either the IscU proteins or NifU, putative, while the NFU1 mainly consisted of either NFU1 proteins or NifU like proteins, but no IscU protein. This is in accordance to the conserved domain analysis results which suggested NIFU, putative protein to possess the IscU like superfamily domain. Based on these observations, from this point forward we will designate NIFU, putative protein as IscU protein, putative.

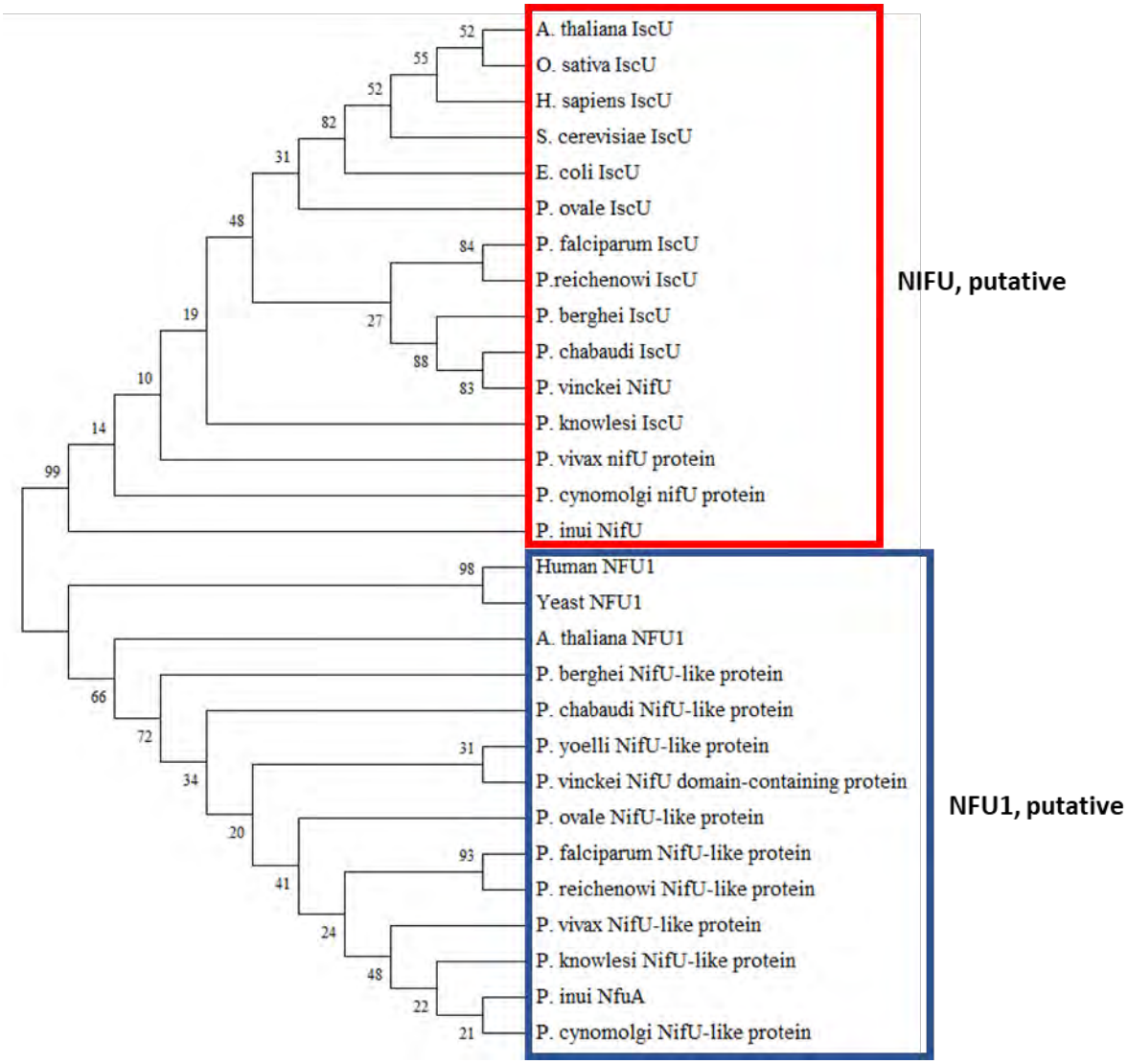

Figure 5.3: Phylogenetic analysis of *P. vivax* NIFU, putative and *P. vivax* NFU1 protein sequences. Bootstrapping was done for 1000 iterations, and the percentage of trees in which the associated taxa clustered together is shown next to branches.

5.2.3 Primer designing and amplification of PvIscU, putative gene

After confirming the *Pv*NIFU, putative protein as IscU protein, putative, we used the gene sequence of *P. vivax Salvador I* (Gene Id: PVX_117755) for designing gene specific primers **(Figure 5.4)**. The *Pv*NIFU, putative gene is 811bp long and is present on chromosome 12, spanning the 2,114,375 - 2,115,185 (-) region. The gene also includes a 5' UTR region and encodes a protein of 170 amino acids (corresponding to 513bp without 5' UTR region). Amplification of full-length gene (without UTR) was obtained from parasite DNA isolated from *P. vivax* clinical isolates using primers SGNFU: 5′ GTG CAT ATG ATG ATG GCT ACT TTC CTC -3' and SGNFD: 5' GCC

GTC GAC TCA ATT TAT CAC TTT TTC TCT -3' following conditions given in **Table 5.1**. The obtained amplicons **(Figure 5.5)** were purified using a QIAquick Gel Extraction kit, commercially sequenced, and analysed as mentioned in the Chapter 2-Materials and Methods.

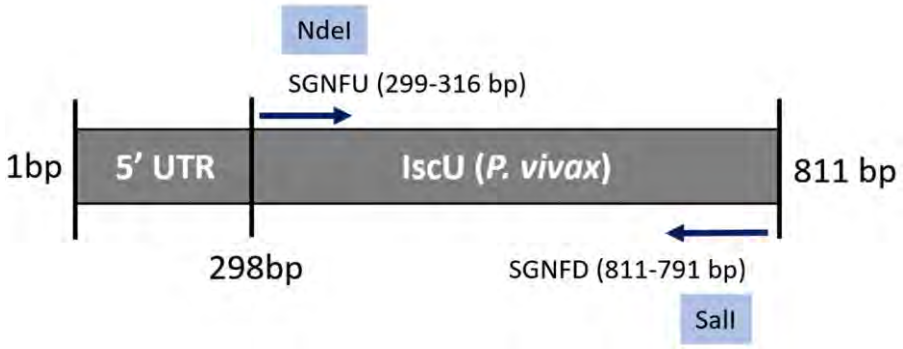

Figure 5.4: Position of primers used for amplification of *P. vivax IscU* gene

Table 5.1: Reaction conditions used for amplification of I*scU* gene from *P. vivax*

Pre-Denaturation	94 °C for 3 min	
Denaturation	94 °C for 1 min	x35
Annealing	53.5 °C for 1 min	
Extension	72 °C for 2 min	
Post Extension	72 °C for 4 min	

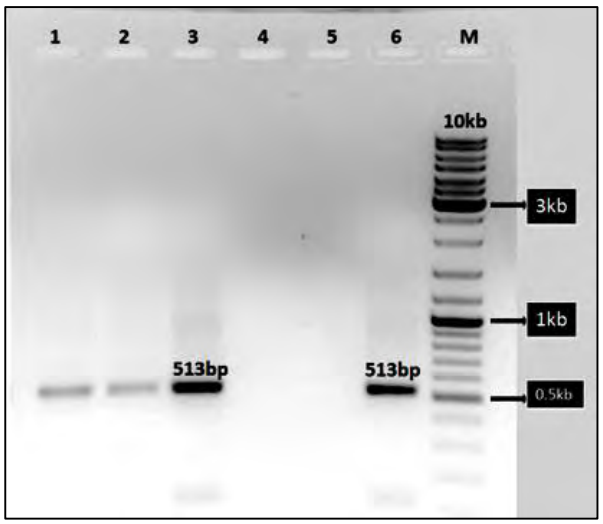

Figure 5.5: Amplification of *IscU* gene from *P. vivax* clinical isolates (Parasite DNA sample no. 1-6, M: Gene Ruler Ladder mix Fermentas SM0331)

5.2.4 Multiple sequence alignment and Signature Motif Analysis

The obtained amplicons from the *P. vivax* Indian isolate was commercially sequenced and compared against different *Plasmodium spp*., prokaryotes, and other eukaryotes using multiple sequence alignment tool Clustal Omega. Percent identity matrix and sequence alignment of *Pv*IscU with other *Plasmodium spp*., showed 78 to 99% similarity, with a percent identity of ~97% with *P. cynomolgi*, ~96% with *P. knowlesi*, and ~80% with *P. falciparum* **(Figure 5.6)**. When aligned with other eukaryotes, *Pv*IscU showed 60% identity with *E. coli* and ~55% with higher eukaryotes, suggesting high sequence conservation of IscU among living organisms **(Figure 5.7).**

P_vivax_indian	100.00	100.00	83.12	81.37	78.62	78.12	78.75	78.75	80.75	81.88	97.04	95.27	96.45
P_vivax	100.00	100.00	82.61	80.86	78.75	78.26	78.88	78.88	80.25	81.99	97.06	95.29	96.47
P_malariae	83.12	82.61	100.00	83.12	81.65	80.50	80.50	80.50	82.50	85.09	83.85	83.85	84.47
P_falciparum	81.37	80.86	83.12	100.00	82.50	82.61	80.75	80.75	99.38	79.38	80.25	80.25	82.10
P_chabaudi	78.62	78.75	81.65	82.50	100.00	98.75	95.00	96.25	81.88	82.28	79.38	79.38	80.00
P_vinckei	78.12	78.26	80.50	82.61	98.75	100.00	95.03	96.27	81.99	81.76	78.88	78.88	78.88
P_berghei	78.75	78.88	80.50	80.75	95.00	95.03	100.00	98.76	80.12	83.02	79.50	79.50	79.50
P_yoelii	78.75	78.88	80.50	80.75	96.25	96.27	98.76	100.00	80.12	83.02	79.50	79.50	79.50
P_reichenowi	80.75	80.25	82.50	99.38	81.88	81.99	80.12	80.12	100.00	78.75	79.63	79.63	81.48
P_ovale	81.88	81.99	85.09	79.38	82.28	81.76	83.02	83.02	78.75	100.00	83.85	82.61	82.61
P_cynomolgi	97.04	97.06	83.85	80.25	79.38	78.88	79.50	79.50	79.63	83.85	100.00	95.29	94.12
P_inui	95.27	95.29	83.85	80.25	79.38	78.88	79.50	79.50	79.63	82.61	95.29	100.00	94.12
P_knowlesi	96.45	96.47	84.47	82.10	80.00	78.88	79.50	79.50	81.48	82.61	94.12	94.12	100.00

Figure 5.6: Percent identity of *Pv*IscU protein sequence from Indian field isolates with IscU sequence from other *Plasmodium* species

P_vivax_indian	100.00	100.00	80.62	79.87	51.63	54.97	53.90	61.60
P_vivax	100.00	100.00	80.12	80.00	51.30	54.61	53.55	61.11
P_falciparum	80.62	80.12	100.00	80.75	54.05	55.94	54.11	60.32
P_berghei	79.87	80.00	80.75	100.00	52.38	56.34	55.17	61.90
S_cerevisiae	51.63	51.30	54.05	52.38	100.00	63.82	61.15	70.31
A_thaliana	54.97	54.61	55.94	56.34	63.82	100.00	67.08	71.88
H_sapiens	53.90	53.55	54.11	55.17	61.15	67.08	100.00	74.22
E_coli	61.60	61.11	60.32	61.90	70.31	71.88	74.22	100.00

Figure 5.7: Percent identity of *Pv*IscU protein sequence from Indian field isolates with that from other *Plasmodium* species, prokaryotes, and higher eukaryotes

Given its role as a scaffold protein, the residues implicated in [2Fe-2S] cluster dynamics of IscU were also examined for their conservation. The conserved residue analysis of *Pv*IscU showed the presence of three conserved Cysteine residues [Cys81, Cys106, and Cys149], Aspartic acid [Asp83], and Histidine [His148] known to be involved in [2Fe-2S] assembly (Tanaka et al., 2019; Kunichika et al., 2021).

Other than these conserved amino acid residues, a specific signature motif LPPVK is also found throughout the IscU orthologues (Campbell et al., 2021). This motif is mainly responsible for interaction dynamics between i) frataxin and ISCU and ii) Chaperones (HSPA9 and HSCB), and ISCU during [2Fe-2S] cluster formation and release mechanism (Campbell et al., 2021). This motif was also present in *Pv*IscU (142-146 aa), suggesting a high probablity of its role in mitochondrial [2Fe-2S] cluster assembly and transfer **(Figure 5.8)**.

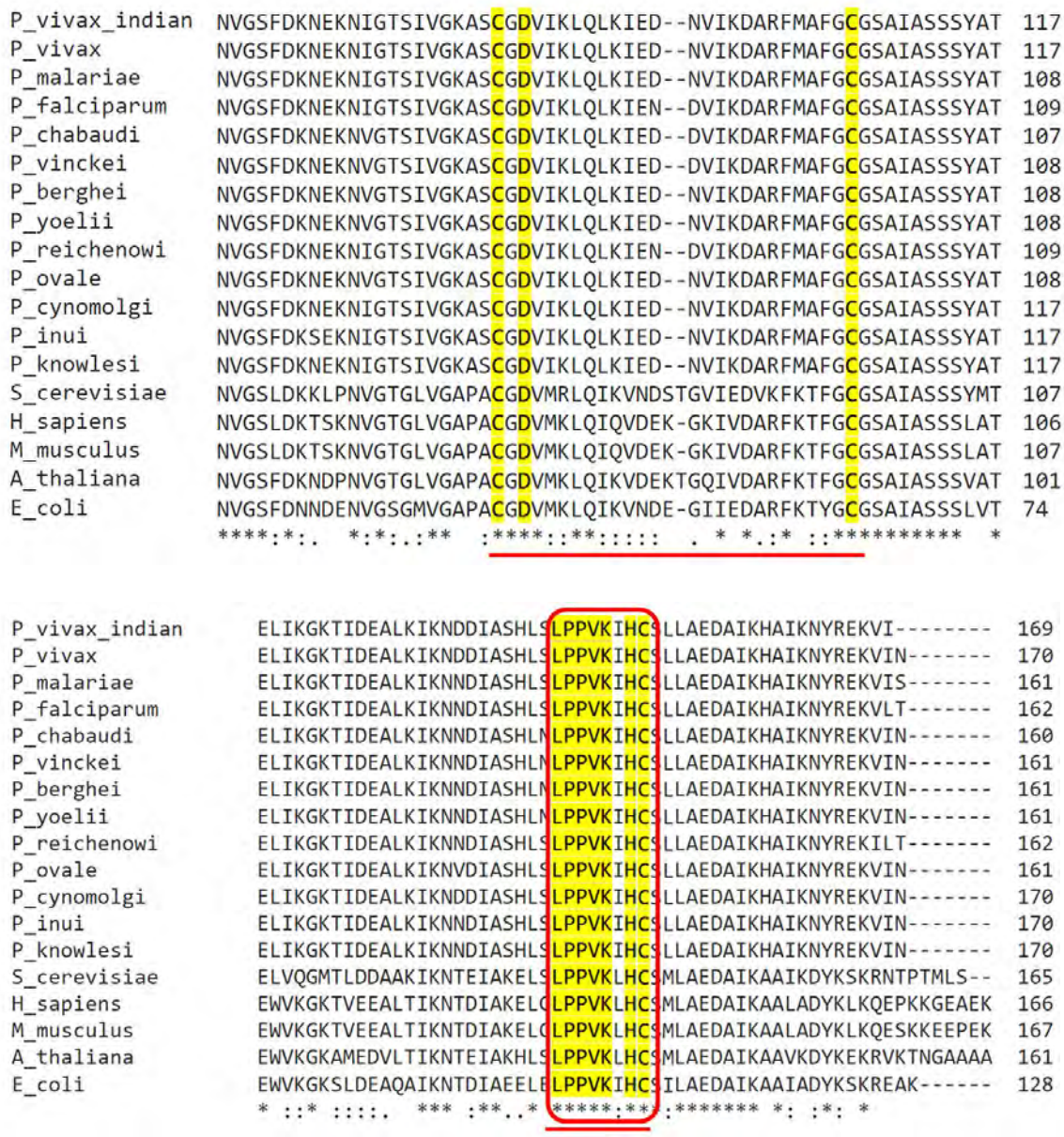

Figure 5.8: Multiple sequence alignment of *P. vivax* IscU sequence from Indian clinical isolates with *Plasmodium spp*., higher eukaryotes, and *E. coli*

5.2.5 Cloning and expression of PvIscU gene

Once the amplicons were confirmed through sequencing, they were subjected to cloning into the TA cloning vector, after which the recombinant clones were confirmed by colony PCR **(Figure 5.9)** and digestion with restriction enzymes like ApoI and PvuII to confirm the orientation of the insert **(Figure 5.10)**.

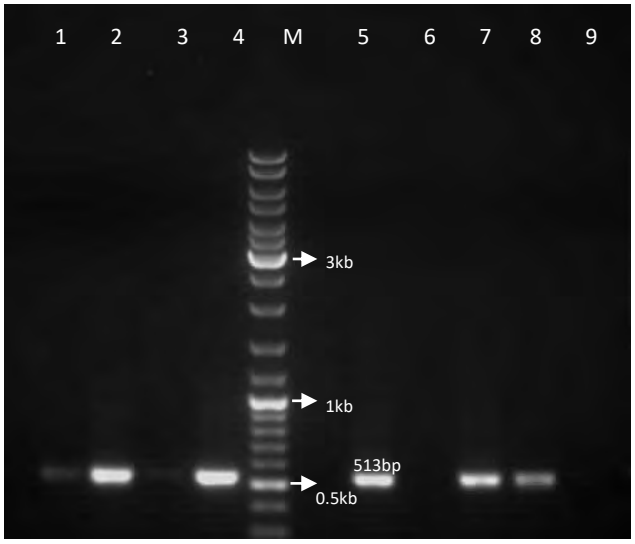

Figure 5.9: Colony PCR to check for the colonies showing recombinant construct in TA vector. (M: Gene Ruler DNA Ladder Mix SM0331; 1- 9: colony number obtained after vector insert ligation and transformation)

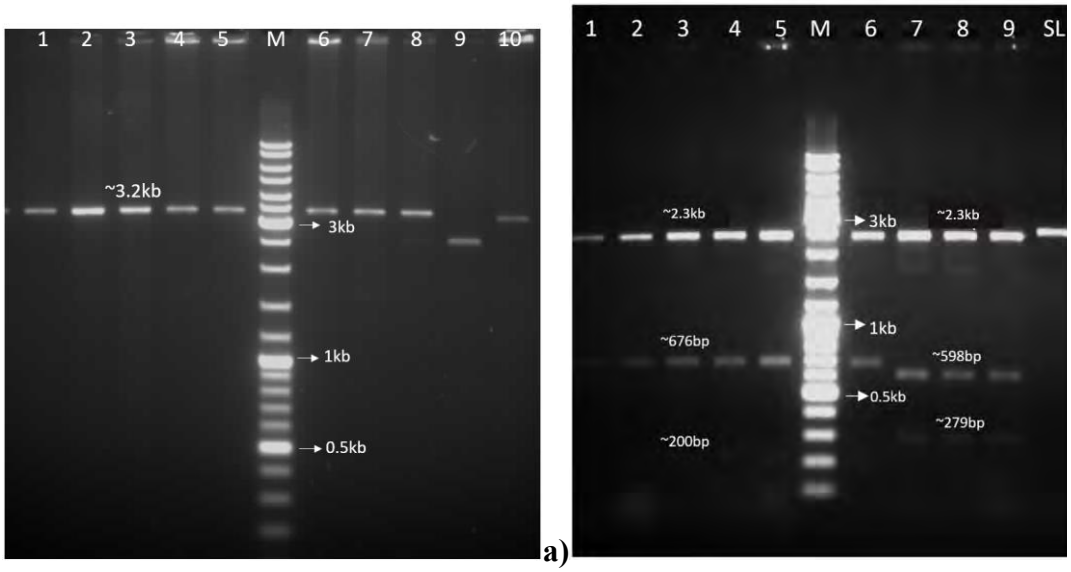

a)

Figure 5.10: **Restriction analysis of *Pv*IscU-TA clone with a) ApoI enzyme b) PvuII enzyme** (M: Gene Ruler DNA Ladder Mix Fermentas SM0331; SL: self-ligated colony; 1-10: colony number after vector insert ligation and transformation)

Once the cloning of *Pv*IscU gene was confirmed in the TA cloning vector, sub-cloning of the gene was performed in the expression plasmid pRSETA for recombinant protein expression. The vector (pRSETA) and the *Pv*IscU-TA clone were double digested using SacI and BglII restriction endonucleases **(Figure 5. 11)**, ligated and transformed into *E. coli* DH5a competent cells. The obtained putative recombinant clones were screened for clone confirmation using Colony PCR **(Figure 5.12)**.

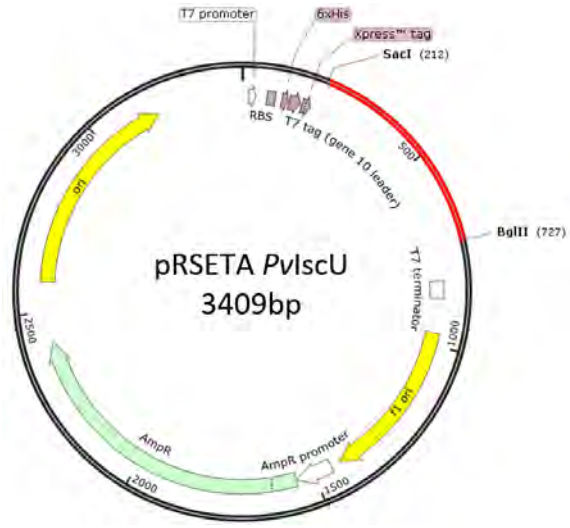

Figure 5.11: The pRSET A-*Pv*IscU clone map: The red part depicts the *Pv*IscU gene, and the black part shows the pRSET A backbone. Restriction sites mentioned were used during cloning and Restriction Endonuclease digestion analysis.

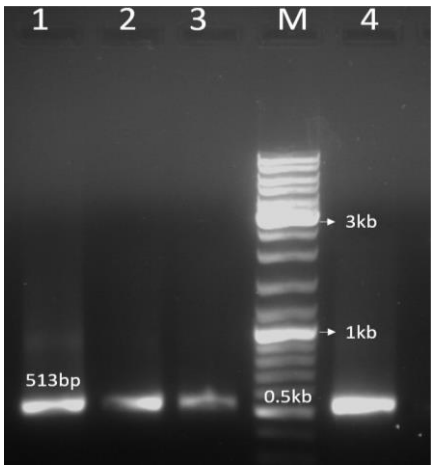

Figure 5.12: Colony PCR to check for the colonies showing recombinant construct in pRSETA vector. (M: Gene Ruler DNA Ladder Mix SM0331; 1- 4: colony number obtained after vector insert ligation and transformation)

The recombinant colonies (PvNIFU/IscU-pRSETA) that exhibited positive colony PCR results were further digested with PvuII (presence of PvuII site in the insert at the 58th position and in pRSETA at the 224th position) to confirm the presence of insert and its correct orientation. The bands observed at ~3 kb and ~464 bp validated the presence of PvNIFU/IscU in the correct orientation, as shown in **Figure 5.13**. Additionally, the putative clones were sent for DNA sequencing to ensure the insert orientation and the presence of the start codon in-frame.

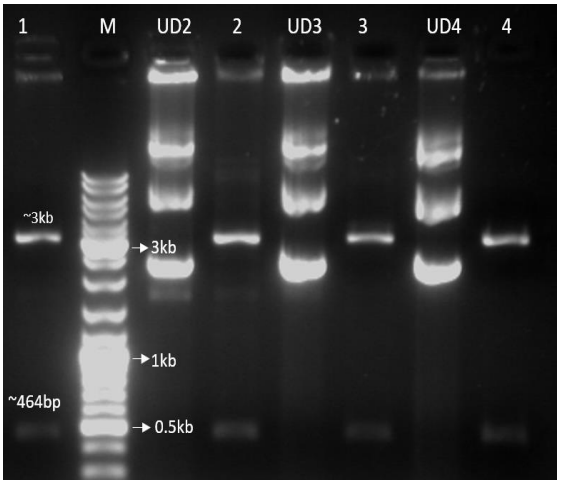

Figure 5.13: Restriction analysis of *Pv*IscU-pRSETA with PvuII enzyme for confirming recombinant construct and orientation (M: Gene Ruler DNA Ladder Mix Fermentas SM0331; UD 2-4: Undigested plasmid 2-4, 1-4: digested plasmid for colony number 1-4)

After successful clone confirmation, the obtained recombinant molecule was transformed in *E. coli* BL21 (DE3) pLysS host cells to express the *Pv*IscU protein. For this, 5% inoculum from 12hr primary clone culture was used to start the secondary culture, which was induced with 0.5mM IPTG when the OD_{600} reached 0.5-0.6. Samples were collected at different time points at 0, 2, 4, 6hr post-IPTG induction. The collected samples were pelleted, resuspended in 2X Lysis buffer, and checked on SDS PAGE. The presence of protein was checked after staining with Coomassie brilliant blue R250 **(Figure 5.14)**. The Recombinant *Pv*IscU protein was expressed as a fusion protein of ~22 kDa carrying a 6X-His tag.

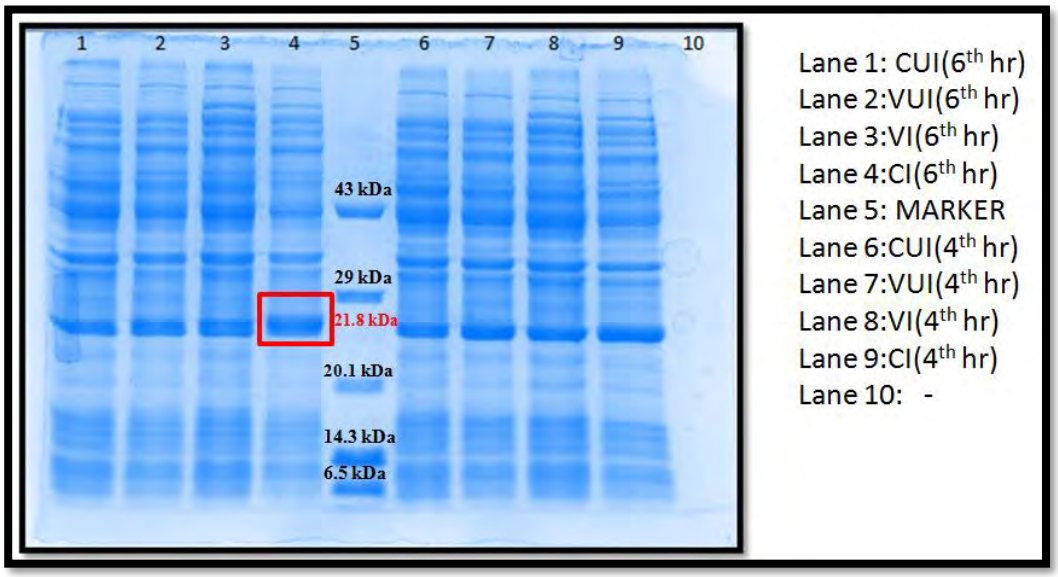

Figure 5.14: Overexpression of full-length *Pv*IscU protein in *E. coli.* (M: Protein Low Molecular Weight Marker (Genei); VUI: pRSETA vector uninduced; VI: pRSETA vector induced; CUI: pRSETA *Pv*IscU clone uninduced; CI: pRSETA *Pv*IscU clone induced

The protein expression was further validated by western blot analysis **(Figure 5.15)** using an anti-His antibody (Qiagen, USA) as per the manufacturer's protocol. A band, at ~22 kDa in the recombinant clone-induced sample, shows the desired protein.

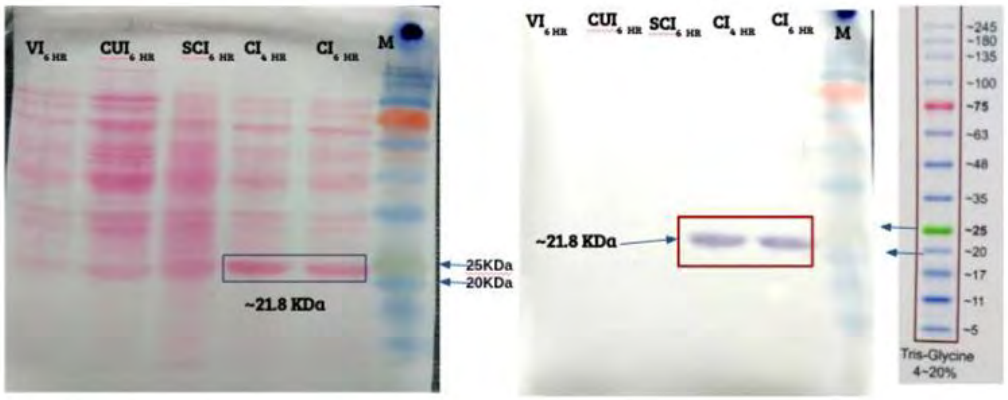

a) Membrane stained with Ponceau stain **b) Membrane after western blot**

Figure 5.15: Expression of full-length *Pv*IscU protein in *E. coli* BL21(DE3) pLysS confirmed by western blot using anti-His antibodies.

After successfully confirming the over-expressed *Pv*IscU protein, we proceeded with protein purification for downstream experiments like biochemical assay and protein sub-cellular localization. As recombinant *Pv*IscU possess a 6X-His tag at the N-terminal region, the protein was purified by performing Ni-NTA chromatography. Multiple eluent fractions were collected and analyzed on SDS-PAGE **(Figure 5.16).** The eluent fraction(s) with maximum intensity and minimum/absence of non-specific bands were included for further experiments.

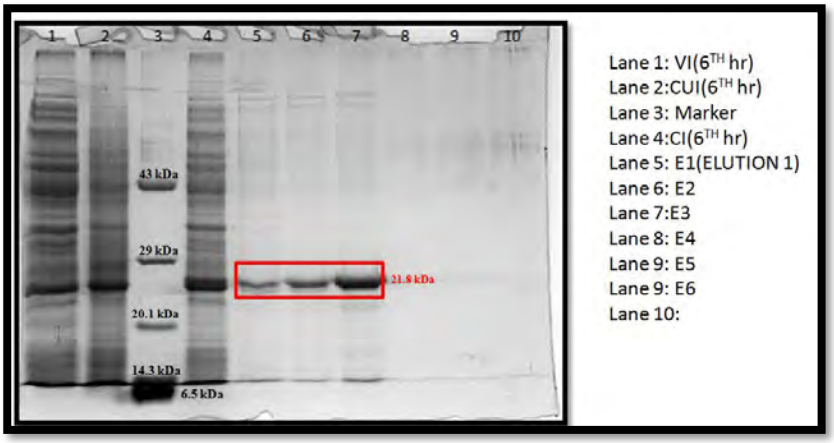

Figure 5.16: Purification of His Tagged *Pv*IscU Protein. M: Protein Low Molecular weight Marker (Genei); CI: pRSETA-*Pv*IscU clone induced sample; CUI: pRSETA-*Pv*IscU clone uninduced sample; VI: pRSETA induced sample

5.2.6 Subcellular Localization of PvIscU protein

5.2.6.1 In silico targeting predictions for PvIscU protein

Targeting predictions with servers detailed in Chapter 2 suggested no cytoplasmic or nuclear localization for *Pv*IscU protein. When subjected to PlasmoAP, an apicoplast targeting peptide was observed, but no signal peptide could be detected suggesting no apicoplast targeting for the protein. However, Mitoprot II predicted a mitochondrial localization for the protein with a high score of 0.94 **(Figure 5.17)**.

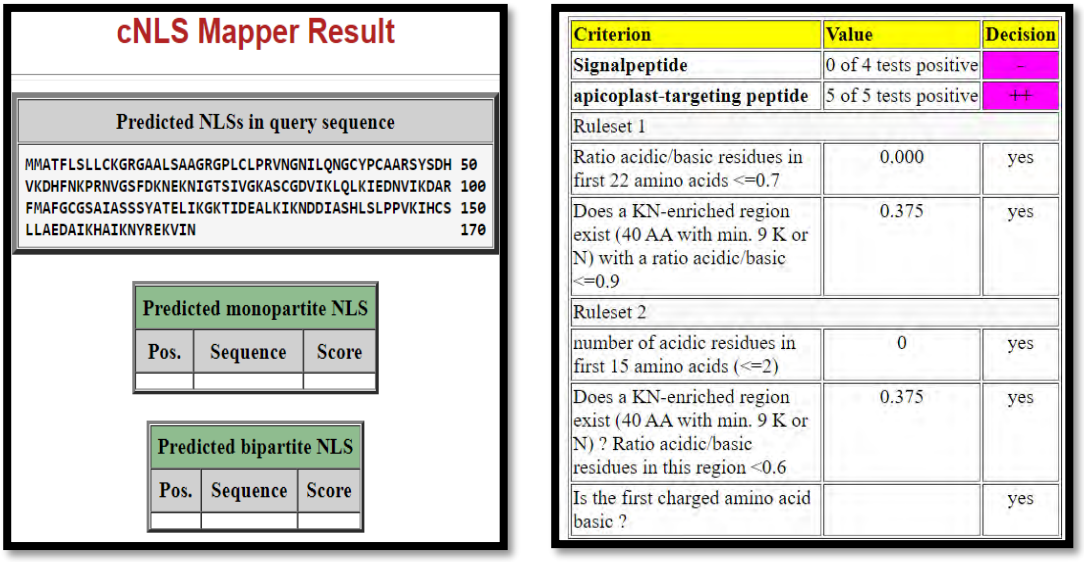

(a) **(b)**

(c)

Figure 5.17: Prediction of targeting for *Pv*IscU using a) cNLS Mapper, b) PlasmoAP, and c) Mitoprot II software

5.2.6.2 Antibody Raising and Immunolocalization

After targeting predictions, to confirm the subcellular localization of *Pv*IscU, antibodies were raised against recombinant *Pv*IscU in mice as per the procedure detailed in Chapter 2. The generated antibodies were subjected to ELISA for antibody titer calculation to determine the optimal antibody dilutions for downstream experiments. For the same, the test readings of sera after different booster doses of protein were compared with sera collected from mice injected with 1X PBS along with Freund's Adjuvant as control. Pre-immune sera were also collected to check the presence of any cross-reactive antibodies. An increased antibody titer was observed for the booster doses **(Figure 5.18)**.

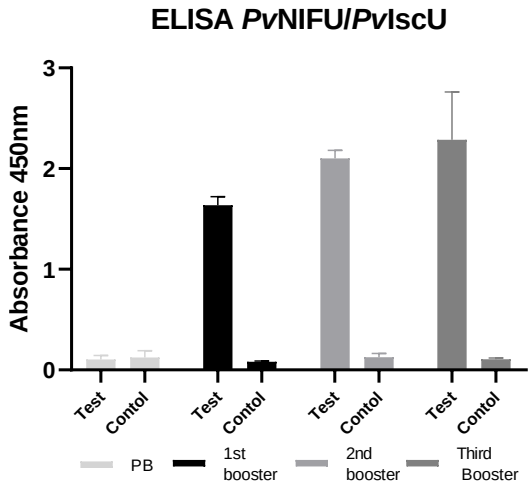

Figure 5.18: Antibody titre of PvIscU protein by performing ELISA [Antibody dilution 1:1000] (PB: Pre-bleed sera)

The raised antibodies were then used on methanol fixed *P. vivax*-infected blood smears after permeabilizing them with Saponin and Triton X-100 to analyze the subcellular localization of *Pv*IscU protein. For localization of *Pv*IscU protein, polyclonal anti-*Pv*IscU (1:500) sera was added to *P. vivax*-infected blood smears followed by FITC 488 conjugate (1:200). For mitochondrial co-localization, the smear was further treated with mitochondria specific Prohibitin Polyclonal Rabbit Antibody (1:500) followed by goat anti-rabbit IgG Alexa 647 conjugate (1:200). The cells were counterstained with DAPI and Qdot 565 Streptavidin Conjugate for visualizing the parasites' nucleus and Apicoplast, respectively. After mounting with Vectashield, slides were observed under confocal microscope using the respective filters. A bright field was used to identify the RBCs infected with the parasite, while the green fluorescence was used to localize the *Pv*IscU protein. The blue, red, and pink fluorescence was observed for the nucleus, mitochondria, and Apicoplast, respectively **(Figure 5.19)**.

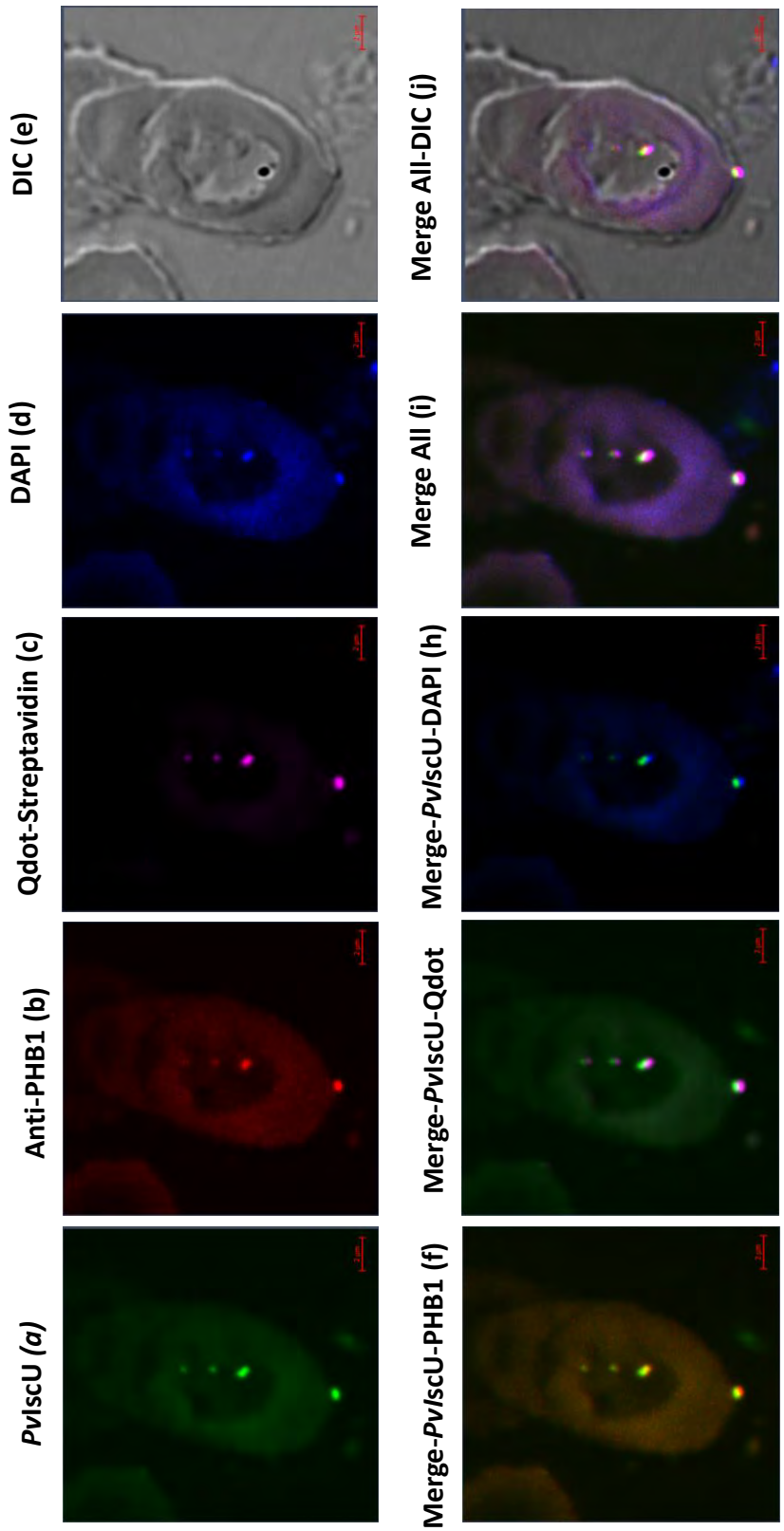

Figure 5.19: Sub-cellular localization of *Pv*IscU protein in smears prepared from *P. vivax* Indian field isolates. 63X Magnification a) The full-length recombinant *Pv*IscU protein was tagged with FITC 488 and visualized as a green fluorescence. **b)** The parasite's mitochondria were further stained with Mitochondria specific Prohibitin Polyclonal Rabbit Antibody and Alexa 647 (red), **c)** The parasite's Apicoplast was further stained with Q-dot 565 (pink), and **d)** DAPI (blue) was used to identify the nucleus. **e)** The DIC bright field image shows the presence of a Parasite inside an infected RBC. Image z-stacks were deconvolved and then presented as a single combined image. The merged image of *Pv*IscU with different antibodies/ dyes is given as **[f to j]**.

The *Pv*IscU protein was found to be localized as a green fluorescing spot with an overlapping red spot of mitochondria resulting in yellow colour and indicating mitochondrial localization of the protein. However, the *Pv*IscU green fluorescing spot did not overlap with the pink or blue fluorescing spot, indicating it is not localized to Apicoplast or nucleus. This study confirms that the *Pv*IscU protein is functionally active in mitochondria **(Figure 5.19)**.

5.2.7 Binding of [Fe-S] clusters on PvIscU protein

As discussed above, our conserved domain and signature motif analysis identified *Pv*IscU, putative to possess [Fe-S] cluster assembly scaffold IscU domain and various [Fe-S] coordinating critical amino acid residues (Cysteine, aspartate, and Histidine). In order to determine the functional role of *Pv*IscU as an ISC scaffold protein, first we generated a three dimensional model of *Pv*IscU using homology modeling followed by *in silico* docking of [Fe-S] clusters on the protein. After successful docking, these clusters were biochemically reconstituted on the protein to determine the *in vitro* binding of [Fe-S] clusters on the *Pv*IscU protein.

5.2.7.1 Three Dimensional Model Generation and Energy Minimization for PvIscU protein

A three-dimensional (3D) model for *Pv*IscU was generated through Modeller 9v.18, a structural homology modeling server. For the same, *Pv*IscU sequence was submitted to HHpred software to search for the potential templates. Amongst the potential templates obtained, the crystal structure of *Methanothrix thermoacetophila* IscU (PDB; A chain of 7C8M) protein with 3.50 Å resolution was selected (Kunichika et al., 2021), which showed an amino acid identity of 44.09% with *Pv*IscU protein sequence. The obtained structure was further refined by performing energy minimization **(Figure 5.20)** using the online server YASARA (Krieger et al., 2009).

To determine the integrity of the model, the obtained structure was evaluated using different online servers available on UCLA-DOE LAB SAVES v6.0. The structure when subjected to PROCHECK, showed a G- factor 'BETTER'. Majority of the amino acid residues (97.3%) in Ramachandran Plot were placed in favorable regions (90.9% core (most favored), 5.5% (additionally allowed), and 0.9% (generously allowed)) except 2.3%, that were present in the disallowed regions **(Figure 5.21 a)**. The

VERIFY3D for *Pv*IscU model showed 97.54% of the residues with averaged 3D-1D score >= 0.2 while as per the ERRAT score, 95.37% of the amino acid residues represented that molecular geometry of the model is of good quality **(Figure 5.21 b)**.

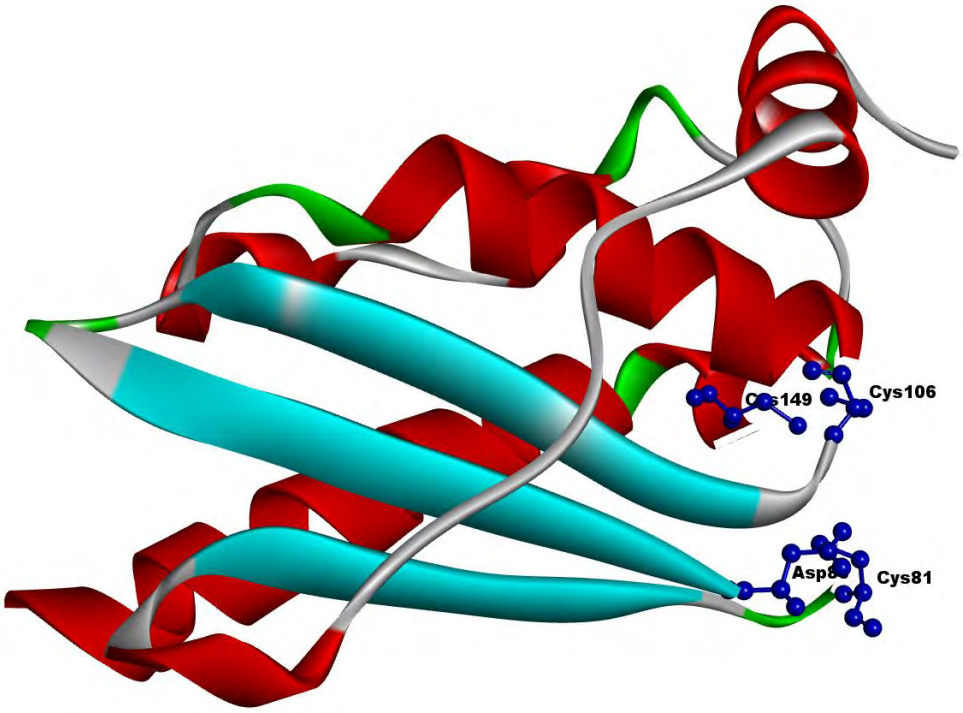

Figure 5.20: *Pv*IscU protein structure prediction: The crystal structure of *M. thermoacetophila* IscU (PDB Id: 7C8M) was used as a template. The conserved cysteine and aspartic acid residues are involved in [Fe-S] binding are shown in blue.

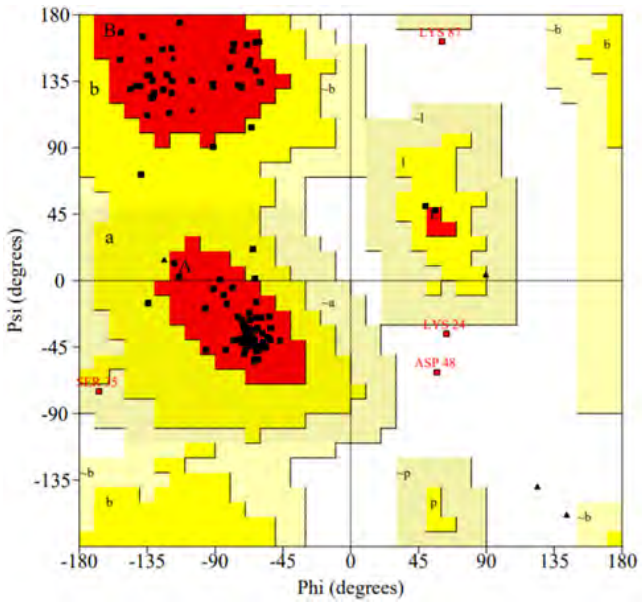

Figure 5.21a: Validation of 3D structures of *Pv*IscU using Ramachandran Plot

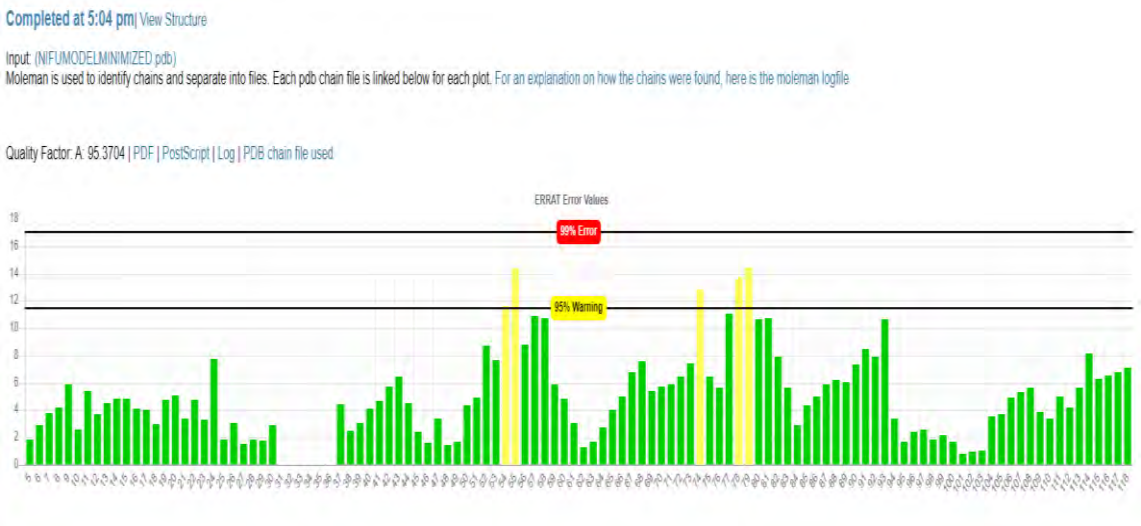

Figure 5.21b: Validation of 3D structures of *Pv*IscU using ERRAT score

The obtained monomeric structure of *Pv*IscU consisted of three alpha helices and seven beta strands running anti-parallel to each other. The generated *Pv*IscU structure showed a high level of sequence conservation amongst the essential cysteine residues involved in the interaction of ISCU scaffold protein with iron-sulfur cluster, which includes Cys81, Cys106, and Cys149 and an Aspartic acid residue Asp83 **(Figure 5.20)**.

5.2.7.2 In silico docking of [Fe-S] clusters on the PvIscU protein

After the three dimensional model was generated, to analyze the binding of [Fe-S] clusters to *Pv*IscU protein and to validate the types of residues involved in [Fe-S] binding, we went ahead with the molecular docking of *Pv*IscU and [2Fe-2S] using AutoDock Vina software (Trott and Olson, 2010). The [2Fe-2S] ligand selection for docking was solely based on interspecies literature survey, which suggests that ISCU protein exists in dimer form, and is involved in [2Fe-2S] scaffolding activity. Once the binding cavity was determined, the [2Fe-2S] was docked against the *Pv*IscU at the active site containing conserved cysteine (Cys81, Cys106, and Cys149) and aspartic acid (Asp83) residues. The distances between the conserved cysteine residues and [2Fe-2S] cluster were within 4 Å, indicating good affinity of [2Fe-2S] towards the *Pv*IscU active site **(Figure 5.22)**. Besides conserved cysteine and Aspartic acid, Ala109 and Lys146 also interacted with [2Fe-2S], where Lys146 belongs to the conserved LPPVK motif **(Figure 5.22)**. All the residues involved in the interaction with the [2Fe-2S] cluster are given in **Table 5.2**

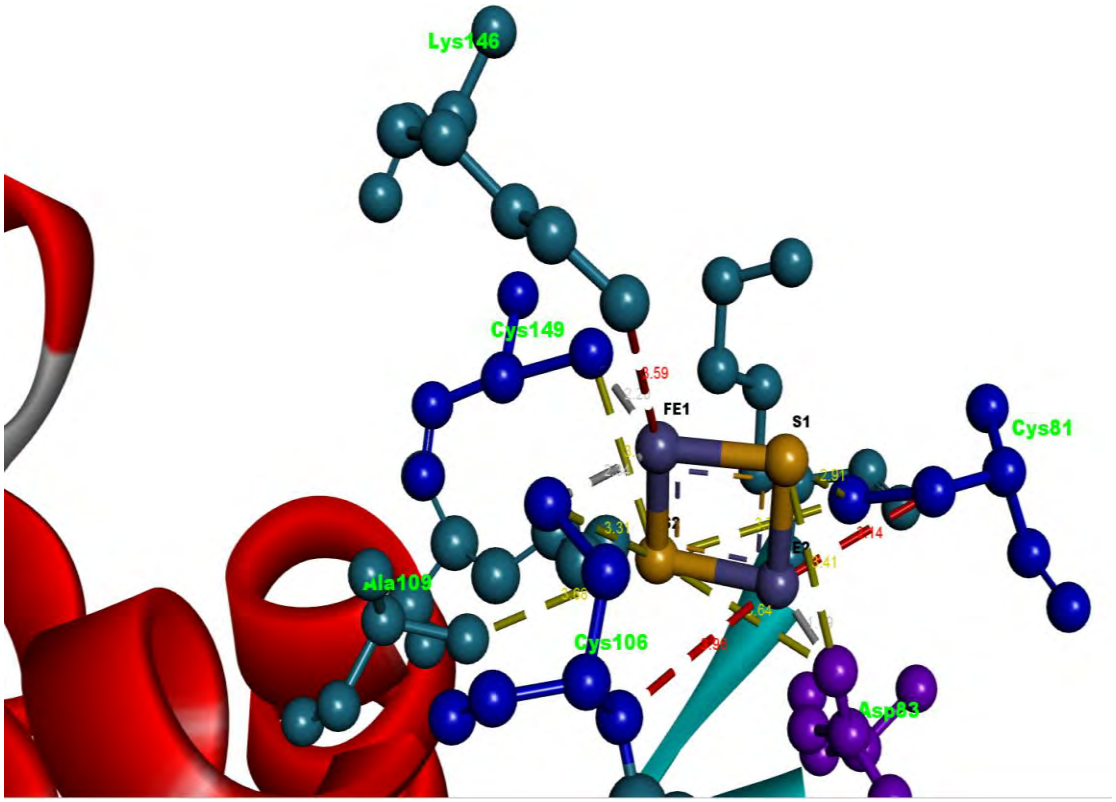

Figure 5.22 Docking of [2Fe-2S] cluster on *Pv*IscU protein. The interaction of Cysteine residues with [2Fe-2S] are labelled as blue and with Aspartic acid as violet.

Table 5.2: Residues in the *Pv*IscU active site interacting with the [2Fe-2S] cluster.

[2Fe-2S]	Interacting Residues
FE1	Lys146 [3.59 Å], Cys106 [2.34 Å] and Cys149 [2.20 Å]
FE2	Asp83 [1.69 Å], Cys81 [3.14 Å], and Cys106 [3.96 Å]
S1	Asp83 [3.41 Å], and Cys81 [2.91 Å]
S2	Asp83 [3.64 Å], Cys81 [3.77 Å], Ala109 [3.68 Å], Cys106 [3.31 Å] and Cys149 [3.39 Å]

5.2.7.3 Chemical Reconstitution of [Fe-S] clusters on purified PvIscU Protein

After confirming the *in silico* binding of [2Fe-2S] clusters to the *Pv*IscU protein, we further validated the formation of these clusters *in vitro*, by biochemically reconstituting [Fe-S] clusters on the protein using external iron and sulfur source. This

was required as the protein was purified in aerobic conditions resulting in [Fe-S] cluster removal.

To chemically reconstitute [Fe-S] clusters onto *Pv*IscU, different protein concentrations, such as 5, 10, and 20 µM of purified proteins were anaerobically incubated in reconstitution buffer (50 mM Tris-HCl, 200 mM NaCl, pH 8) for 1 hr at 25°C in a reaction chamber. Subsequently, these mixtures were anaerobically incubated with a five-fold molar excess of Na_2S and Fe $(NH_4)_2(SO_4)_2$ in the presence of Dithiothreitol (DTT). After 3-4 hours of incubation, the formation of [Fe-S] clusters on the protein was validated using UV-vis spectroscopy. The UV-visible spectral analysis of the reconstituted protein showed a peak between 420-470 nm (~420nm and ~456nm) **(Figure 5.23)**, suggesting the formation of holo-*Pv*IscU. In the case of 5 and 10 µM of protein, the reconstituted protein showed a peak at ~456 nm, which is a signature peak for [2Fe-2S] on IscU orthologue. However, for higher concentration such as 20 µM *Pv*IscU or above, we observed an additional peak at ~420 nm, alongside the ~456 nm peak **(Figure 5.23 and Figure 5.24)** suggesting some concentration-based peak variation. It is worth noting that at all protein concentrations, the ~456 nm peak remains constant. Thus, this variation needs further validation through EPR studies to identify the types of [Fe-S] clusters coordinating on *Pv*IscU.

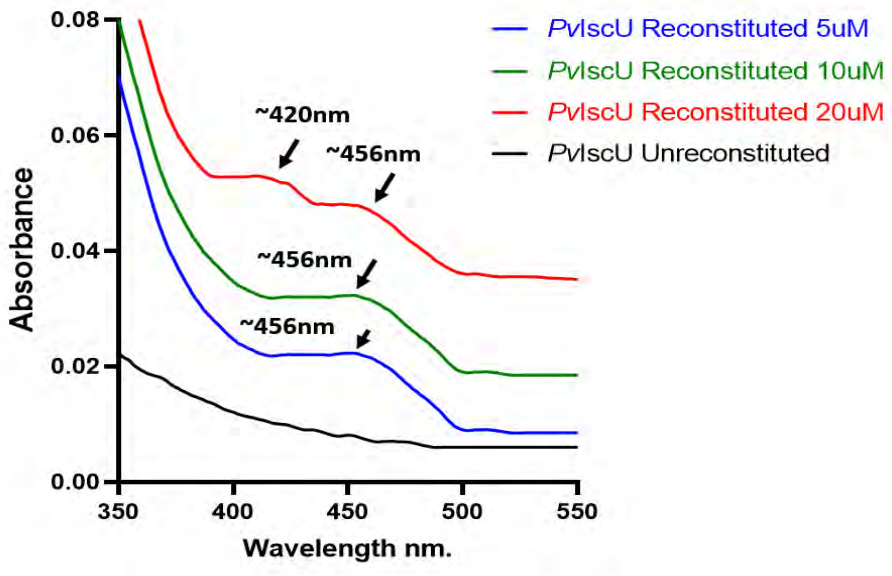

Figure 5.23 UV-vis spectral analysis of chemically reconstituted *Pv*IscU. *Pv*IscU after Chemical reconstitution is shown as Blue (5 µM), Green (10 µM), and Red (20 µM), which represents different protein concentrations. Purified *Pv*IscU before chemical Reconstitution is depicted as Black

It has been reported that Zn^{2+} binding to IscU stabilizes the protein conformation by ligating directly at the active site, which adapts a conformation like [2Fe-2S] bound IscU. Once Zn^{2+} stabilizes IscU, [Fe-S] reconstitution is inhibited because of already coordinated Zn^{2+} at the scaffold's active site (Lewis et al., 2019; Lin et al., 2020). Thus to check the effect of zinc on *Pv*IscU scaffolding activity in terms of its [Fe-S] cluster binding, we performed the chemical reconstitution of [Fe-S] in similar manner as described above but this time the *Pv*IscU was preloaded with Zinc (Zn-*Pv*IscU) in the reaction system (Na_2S, Fe $(NH_4)_2(SO_4)_2$ and DTT). To generate Zn-*Pv*IscU, purified *Pv*IscU was incubated with one molar equivalent of $ZnSO_4$ in reconstitution buffer followed by desalting with Amicon filter (10kD) to remove excess Zinc (Lewis et al., 2019; Gervason et al., 2019). Zn-*Pv*IscU showed no peaks specific for [Fe-S] formation, showing the negative effect of zinc on *Pv*IscU scaffolding or [Fe-S] forming capability (**Figure 5.24**).

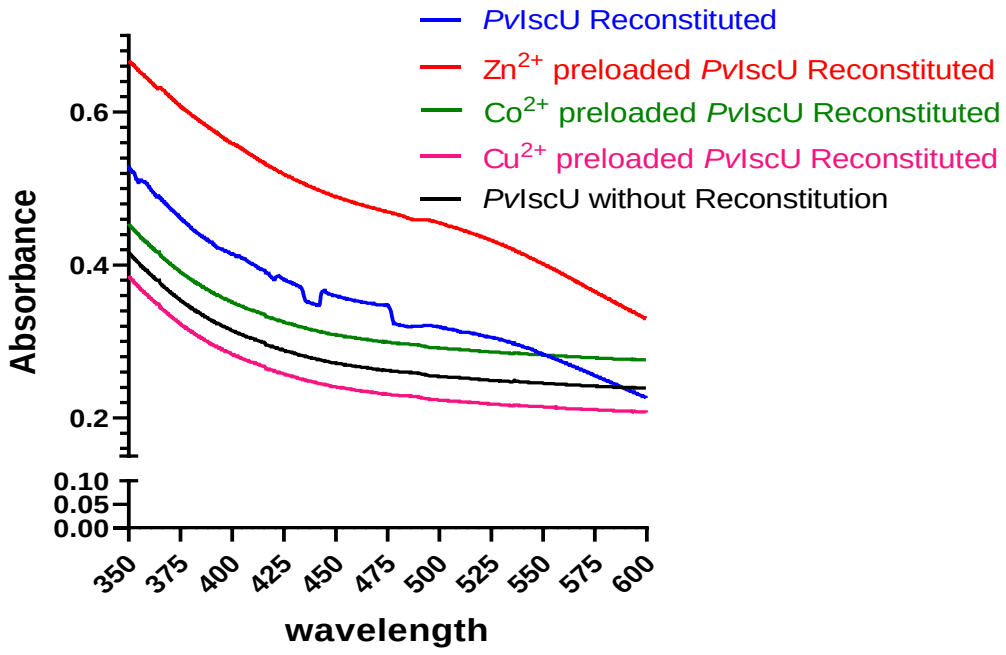

Figure 5.24: **UV-vis spectral analysis of chemically reconstituted *Pv*IscU with different metals**. *Pv*IscU without any metal (Blue), *Pv*IscU with Zinc (Red), Cobalt preloaded on *Pv*IscU (Green), and Copper preloaded on *Pv*IscU (Pink). Purified *Pv*IscU before chemical Reconstitution (Black).

We further wanted to investigate the impact of other divalent metal ions on the reconstitution capability of *Pv*IscU. For the same, we chose Cu^{2+} and Co^{2+}, which have

different coordination geometries. Cu^{2+} ions are expected to adopt trigonal-pyramidal or square-planar coordination in proteins, while Co^{2+} ions potentially adopt octahedral coordination. Circular dichroism spectral analysis revealed that amongst Zn^{2+}, Cu^{2+}, and Co^{2+}, only Cu^{2+}, did not affect the secondary structure of IscU, unlike Co^{2+} and Zn^{2+} (Roy et al., 2017). However, similar to zinc, both copper and cobalt inhibited cluster formation on *Pv*IscU, regardless of whether it was preloaded onto the protein or added separately during the reconstitution (**Figures 5.24**).

5.2.7.4 Iron and Sulphur Determination by Rapid Colorimetric Assays

After chemical reconstitution and [Fe-S] peak validation through UV-vis spectrometry, the molar ratio of bound iron and sulfur to *Pv*IscU protein was determined using Ferrozine and methylene blue assays for iron and sulfur, respectively (Methodology given in Chapter 2). Initially standard graphs were generated for iron and sulfur using known concentrations of Fe and S and absorbance recorded for each concentration after performing the respective assays **(Figure 5.25)**. Later the molar concentration of iron and sulfur was determined for the chemically reconstituted *Pv*IscU sample by extrapolating the obtained absorbance for reconstituted sample on these standard graphs. The total iron and sulfur content of reconstituted *Pv*IscU was calculated as 2.19µM (µmole protein)$^{-1}$ and 2.06µM (µmole protein)$^{-1}$ respectively indicating equimolar binding of [Fe-S].

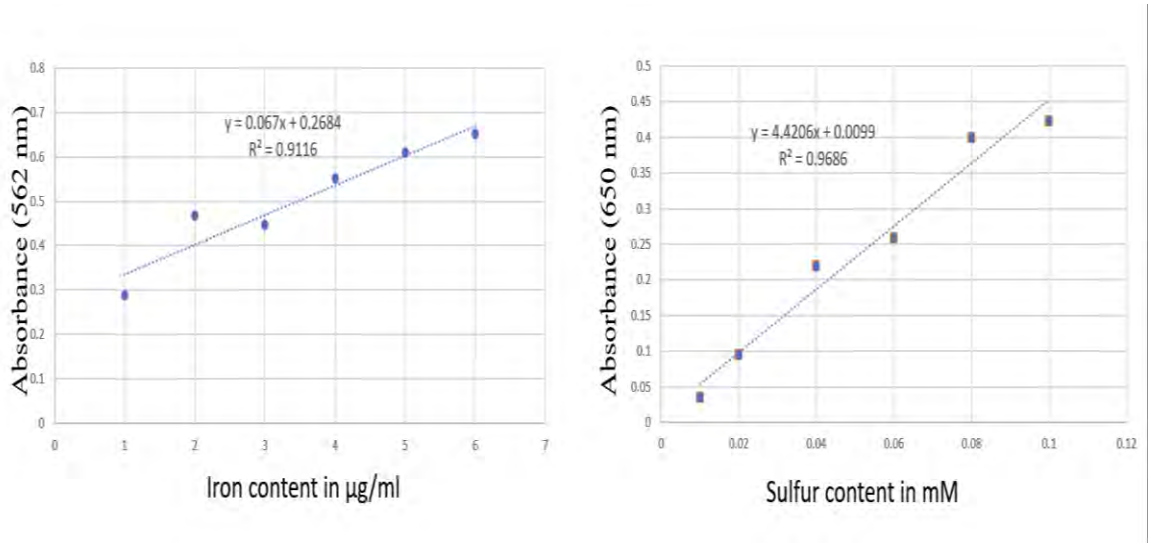

Figure 5.25: Determination of Iron and Sulfur Content by Ferrozine and Methylene blue assay respectively

5.3 Discussion

The scaffold protein is one of the integral protein of any [Fe-S] biogenesis pathway. For the mitochondrial [Fe-S] cluster assembly pathways, IscU is one of the U-type scaffold proteins that provide the structural architecture onto which [2Fe-2S] assembly occurs. ISC scaffold orthologues from M. *thermoacetophila, E. coli*, yeast, and humans have been shown 50-75% of sequence identity with *Plasmodium*, suggesting evolutionary conservation of the protein. Recently Sadik et al. reported the *P. falciparum* ISC scaffold complex which consists of dimeric hetero-hexamer with each hexamer consisting of [2*Pf*IscS-2*Pf*Isd11-2*Pf*IscU] and their localization to mitochondria suggesting the organelle as its functional site (Sadik et al., 2021). However, this protein has not been detailed from *P. vivax*, another major human malaria parasite. In addition, there is much more to explore regarding the metamorphic nature of ISC scaffold protein and the effect of various metals on its activity.

The IscU scaffold proteins have a significant domain architecture that is accountable for [2Fe-2S] assembly at the protein's active sites that includes i) Three conserved cysteine residues, aspartic acid, and Histidine residues mainly involved in [2Fe-2S] assembly and ii) presence of LPPVK motif (Campbell et al., 2021). Conserved domain and signature motif analysis of *Pv*NifU, putative showed the presence of these highly conserved residues involved in [Fe-S] cluster binding as well as the LPPVK motif, suggesting its role as the scaffold protein (IscU) in the ISC pathway. The phylogenetic tree generated based on IscU and NifU sequences from different organisms also placed NifU, putative in the cluster of IscU protein, further suggesting its role as IscU protein. This was further confirmed by performing subcellular localization studies, where *Pv*NIFU, putative (as per PlasmoDB database) was shown to localize to mitochondria, confirming its role in mitochondrial ISC machinery. This protein (*Pv*IscU, putative), when amplified and sequenced from *P. vivax* clinical Indian isolates, showed 78-99% identity with other *Plasmodium spp.,* 60% identity with *E. coli* IscU and ~55% identity with higher eukaryotes, suggesting high sequence conservation for IscU among living domains.

To gain insights into the [Fe-S] cluster binding capacity of *Pv*IscU, the homology model generated for *Pv*IscU was docked with [2Fe-2S] cluster. As described previously using

various spectroscopic and structural studies, the *Pv*IscU protein was also observed to coordinate [2Fe-2S] cluster by utilizing the three conserved cysteine residues Cys81, Cys106, and Cys149 (C37, C63, and C106 in *E. coli* IscU) and Asp83 (D39 in *E. coli* IscU), indicating affinity of the cluster to the protein's active site (Tanaka et al.,2019). Further, the [Fe-S] cluster interaction with IscU was confirmed by chemically reconstituting [Fe-S] clusters on the *Pv*IscU protein under anaerobic conditions. UV-vis spectral analysis showed peaks between 420-470nm indicating the formation of [Fe-S] clusters onto *Pv*IscU. The spectral data obtained for holo-*Pv*IscU aligned with the ~456 nm peak mentioned in *E. coli* IscU for [2Fe-2S] (Bitoun et al., 2008; Kim et al., 2012; Olson et al., 2000; Yang et al., 2006). It has been suggested in various reports published previously that peaks corresponding to ~420nm, ~456nm represent [2Fe-2S] clusters (Sadik et al., 2021), thus indicating formation of [2Fe-2S] clusters on *Pv*IscU as well. However, EPR must be performed to establish the types of clusters formed on *Pv*IscU.

Among the various scaffold proteins, IscU is called a "Metamorphic protein" because it can change the protein conformation from Disordered to ordered and vice versa according to the availability of divalent metal ions, cofactors, and specific ISC pathway chaperones (HscA and HscB). The ISC scaffold conformational shift cycle is likely accountable for cluster assembly dynamics and related protein interactions (Kim et al., 2012; Markley et al., 2013). Many reports have suggested the affinity of IscU with specific divalent metal ions such as Fe^{2+} and Zn^{2+}. However, the physiological role of zinc is still under exploration; but, it is suggested that its presence can modulate scaffolding activity during dynamic reactions (Lewis et al., 2019). Thus, in this study, we have analysed the effect of Zinc and other divalent cations on the ability of *Pv*IscU to reconstitute [Fe-S] clusters. Zn^{2+} and [2Fe-2S] both are reported to bind at the IscU [Disordered] active site, which means either of the ligands can interact at the active site and in presence of any of these ligands (Zn^{+2} or [2Fe-2S]), IscU [Disordered] can convert to IscU [Stable/ ordered], which then loses affinity for the other. It is reported that when zinc was added during the chemical reconstitution assay, there was an inhibition in [2Fe-2S] formation onto IscU, which is also suggestive of the same ligand binding site for Zn^{2+} and [2Fe-2S] onto ISC scaffold (Hinton et al., 2022; Lin et al., 2020). When we biochemically reconstituted the [Fe-S] clusters on the purified recombinant *Pv*IscU protein, we found typical [Fe-S] cluster specific peak in UV-vis spectroscopy, but in the presence of zinc, the [Fe-S] cluster specific peak could not be

observed indicating inhibition of cluster assembly in the presence of zinc and suggesting the regulatory role of Zinc in ISC machinery. Similar results were obtained for other divalent cations like Co^{2+} and Cu^{2+}. However, further protein conformational studies must be done on Zn-*Pv*IscU and *Pv*IscU to analyze the ordered and disordered states of the proteins to correlate with other ISC scaffold orthologues.

Chapter 6

Conclusions and Future Perspectives

Conclusions and Future Perspectives

6.1 Specific Conclusions

The main objective of this work was to characterize component(s) of Cytoplasmic (CIA) and mitochondrial (ISC) [Fe-S] cluster biogenesis pathways from *Plasmodium vivax* at a functional level using various molecular biology techniques, protein-activity-based assays, subcellular localization studies, *in silico* modelling and docking approaches. Thus, we initiated our studies by identification of the genes encoding for the components of CIA and ISC pathways in *Plasmodium vivax* from the PlasmoDB database based on their conserved domains and signature motifs. After performing various sequence alignments and functional domain analysis, Dre2, putative protein (PVX_089130) involved in CIA pathway and NifU protein, putative (PVX_117755) further designated as *Pv*IscU protein, putative in ISC pathway were chosen for further studies.

6.1.1 Specific Conclusions for PvDre2

*Pv*Dre2 gene was amplified from *P. vivax* clinical isolates and sequenced to analyse for mutations, if any. Extensive sequence analysis for *Pv*Dre2 revealed below mentioned points:

i) Comparative Conserved Domain and Signature Motif analysis of *Pv*Dre2 across inter and intra species showed presence of an evolutionary conserved C-terminal Cytokine-induced anti-apoptosis inhibitor 1 (CIAPIN1) domain. The domain showed high sequence conservation at Motif-II [$CX_2CX_7CX_2C$], whereas Motif-I [CX_8CX_2CXC] showed only three out of four cysteine residues to be conserved. However, this fourth cysteine was present in all the rodent malaria parasites such as *P. berghei, P. chabaudi*, *P. yoelii* and *P. vinckei* similar to other Apicomplexans and higher eukaryotes.

ii) Homology based CDD search was unable to determine N-terminal methyl transferase like domain for *Plasmodium* suggesting no methyl transferase like activity for the protein. However, the presence of a hydrophobic patch suggests multiple interacting partners for the protein which is also indicated by the disordered regions present in the linker portion of the protein. This was further supported by co-immunoprecipitation of parasite lysate with anti-*Pv*Dre2 sera,

which suggested interaction of Dre2 with proteins involved in pathways such as Golgi trafficking, ribosome biogenesis, DNA repair etc.

iii) Clustal alignment of *Pv*Dre2 sequence obtained from Indian isolates and *P. vivax* Sal1 PVX_089130 showed an Asparagine to Tyrosine change towards the N-terminal of the protein in one of the samples.

iv) *Pv*Dre2 was observed to form [Fe-S] clusters both *in silico* and *in vitro* under anaerobic conditions proving the function of *Pv*Dre2 as a [Fe-S] binding protein. *In silico* docking studies of *Pv*Dre2 with [2Fe-2S] and [4Fe-4S] at C-terminal CIAPIN1 domain showed essential interactions with conserved cysteine residues present in Motif-I (Cys170, Cys173 and Cys175) and Motif-II (Cys205, Cys208, Cys216 and Cys219) respectively. The distances between these conserved cysteine residues and the corresponding iron atoms of the Motif-I and Motif-II were all found to be within 3.5A° indicating good affinity of clusters for the *Pv*Dre2 active site.

v) Immunolocalization studies performed for *Pv*Dre2 on *P. vivax* infected blood smears prepared from patient's blood using antibodies raised against recombinant *Pv*Dre2 protein suggested mitochondrial localization. Also the presence of CXXC twin motifs at C-terminal CIAPIN1 domain suggested it to be localized to inter-membranous mitochondrial space.

vi) *Pv*Dre2 heterologous expression in *E. coli* showed iron accumulation and reduced bacterial growth due to Fe-mediated oxidative stress generation. This led to various membrane deformities like blebbing, cavity formation, intracellular exudation etc. However, *Pv*Dre2 expressing *E. coli* cells were able to rescue their growth in the late phases of protein expression via activation of genes involved in *E. coli* stress pathway. Also, this cell death was restored to normal upon exogenous addition of Artemether which suggests potential interaction between *Pv*Dre2 and Artemether.

6.1.2 Specific Conclusions for PvNIFU/IscU

i) Based on the presence of conserved IscU domain containing LPPVK motif and positioning in the same clade with the IscU proteins in the phylogenetic tree, the NifU protein, putative (PVX_117755) was designated as *Pv*IscU protein, putative functional in the ISC pathway localized to mitochondria. The gene encoding this protein was amplified and sequenced from clinical *P. vivax* isolates which exhibited a high conservation for this protein.

ii) Immunolocalization studies for *PvIscU* using antibodies raised against recombinant protein on *P. vivax* infected blood smears from patients suggested mitochondrial localization, which further confirms its association with parasite's mitochondrial ISC machinery.

iii) *In silico* docking studies of *PvIscU* with [2Fe-2S] cluster at the active site showed interactions with conserved cysteine residues, where the distances between the conserved cysteine residues and the corresponding iron atoms of the [2Fe-2S] were all within 2.9 A° indicating high affinity of [2Fe-2S] clusters towards *PvIscU* active site.

iv) Chemically reconstituted *Pv*IscU showed peak between ~420nm and ~465nm indicating the formation of [Fe-S] clusters. However, when zinc was added along with exogenous iron and sulfur source, these peaks disappeared showing effect of zinc on *PvIscU* scaffolding or [Fe-S] cluster forming capability, suggesting similar binding sites for the two.

In conclusion, to the best of our knowledge, this research provides the first report of characterization of any component of the cytosolic [Fe-S] cluster biogenesis (CIA) pathway from *Plasmodium*. Along with the functional characterization of *Pv*Dre2, this study also reports potential interaction of Artemisinin (Artemether) with *Pv*Dre2 which brings us one step close towards exploring mode of action of Artemisinin. Other than CIA pathway, this research also focuses on the characterization of ISC pathway scaffold protein *PvIscU* where the regulatory role of divalent metals such as Zinc and Cobalt was investigated for the assembly of [Fe-S] clusters on IscU. Thus this research helps us understand the [Fe-S] cluster biogenesis machinery of *Plasmodium* in a better perspective that may be useful for designing new inhibitors to target the malaria parasite.

6.2 Future Perspectives

This work can be further extended in the following aspects:

- Functional characterization of all the remaining components of the CIA pathway from *Plasmodium* and detailing the cross-talk between the CIA and ISC pathways of [Fe-S] cluster biogenesis in the parasite.
- The Dre2 protein is a part of CIA pathway electron transport system that involves another protein Tah18. Other than CIA pathway, their interaction and

dynamics have been reported in oxidative stress conditions, where upon stress, Tah18 gets separated from Dre2 and localizes to mitochondria and induces apoptosis in higher eukaryotes. As *Pv*Dre2 and *Pv*Tah18 interaction is not known in the parasite, thus a future study under the influence of oxidative stress can also be conducted to identify fate of these proteins.

- *Pv*Dre2 co-immunoprecipitation data can be further analysed to get insights into its non-canonical role in various essential pathways.
- Molecular mechanism involved in the interaction between *Pv*Dre2 and Artemisinin needs to be further elucidated.
- *Pv*IscU co-immunoprecipitation can be performed to get insights into its interacting partners.

References

References

Adam, A. C., Bornhövd, C., Prokisch, H., Neupert, W., & Hell, K. (2006). The Nfs1 interacting protein Isd11 has an essential role in Fe/S cluster biogenesis in mitochondria. *The EMBO journal*, *25*(1), 174-183.

Ahmad, S. S., Rahi, M., & Sharma, A. (2021). Relapses of Plasmodium vivax malaria threaten disease elimination: time to deploy tafenoquine in India? *BMJ Global Health*, *6*(2), e004558.

Altschul, S. F., Madden, T. L., Schäffer, A. A., Zhang, J., Zhang, Z., Miller, W., & Lipman, D. J. (1997). Gapped BLAST and PSI-BLAST: a new generation of protein database search programs. *Nucleic acids research*, *25*(17), 3389-3402.

Amitai, S., Kolodkin-Gal, I., Hananya-Meltabashi, M., Sacher, A., & Engelberg-Kulka, H. (2009). Escherichia coli MazF leads to the simultaneous selective synthesis of both "death proteins" and "survival proteins". *PLoS genetics*, *5*(3), e1000390.

Anwar, S., Dikhit, M. R., Singh, K. P., Kar, R. K., Zaidi, A., Sahoo, G. C., ... & Ali, V. (2014). Interaction between Nbp35 and Cfd1 proteins of cytosolic Fe-S cluster assembly reveals a stable complex formation in Entamoeba histolytica. *PLoS One*, *9*(10), e108971.

Aurrecoechea, C., Brestelli, J., Brunk, B. P., Dommer, J., Fischer, S., Gajria, B., ... & Wang, H. (2009). PlasmoDB: a functional genomic database for malaria parasites. *Nucleic acids research*, *37*(suppl_1), D539-D543.

Backes, S., Garg, S. G., Becker, L., Peleh, V., Glockshuber, R., Gould, S. B., & Herrmann, J. M. (2019). Development of the mitochondrial intermembrane space disulfide relay represents a critical step in eukaryotic evolution. *Molecular biology and evolution*, *36*(4), 742-756.

Baek, M., DiMaio, F., Anishchenko, I., Dauparas, J., Ovchinnikov, S., Lee, G. R., ... & Baker, D. (2021). Accurate prediction of protein structures and interactions using a three-track neural network. *Science*, *373*(6557), 871-876.

Banci, L., Bertini, I., Ciofi-Baffoni, S., Boscaro, F., Chatzi, A., Mikolajczyk, M., ... & Winkelmann, J. (2011). Anamorsin is a [2Fe-2S] cluster-containing substrate of the

Mia40-dependent mitochondrial protein trapping machinery. *Chemistry & biology*, *18*(6), 794-804.

Banci, L., Ciofi-Baffoni, S., Mikolajczyk, M., Winkelmann, J., Bill, E., & Pandelia, M. E. (2013). Human anamorsin binds [2Fe–2S] clusters with unique electronic properties. *JBIC Journal of Biological Inorganic Chemistry*, *18*, 883-893.

Banci, L., Ciofi-Baffoni, S., Gajda, K., Muzzioli, R., Peruzzini, R., & Winkelmann, J. (2015). N-terminal domains mediate [2Fe-2S] cluster transfer from glutaredoxin-3 to anamorsin. *Nature Chemical Biology*, *11*(10), 772.

Bandyopadhyay, S., Naik, S. G., O'Carroll, I. P., Huynh, B. H., Dean, D. R., Johnson, M. K., & Dos Santos, P. C. (2008). A proposed role for the Azotobacter vinelandii NfuA protein as an intermediate iron-sulfur cluster carrier. *Journal of Biological Chemistry*, *283*(20), 14092-14099.

Bannister, L. H., Hopkins, J. M., Fowler, R. E., Krishna, S., & Mitchell, G. H. (2000). A brief illustrated guide to the ultrastructure of Plasmodium falciparum asexual blood stages. *Parasitology today*, *16*(10), 427-433.

Barras, F., Loiseau, L., & Py, B. (2005). How Escherichia coli and Saccharomyces cerevisiae build Fe/S proteins. *Advances in microbial physiology*, *50*, 41-101.

Bernard, D. G., Netz, D. J., Lagny, T. J., Pierik, A. J., & Balk, J. (2013). Requirements of the cytosolic iron–sulfur cluster assembly pathway in Arabidopsis. *Philosophical Transactions of the Royal Society B: Biological Sciences*, *368*(1622), 20120259.

Berndt, C., Christ, L., Rouhier, N., & Mühlenhoff, U. (2021). Glutaredoxins with iron-sulphur clusters in eukaryotes-structure, function and impact on disease. *Biochimica et Biophysica Acta (BBA)-Bioenergetics*, *1862*(1), 148317.

Bertini, I., Cowan, J. A., Del Bianco, C., Luchinat, C., & Mansy, S. S. (2003). Thermotoga maritima IscU. Structural characterization and dynamics of a new class of metallochaperone. *Journal of molecular biology*, *331*(4), 907-924.

Betinol, I. O., Nader, S., & Mansy, S. S. (2021). Spectral decomposition of iron-sulfur clusters. *Analytical Biochemistry*, *629*, 114269.

Birnboim, H., & Doly, J. (1979). A rapid alkaline extraction procedure for screening recombinant plasmid DNA. *Nucleic acids research*, *7*(6), 1513-1523.

Bitoun, J. P., Wu, G., & Ding, H. (2008). Escherichia coli FtnA acts as an iron buffer for re-assembly of iron–sulfur clusters in response to hydrogen peroxide stress. *Biometals*, *21*, 693-703.

Blahut, M., Sanchez, E., Fisher, C. E., & Outten, F. W. (2020). Fe-S cluster biogenesis by the bacterial Suf pathway. *Biochimica et Biophysica Acta (BBA)-Molecular Cell Research*, *1867*(11), 118829.

Bondos, S. E., Dunker, A. K., & Uversky, V. N. (2022). Intrinsically disordered proteins play diverse roles in cell signaling. *Cell Communication and Signaling*, *20*(1), 20.

Bradford, M. M. (1976). A rapid and sensitive method for the quantitation of microgram quantities of protein utilizing the principle of protein-dye binding. *Analytical biochemistry*, *72*(1-2), 248-254.

Braymer, J. J., Freibert, S. A., Rakwalska-Bange, M., & Lill, R. (2021). Mechanistic concepts of iron-sulfur protein biogenesis in Biology. *Biochimica et Biophysica Acta (BBA)-Molecular Cell Research*, *1868*(1), 118863.

Braymer, J. J., & Lill, R. (2017). Iron–sulfur cluster biogenesis and trafficking in mitochondria. *Journal of Biological Chemistry*, *292*(31), 12754-12763.

Buzas, D. M., Nakamura, M., & Kinoshita, T. (2014). Epigenetic role for the conserved Fe-S cluster biogenesis protein AtDRE2 in Arabidopsis thaliana. *Proceedings of the National Academy of Sciences*, *111*(37), 13565-13570.

Bych, K., Netz, D. J., Vigani, G., Bill, E., Lill, R., Pierik, A. J., & Balk, J. (2008). The essential cytosolic iron-sulfur protein Nbp35 acts without Cfd1 partner in the green lineage. *Journal of Biological Chemistry*, *283*(51), 35797-35804.

Campbell, C. J., Pall, A. E., Naik, A. R., Thompson, L. N., & Stemmler, T. L. (2021). Molecular Details of the Frataxin–Scaffold Interaction during Mitochondrial Fe–S Cluster Assembly. *International Journal of Molecular Sciences*, *22*(11), 6006.

Camponeschi, F., Prusty, N. R., Heider, S. A. E., Ciofi-Baffoni, S., & Banci, L. (2020). GLRX3 acts as a [2Fe–2S] cluster chaperone in the cytosolic iron–sulfur assembly machinery transferring [2Fe–2S] clusters to NUBP1. *Journal of the American Chemical Society*, *142*(24), 10794-10805.

Cardenas, C., Miller, R. A., Smith, I., Bui, T., Molgo, J., Müller, M., ... & Foskett, J. K. (2010). Essential regulation of cell bioenergetics by constitutive InsP3 receptor Ca2+ transfer to mitochondria. *Cell*, *142*(2), 270-283.

Carter, R., & Graves, P. M. (1988). Gametocytes. *Malaria: principles and practice of malariology. Volume 1.*, 233-305.

CDC Malaria Programme 2021
https://www.cdc.gov/malaria/resources/cdc_malaria_program_ 2021.html

CDC Malaria Programme 2022
https://www.cdc.gov/malaria/resources/cdc_malaria_program_2022.html

Chandramouli, K., Unciuleac, M. C., Naik, S., Dean, D. R., Huynh, B. H., & Johnson, M. K. (2007). Formation and properties of [4Fe-4S] clusters on the IscU scaffold protein. *Biochemistry*, *46*(23), 6804-6811.

Chang, L., Zhang, X., Gong, P., Wang, Y., Du, B., & Li, J. (2019). Identification and characterization of Letm1 gene in Toxoplasma gondii. *Acta Biochimica et Biophysica Sinica*, *51*(1), 78-87.

Charan, M., Singh, N., Kumar, B., Srivastava, K., Siddiqi, M. I., & Habib, S. (2014). Sulfur mobilization for Fe-S cluster assembly by the essential SUF pathway in the Plasmodium falciparum apicoplast and its inhibition. *Antimicrobial agents and chemotherapy*, *58*(6), 3389-3398.

Charan, M., Choudhary, H. H., Singh, N., Sadik, M., Siddiqi, M. I., Mishra, S., & Habib, S. (2017). [Fe–S] cluster assembly in the apicoplast and its indispensability in mosquito stages of the malaria parasite. *The FEBS journal*, *284*(16), 2629-2648.

Ciofi-Baffoni, S., & Andreini, C. (2022). The Intriguing Role of Iron-Sulfur Clusters in the CIAPIN1 Protein Family. *Inorganics*, *10*(4), 52.

Claros, M. G., & Vincens, P. (1996). Computational method to predict mitochondrially imported proteins and their targeting sequences. *European journal of biochemistry*, *241*(3), 779-786.

Colin, F., Martelli, A., Clémancey, M., Latour, J. M., Gambarelli, S., Zeppieri, L., ... & Ollagnier de Choudens, S. (2013). Mammalian frataxin controls sulfur production

and iron entry during de novo Fe4S4 cluster assembly. *Journal of the American Chemical Society*, *135*(2), 733-740.

Colovos, C., & Yeates, T. O. (1993). Verification of protein structures: patterns of nonbonded atomic interactions. *Protein science*, *2*(9), 1511-1519.

Corless, E. I., Mettert, E. L., Kiley, P. J., & Antony, E. (2020). Elevated expression of a functional Suf pathway in Escherichia coli BL21 (DE3) enhances recombinant production of an iron-sulfur cluster-containing protein. *Journal of Bacteriology*, *202*(3), 10-1128.

Cory, S. A., Van Vranken, J. G., Brignole, E. J., Patra, S., Winge, D. R., Drennan, C. L., ... & Barondeau, D. P. (2017). Structure of human Fe–S assembly subcomplex reveals unexpected cysteine desulfurase architecture and acyl-ACP–ISD11 interactions. *Proceedings of the National Academy of Sciences*, *114*(27), E5325-E5334.

Dai, Z., Tonelli, M., & Markley, J. L. (2012). Metamorphic protein IscU changes conformation by cis–trans isomerizations of two peptidyl–prolyl peptide bonds. *Biochemistry*, *51*(48), 9595-9602.

Das, A., Holloway, B., Collins, W. E., Shama, V. P., Ghosh, S. K., Sinha, S., ... & Lal, A. A. (1995). Species-specific 18S rRNA gene amplification for the detection ofP. falciparumandP. vivaxmalaria parasites. *Molecular and cellular probes*, *9*(3), 161-165.

Das, A., & Pakalapati, D. (2017). A set of oligonucleotide primers useful for the species specific detection of plasmodium species. Indian Patent Application No. IN281595, India Science, Technology & Innovation, https://www.indiascienceandtechnology.gov.in/innovations/patents/in281595-set-oligonucleotide-primers-useful-species-specific-detection-plasmodium-species

Doolan, D., Dobano, C., & Baird, J. (2009). Acquired immunity to malaria. 610 Clin Microbiol Rev 22: 13-36. *Table of Contents*, *611*.

Eichner, M., Diebner, H. H., Molineaux, L., Collins, W. E., Jeffery, G. M., & Dietz, K. (2001). Genesis, sequestration and survival of Plasmodium falciparum gametocytes: parameter estimates from fitting a model to malariatherapy

data. *Transactions of the Royal Society of Tropical Medicine and Hygiene*, *95*(5), 497-501.

Eisenberg, D., Lüthy, R., & Bowie, J. U. VERIFY3D: assessment of protein models with three-dimensional profiles. InMethods in enzymology 1997 Jan 1 (Vol. 277, pp. 396-404). *Academic Press. DOI*, *10*, s0076-6879.

Eramian, M. Y. S., Pieper, U., & Sali, A. (2006). Comparative protein structure modeling using MODELLER. *Current protocols in bioinformatics*, *5*(1-5), 6.

Erental, A., Sharon, I., & Engelberg-Kulka, H. (2012). Two programmed cell death systems in Escherichia coli: an apoptotic-like death is inhibited by the mazEF-mediated death pathway. *PLoS biology*, *10*(3), e1001281.

Escalante, A. A., Cornejo, O. E., Freeland, D. E., Poe, A. C., Durrego, E., Collins, W. E., & Lal, A. A. (2005). A monkey's tale: the origin of Plasmodium vivax as a human malaria parasite. *Proceedings of the National Academy of Sciences*, *102*(6), 1980-1985.

Ezratty, E. J., Bertaux, C., Marcantonio, E. E., & Gundersen, G. G. (2009). Clathrin mediates integrin endocytosis for focal adhesion disassembly in migrating cells. *Journal of Cell Biology*, *187*(5), 733-747.

Felsenstein, J. (1985). Confidence limits on phylogenies: an approach using the bootstrap. *evolution*, *39*(4), 783-791.

Fish, W. W. (1988). Rapid colorimetric micromethod for the quantitation of complexed iron in biological samples in Methods in Enzymology (Riordan, JF and Vallee, BL, eds.) Vol. 158A.

Flannery, E. L., Markus, M. B., & Vaughan, A. M. (2019). Plasmodium vivax. *Trends in parasitology*, *35*(7), 583-584.

Foth, B. J., Ralph, S. A., Tonkin, C. J., Struck, N. S., Fraunholz, M., Roos, D. S., ... & McFadden, G. I. (2003). Dissecting apicoplast targeting in the malaria parasite Plasmodium falciparum. *Science*, *299*(5607), 705-708.

Fox, N. G., Yu, X., Feng, X., Bailey, H. J., Martelli, A., Nabhan, J. F., ... & Han, S. (2019). Structure of the human frataxin-bound iron-sulfur cluster assembly complex provides insight into its activation mechanism. *Nature communications*, *10*(1), 2210.

Fraga, H., & Ventura, S. (2012). Protein oxidative folding in the intermembrane mitochondrial space: more than protein trafficking. *Current Protein and Peptide Science*, *13*(3), 224-231.

Frazzon, J., & Dean, D. R. (2003). Formation of iron–sulfur clusters in bacteria: an emerging field in bioinorganic chemistry. *Current opinion in chemical biology*, *7*(2), 166-173.

Frey, A. G., Palenchar, D. J., Wildemann, J. D., & Philpott, C. C. (2016). A Glutaredoxin· BolA Complex Serves as an Iron-Sulfur Cluster Chaperone for the Cytosolic Cluster Assembly Machinery*♦. *Journal of Biological Chemistry*, *291*(43), 22344-22356.

Gao, F. (2020). Iron–sulfur cluster biogenesis and iron homeostasis in cyanobacteria. *Frontiers in Microbiology*, *11*, 165.

Gervason, S., Larkem, D., Mansour, A. B., Botzanowski, T., Müller, C. S., Pecqueur, L., ... & D'autréaux, B. (2019). Physiologically relevant reconstitution of iron-sulfur cluster biosynthesis uncovers persulfide-processing functions of ferredoxin-2 and frataxin. *Nature communications*, *10*(1), 3566.

Gisselberg, J. E., Dellibovi-Ragheb, T. A., Matthews, K. A., Bosch, G., & Prigge, S. T. (2013). The suf iron-sulfur cluster synthesis pathway is required for apicoplast maintenance in malaria parasites. *PLoS pathogens*, *9*(9), e1003655.

Grossman, J. D., Gay, K. A., Camire, E. J., Walden, W. E., & Perlstein, D. L. (2019). Coupling nucleotide binding and hydrolysis to iron–sulfur cluster acquisition and transfer revealed through genetic dissection of the Nbp35 ATPase site. *Biochemistry*, *58*(15), 2017-2027.

Gupta, V., Sendra, M., Naik, S. G., Chahal, H. K., Huynh, B. H., Outten, F. W., ... & Ollagnier de Choudens, S. (2009). Native Escherichia coli SufA, coexpressed with SufBCDSE, purifies as a [2Fe− 2S] protein and acts as an Fe− S transporter to Fe− S target enzymes. *Journal of the American Chemical Society*, *131*(17), 6149-6153.

Hao, Z., Li, X., Qiao, T., Du, R., Zhang, G., & Fan, D. (2006). Subcellular localization of CIAPIN1. *Journal of Histochemistry & Cytochemistry*, *54*(12), 1437-1444.

Haussig, J. M., Matuschewski, K., & Kooij, T. W. (2013). Experimental genetics of Plasmodium berghei NFU in the apicoplast iron-sulfur cluster biogenesis pathway. *PloS one*, *8*(6), e67269.

Haussig, J. M., Matuschewski, K., & Kooij, T. W. (2014). Identification of vital and dispensable sulfur utilization factors in the Plasmodium apicoplast. *PloS one*, *9*(2), e89718.

Haynes, R. K., Chan, W. C., Wong, H. N., Li, K. Y., Wu, W. K., Fan, K. M., ... & Monti, D. (2010). Facile oxidation of leucomethylene blue and dihydroflavins by artemisinins: relationship with flavoenzyme function and antimalarial mechanism of action. *ChemMedChem*, *5*(8), 1282-1299.

Hazan, R., Sat, B., & Engelberg-Kulka, H. (2004). Escherichia coli mazEF-mediated cell death is triggered by various stressful conditions. *Journal of bacteriology*, *186*(11), 3663-3669.

Hinton, T. V., Batelu, S., Gleason, N., & Stemmler, T. L. (2022). Molecular characteristics of proteins within the mitochondrial Fe-S cluster assembly complex. *Micron*, *153*, 103181.

Hollingsworth, S. A., & Karplus, P. A. (2010). A fresh look at the Ramachandran plot and the occurrence of standard structures in proteins.

Honarmand Ebrahimi, K., Ciofi-Baffoni, S., Hagedoorn, P. L., Nicolet, Y., Le Brun, N. E., Hagen, W. R., & Armstrong, F. A. (2022). Iron–sulfur clusters as inhibitors and catalysts of viral replication. *Nature Chemistry*, *14*(3), 253-266.

Howes, R. E., Battle, K. E., Mendis, K. N., Smith, D. L., Cibulskis, R. E., Baird, J. K., & Hay, S. I. (2016). Global epidemiology of Plasmodium vivax. *The American journal of tropical medicine and hygiene*, *95*(6 Suppl), 15.

Hung, H. I., Schwartz, J. M., Maldonado, E. N., Lemasters, J. J., & Nieminen, A. L. (2013). Mitoferrin-2-dependent mitochondrial iron uptake sensitizes human head and neck squamous carcinoma cells to photodynamic therapy. *Journal of Biological Chemistry*, *288*(1), 677-686.

Imlay, J. A. (2003). Pathways of oxidative damage. *Annual Reviews in Microbiology*, *57*(1), 395-418.

Imlay, J. A. (2006). Iron-sulphur clusters and the problem with oxygen. *Molecular microbiology*, *59*(4), 1073-1082.

Ismail, H. M., Barton, V., Phanchana, M., Charoensutthivarakul, S., Wong, M. H., Hemingway, J., ... & Ward, S. A. (2016). Artemisinin activity-based probes identify multiple molecular targets within the asexual stage of the malaria parasites Plasmodium falciparum 3D7. *Proceedings of the National Academy of Sciences*, *113*(8), 2080-2085.

Jacobson, M. R., Cash, V. L., Weiss, M. C., Laird, N. F., Newton, W. E., & Dean, D. R. (1989). Biochemical and genetic analysis of the nifUSVWZM cluster from Azotobacter vinelandii. *Molecular and General Genetics MGG*, *219*, 49-57.

Janse, C. J., van der Klooster, P. F., van der Kaay, H. J., van der Ploeg, M., & Overdulve, J. P. (1986). DNA synthesis in Plasmodium berghei during asexual and sexual development. *Molecular and biochemical parasitology*, *20*(2), 173-182.

Jonscher, E. G. W. (2018). *Identification of proteins involved in host cell cytosol uptake in the human Malaria parasite Plasmodium falciparum* (Doctoral dissertation, Staats-und Universitätsbibliothek Hamburg Carl von Ossietzky).

Jones, M. K., & Good, M. F. (2006). Malaria parasites up close. *Nature medicine*, *12*(2), 170-171.

Kassube, S. A., & Thomä, N. H. (2020). Structural insights into Fe–S protein biogenesis by the CIA targeting complex. *Nature structural & molecular biology*, *27*(8), 735-742.

Ke, H., & Mather, M. W. (2017). + Targeting mitochondrial functions as antimalarial regime, what is next?. *Current Clinical Microbiology Reports*, *4*, 175-191.

Kiley, P. J., & Beinert, H. (2003). The role of Fe–S proteins in sensing and regulation in bacteria. *Current opinion in microbiology*, *6*(2), 181-185.

Kim, J. H., Tonelli, M., & Markley, J. L. (2012). Disordered form of the scaffold protein IscU is the substrate for iron-sulfur cluster assembly on cysteine desulfurase. *Proceedings of the National Academy of Sciences*, *109*(2), 454-459.

Kim, S., Chen, J., Cheng, T., Gindulyte, A., He, J., He, S., ... & Bolton, E. E. (2023). PubChem 2023 update. *Nucleic acids research*, *51*(D1), D1373-D1380.

Kitaoka, S., Wada, K., Hasegawa, Y., Minami, Y., Fukuyama, K., & Takahashi, Y. (2006). Crystal structure of Escherichia coli SufC, an ABC-type ATPase component of the SUF iron–sulfur cluster assembly machinery. *FEBS letters*, *580*(1), 137-143.

Kochar, D. K., Saxena, V., Singh, N., Kochar, S. K., Kumar, S. V., & Das, A. (2005). *Plasmodium vivax* malaria. *Emerging infectious diseases*, *11*(1), 132.

Kochar, D. K., Das, A., Kochar, S. K., Saxena, V., Sirohi, P., Garg, S., ... & Gupta, V. (2009). Severe Plasmodium vivax malaria: a report on serial cases from Bikaner in northwestern India. *The American journal of tropical medicine and hygiene*, *80*(2), 194-198.

Koenderink, J. B., Kavishe, R. A., Rijpma, S. R., & Russel, F. G. (2010). The ABCs of multidrug resistance in malaria. *Trends in parasitology*, *26*(9), 440-446.

Kosugi, S., Hasebe, M., Tomita, M., & Yanagawa, H. (2009). Systematic identification of cell cycle-dependent yeast nucleocytoplasmic shuttling proteins by prediction of composite motifs. *Proceedings of the National Academy of Sciences*, *106*(25), 10171-10176.

Krieger, E., Joo, K., Lee, J., Lee, J., Raman, S., Thompson, J., ... & Karplus, K. (2009). Improving physical realism, stereochemistry, and side-chain accuracy in homology modeling: four approaches that performed well in CASP8. *Proteins: Structure, Function, and Bioinformatics*, *77*(S9), 114-122.

Kumar, B., Chaubey, S., Shah, P., Tanveer, A., Charan, M., Siddiqi, M. I., & Habib, S. (2011). Interaction between sulphur mobilisation proteins SufB and SufC: evidence for an iron–sulphur cluster biogenesis pathway in the apicoplast of Plasmodium falciparum. *International journal for parasitology*, *41*(9), 991-999.

Kumar, S., Stecher, G., Li, M., Knyaz, C., & Tamura, K. (2018). MEGA X: molecular evolutionary genetics analysis across computing platforms. *Molecular biology and evolution*, *35*(6), 1547.

Kunichika, K., Nakamura, R., Fujishiro, T., & Takahashi, Y. (2021). The Structure of the Dimeric State of IscU Harboring Two Adjacent [2Fe–2S] Clusters Provides Mechanistic Insights into Cluster Conversion to [4Fe–4S]. *Biochemistry*, *60*(20), 1569-1572.

Larkin, M. A., Blackshields, G., Brown, N. P., Chenna, R., McGettigan, P. A., McWilliam, H., ... & Higgins, D. G. (2007). Clustal W and Clustal X version 2.0. *bioinformatics*, *23*(21), 2947-2948.

Laskowski, R. A., MacArthur, M. W., Moss, D. S., & Thornton, J. M. (1993). PROCHECK: a program to check the stereochemical quality of protein structures. *Journal of applied crystallography*, *26*(2), 283-291.

Le, T. L., Yap, A. S., & Stow, J. L. (1999). Recycling of E-cadherin: a potential mechanism for regulating cadherin dynamics. *The Journal of cell biology*, *146*(1), 219-232.

Lee, H., & Lee, D. G. (2019). Programmed cell death in bacterial community: mechanisms of action, causes and consequences.

Leimkühler, S. (2020). The biosynthesis of the molybdenum cofactors in Escherichia coli. *Environmental Microbiology*, *22*(6), 2007-2026.

Lewis, B. E., Mason, Z., Rodrigues, A. V., Nuth, M., Dizin, E., Cowan, J. A., & Stemmler, T. L. (2019). Unique roles of iron and zinc binding to the yeast Fe–S cluster scaffold assembly protein “Isu1”. *Metallomics*, *11*(11), 1820-1835.

Li, Y., Tran, Q., Shrestha, R., Piao, L., Park, S., Park, J., & Park, J. (2019). LETM1 is required for mitochondrial homeostasis and cellular viability. *Molecular Medicine Reports*, *19*(5), 3367-3375.

Lill, R., & Freibert, S. A. (2020). Mechanisms of mitochondrial iron-sulfur protein biogenesis. *Annual review of biochemistry*, *89*, 471-499.

Lin, C. W., McCabe, J. W., Russell, D. H., & Barondeau, D. P. (2020). Molecular mechanism of ISC iron–sulfur cluster biogenesis revealed by high-resolution native mass spectrometry. *Journal of the American Chemical Society*, *142*(13), 6018-6029.

Livak, K. J., & Schmittgen, T. D. (2001). Analysis of relative gene expression data using real-time quantitative PCR and the $2^{-\Delta\Delta CT}$ method. *methods*, *25*(4), 402-408.

Lovell, S. C., Davis, I. W., Arendall III, W. B., De Bakker, P. I., Word, J. M., Prisant, M. G., ... & Richardson, D. C. (2003). Structure validation by Cα geometry: ϕ, ψ and Cβ deviation. *Proteins: Structure, Function, and Bioinformatics*, *50*(3), 437-450.

Maio, N., & Rouault, T. A. (2020). Outlining the complex pathway of mammalian Fe-S cluster biogenesis. *Trends in biochemical sciences*, *45*(5), 411-426.

Marchler-Bauer, A., Derbyshire, M. K., Gonzales, N. R., Lu, S., Chitsaz, F., Geer, L. Y., ... & Bryant, S. H. (2015). CDD: NCBI's conserved domain database. *Nucleic acids research*, *43*(D1), D222-D226.

Markley, J. L., Kim, J. H., Dai, Z., Bothe, J. R., Cai, K., Frederick, R. O., & Tonelli, M. (2013). Metamorphic protein IscU alternates conformations in the course of its role as the scaffold protein for iron–sulfur cluster biosynthesis and delivery. *FEBS letters*, *587*(8), 1172-1179.

Matteucci, S., Camponeschi, F., Clémancey, M., Ciofi-Baffoni, S., Blondin, G., & Banci, L. (2021). In Cellulo Mössbauer and EPR studies bring new evidence to the long-standing debate on iron–sulfur cluster binding in human anamorsin. *Angewandte Chemie*, *133*(27), 14967-14971.

McBroom, A. J., & Kuehn, M. J. (2007). Release of outer membrane vesicles by Gram-negative bacteria is a novel envelope stress response. *Molecular microbiology*, *63*(2), 545-558.

McGuffin, L. J., Bryson, K., & Jones, D. T. (2000). The PSIPRED protein structure prediction server. *Bioinformatics*, *16*(4), 404-405.

McQuillan, J. S., & Shaw, A. M. (2014). Differential gene regulation in the Ag nanoparticle and Ag+-induced silver stress response in Escherichia coli: A full transcriptomic profile. *Nanotoxicology*, *8*(sup1), 177-184.

Mihara, H., & Esaki, N. (2002). Bacterial cysteine desulfurases: their function and mechanisms. *Applied microbiology and biotechnology*, *60*, 12-23.

Morse, E. M., Brahme, N. N., & Calderwood, D. A. (2014). Integrin cytoplasmic tail interactions. *Biochemistry*, *53*(5), 810-820.

Mühlenhoff, U., Richhardt, N., Ristow, M., Kispal, G., & Lill, R. (2002). The yeast frataxin homolog Yfh1p plays a specific role in the maturation of cellular Fe/S proteins. *Human molecular genetics*, *11*(17), 2025-2036.

Muhlenhoff, U., Balk, J., Richhardt, N., Kaiser, J. T., Sipos, K., Kispal, G., & Lill, R. (2004). Functional characterization of the eukaryotic cysteine desulfurase Nfs1p from Saccharomyces cerevisiae. *Journal of Biological Chemistry*, *279*(35), 36906-36915.

Netz, D. J., Pierik, A. J., Stümpfig, M., Mühlenhoff, U., & Lill, R. (2007). The Cfd1–Nbp35 complex acts as a scaffold for iron-sulfur protein assembly in the yeast cytosol. *Nature chemical biology*, *3*(5), 278-286.

Netz, D. J., Stümpfig, M., Doré, C., Mühlenhoff, U., Pierik, A. J., & Lill, R. (2010). Tah18 transfers electrons to Dre2 in cytosolic iron-sulfur protein biogenesis. *Nature chemical biology*, *6*(10), 758-765.

Netz, D. J., Mascarenhas, J., Stehling, O., Pierik, A. J., & Lill, R. (2014). Maturation of cytosolic and nuclear iron–sulfur proteins. *Trends in cell biology*, *24*(5), 303-312.

Netz, D. J., Genau, H. M., Weiler, B. D., Bill, E., Pierik, A. J., & Lill, R. (2016). The conserved protein Dre2 uses essential [2Fe–2S] and [4Fe–4S] clusters for its function in cytosolic iron–sulfur protein assembly. *Biochemical Journal*, *473*(14), 2073-2085.

Nkhoma, S. C., Nair, S., Cheeseman, I. H., Rohr-Allegrini, C., Singlam, S., Nosten, F., & Anderson, T. J. (2012). Close kinship within multiple-genotype malaria parasite infections. *Proceedings of the Royal Society B: Biological Sciences*, *279*(1738), 2589-2598.

Oladipo, H. J., Tajudeen, Y. A., Oladunjoye, I. O., Yusuff, S. I., Yusuf, R. O., Oluwaseyi, E. M., ... & El-Sherbini, M. S. (2022). Increasing challenges of malaria control in sub-Saharan Africa: Priorities for public health research and policymakers. *Annals of Medicine and Surgery*, *81*, 104366.

Olson, J. W., Agar, J. N., Johnson, M. K., & Maier, R. J. (2000). Characterization of the NifU and NifS Fe− S cluster formation proteins essential for viability in Helicobacter pylori. *Biochemistry*, *39*(51), 16213-16219.

Olson, J. W., Mehta, N. S., & Maier, R. J. (2001). Requirement of nickel metabolism proteins HypA and HypB for full activity of both hydrogenase and urease in Helicobacter pylori. *Molecular microbiology*, *39*(1), 176-182.

Outten, F. W., Djaman, O., & Storz, G. (2004). A suf operon requirement for Fe–S cluster assembly during iron starvation in Escherichia coli. *Molecular microbiology*, *52*(3), 861-872.

Pakalapati, D., Garg, S., Middha, S., Acharya, J., Subudhi, A. K., Boopathi, A. P., ... & Das, A. (2013). Development and evaluation of a 28S rRNA gene-based nested PCR assay for P. falciparum and P. vivax. *Pathogens and global health*, *107*(4), 180-188.

Pakalapati, D., Garg, S., Middha, S., Kochar, A., Subudhi, A. K., Arunachalam, B. P., ... & Das, A. (2013). Comparative evaluation of microscopy, OptiMAL® and 18S rRNA gene based multiplex PCR for detection of Plasmodium falciparum & Plasmodium vivax from field isolates of Bikaner, India. *Asian Pacific Journal of Tropical Medicine*, *6*(5), 346-351.

Pala, Z. R., Saxena, V., Saggu, G. S., Yadav, S. K., Pareek, R. P., Kochar, S. K., ... & Garg, S. (2016). Structural and functional characterization of an iron–sulfur cluster assembly scaffold protein-SufA from Plasmodium vivax. *Gene*, *585*(1), 159-165.

Pala, Z. R., Saxena, V., Saggu, G. S., & Garg, S. (2018). Recent advances in the [Fe–S] cluster biogenesis (SUF) pathway functional in the apicoplast of Plasmodium. *Trends in Parasitology*, *34*(9), 800-809.

Pala, Z. R., Saxena, V., Saggu, G. S., Mani, S. K., Pareek, R. P., Kochar, S. K., ... & Garg, S. (2019). Functional analysis of iron-sulfur cluster biogenesis (SUF pathway) from Plasmodium vivax clinical isolates. *Experimental parasitology*, *198*, 53-62.

Pan, X., Zaarur, N., Singh, M., Morin, P., & Kandror, K. V. (2017). Sortilin and retromer mediate retrograde transport of Glut4 in 3T3-L1 adipocytes. *Molecular biology of the cell*, *28*(12), 1667-1675.

Pandey, A. K., Pain, J., Dancis, A., & Pain, D. (2019). Mitochondria export iron–sulfur and sulfur intermediates to the cytoplasm for iron–sulfur cluster assembly and tRNA thiolation in yeast. *Journal of Biological Chemistry*, *294*(24), 9489-9502.

Pareek, V., Gupta, R., Devineau, S., Sivasankaran, S. K., Bhargava, A., Khan, M. A., ... & Panwar, J. (2022). Does silver in different forms affect bacterial susceptibility and resistance? A mechanistic perspective. *ACS Applied Bio Materials*, *5*(2), 801-817.

Park, K. A., Yun, N., Shin, D. I., Choi, S. Y., Kim, H., Kim, W. K., ... & Oh, Y. J. (2011). Nuclear translocation of anamorsin during drug-induced dopaminergic neurodegeneration in culture and in rat brain. *Journal of neural transmission*, *118*, 433-444.

Pastore, A., & Puccio, H. (2013). Frataxin: a protein in search for a function. *Journal of neurochemistry*, *126*, 43-52.

Patra, S., & Barondeau, D. P. (2019). Mechanism of activation of the human cysteine desulfurase complex by frataxin. *Proceedings of the National Academy of Sciences*, *116*(39), 19421-19430.

Peleh, V., Riemer, J., Dancis, A., & Herrmann, J. M. (2014). Protein oxidation in the intermembrane space of mitochondria is substrate-specific rather than general. *Microbial cell*, *1*(3), 81.

Peña-Diaz, P., & Lukeš, J. (2018). Fe–S cluster assembly in the supergroup Excavata. *JBIC Journal of Biological Inorganic Chemistry*, *23*(4), 521-541.

Pérard, J., & Ollagnier de Choudens, S. (2018). Iron–sulfur clusters biogenesis by the SUF machinery: close to the molecular mechanism understanding. *JBIC Journal of Biological Inorganic Chemistry*, *23*, 581-596.

Petrovic, A., Davis, C. T., Rangachari, K., Clough, B., Wilson, R. J. M., & Eccleston, J. F. (2008). Hydrodynamic characterization of the SufBC and SufCD complexes and their interaction with fluorescent adenosine nucleotides. *Protein Science*, *17*(7), 1264-1274.

Pettersen, E. F., Goddard, T. D., Huang, C. C., Couch, G. S., Greenblatt, D. M., Meng, E. C., & Ferrin, T. E. (2004). UCSF Chimera—a visualization system for exploratory research and analysis. *Journal of computational chemistry*, *25*(13), 1605-1612.

Pieperhoff, M. S., Schmitt, M., Ferguson, D. J., & Meissner, M. (2013). The role of clathrin in post-Golgi trafficking in Toxoplasma gondii. *PLoS One*, *8*(10), e77620.

Prichard, K. L., O'Brien, N. S., Murcia, S. R., Baker, J. R., & McCluskey, A. (2022). Role of clathrin and dynamin in clathrin mediated endocytosis/synaptic vesicle recycling and implications in neurological diseases. *Frontiers in Cellular Neuroscience*, *15*, 754110.

Prilusky, J., Felder, C. E., Zeev-Ben-Mordehai, T., Rydberg, E. H., Man, O., Beckmann, J. S., ... & Sussman, J. L. (2005). FoldIndex©: a simple tool to predict whether a given protein sequence is intrinsically unfolded. *Bioinformatics*, *21*(16), 3435-3438.

Pyrih, J., Žárský, V., Fellows, J. D., Grosche, C., Wloga, D., Striepen, B., ... & Tachezy, J. (2021). The iron-sulfur scaffold protein HCF101 unveils the complexity of organellar evolution in SAR, Haptista and Cryptista. *BMC Ecology and Evolution*, *21*(1), 1-19.

Rathore, D., Wahl, A. M., Sullivan, M., & McCutchan, T. F. (2001). A phylogenetic comparison of gene trees constructed from plastid, mitochondrial and genomic DNA of Plasmodium species. *Molecular and biochemical parasitology*, *114*(1), 89-94.

Ratledge, C., & Dover, L. G. (2000). Iron metabolism in pathogenic bacteria. *Annual reviews in microbiology*, *54*(1), 881-941.

Roier, S., Zingl, F. G., Cakar, F., Durakovic, S., Kohl, P., Eichmann, T. O., ... & Schild, S. (2016). A novel mechanism for the biogenesis of outer membrane vesicles in Gram-negative bacteria. *Nature communications*, *7*(1), 10515.

Rouault, T. A., & Tong, W. H. (2008). Iron–sulfur cluster biogenesis and human disease. *Trends in Genetics*, *24*(8), 398-407.

Roy, P., Bauman, M. A., Almutairi, H. H., Jayawardhana, W. G., Johnson, N. M., & Torelli, A. T. (2017). Comparison of the response of bacterial IscU and SufU to Zn2+ and select transition-metal ions. *ACS chemical biology*, *13*(3), 591-599.

Russell, D. W., & Sambrook, J. (2001). *Molecular cloning: a laboratory manual* (Vol. 1, p. 112). Cold Spring Harbor, NY: Cold Spring Harbor Laboratory.

Ruzicka, F. J., & Beinert, H. E. L. M. U. T. (1978). The soluble “high potential” type iron-sulfur protein from mitochondria is aconitase. *Journal of Biological Chemistry*, *253*(8), 2514-2517.

Sadik, M., Afsar, M., Ramachandran, R., & Habib, S. (2021). [Fe–S] biogenesis and unusual assembly of the ISC scaffold complex in the Plasmodium falciparum mitochondrion. *Molecular Microbiology*, *116*(2), 606-623.

Saito, Y., Santosa, V., Ishiguro, K. I., & Kanemaki, M. T. (2022). MCMBP promotes the assembly of the MCM2–7 hetero-hexamer to ensure robust DNA replication in human cells. *Elife*, *11*, e77393.

Saitou, N., & Nei, M. (1987). The neighbor-joining method: a new method for reconstructing phylogenetic trees. *Molecular biology and evolution*, *4*(4), 406-425.

Šali, A., & Blundell, T. L. (1993). Comparative protein modelling by satisfaction of spatial restraints. *Journal of molecular biology*, *234*(3), 779-815.

Sangaré, L. O., Alayi, T. D., Westermann, B., Hovasse, A., Sindikubwabo, F., Callebaut, I., ... & Tomavo, S. (2016). Unconventional endosome-like compartment and retromer complex in Toxoplasma gondii govern parasite integrity and host infection. *Nature communications*, *7*(1), 11191.

Sato, S., Rangachari, K., & Wilson, R. J. M. (2003). Targeting GFP to the malarial mitochondrion. *Molecular and biochemical parasitology*, *130*(2), 155-158.

Sato, S. (2021). Plasmodium—a brief introduction to the parasites causing human malaria and their basic biology. *Journal of physiological anthropology*, *40*(1), 1-13.

Saxena, V., Garg, S., Ranjan, S., Kochar, D., Ranjan, A., & Das, A. (2007). Analysis of elongation factor Tu (tuf A) of apicoplast from Indian Plasmodium vivax isolates. *Infection, Genetics and Evolution*, *7*(5), 618-626.

Saxena, V., Garg, S., Tripathi, J., Sharma, S., Pakalapati, D., Subudhi, A. K., ... & Das, A. (2012). Plasmodium vivax apicoplast genome: a comparative analysis of major genes from Indian field isolates. *Acta tropica*, *122*(1), 138-149.

Schrodinger, L. L. C. (2015). The PyMOL molecular graphics system. *Version*, *1*, 8.

Srinivas, (2015, February 25). Malaria Parasite. Malaria Site https://www.malariasite.com/malaria-parasites/

DeLano, W. L. (2017). The PyMOL Molecular Graphics System, version 2.0; Schrodinger, Inc. *New York*.

Schwenkert, S., Netz, D. J., Frazzon, J., Pierik, A. J., Bill, E., Gross, J., ... & Meurer, J. (2010). Chloroplast HCF101 is a scaffold protein for [4Fe-4S] cluster assembly. *Biochemical Journal*, *425*(1), 207-218.

Seeber, F. (2002). Biogenesis of iron–sulphur clusters in amitochondriate and apicomplexan protists. *International journal for parasitology*, *32*(10), 1207-1217.

Sekar, V. (1987). A Rapid Screening-Procedure for the Identification of Recombinant Bacterial Clones. *Biotechniques*, *5*(1), 11-13.

Shibayama, H., Takai, E., Matsumura, I., Kouno, M., Morii, E., Kitamura, Y., ... & Kanakura, Y. (2004). Identification of a cytokine-induced antiapoptotic molecule anamorsin essential for definitive hematopoiesis. *The Journal of experimental medicine*, *199*(4), 581-592.

Siddiqui, G., Giannangelo, C., De Paoli, A., Schuh, A. K., Heimsch, K. C., Anderson, D., ... & Creek, D. J. (2022). Peroxide antimalarial drugs target redox homeostasis in Plasmodium falciparum infected red blood cells. *ACS infectious diseases*, *8*(1), 210-226.

Siegel, L. M. (1965). A direct microdetermination for sulfide. *Analytical biochemistry*, *11*(1), 126-132.

Sigrist, C. J., Cerutti, L., Hulo, N., Gattiker, A., Falquet, L., Pagni, M., ... & Bucher, P. (2002). PROSITE: a documented database using patterns and profiles as motif descriptors. *Briefings in bioinformatics*, *3*(3), 265-274.

Söding, J., Biegert, A., & Lupas, A. N. (2005). The HHpred interactive server for protein homology detection and structure prediction. *Nucleic acids research*, *33*(suppl_2), W244-W248.

Soler, N., Craescu, C. T., Gallay, J., Frapart, Y. M., Mansuy, D., Raynal, B., ... & Vernis, L. (2012). AS-adenosylmethionine methyltransferase-like domain within the essential, Fe-S-containing yeast protein Dre2. *The FEBS journal*, *279*(12), 2108-2119.

Song, G., Cheng, C., Li, Y., Shaw, N., Xiao, Z. C., & Liu, Z. J. (2014). Crystal structure of the N-terminal methyltransferase-like domain of anamorsin. *Proteins: Structure, Function, and Bioinformatics*, *82*(6), 1066-1071.

Srikumar, S., Kröger, C., Hébrard, M., Colgan, A., Owen, S. V., Sivasankaran, S. K., ... & Hinton, J. C. (2015). RNA-seq brings new insights to the intra-macrophage transcriptome of Salmonella Typhimurium. *PLoS pathogens*, *11*(11), e1005262.

Srivastava, A., Garg, S., Jain, R., Ayana, R., Kaushik, H., Garg, L., ... & Singh, S. (2019). Identification and functional characterization of a bacterial homologue of Zeta toxin in Leishmania donovani. *FEBS letters*, *593*(11), 1223-1235.

Stehling, O., Vashisht, A. A., Mascarenhas, J., Jonsson, Z. O., Sharma, T., Netz, D. J., ... & Lill, R. (2012). MMS19 assembles iron-sulfur proteins required for DNA metabolism and genomic integrity. *Science*, *337*(6091), 195-199.

Szklarczyk, D., Morris, J. H., Cook, H., Kuhn, M., Wyder, S., Simonovic, M., ... & Von Mering, C. (2016). The STRING database in 2017: quality-controlled protein–protein association networks, made broadly accessible. *Nucleic acids research*, gkw937.

Takahashi, Y., & Tokumoto, U. (2002). A Third Bacterial System for the Assembly of Iron-Sulfur Clusters with Homologs in Archaea and Plastids* 210. *Journal of Biological Chemistry*, *277*(32), 28380-28383.

Tanaka, N., Yuda, E., Fujishiro, T., Hirabayashi, K., Wada, K., & Takahashi, Y. (2019). Identification of IscU residues critical for de novo iron–sulfur cluster assembly. *Molecular Microbiology*, *112*(6), 1769-1783.

Tokumoto, U., Kitamura, S., Fukuyama, K., & Takahashi, Y. (2004). Interchangeability and distinct properties of bacterial Fe-S cluster assembly systems: functional replacement of the isc and suf operons in Escherichia coli with the nifSU-like operon from Helicobacter pylori. *Journal of biochemistry*, *136*(2), 199-209.

Toyofuku, M., Nomura, N., & Eberl, L. (2019). Types and origins of bacterial membrane vesicles. *Nature Reviews Microbiology*, *17*(1), 13-24.

Trott, O., & Olson, A. J. (2010). AutoDock Vina: improving the speed and accuracy of docking with a new scoring function, efficient optimization, and multithreading. *Journal of computational chemistry*, *31*(2), 455-461.

Tsai, C. L., & Barondeau, D. P. (2010). Human frataxin is an allosteric switch that activates the Fe− S cluster biosynthetic complex. *Biochemistry*, *49*(43), 9132-9139.

Tsaousis, A. D., Gentekaki, E., Eme, L., Gaston, D., & Roger, A. J. (2014). Evolution of the cytosolic iron-sulfur cluster assembly machinery in Blastocystis species and other microbial eukaryotes. *Eukaryotic cell*, *13*(1), 143-153.

Tu, J., Zhao, Q., Wei, L., & Yang, Q. (2012). Heavy metal concentration and speciation of seven representative municipal sludges from wastewater treatment plants in Northeast China. *Environmental monitoring and assessment*, *184*, 1645-1655.

Untergasser, A., Cutcutache, I., Koressaar, T., Ye, J., Faircloth, B. C., Remm, M., & Rozen, S. G. (2012). Primer3—new capabilities and interfaces. *Nucleic acids research*, *40*(15), e115-e115.

Van Dooren, G. G., Stimmler, L. M., & McFadden, G. I. (2006). Metabolic maps and functions of the Plasmodium mitochondrion. *FEMS microbiology reviews*, *30*(4), 596-630.

Vernis, L., Facca, C., Delagoutte, E., Soler, N., Chanet, R., Guiard, B., ... & Baldacci, G. (2009). A newly identified essential complex, Dre2-Tah18, controls mitochondria integrity and cell death after oxidative stress in yeast. *PloS one*, *4*(2), e4376.

Vriend, G. (1990). WHAT IF: a molecular modeling and drug design program. *Journal of molecular graphics*, *8*(1), 52-56.

Wang, J., Huang, L., Li, J., Fan, Q., Long, Y., Li, Y., & Zhou, B. (2010). Artemisinin directly targets malarial mitochondria through its specific mitochondrial activation. *Plos one*, *5*(3), e9582.

Wang, X., Chen, X., Sun, L., & Qian, W. (2019). Canonical cytosolic iron-sulfur cluster assembly and non-canonical functions of DRE2 in Arabidopsis. *PLoS Genetics*, *15*(4), e1008094.

Weiler, B. D., Brück, M. C., Kothe, I., Bill, E., Lill, R., & Mühlenhoff, U. (2020). Mitochondrial [4Fe-4S] protein assembly involves reductive [2Fe-2S] cluster fusion on ISCA1–ISCA2 by electron flow from ferredoxin FDX2. *Proceedings of the National Academy of Sciences*, *117*(34), 20555-20565.

World Health Organization. (2021). *World malaria report 2021*. World Health Organization.

World Health Organization. (2022). *World malaria report 2022*. World Health Organization.

Yamaguchi, K., Yoshimura, Y., Nakagawa, S., Mezaki, H., Yoshimura, S., & Kawasaki, T. (2019). OsDRE2 contributes to chitin-triggered response through its

interaction with OsRLCK185. *Bioscience, Biotechnology, and Biochemistry*, *83*(2), 281-290.

Yang, J., Bitoun, J. P., & Ding, H. (2006). Interplay of IscA and IscU in biogenesis of iron-sulfur clusters. *Journal of Biological Chemistry*, *281*(38), 27956-27963.

Yoshikawa, Y., Nasuno, R., Kawahara, N., Nishimura, A., Watanabe, D., & Takagi, H. (2016). Regulatory mechanism of the flavoprotein Tah18-dependent nitric oxide synthesis and cell death in yeast. *Nitric Oxide*, *57*, 85-91.

Zhang, Y., Lyver, E. R., Nakamaru-Ogiso, E., Yoon, H., Amutha, B., Lee, D. W., ... & Dancis, A. (2008). Dre2, a conserved eukaryotic Fe/S cluster protein, functions in cytosolic Fe/S protein biogenesis. *Molecular and cellular biology*, *28*(18), 5569-5582.

Zhang, Y., Yang, C., Dancis, A., & Nakamaru-Ogiso, E. (2016). EPR studies of wild type and mutant Dre2 identify essential [2Fe–-2S] and [4Fe–-4S] clusters and their cysteine ligands. *The journal of biochemistry*, mvw054.

Zheng, L., Cash, V. L., Flint, D. H., & Dean, D. R. (1998). Assembly of iron-sulfur clusters: identification of an iscSUA-hscBA-fdx gene cluster from Azotobacter vinelandii. *Journal of Biological Chemistry*, *273*(21), 13264-13272.

Zheng, M., Wang, X., Templeton, L. J., Smulski, D. R., LaRossa, R. A., & Storz, G. (2001). DNA microarray-mediated transcriptional profiling of the Escherichia coli response to hydrogen peroxide. *Journal of bacteriology*, *183*(15), 4562-4570.

Zhou, B., Yang, C., Yan, X., Shi, Z., Xiao, H., Wei, X., ... & Wu, Z. (2021). LETM1 knockdown promotes autophagy and apoptosis through AMP-activated protein kinase phosphorylation-mediated Beclin-1/Bcl-2 complex dissociation in hepatocellular carcinoma. *Frontiers in Oncology*, *10*, 606790.

List of Publications in cited Journals (SCI)

- **Bub, Nidhi Kirtikumar**, Sakshi Anand, Swati Garg, Vishal Saxena, Dhanabala Subhiksha Rajesh Khanna, Deeptanshu Agarwal, Sanjay Kumar Kochar, Shailja Singh, and Shilpi Garg*. "*Plasmodium* Iron-Sulfur [Fe-S] cluster assembly protein Dre2 as a plausible target of Artemisinin: Mechanistic insights derived in a prokaryotic heterologous system." *Gene* 869 (2023): 147396.
- **Nidhi Kirtikumar Bub**, Vishal Saxena, Dhanabala Subhiksha Rajesh Khanna, Sayantani Chatterjee, Ankush Bhardwaj, Sanjay Kumar Kochar, Shilpi Garg* "Characterization of a cytoplasmic [Fe-S] cluster assembly protein Dre2 from *Plasmodium vivax* clinical isolates." (Under review)
- **Nidhi Kirtikumar Bub**, Vishal Saxena, Sweta Chauhan, Sahitya Murali, Sanjay Kumar Kochar, Shilpi Garg* "Insight into the metamorphic property of IscU from *Plasmodium vivax*" (Under preparation)

List of National and International Conferences attended

Poster Presentation

- **Nidhi K. Bub**, Aishwarya Singh, Anubhuti Mishra, Vishal Saxena, Shilpi Garg. **"Molecular Characterization of [Fe-S] Cluster Pathways from *Plasmodium"*** in International Conference on Life Science Research and its Interface with Engineering and Allied Sciences 1st-3rd November 2018, organized by BITS Pilani, India
- **Nidhi K. Bub**, Vishal Saxena, Shilpi Garg. "**Characterization of *Pv*Dre2 involved in cytosolic [Fe-S] iron-sulfur cluster assembly (CIA) Pathway from *P. vivax"*** in Biomics'19 April 27, 2019, organized by NIIT University Neemrana, Rajasthan, India
- **Nidhi K. Bub**, Vishal Saxena, Deeptanshu Agarwal, Dhanabala Subhiksha R K, Ankush Bhardwaj, Shilpi Garg. **"Investigation of Cytoplasmic Fe-S Cluster Assembly pathway from *P. vivax* with special emphasis on Dre2/ Anamorsin protein"** in 32nd Annual Molecular Parasitology Meeting 5th-9th October 2021, organized at Marine Biological Laboratory, Woods Hole, MA, USA
- **Nidhi K. Bub**, Vishal Saxena, Sweta Chauhan, Shilpi Garg. **"Characterization of Scaffold protein IscU/NifU from *P. vivax* ISC pathway"** in 15th International Conference on Vector Borne Diseases (ICOV-15) 15th-17th February 2023, organized by ICMR-NIMR and National Academy of Vector Borne Diseases (NAVBD), Goa, India

Details of the workshop attended:

- Workshop on Biosafety and Biohazards organized by Dept. of Biological Sciences, BITS – Pilani Campus, Rajasthan, India. 2022
- MHRD –Global Initiative on Academic Network (GIAN) workshop on "Malaria Control Strategies: Drug Design and Vaccine Development," organized by the School of Life Sciences, University of Hyderabad, India. 2019
- Workshop on Analytical Instruments for Chemical and Environmental Engineers (WAICEE - 2019) organized by IIChE Pilani Regional Centre & Department of Chemical Engineering, BITS – Pilani Campus, India. 2019

Details of Awards and Fellowships

- Junior Research Fellowship-National Eligibility Test (JRF-NET) (Life Sciences), CSIR - UGC, Department of Higher Education, Government of India. 2016
- Junior Research Fellowship (DBT-JRF), Department of Biotechnology, Ministry of Science and Technology, Government of India, to pursue Doctoral Research. 2017 – 2019
- Senior Research Fellowship (DBT-SRF), Department of Biotechnology, Ministry of Science and Technology, Government of India, to pursue Doctoral Research. 2019 – 2022
- Best Poster Award, International Conference on Life Science Research and its Interface with Engineering and Allied Sciences, Organized by BITS Pilani, India. 2018

Biography of Prof. Shilpi Garg

Prof. Shilpi Garg is working as a full-time Professor in Department of Biological Sciences, Birla Institute of Technology and Science, Pilani. She completed her Ph.D. in "Studies on the Drug Resistance Genes in *Plasmodium falciparum* and *Plasmodium vivax* from India" from Department of Biological Sciences, Birla Institute of Technology and Science, Pilani, in 2009. After PhD, she joined as a Research Associate in a DBT-sponsored project entitled "A Systems Biology approach towards understanding Severe Malaria with special reference to the Transcriptome and Proteome of the Parasite and the Host". She was also awarded the prestigious UGC-Dr. D. S. Kothari Post-Doctoral fellowship in 2010. She joined the Department of Biological Sciences as an Assistant Professor in 2012 and became Associate Professor in 2018 and Professor in 2023. Currently she is also serving as a Faculty-In-Charge for "Institute Functions and Infant Care Center". During her tenure at BITS, she has handled and completed research projects from various funding agencies like DST, UGC, ICMR etc.

She was also the recipient of "University Immersion Award" for a research visit to the University of Melbourne, Australia and was also awarded "Outstanding Woman Researcher in Molecular Biology" at the 8th Venus International Women Awards (VIWA 2023) this year. Under her supervision two students have completed their PhD and currently she is guiding 4 students each as a Supervisor and Co-supervisor. She has over 20 years of experience in teaching and research and has supervised many graduate and post-graduate student theses. She has delivered invited talks and chaired scientific sessions at various national and international conferences. Her current research focuses on various aspects related to the malaria parasite *Plasmodium* like "[Fe-S] cluster biogenesis pathways, cold shock proteins from *Plasmodium* and apoptotic machinery of the parasite. She has published over 40 research papers in international peer-reviewed journals of repute and authored chapters in various books.

Biography of the Candidate Ms. Nidhi Bub

Nidhi Bub completed her B.Sc. Biotechnology (2011-2014) from Shree M. & N Virani Science college (Atmiya University), Gujarat, and M.Sc. Biotechnology (2014-2016) from Maharaja Sayajirao University of Baroda, Gujarat. During her Masters, she was involved in a project entitled "Study of putative Prion forming gene MOT3 in *Candida glabrata*" under the supervision of Prof. Johannes Manjrekar, Genome Research Centre, Maharaja Sayajirao University of Baroda. This experience provided her with valuable insights into the intricate world of Molecular Biology and sparked her interest in Infection biology. She had also qualified CSIR-UGC NET-JRF, Graduate Aptitude Test in Engineering (GATE) and Gujarat State Eligibility Test (GSET). Following her interest in infection biology, she joined Prof. Shilpi Garg's Molecular Parasitology and Vector Biology lab at the Department of Biological Sciences, BITS-Pilani, Rajasthan, to pursue her doctoral research in *Plasmodium* biology. For doctoral research she availed JRF (2017-2019) and SRF (2019-2022) fellowship from Department of Biotechnology, Govt. of India. She had been associated for over five years in teaching various theoretical and practical courses in the Department of Biological Sciences. During her PhD she has mentored projects and master's thesis students with her Ph.D. supervisor. Her doctoral research primarily focused on the characterization of Iron-Sulfur [Fe-S] cluster biogenesis pathways from *Plasmodium vivax*, where she has studied various components from Cytoplasmic and Mitochondrial Fe-S biogenesis pathway. She has published research articles in various journals of international repute and has presented her research work in national and international conferences.